

**Structural and functional progression in
glaucoma: some aspects**

Eleni Malissova

Doctor of Philosophy

**Cardiff School of Optometry and Vision
Sciences**

Cardiff University

2015

**NOTICE OF SUBMISSION OF THESIS FORM:
POSTGRADUATE RESEARCH**

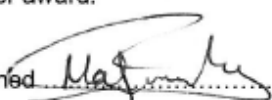


APPENDIX 1:

Specimen layout for Thesis Summary and Declaration/Statements page to be included in a Thesis

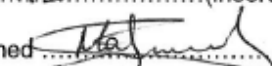
DECLARATION

This work has not been submitted in substance for any other degree or award at this or any other university or place of learning, nor is being submitted concurrently in candidature for any degree or other award.

Signed  (candidate) Date 30/04/2015

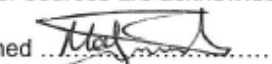
STATEMENT 1

This thesis is being submitted in partial fulfillment of the requirements for the degree of PhD (insert MCh, MD, MPhil, PhD etc, as appropriate)

Signed  (candidate) Date 30/04/2015


STATEMENT 2

This thesis is the result of my own independent work/investigation, except where otherwise stated. Other sources are acknowledged by explicit references. The views expressed are my own.

Signed  (candidate) Date 30/04/2015

STATEMENT 3

I hereby give consent for my thesis, if accepted, to be available online in the University's Open Access repository and for inter-library loan, and for the title and summary to be made available to outside organisations.

Signed  (candidate) Date 30/04/2015

To Vasílikí and Lampros, my parents

Structural and functional progression in glaucoma: some aspects

This thesis explored some aspects of the relationship between structural progression of the glaucomatous optic nerve head (ONH) and functional progression of the visual field.

Sixty-one individuals with a longitudinal series of ONH images were manually identified from a database of approximately 2800 individuals attending a hospital glaucoma clinic. The ONH images obtained from the various photographic sources were equalized, for each individual, in terms of ONH size.

Custom-software was designed to enable the viewing of consecutive and chronologically different ONH image-pairs under monoscopic and stereoscopic conditions, with and without sequential flicker. The efficacy, for the identification of progressive glaucomatous loss, amongst the 61 individuals, of the four viewing techniques was qualitatively evaluated by two ophthalmologists. Stereo-flicker identified the largest number of cases of progression, although little agreement was present between the two ophthalmologists.

The digital characteristics of the ONH images from 27 of the 61 individuals enabled quantitative digital stereo-planimetry. A weak positive curvilinear association was present, at baseline, between the reduction in the neuroretinal rim area and the outcomes of perimetry, including residual retinal ganglion cell (RGC) count. However, little agreement was again present between the two ophthalmologists. Little association was present with either ophthalmologist between progressive structural damage and functional damage.

A separate manual search of 1000 individuals with glaucoma archived in 'Open eyes' identified 112 individuals with a minimum of 5 visual field examinations over a minimum of 5 years. The outcomes at each stimulus location of the differential light sensitivity, expressed in decibels (dB), and of the residual RGC count, against time to follow-up, were compared using univariate linear regression analysis. In general, residual RGC count identified progression, in terms of a greater statistical significance and/ or of more stimulus locations, at an earlier stage of the disease than sensitivity expressed in dB.

Acknowledgments

I would like first to express my sincere thanks to my supervisor Professor John Wild, for his guidance, assistance and support throughout my studies.

I would like to thank Dr Gavin Powell, Cardiff School of Computer Science and Informatics, Cardiff University, for the development of the software utilities for digital stereo-flicker chronoscopy and planimetry, Dr Carlo Knupp, Senior Lecturer, Cardiff School of Optometry and Vision Sciences for the development of the application used to convert the dB values into RGC values and Mr David Shaw, Senior Medical Statistician, who performed the univariate linear regression analysis for the purposes of a study. I also wish to thank all my colleagues and staff in Cardiff School of Optometry and Vision Sciences, Cardiff University for their help and support with special thanks to Mrs Susan Hobbs.

I am grateful to Mr Ian Cunliffe, Consultant Ophthalmologist and Mr Mike Austin, Consultant Ophthalmologist, for their assistance with the project.

I would like to extend a special thanks to my precious friends Dr Kholoud Alshaghroud, and Miss Rena Karapetrou, as well as, my lovely brother Giorgos for their continuous encouragement and support.

Finally, I would like express my gratitude to my great parents Vasiliki and Lampros, for their love, support and their advice that with patience, work and perseverance I can achieve my goals.

Table of Contents

Chapter	Title	Page
Chapter 1	Fundamentals of the optic nerve head appearance, of digital optic nerve head imaging and of perimetry	
1.1	The normal optic nerve head (ONH)	1
1.2	Glaucoma	5
1.2.1	Classification of Glaucoma	6
1.2.1.1	Primary open-angle glaucoma (POAG)	6
1.2.1.2	Normal-tension glaucoma (NTG)	6
1.2.1.3	Ocular Hypertension (OHT)	7
1.2.1.4	Glaucoma Suspect	7
1.2.1.5	Primary angle-closure glaucoma (PACG)	8
1.2.2	Primary risk factors for glaucoma	8
1.2.2.1	Family history	8
1.2.2.2	Ageing	9
1.2.2.3	Ethnicity	9
1.2.2.4	Central corneal thickness (CCT)	10
1.2.2.5	Intraocular pressure (IOP)	11
1.2.3	Secondary risk factors for glaucoma	12
1.2.3.1	Ocular perfusion pressure (OPP)	12
1.2.3.2	Diabetes - High Myopia - Axial length	12
1.2.3.3	Peripapillary Atrophy (PPA)	13

1.2.3.4	Disc Haemorrhage (DH)	13
1.2.3.5	Gender	13
1.3	The ONH in primary open-angle glaucoma	14
1.3.1	Introduction	14
1.3.2	Neuroretinal rim (NRR)	14
1.3.3	Measurement of the predominant ONH features in glaucoma	14
1.3.4	Peripapillary atrophy (PPA)	15
1.3.5	Disc Haemorrhage (DH)	16
1.3.6	Vasculature	16
1.3.7	Laminar pores	16
1.3.8	Pallor	17
1.3.9	The Retinal Nerve fibre Layer (RNFL) in open-angle glaucoma	17
1.4	Pathophysiology of glaucoma	18
1.4.1	Apoptosis	19
1.4.2	Cell shrinkage	19
1.4.3	Mechanical and Ischemic mechanism	20
1.4.3.1	Mechanical mechanism	21
1.4.3.2	Ischaemic mechanism	21
1.4.4	Treatment modalities in glaucoma	22
1.5	Types of ONH photography	22
1.5.1	Analogue photography	22
1.5.2	Digital photography	22

1.6	Fundamentals of perimetry	26
1.6.1	The normal visual field	26
1.6.2	Differential light sensitivity	26
1.6.3	Kinetic perimetry	27
1.6.4	Standard automated perimetry (SAP)	28
1.6.4.1	Threshold algorithms	30
1.6.4.2	Stimulus Program	34
1.6.4.3	Variability of the threshold estimate	35
1.7	Classification of visual field defects	35
1.8	The Single Field printout of the central field	36
1.8.1	Estimated values of sensitivity	37
1.8.2	Grayscale	38
1.8.3	Total Deviation values	38
1.8.4	Pattern Deviation values	38
1.8.5	Total Deviation probability values	40
1.8.6	Pattern Deviation probability values	40
1.8.7	Visual field indices	41
1.8.7.1	Mean Deviation (MD)	41
1.8.7.2	Pattern Standard Deviation (PSD)	42
1.8.7.3	Visual Field Index (VFI)	42
1.8.7.4	Glaucoma Hemifield Test (GHT)	43
1.8.8	Reliability parameters	44

1.8.8.1	False-Negative (FN) Catch Trials	44
1.8.8.2	False-Positive (FP) Catch Trials	45
1.8.8.3	Fixation Stability	45
1.8.8.4	Perimetric learning effect and fatigue effect	46
1.9	The identification of progressive visual field loss	48
1.9.1	Empirical Clinical Judgement	49
1.9.2	Defect Classification Systems	49
1.9.3	Trend Analysis	50
1.9.4	Event Analysis	50
Chapter 2 Rational for the Research		
2.1	Introduction to structural and functional characteristics of the ONH	52
2.2	Previous work	53
2.3	Overall and specific aims of the work	54
2.4	Experimental Studies	56
2.5	Logistics	57
Chapter 3 Characteristics of the individuals within the database compiled for the research		
3.1	Acquisition of the various cohorts	63
3.2	Evaluation of structural and/or functional progressive loss (Chapter 5 and Chapter 6)	64
3.2.1	Optic nerve head (ONH) images	64
3.2.2	Visual field examination time series	66
3.3	The characteristics of the various cohorts with ONH stereo-images and visual field examinations	67

3.3.1	Resultant cohort for the qualitative assessment of progressive glaucomatous ONH damage using both mono- and stereo-flicker chronoscopy (Chapter 5)	74
3.3.2	Resultant cohort for the quantitative assessment of progressive structural and functional glaucomatous damage (Chapter 6)	79
3.3.3	Resultant cohort for the pointwise linear regression of residual retinal ganglion cell (RGC) count (Chapter 7)	84
Chapter 4	Optic nerve head image registration, sizing and alignment, and viewing	
4.1	Aim	88
4.2	Hardware	88
4.3	Software	89
4.4	Equalizing the ONH image size from the various photographic sources	96
4.5	Results	100
4.6	Discussion	102
Chapter 5	The qualitative assessment of progressive glaucomatous ONH damage using both mono- and stereo-flicker chronoscopy	
5.1	Introduction	104
5.2	Aim	105
5.3	Methods	106
5.4	Results	112
5.4.1	Designation of glaucoma	118

5.4.2	Designation of progressive glaucomatous ONH damage	123
5.4.3	Comparison of definite progression to that of the corresponding visual field outcome	129
5.5	Discussion	133
Chapter 6	The quantitative assessment of progressive structural and functional glaucomatous damage	
6.1	Introduction	137
6.2	Aim	139
6.3	Methods	139
6.4	Results	150
6.5	Discussion	166
Chapter 7	Pointwise linear regression of residual RGC count	
7.1	Introduction	171
7.2	Aim	174
7.3	Methods	174
7.4	Results	179
7.4.1	Global approach	180
7.4.2	Pointwise approach	183
7.5	Discussion	193
Chapter 8	Overall Discussion, conclusion and future work	
8.1	Optic nerve head image registration, sizing and alignment, and viewing	198

8.2	The qualitative assessment of progressive glaucomatous ONH damage using both mono- and stereo-flicker chronoscopy	199
8.3	The quantitative assessment of progressive structural and functional glaucomatous damage	200
8.4	Pointwise linear regression of residual RGC count	202
	References	206

List of acronyms used in the text

Abbreviation	Interpretation
α -zone	Alpha zone
asb	Apostilb
β -zone	Beta zone
CCD	Charge couple device
CCT	Central corneal thickness
CDR	cup-to-disc ratio
CSLO	Confocal scanning laser ophthalmoscopy
dB	Decibel
DD	Diffuse Defect
dD	Disc diameter
DH	Disc haemorrhage
dpi	Dots per inch
EGS	European Glaucoma Society
ERF	Error Related Factor
FOS	Frequency-of-Seeing curve
FN	False-Negative
FP	False-Positive
GH	General Height
.gif	Graphics interchange format
GHT	Glaucoma Hemifield Test
GPA	Guided Progression Analysis
HFA	Humphrey Field Analyzer
HRT	Heidelberg Retinal Tomography
IOL	Intraocular lens implementation
IOP	Intraocular pressure
.jpeg	Joint photographic experts group
LC	Lamina cribrosa
LD	Local Defect
MD	Mean Deviation
NRR	Neuroretinal rim
NTG	Normal-tension glaucoma

OCT	Optical coherence tomography
OHT	Ocular hypertension
OHTS	Ocular Hypertension Treatment Study
ONH	Optic nerve head
OPP	Ocular perfusion pressure
PMS	Patient management system
PSD	Pattern Standard Deviation
PPA	Peripapillary atrophy
PIGM	Pigment dispersion glaucoma
PLR	Pointwise linear regression analysis
.png	Portable network graphics
POAG	Primary open-angle glaucoma
PACG	Primary angle-closure glaucoma
PEXG	Pseudo-exfoliation glaucoma
RGB	Red, Green, Blue
RGC	Retinal ganglion cell
RNFL	Retinal nerve fibre layer
RPE	Retinal pigment epithelium
Rw/Dd	Rim width-to-disc ratio
SLP	Scanning laser polarimetry
SKP	Semi-automated kinetic perimetry
STP	Size Threshold Perimetry
SAS	Statistical Analysis System
SAP	Standard automated perimetry
SITA	Swedish Interactive Threshold Algorithm
.tiff	Tagged image file format
AGIS	The Advanced Glaucoma Intervention Study
CIGTS	The Collaborative Initial Glaucoma Treatment Study
CNTGS	The Collaborative Normal-Tension Glaucoma Study
EMGT	The Early Manifest Glaucoma Trial

EGPS	The European Glaucoma Prevention Study
LoGTS	The Low-Pressure Glaucoma Treatment Study
UHW	University Hospital of Wales
VCDR	Vertical cup-to-disc ratio
VFI	Visual Field Index

List of Figures

Figure	Title	Page
Chapter 1	Fundamentals of the optic nerve head appearance, of digital optic nerve head imaging and of perimetry	
Figure 1.1	The Single Field Printout for Program 24-2 and the SITA Fast algorithm in the left eye of a patient with an age-related cataract and NTG.	37
Chapter 2	Rational for the Research	
-	No figures listed.	-
Chapter 3	Characteristics of the individuals within the database compiled for the research	
Figure 3.1	The distribution of the ONH and visual field examination in 27 patients with two or more ONH stereo-images with at least one visit conducted through Topcon TRC-EX and five or more reliable visual field examinations.	83
Chapter 4	Optic nerve head image registration, sizing and alignment, and viewing	
Figure 4.1	A screenshot of the biographical information, the designation of each ONH image for the given stereo-pair, the keratometry values, the refraction, the name of the camera and the date of examination for a given individuals as presented from the software.	89
Figure 4.2.	A screenshot of the multiple align box used for image alignment.	90
Figure 4.3	A screen capture of the database illustrating an ONH image for the right and left eyes, respectively, of a given individual at each of seven visits. The two images contained within the automatically generated red square, indicate the two time points, selected by the operator, for the	91

	given chronological comparison of the ONH characteristics.	
Figure 4.4.	A screen capture of the database illustrating an ONH image for the right and left eyes, respectively, of a given individual at each of five visits.	92
Figure 4.5	Multiple align box option	94
Figure 4.6	A schematic illustrating the procedure for the manual resizing of the original photographic images for any visit (A, B, D) and the manually resized and aligned stereo-pairs (E) relative to those between Visits 1 and 2 (C). The associated vector comparisons for the calculation of the scaling factor are also shown.	97
Figure 4.7.	Two examples of the position of a vessel bifurcation, indicated by the ✓ symbol, considered suitable for the vector analysis. The X symbols represent unsuitable, positions of the same bifurcations.	99
Figure 4.8	The eight features (a to h inclusive) selected for the vector analysis, and the corresponding 28 vectors, illustrated for a given stereo-pair for a given individual.	99
Chapter 5	The qualitative assessment of progressive glaucomatous ONH damage using both mono- and stereo-flicker chronoscopy	
Figure 5.1	A schematic illustrating, by visit, the pseudo-randomization of the four viewing techniques across the 61 individuals.	111
Figure 5.2	The non-colour balanced ONH images, between Visits 1 and 2, for each of the four cases of non-glaucoma incorrectly designated as ‘glaucoma’ by both observers.	121

Figure 5.3	The non-colour balanced ONH images, between Visits 1 and 2, for each of the four cases of non-glaucoma incorrectly designated as ‘non-glaucoma’ by both observers.	123
Chapter 6	The quantitative assessment of progressive structural and functional glaucomatous damage	
Figure 6.1	The pseudo-randomized order of presentation of the mono- and stereo-viewing techniques between images and between visits.	143
Figure 6.2	The ONH sectors from Wirtschafter and colleagues (1982) (top) and the mapping of the visual field to the ONH sectors, to estimate the RGC number of a given ONH sector subserving the given stimulus location, based upon the work of Garway-Heath and colleagues (2000) (bottom).	148
Figure 6.3	An example of the output from the application coded to calculate the RGC at each of the ONH sectors based upon the Program 24-2 stimulus grid of the HFA.	148
Figure 6.4	The between-observer difference in the NRR area (mm^2) at baseline between Observer B and A against the mean of the NRR area (mm^2) derived by the two observers. The solid line indicates the mean of the differences and the dotted line the 95% limits of agreement.	152
Figure 6.5	The true NRR area (mm^2) against the true ONH area (mm^2) at the baseline photographic visit by observer for the 23 individuals who had undertaken perimetry reliably (top) Observer A; (bottom) Observer B.	153
Figure 6.6	The VFI (%) at the baseline visual field examination against the true NRR area (mm^2) at the baseline photographic visit for the 23	154

	individuals for ‘Observer A’ (top) and ‘Observer B’ (bottom).	
Figure 6.7	The MD (dB) at the baseline visual field examination against the true NRR area (mm ²) at the baseline photographic visit for the 23 individuals for ‘Observer A’ (top) and ‘Observer B’ (bottom).	155
Figure 6.8	The number of RGCs (millions) at the baseline visual field examination against the true NRR area (mm ²) at the baseline photographic visit for the 23 individuals for ‘Observer A’ (top) and ‘Observer B’ (bottom).	156
Figure 6.9	The between-observer difference in the proportionate change in the NRR area (%) at baseline between Observer B and A against the mean of the proportionate change in the NRR area (%) derived by the two observers.	157
Figure 6.10	The proportionate change (%) in VFI from the baseline to the last visit against the corresponding proportionate change in the NRR (%), for Observer A (top) and Observer B (bottom).	159
Figure 6.11	The proportionate change in MD (%) from the baseline to the last visit against the corresponding proportionate change in the NRR (%), for Observer A (top) and Observer B (bottom).	161
Figure 6.12	The proportionate change in the number of RGCs (%) from the baseline to the last visit against the corresponding proportionate change in the NRR (%), for Observer A (top) and Observer B (bottom).	162
Figure 6.13	The proportionate change in the superior number of RGCs (%) from the baseline to the last visit against the corresponding proportionate change in	163

- the superior NRR area (%), for Observer A (top) and Observer B (bottom).
- Figure 6.14 The proportionate change in the inferior number of RGCs (%) from the baseline to the last visit against the corresponding proportionate change in the inferior NRR area (%), for Observer A (top) and Observer B (bottom). 164
- Figure 6.15 The between-observer difference in the proportionate change of the NRR area (%) against the time interval (years). 165
- Chapter 7 Pointwise linear regression of residual retinal ganglion cell count**
- Figure 7.1 The relationship between the various transformations of the mean differential light sensitivity recorded with stimulus size III using Program 24-2 and specified in dB. Note the differences in the scaling of the various axis. 173
- Figure 7.2 The output of the univariate linear regression analysis illustrating the slope of each of the three visual field indices, MD, PSD and VFI, and of the global residual RGC count against time to follow-up; the lower and upper 95% confidence limits of the estimate and the statistical significance of the estimate, at each stimulus location arranged in Program 24-2 format. Outcomes exhibiting a statistical significant estimate of the slope are highlighted in yellow. 176
- Figure 7.3a The slope of the univariate linear regression of differential light sensitivity (dB) against time to follow-up, the lower and upper 95% confidence limits of the estimate and the statistical significance of the estimate, at each stimulus location arranged in Program 24-2 format. 178

Figure 7.3b	The slope of the univariate linear regression of residual RGC count against time to follow-up, the lower and upper 95% confidence limits of the estimate and the statistical significance of the estimate, at each stimulus location arranged in Program 24-2 format.	178
Figure 7.4	An illustration of the significance printout, is given in Figures 7.3. The statistical significance of the estimate of the slope of the univariate linear regression of differential light sensitivity (dB) (top) and residual RGC count (bottom) against time to follow-up arranged in Program 24-2 format for the individual presented in Figures 7.3 a and b.	179
Figure 7.5	The relationship of the number of statistically significant progressive slopes between the various indices.	182
Figure 7.6	The number of individuals against the number of statistically significant negative slopes for each regression outcome.	185
Figure 7.7	The number of individuals against the number of additional statistically significant negative slopes for each regression outcome.	186
Figure 7.8	The relationship between the number of statistically significant negative slopes and the corresponding number of positive slopes for the absolute values of sensitivity (dB). The figure adjacent to a symbol indicates the number of overlapping data points.	187
Figure 7.9	The relationship between the number of statistically significant negative slopes and the corresponding number of positive slopes for the residual RGC count. The figure adjacent to a symbol indicates the number of overlapping data	187

points.

Figure 7.10 The number of locations exhibiting a statistically significant negative slope for each regression outcome, but with one outcome manifesting a more statistically significant slope compared to the other, by the mean of the absolute sensitivity at the two baseline examinations. 189

Figure 7.11 The number of additional locations exhibiting a statistically significant negative slope for one outcome compared to the absence of progression with the other outcome, by the mean of the absolute sensitivity at the two baseline examinations. Note the scaling of both the ordinate and the abscissa is different to that of Figure 7.10. 191

List of Tables

Table	Title	Page
Chapter 1	Fundamentals of the optic nerve head appearance, of digital optic nerve head imaging and of perimetry	
-	No tables listed.	-
Chapter 2	Rational for the Research	
-	No tables listed.	-
Chapter 3	Characteristics of the individuals within the database compiled for the research	
Table 3.1	The number of stereo-images by the number of photographic visits, and the mode and resolution of photography at each visit, for the 212 individuals with two or more stereo-images.	66
Table 3.2	The number of individuals by the frequency of the available ONH images and visual field examinations.	68
Table 3.3	The number of stereo-images by the number of photographic visits, and the mode and resolution of photography at each visit, for the 116 individuals with two or more stereo-images and three or more reliable visual field examinations.	69
Table 3.4	The number of ONH stereo-images by the number of visual field examinations for the 116 individuals with two or more stereo-images and three or more reliable visual field examinations.	69
Table 3.5	The number and the corresponding percentage (%) of visits where the photography and visual field examinations were undertaken on the same day for the 116 individuals with two or more stereo-images and three or more reliable visual field examinations.	70

Table 3.6	The cumulative distribution of the 116 patients (cells) with two or more stereo-images and three or more reliable visual field examinations by the number of, and interval between, the corresponding photographic and visual field examinations.	70
Table 3.7	The number of ONH stereo-images by the number of visual field examinations for the 97 individuals with two or more stereo-images and three or more reliable visual field examinations and with the pairs of respective examinations conducted within 12 months of each other.	71
Table 3.8	The number of stereo-images by the number of photographic visits, and the mode and resolution of photography at each visit, for the 74 individuals with two or more stereo-images and five or more reliable visual field examinations.	72
Table 3.9	The number of ONH stereo-images by the number of visual field examinations for the 74 individuals with two or more stereo-images and five or more reliable visual field examinations.	72
Table 3.10	The number and the corresponding percentage (%) of visits where the photography and visual field examinations were undertaken on the same day for the 74 individuals with two or more stereo-images and five or more reliable visual field examinations and with at least one pair of respective examinations conducted within 12 months of each other.	73
Table 3.11	The cumulative distribution of the 74 patients (cells) with two or more ONH stereo-images and five or more reliable visual field examinations by the number of, and interval between, the	73

	corresponding photographic and visual field examinations.	
Table 3.12	The number of ONH stereo-images by the number of visual field examinations for the 68 individuals with two or more stereo-images and five or more reliable visual field examinations and with at least one pair of respective examinations conducted within 12 months of each other.	74
Table 3.13	The number of stereo-images by the number of photographic visits, and the mode and resolution of photography at each visit, for the 61 individuals with two or more stereo-images and five or more reliable visual field examinations and with at least one pair of respective examinations conducted within 12 months of each other.	75
Table 3.14	The number of ONH stereo-images by the number of visual field examinations for the 61 individuals with two or more stereo-images and five or more reliable visual field examinations and with at least one pair of respective examinations conducted within 12 months of each other.	75
Table 3.15	The demographic characteristics of the most severely affected eye, by diagnosis, for the 61 individuals with two or more stereo-images and five or more reliable visual field examinations conducted within 12 months of each other.	77
Table 3.16	The clinical characteristics of the most severely affected eye, by diagnosis, for the 61 individuals with two or more stereo-images and five or more reliable visual field examinations.	78
Table 3.17	The number of stereo-images by the number of photographic visits, and the mode and resolution of photography at each visit, for the 27 individuals	79

with two or more stereo-images and five or more reliable visual field examinations with at least one pair of examinations conducted within 12 months of each other and with at least one photographic examination undertaken with the Topcon TRC-Ex camera.

Table 3.18	The number of ONH stereo-images by the number of visual field examinations for the 27 individuals with two or more stereo-images and five or more reliable visual field examinations with at least one pair of respective examinations conducted within 12 months of each other and with at least one photographic examination undertaken with the Topcon TRC-Ex camera.	80
Table 3.19	The demographic characteristics, of the most severely affected eye, by diagnosis, for the 27 individuals with two or more stereo-images and at least one visit conducted through Topcon TRC-EX and five or more reliable visual field examinations conducted within 12 months of each other.	81
Table 3.20	The perimetric and clinical characteristics, at the entry visit, of the 27 individuals with two or more stereo-images and at least one visit conducted through Topcon TRC-EX and five or more reliable visual field examinations conducted within 12 months of each other.	82
Table 3.21	The demographic characteristics of the most severely affected eye, by diagnosis, for the 112 individuals with five or more reliable visual field examinations over a minimum follow-up of 5 years.	86
Table 3.22	The perimetric characteristics at the entry visit, of the most severely affected eye, by diagnosis, for	87

the 112 individuals with five or more reliable visual field examinations over a minimum follow-up of 5 years.

Chapter 4 Optic nerve head image registration, sizing and alignment, and viewing

Table 4.1 The summary statistics for the proportionate difference, in the magnitudes of the x and y coordinates of all 28 vectors considered together, between the original image and the manually resized image for each given imaging modality, at a randomly selected visit, amongst the 27 individuals. 100

Table 4.2 The summary statistics median for the proportionate difference, in the magnitudes of the x and y coordinates of all 28 vectors considered together, between the manually resized and aligned images, by paired photographic modalities, at a randomly selected between-visit comparison, amongst the 27 individuals. 101

Chapter 5 The qualitative assessment of progressive glaucomatous ONH damage using both mono- and stereo-flicker chronoscopy

Table 5.1 The demographic characteristics of the randomly assigned eye of the 61 individuals at the baseline visit. 107

Table 5.2 The clinical characteristics of the randomly assigned eye of the 61 individuals at the baseline visit. 108

Table 5.3 The median of the image quality, scored on a 0-5 scale, by observer and by viewing technique, for the 50 individuals with glaucoma (top) and for the 11 individuals with ocular hypertension (bottom), evaluated at each of the first three visits. 113

Table 5.4	The mean of the differences, and the corresponding 95% limits of agreement, for the within-observer ‘test-retest’ variability in the assessment of image quality for each of the viewing techniques, for each observer, within the first three visits, for the individuals with glaucoma (top) and the between-observer variability in the assessment of image quality for the second of the two image evaluations for each of the viewing techniques within the first three visits (bottom).	114
Table 5.5	The mean of the differences, and the corresponding 95% limits of agreement, for the within-observer ‘test-retest’ variability in the assessment of image quality for each of the viewing techniques, for each observer, within the first three visits, for the individuals with ocular hypertension (top) and the between-observer variability in the assessment of image quality for the second of the two image evaluations for each of the viewing techniques within the first three visits (bottom).	115
Table 5.6	Top: The median (lower and upper quartiles; range) of the time (seconds) taken to reach an outcome in terms both of diagnosis and of progression for each paired-comparison, by observer and by viewing technique, for the 50 individuals with glaucoma. Bottom: The mean of the differences between the two observers, and the corresponding 95% limits of agreement, for the time to reach an outcome in terms both of diagnosis and of progression, by viewing technique, at each of the first three visits.	116

Table 5.7	Top: The median (lower and upper quartiles; range) of the time (seconds) taken to reach a diagnostic outcome for each paired comparison, by observer and by viewing technique, for the 11 individuals with ocular hypertension. Bottom: The mean of the differences between the two observers, and the corresponding 95% limits of agreement, for the time to reach a diagnostic outcome, by viewing technique, at each of the first three visits.	117
Table 5.8	The number of ‘glaucoma’ to ‘non-glaucoma’ cases, by observer and by viewing technique, for the 50 individuals with glaucoma and for the 11 individuals with ocular hypertension between Visit 1 and Visit 2 (left column) and for the 30 individuals with glaucoma and 5 individuals with ocular hypertension between Visits 1, 2 and 3 (middle columns). The fourth column represents the outcomes from the 82 comparisons of the ONH images from the 17 individuals (14 with glaucoma and 3 with ocular hypertension) with four or more ONH images.	119
Table 5.9	The number of cases with non-progression by observer, by number of visits and by viewing technique, for the 50 individuals with glaucoma.	126
Table 5.10	The number of cases with definite progression and with possible progression (in parenthesis) by observer, by number of visits and by viewing technique, for the 50 individuals with glaucoma.	127
Table 5.11	The number of instances in which the given viewing technique identified definite progression at an earlier stage compared to each of the remaining three viewing techniques, by observer, by number of visits, amongst the 50 progressed	128

individuals with glaucoma. The figure in parenthesis indicates the number of instances where agreement was present for both observers.

Table 5.12	The outcome for the 4 cases of ocular hypertension incorrectly designated as glaucoma by both observers, by viewing technique and by ranking of the earliest identification of definite progression.	128
Table 5.13	The outcomes of the three separate visual field progression criteria, MD, VFI and EMGT GPA in isolation, and in combination, for the 50 individuals with glaucoma and the 11 individuals with ocular hypertension.	129
Table 5.14	The frequency of visual field progression for each of the three separate visual field progression criteria, MD, VFI and EMGT GPA in isolation and combined, for the 14 cases of definite progression confirmed by both observers using stereo-flicker chronoscopy and for the 20 and 22 cases, respectively, of definite progression for Observer 'A' and Observer 'B', alone.	130
Table 5.15	The frequency of visual field progression for each of the three separate visual field progression criteria, MD, VFI and EMGT GPA in isolation and in combination for the 7 cases of non-progression of the ONH confirmed by both observers using stereo-flicker chronoscopy and for the 11 and 15 cases, respectively, of non-progression for Observer 'A' and Observer 'B', alone.	131
Table 5.16	The number of the perimetric and the photographic visits (median, lower and upper quartiles; range) for the 7 out of 14 cases of definite progression confirmed by both observers using stereo-flicker chronoscopy and who exhibited visual field	132

progression (left-hand column); for the 7 out the 14 cases of definite progression confirmed by both observers using stereo-flicker chronoscopy and who did not exhibit visual field progression (middle-left column); for the 4 out of 7 cases of non-progression of the ONH confirmed by both observers using stereo-flicker chronoscopy and who exhibited visual field progression (middle-right column); and for the 3 of the 7 cases of non-progression of both the ONH and the visual field.

Chapter 6 The quantitative assessment of progressive structural and functional glaucomatous damage

Table 6.1	The demographic characteristics of the randomly assigned eye of the 27 individuals at the baseline visit.	141
Table 6.2	The clinical characteristics of the randomly assigned eye of the 27 individuals at the baseline visit.	142
Table 6.3	The median of the times (minutes) to complete planimetry of the 23 images acquired at the second photographic visit, by diagnosis, by observer and by viewing technique, together with the mean of the differences between the two observers, and the corresponding 95% limits of agreement.	150
Table 6.4	The descriptive statistics for the true values of the ONH area, NRR area, cup area, ONH diameter, and CDR for the 20 individuals with glaucoma (top) and for the 3 individuals with ocular hypertension (bottom), by observer and by viewing technique.	151
Table 6.5	The frequency of visual field progression by trend-analysis (the statistical significance of the slopes of the VFI and MD against time to follow-up) and by	158

event-analysis (EMGT GPA progression criteria) amongst the 23 individuals.

Chapter 7 Pointwise linear regression of residual retinal ganglion cell count

Table 7.1	Table 7.1. The summary statistics for the age and gender characteristics of the 112 individuals together with the number of visual field examinations; the duration of visual field follow-up; the visual field indices and the residual RGC count of the baseline visual field in the randomly selected eye.	180
Table 7.2	The number of statistically significant progressive slopes by each of the various visual field indices and by the global residual RGC count for each eye.	180
Table 7.3.	The summary statistics of the slope of the given visual field index against time to follow-up for the total number of progressive slopes, of statistically significant progressive slopes, of improving slopes, and of statistically significant improving slopes.	181
Table 7.4	The number of statistically significant improving slopes by each of the various visual field indices and by the global residual RGC count for each eye.	182
Table 7.5	The outcomes illustrated in Figure 7.5, expressed in tabulated format.	183
Table 7.6.	The summary statistics of the number of locations for the 102 individuals associated with a statistically significant negative slope for the absolute values of sensitivity (dB) and for the residual RGC count, against time to follow-up.	184
Table 7.7	The summary statistics of the distributions of the statistically significant negative and positive slopes for residual RGC count, and for the absolute values of sensitivity (dB), against time to follow-up,	186

respectively, amongst the 22 individuals.

Table 7.8. The summary statistics of the absolute values of sensitivity (dB) averaged across Visits 1 and 2. 190

Table 7.9 The summary statistics of the number of locations for the 10 individuals associated with a statistically significant positive slope for the absolute values of sensitivity (dB) and for the residual RGC count, against time to follow-up. 192

Chapter 1

Fundamentals of the optic nerve head appearance, of digital optic nerve head imaging and of perimetry

1.1 The normal optic nerve head (ONH)

The optic nerve head (ONH) is situated approximately 1.5° below and 15° nasally from the fovea and is a vertical oval subtending 7.5° by 5.5°. It contains the axons of the retinal ganglion cells (RGC) gathered into bundles of approximately 20µm in diameter (Jonas et al. 1999; Sramek 2002; Oddone and Centofanti 2005).

The predominant features of the ONH are the optic cup and the neuroretinal rim (NRR). The normal cup is horizontally oval: the horizontal diameter is approximately 8% wider than the vertical diameter (Varma 1993; Sanfilippo et al. 2009). The NRR contains between 800,000 and 1,500,000 axons, with an average of 1,200,000 (Wynsberghe et al. 1995; Levin 1999) and comprises the area between the border of the cup and the edge of the ONH. The NRR is, therefore, defined by the vertical shape of the ONH and the horizontal shape of the cup. The vertical cup-to-disc ratio (VCDR) can be used to describe the predominant features of the ONH (Quigley et al. 2008; Lee et al. 2010; Stone et al. 2010; Breusegem et al. 2011; Swamy et al. 2012). The normal value ranges from 0.43 to 0.50; however, 5% of normal individuals exhibit a cup-to-disc ratio (CDR) of 0.7 (Boland and Quigley 2007; Bourne 2012). The NRR

area and the cup area each exhibit a positive linear correlation with the ONH size (Hoffmann et al. 2007). The VCDR increases by 0.1 between the ages of 30 to 70 years (Garway-Heath et al. 1997).

The axons temporal to the macula in one horizontal hemifield follow an arcuate course around the macula, termed the papillomacular bundle, and enter the temporal sectors of the ONH. The axons from the more peripheral temporal region follow a course around the papillomacular bundle and enter the ONH at the superior or inferior pole respectively. Nasally, the axons follow a radial course and enter the nasal sectors of the ONH (Varma 1993; Maresco 2002; Hoffmann et al. 2007; Morrison 2007). The peripapillary retinal nerve fibre layer (RNFL) is, therefore, thickest at the upper and lower poles (Radius 1987; Azuara-Blanco et al. 2002a; Heijl and Patella 2002). Four types of ganglion cell have been identified in human: the midget cells, which form 89-90% of the population (Dacey and Lee 1994); the parasol cells (Dacey and Brace 1992); the small bistratified cells (Kaas et al. 1978; Dacey 1993); and the melanopsin-containing cells (Hankins et al. 2008; Li et al. 2012).

Within the ONH, collagenous extensions from the surrounding sclera form a fine meshwork, the lamina cribrosa (LC) (Oddone and Centofanti 2005). The main role of the LC is to provide mechanical support for the axon bundles and to maintain the intraocular pressure (IOP) gradient. The main glial element are the astrocytes which support the passage of the axon bundles through the pores between the collagen thereby isolating individual axon bundles from one another and from the blood vessels (Radius 1987; Maresco 2002). The LC is

slightly concave with its largest pores located superiorly and inferiorly (Hoffmann et al. 2007; Lawrenson 2007; Park et al. 2013). Elevated IOP can lead to posterior bowing of the LC and this displacement leads to a deformation of the pores with subsequent axonal damage (Radius and Gonzales 1981; Varma 1993; Caprioli and Coleman 2010). The NRR area exhibits considerable variability between individuals depending upon the density and diameter of the axons and upon differences in the LC and in the proportion of glial cells (Fingeret et al. 2005; Rolando 2005; Hoffmann et al. 2007; Sanfilippo et al. 2009). The size of the LC pores is positively correlated with the size of the ONH. Large ONHs exhibit large pores and the axons are more sparsely arranged through the LC with less compression whilst the opposite occurs with small ONHs (Healey and Mitchell 2004; Lee et al. 2012a; Park and Park 2012).

The central retinal artery and vein emerge from the ONH and branch to supply the four quadrants of the retina. The ONH can thus be located by the point of convergence of the vessels (Sramek 2002; Oddone and Centofanti 2005). The exit position of the central vessel trunk can influence the local susceptibility of the NRR to damage (Jonas et al. 2001).

The ONH margin is surrounded by Elschnig's ring which is composed of white neuroglial tissue and separates the ONH from the retinal pigment epithelium (RPE) (Roff et al. 2001; Cankaya and Simsek 2012; Chauhan et al. 2012). The fine capillaries are responsible for the pink colour of the ONH.

In approximately 15%-20% of cases, the normal ONH can be associated with

peripapillary atrophy (PPA), which is an age-related degeneration of the retinal pigment epithelium and Bruch's membrane, and which is associated with a thinning of the chorioretina, and/ or an abnormal pigmentation and colour, in the immediate peripapillary region. Peripapillary atrophy comprises the more peripheral alpha (α) zone, the inner edge of which forms the border with the outer edge of the more central beta (β) zone. The inner edge of the β -zone forms the border with Elschnig's ring (Healey et al. 2007; Radcliffe et al. 2008; See et al. 2009; Teng et al. 2010; VanderBeek et al. 2010; Jonas et al. 2012; Lee et al. 2012b). The β -zone is mostly present in glaucoma.

The area of the normal ONH follows a near Gaussian distribution. Estimates of the mean area range from 2.1 mm² (SD 0.47) (Sung et al. 2009) to 2.61 mm² (SD 0.68) (Xu et al. 2008; Sanfilippo et al. 2009). The corresponding NRR area ranges from 1.50 mm² (SD 0.63) (Xu et al. 2008) to 2.03 mm² (SD 0.51) (Sung et al. 2009).

The CDR is traditionally utilized to quantify the predominant features of the ONH, (Quigley et al. 2008; Lee et al. 2010; Stone et al. 2010; Breusegem et al. 2011; Swamy et al. 2012). The VCDR is the most useful ratio (Jonas et al. 2000; Chandra et al. 2013). The VCDR in the normal eye ranges from 0.29 (SD 0.16) (Sung et al. 2009) to 0.54 (SD 0.26) (Jonas et al. 2000). The CDR increases by 0.1 between 30 and 70 years of age (Garway-Heath et al. 1997).

1.2 Glaucoma

Glaucoma is the largest cause of irreversible vision loss, worldwide (Friedman et al. 2006; Broman et al. 2008; Gardiner et al. 2011). It affects approximately 70 million people, worldwide, of whom approximately 10% are estimated to be bilaterally blind (Quigley and Broman 2006). By 2020, it is estimated that approximately 79.4 million people, worldwide, will have glaucoma (Garway-Heath et al. 2013) and 10% of these will be bilaterally blind (Quigley and Broman 2006). Approximately 50% of cases remain undetected due to the asymptomatic nature of the disease (Cedrone et al. 2008; Taylor 2009; Kim and Varma 2010; Heijl et al. 2013a; Weinreb et al. 2014).

Glaucoma is not a single disease entity and the glaucomas can be defined as a group of optic neuropathies characterized by progressive neuro-degeneration of the RGCs (Weinreb et al. 2014). The aetiology is multi-factorial (see Section 1.2.2) and results in characteristic changes at the ONH comprising focal and/ or generalized thinning of the NRR with excavation and enlargement of the cup and deformation of the LC, and in a thinning of the RNFL, leading to corresponding visual field loss (Baltmr et al. 2010; Casson et al. 2012b; Morgan 2012; Park et al. 2013; Williams et al. 2013). The type and location of the field loss reflects that of the damage to the axons.

1.2.1 Classification of Glaucoma

Glaucoma is generally a primary condition (Leske 1983; Litwak 2001; Musch et al. 2012); however, glaucoma can occur due to secondary causes including trauma, corticosteroid use, inflammation, uveal melanoma, and pupillary block, (Bock et al. 2010; De Moraes et al. 2011; Casson et al. 2012b; Weinreb et al. 2014). The glaucomas are further classified in terms of the patency of the anterior chamber angle, i.e., whether it is open or closed. An open angle is essential for drainage of the aqueous humour and thereby the maintenance of normal IOP.

1.2.1.1 Primary open-angle glaucoma (POAG)

Primary open-angle glaucoma (POAG) is the most prevalent form (Jonas et al. 2006; O'Neill et al. 2010; Kamdeu Fansi et al. 2011; Syed et al. 2012; Rao et al. 2013a). It is characterized by an IOP beyond the normal range, i.e., ≥ 22 mmHg (Jonas et al. 2000; Gardiner et al. 2011) in the presence of an open anterior chamber angle (Moore et al. 2008; Wesselink et al. 2009; Eilaghi et al. 2010; Boland and Quigley 2011; Garway-Heath et al. 2013; Rao et al. 2013b; Weinreb et al. 2014).

1.2.1.2 Normal-tension glaucoma (NTG)

Primary open-angle glaucoma in the presence of an IOP within the normal range, i.e., 10-21mmHg is termed normal-tension glaucoma (NTG). The estimates of the prevalence of NTG vary from 25% (Wax 2011) to 50% (Gordon et al. 2002).

1.2.1.3 Ocular Hypertension (OHT)

Ocular hypertension (OHT) describes the condition where the IOP is elevated beyond the normal range, i.e., ≥ 22 mmHg, in the absence both of structural and functional abnormality. Approximately 1%-2% of individuals will convert to POAG and this figure is slightly reduced if the IOP is medically lowered (Ocular Hypertension Treatment Study [OHTS]) (Kass et al. 2002; Laemmer et al. 2007). Individuals who convert to POAG progress faster than those with NTG (Chauhan et al. 2009; Fukuchi et al. 2010).

1.2.1.4 Glaucoma Suspect

The category ‘Glaucoma Suspect’ is a subjective entity based upon the anomalous appearance of the ONH or other specific feature, such as the retinal nerve fibre layer, that indicates a possible likelihood of developing glaucoma (Garway-Heath et al. 1998a; Larrosa et al. 2012).

The classification of pseudo-exfoliation glaucoma (PEXG) and of pigment dispersion glaucoma (PIGM) is equivocal in that they can be considered as primary (Lindberg 1989) or secondary conditions (Cavallerano 2001; Foster et al. 2002). Pseudo-exfoliation glaucoma is considered to be the most common type of secondary open-angle glaucoma (Ritch 2001; Leske et al. 2007; Anastasopoulos et al. 2015). Pigment dispersion glaucoma is associated with young individuals with higher degrees of myopia (Azulara-Blanco et al. 2002b; Musch et al. 2012).

1.2.1.5 Primary angle-closure glaucoma (PACG)

Primary angle-closure glaucoma (PACG) arises from an anatomically closed angle (when $\geq 270^\circ$ of the angle is occluded) resulting from apposition of the iris leading to blockage of the trabecular meshwork and consequent prevention of aqueous humour drainage from the eye, resulting in an elevated IOP (Weinreb et al. 2014). The condition can present as an acute primary angle-closure in less than a third of the cases which can manifest as corneal oedema, a dilated non-reactive pupil, conjunctival hyperaemia and a markedly elevated IOP (> 30 mm Hg) in the presence of a shallow anterior chamber (American Academy 2010; Weinreb et al. 2014). In the acute condition, the ONH becomes pale with minimal cupping due to the presence of an acute anterior ischemic neuropathy (Spaeth 1994; Musch et al. 2012).

1.2.2 Primary risk factors for glaucoma

The primary risk factors for glaucoma are family history, ageing, ethnicity, reduced central corneal thickness (CCT) and elevated intraocular pressure (Williams et al. 2013).

1.2.2.1 Family history

One fifth of cases of glaucoma exhibit a positive family history of the disease (Leske 1983; Balasubramanian et al. 2010; Qu et al. 2010; VanderBeek et al. 2010).

1.2.2.2 Ageing

The prevalence of glaucoma in developed countries is 3% in the population older than 40 years (Varma et al. 2011). The prevalence rises to 13% to 15% for those of black African descent aged between 80 and 96 years (Tielsch et al. 1991; Leske et al. 1994; Fansi et al. 2009). The number of treated patients also increases with age: patients aged 85 years or more are 13 times more likely to receive glaucoma therapy compared to those aged between 40 and 64 years (Owen et al. 2008). The prevalence of OHT is greater for those over 50 years (Taylor 2009; Kim and Varma 2010).

1.2.2.3 Ethnicity

The prevalence of glaucoma amongst individuals of African descent is higher than that of Caucasians, with the highest prevalence amongst Afro-Caribbeans (Quigley 1996; Boland and Quigley 2007; Fansi et al. 2009). In general, African-Americans, compared to Caucasian individuals, exhibit a significantly larger ONH (Boland and Quigley 2007), a larger VCDR (Foster et al. 2002), a higher IOP (Leske 1983), a thinner CCT (Fansi et al. 2009), a poorer mean deviation (MD) and a more frequent bilateral presentation of glaucoma (Friedman et al. 2006). The onset of glaucoma amongst those of African descent occurs at an earlier age compared to Chinese, Hispanic and European ethnicities (Samarawickrama et al. 2010). In the Eastern Arabian Peninsula, 77% of all POAG cases are associated with pseudo-exfoliation (Musch et al. 2012).

The estimated prevalence of glaucoma among European Caucasians is 1.0% to 1.5% in 40 to 65 year olds which rises exponentially to 2.0% to 7.0% in those greater than 65 years (Mitchell et al. 1996; Rudnicka et al. 2006; Hoffmann et al. 2007; Samarawickrama et al. 2010). The prevalence amongst the Asian population is similar to the European Caucasian population up to the age of 65 years but is not as high (1.6% to 3.8%) after the age of 70 years (Samarawickrama et al. 2010). The prevalence does not increase with age in Chinese and Hispanics ethnicities (Broman et al. 2008). The NTG exhibits its highest rates compared to POAG amongst Asians and Japanese (Dignam and Stutman 2001; Stein et al. 2011). The prevalence of PACG in the Chinese population is three times higher than that of POAG (Quigley 1996; Jackson 2001; Foster et al. 2002).

1.2.2.4 Central corneal thickness (CCT)

A central corneal thickness (CCT) of ≤ 535 μm is a major risk factor for glaucoma (Muir et al. 2004; Jonas et al. 2006; Coleman and Miglior 2008; Medeiros et al. 2012d; Carbonaro et al. 2014) particularly if the presenting IOP is ≥ 21 mmHg (Leske et al. 1994; Varma et al. 2004; Grewal et al. 2009; Gardiner et al. 2011, 2012b; Jiang et al. 2012b). The CCT may affect the accuracy of applanation tonometry leading either to an underestimation of the true IOP among individuals with thin corneas (≤ 535 μm) or to an overestimation among those with thick corneas (≥ 535 μm) (He et al. 2011; Jiang et al. 2012b; Quaranta et al. 2013).

1.2.2.5 Intraocular pressure (IOP)

Glaucomatous damage may occur at any level of IOP (He et al. 2011; Heijl et al. 2011; Lee et al. 2012a; Polaczek-Krupa and Grabska-Liberek 2012; Heijl et al. 2013a; Quaranta et al. 2013). An elevated IOP of ≥ 21 mmHg is a major risk factor for glaucoma with the risk increasing by 10% (Peeters et al. 2010; Gardiner et al. 2012b; Miglior and Bertuzzi 2013; Sharpe et al. 2013; Panarelli et al. 2015) or by 19% for each mmHg above this value (Rossetti et al. 2010). Intraocular pressure is the only modifiable risk factor for glaucoma. All the major clinical trials (the [OHTS] (Gordon et al. 2002; Kass et al. 2002), the European Glaucoma Prevention Study [EGPS] (Zeyen et al. 2003; Miglior et al. 2007) the Early Manifest Glaucoma Trial [EMGT] (Heijl et al. 2002; Leske et al. 2004), the Collaborative Initial Glaucoma Treatment Study [CIGTS] (Lichter et al. 2001; Musch et al. 2008) and the Advanced Glaucoma Intervention Study [AGIS]) (Gaasterland et al. 1994; Investigators 2000)) confirm that a reduction in IOP delays the onset of glaucomatous progression. The most stringent of these studies, the EMGT, found that, at the 4 year follow-up, 49% of those individuals with POAG but not receiving treatment exhibited glaucomatous progression compared to 30% of those under treatment (Lichter 2003). However, the reduction of IOP in the management of NTG is equivocal in the Collaborative Normal-Tension Glaucoma Study (CNTGS) (The Collaborative Normal-Tension Glaucoma Study and Group. 1998; Pan and Varma 2011; Panarelli et al. 2015) and the Low-Pressure Glaucoma Treatment Study (LoTGS) (Krupin et al. 2005).

IOP fluctuation is also considered to be a separate risk factor for glaucoma (Caprioli and Coleman 2008; Fukuchi et al. 2010).

1.2.3 Secondary risk factors for glaucoma

Secondary risk factors include abnormal ocular perfusion pressure (OPP), systemic hypotension, systemic hypertension, diabetes, high myopia, axial length, peripapillary atrophy, and disc haemorrhage (DH).

1.2.3.1 Ocular perfusion pressure (OPP)

Fluctuation in the ocular perfusion pressure (OPP) resulting from disturbances of the physiological nocturnal reduction in blood pressure and/ or the physiological nocturnal reduction in IOP is a risk factor for NTG due to disruption of the autoregulation of the blood within the eye and consequent optic nerve ischaemia (Caprioli and Coleman 2010; He et al. 2011; Gardiner et al. 2012a; Quaranta et al. 2013). The evidence for either systemic hypotension or systemic hypertension as an independent risk factor for glaucoma is equivocal (Moore et al. 2008; Caprioli and Coleman 2010; Konstas et al. 2010; Coudrillier et al. 2012).

1.2.3.2 Diabetes - High Myopia - Axial length

The presence of diabetes as a risk factor for glaucoma is equivocal (Lichter 2003; He et al. 2011). High myopia and axial length ≥ 24 mm are each

considered to be risk factors in glaucoma (Drance 2008; Teng et al. 2010; Jonas et al. 2012; Lee et al. 2012b).

1.2.3.3 Peripapillary Atrophy (PPA)

The presence of a β -zone of PPA is considered to be a risk factor for glaucoma (Jonas et al. 2004; Radcliffe et al. 2008; Teng et al. 2010; Jonas et al. 2012). The extent of the β -zone in NTG is larger than that in POAG (Broadway et al. 1999; Jonas 2005).

1.2.3.4 Disc Haemorrhage (DH)

The presence of a disc haemorrhage (DH) is considered to be a risk factor for glaucoma: the prevalence is 4-7 % compared to that of approximately 1% in the normal eye (Ahn and Park 2002; Soares et al. 2004; Hoyng 2005). However, 55% of those with POAG will manifest a DH at some point during a follow-up period of eight years (Syed et al. 2012). Disc haemorrhages are visible from 8 days to 12 weeks; thus their diagnostic significance is limited (Ahn and Park 2002; Soares et al. 2004; Hoyng 2005). Disc haemorrhages are considered to be independent of the level of IOP (Bengtsson et al. 2008); however, the opposite hypothesis has been also supported (De Moraes et al. 2012a).

1.2.3.5 Gender

Gender as a risk factor is equivocal (Boland and Quigley 2007; Broman et al. 2008; Kim and Varma 2010).

1.3 The ONH in primary open-angle glaucoma

1.3.1 Introduction

Typical ONH alterations in POAG and NTG comprise diffuse or localized peripapillary RNFL thinning with consequent thinning of the NRR and increase in cupping; increase in PPA; DHs; alterations in the course and/ or diameter of the ONH vascularisation; and NRR pallor (Altangerel et al. 2005; Jonas 2005; Martus et al. 2005; Morgan et al. 2005b; Jampel et al. 2008; Iester et al. 2011; Heijl et al. 2013a; Li et al. 2013). Glaucoma is most prevalent in larger ONHs (Hoffmann et al. 2007) and this is consistent across the different types of glaucoma (Jonas et al. 2004). The ONH in OHT and PEXG is generally smaller than in POAG and NTG (Healey and Mitchell 1999; Hoffmann et al. 2007).

1.3.2 Neuroretinal rim (NRR)

The inferior-temporal and superior-temporal sectors of the ONH are most susceptible to axonal damage (Jonas et al. 1998; Drance 2008). In the later stages of glaucoma, the NRR thinning involves the entire temporal sector and the nasal NRR remains relatively unaffected and the superior-nasal region is wider than the inferior-nasal NRR (Nicolela and Drance 1996; Jonas et al. 1999; Drance 2008) often with a large β -zone of PPA (Jonas et al. 2004).

1.3.3 Measurement of the predominant ONH features in glaucoma

The VCDR in glaucoma can be as low as 0.40 (Tsutsumi et al. 2012). Thus, there is a considerable overlap between the range in the normal eye and that in glaucoma (Greenfield 1997; Hafez et al. 2003). The CDR is not independent

of ONH size in that although the ratio may be the same for different sizes ONHs, the proportion of axons within each NRR is greater for the larger ONH (Jonas et al. 1995; Cankaya and Simsek 2012). Thus the use of CDR is of limited diagnostic utility (Spaeth et al. 2006; Bock et al. 2010) unless it is corrected for the ONH size (Garway-Heath and Hitchings 1998; Jonas et al. 2000; Cankaya and Simsek 2012; Morgan et al. 2012; Tsutsumi et al. 2012). However, the CDR is insufficiently sensitive to delineate subtle focal thinning of the NRR (Chandra et al. 2013).

An alternative approach to the CDR is the rim width-to-disc ratio (Rw/Dd), whereby the shape of the NRR width is described by the ratio of either the inferior NRR (5 to 7 o'clock hours) width or the superior NRR (11 to 1 o'clock hours) width expressed as a ratio of the ONH diameter (Dd) (Jonas et al. 1998; Saito et al. 2010; Tsutsumi et al. 2012; Chandra et al. 2013). Prediction limits based upon the 95th percentile have been proposed for the ratio in normal eyes (Bartz-Schmidt et al. 1999). However, the inferior to temporal neuroretinal rim width ratio and the superior to temporal neuroretinal rim width ratio, alone, are not sufficient indicators for the designation of glaucoma (Jonas et al. 1998). A Rw/Dd of ≤ 0.1 at either the superior or inferior region has been proposed as a criterion for the designation of glaucoma (Tsutsumi et al. 2012).

1.3.4 Peripapillary atrophy (PPA)

In glaucoma, the β -zone of the PPA is situated adjacent to the location of the NRR thinning and is consistent with the orientation of the entry/ exit position of the central retinal vessel trunk (Jonas et al. 2001; Lee et al. 2012b). The β -

zone in myopic eyes is larger temporally (Broadway and Drance 1998; Jonas 2005; Drance 2008; Teng et al. 2010).

1.3.5 Disc Haemorrhage (DH)

Disc haemorrhages are more prevalent in the superior-temporal and inferior-temporal regions of the ONH more frequently towards the ONH margin. They are generally positioned in the superficial RNFL and exhibit a splinter shape. They are associated with local peripapillary RNFL defects and consequent NRR notching/ thinning (Bengtsson et al. 2008; Radcliffe et al. 2008; Uhler and Piltz-Seymour 2008; Pan and Varma 2011). Disc haemorrhages may also be located at the level of the LC where they tend to be circular (Fingeret et al. 2005). The aetiology of DHs remain unclear (Radius 1987; Fingeret et al. 2005; Hasnain 2006), however it is suggested that the presence of focal LC defects are associated with DHs (Park et al. 2013).

1.3.6 Vasculature

Changes in the position and/ or course and/ or calibre of the blood vessels of the ONH, such as bayonetting, barring, and nasal shift, occur concurrently with the major alterations to the ONH arising from glaucoma (Bartz-Schmidt et al. 1999; Yogesan et al. 1999; Saito et al. 2010).

1.3.7 Laminar pores

Visibility of the anterior portion of the LC pores is considered to be indicative of NRR damage. A tilting and/ or stretching of the LC pores from an elevated IOP is detrimental to the passage of the axons through the LC (Radius and

Gonzales 1981; Healey and Mitchell 2004; Park et al. 2013). An elevated IOP results in a more tense posterior displacement of the LC in large discs compared to small discs resulting in a more ‘punched out’ appearance of the cup. However, even small discs can exhibit mechanical deformation of the LC (Hancox O.D 1999; Morrison 2007; Brusini et al. 2010; Guerri et al. 2012) (Pablo et al. 2009; Sanfilippo et al. 2009; Lee et al. 2012a). The displacement and compression of the LC can be reversed following the reduction in IOP arising from trabeculectomy. The resultant alteration in the LC and the consequent modification to the ONH can be misinterpreted as an increase in the NRR (Cymbor et al. 2009; Mansouri et al. 2011; Lee et al. 2012a). The degree of the LC reversal increases with an increase in both the presenting IOP and the IOP immediately prior to trabeculectomy and in the magnitude of the reduction in the IOP following trabeculectomy (He et al. 2011; Lee et al. 2012a); but declines with ageing (Coudrillier et al. 2012).

1.3.8 Pallor

Advanced glaucoma can result in a pale ONH; however, it is important to exclude other aetiologies in less severe cases (Broadway et al. 1999; Jonas et al. 1999; Fingeret et al. 2005; Hasnain 2006; Caprioli and Coleman 2010; O'Neill et al. 2010).

1.3.9 The Retinal Nerve fibre Layer (RNFL) in primary open-angle glaucoma

A global or partial reduction of the axons in the RNFL produces corresponding NRR thinning and visual field loss (Qu et al. 2010; Casson et al. 2012a). In

glaucoma, the RNFL is more susceptible inferior-temporally than superior-temporally and both of these regions are more susceptible than the superior-nasal region. This pattern of loss is reflected in the appearance of the NRR (section NRR 1.3.2). It is rare that RNFL defects initially present in the nasal region. Localized RNFL defects appear as dark wedge-shaped areas entering the ONH and which expand as the disease progresses (Jonas et al. 1999; Grewal et al. 2009; Lee et al. 2012b). Localized RNFL defects can occur in the presence of an apparently normal ONH (Lee et al. 2012b). The RNFL thickness in the normal eye, is positively correlated with ageing and with ONH size and negatively correlated with myopia and increases axial length (Huang et al. 2012).

From an epidemiological point of view the RNFL is susceptible to ageing and is thicker in East Asian population compared to the European Caucasians (Samarawickrama et al. 2010). East Asian children between the ages of 6 and 12 exhibit a 3% to 12% thicker RNFL compared to European Caucasian children of the same age. Although the CDRs were 30% to 40% larger in the East Asian children, the NRR areas appeared to be similar (Samarawickrama et al. 2010).

1.4 Pathophysiology of glaucoma

As was described in Section 1.2, glaucoma is a multifactorial disease entity involving at least several mechanisms (Lieven et al. 2006; Nickells 2007; Johnson and Morrison 2009; Schuman 2012).

1.4.1 Apoptosis

The RGCs die by apoptosis (Levin 1999; Lieven et al. 2006) which is controlled by the caspase family of cysteine aspartyl-specific proteases that cleave a large number of protein substrates. The caspases are present but inactive in healthy RGCs and the cells include inhibitors which bind to the caspases resulting in deactivation (Baltmr et al. 2010; Qu et al. 2010).

Apoptosis can occur extrinsically, intrinsically (Levin 1999; Lieven et al. 2006; Qu et al. 2010; He et al. 2011; Morgan 2012). The trigger for apoptosis can occur from a variety of causes including neurotrophin deprivation (Lieven et al. 2006; Williams et al. 2013), oxidative stress (Baltmr et al. 2010; Caprioli and Coleman 2010), ageing (Maresco 2002; Hoffmann et al. 2007; Morrison 2007), glial cell activation (Nickells 2007; Johnson and Morrison 2009; Schuman 2012), Ca^{2+} excitotoxicity (Kisiswa et al. 2010; Qu et al. 2010), autoimmunity, or vascular perfusion (Levin 1999; He et al. 2011). The mitochondria involve in both apoptotic pathways (Lieven et al. 2006; Qu et al. 2010; Morgan 2012) and can affect the synaptic plasticity through the regulation of apoptosis signalling pathways (Kisiswa et al. 2010; Williams et al. 2013).

1.4.2 Cell shrinkage

It still remains unclear whether the RGCs die by apoptosis in a selective or a non-selective manner (Morgan et al. 2006; Caprioli and Coleman 2010; Morgan 2012; Liu et al. 2014). Prior to the loss of the cell soma, a pruning (or shrinkage) of the dendritic-tree occurs which precedes the dendritic atrophy

(Jakobs et al. 2005; Buckingham et al. 2008; Morgan 2012; Williams et al. 2013; Liu et al. 2014). The dendritic pruning and remodelling prior to cell loss supports the hypothesis that the dendritic changes precede the RGC death in glaucoma. The dendritic remodelling is thought to be a passive activity which may coexist with RGC death. Once an individual cell dies, the remaining RGCs have the capacity to alter their existing dendritic field in an attempt to maintain overall retinal function (Kisiswa et al. 2010; Williams et al. 2013).

The extension of the dendrites is achieved by filopodia process which involves five stages: polarisation in which the dendrites gain their characteristics (diameter, length, growth rate and molecular composition, similar to those found in axons); elongation, where the dendrites extend in a defined direction and increase their diameter; branching, which involves the growth of the dendritic tree until the final dendritic spines; tiling, whereby the dendritic arbours are located in non-overlapping spatial territories; and finally formation of the synapse (Kisiswa et al. 2010; Casson et al. 2012a). The size of the soma is usually preserved until cell death, except in programmed cell death when acute changes in cell volume occur (Morgan 2002; Jakobs et al. 2005; Williams et al. 2013; Liu et al. 2014).

1.4.3 Mechanical and Ischemic mechanism

Although there are many theories about the mechanisms of RGC damage in glaucoma, there is no single cellular or molecular aetiology to characterize the pathogenesis of glaucoma (Caprioli and Coleman 2008; Baltmr et al. 2010). The various mechanisms can co-exist and/ or interact with each other (Baltmr

et al. 2010; Kisiswa et al. 2010; Qu et al. 2010).

1.4.3.1 Mechanical mechanism

As is partially discussed in Section 1.3.7, chronic elevation of IOP induces mechanical stress (force/cross-sectional area) and strain (physical deformation of the tissue) within the LC, leading to LC deformation (laminar bowing), and hence a mechanical compression of the axons. Evidence of axonal transport abnormalities at the ONH, exhibit sectorial anatomical differences in the patterns of LC (Radius 1987; Nickells 2007; Morgan 2012; Park et al. 2013; Williams et al. 2013). In both the acute and chronic forms of IOP elevation, the axonal retrograde transport is interrupted and the neurotrophins from the lateral geniculate nucleus cannot reach the RGC soma. This process initiates cell death and triggers the apoptotic cascade (He et al. 2011; Liu et al. 2014).

1.4.3.2 Ischaemic mechanism

The distortion of the lamina cribrosa also induces compression of the blood vessels within the ONH. This in turn reduces the OPP resulting in local hypoxia. The presence of hypoxia activates the auto-regulation in an attempt to sustain normal blood flow (Baltmr et al. 2010; He et al. 2011). The failure of this auto-regulation produces ischaemia in the axons of the RGCs. The axonal injury leads to insufficient nutrition in the RGC, including a lack of growth factors, subsequent degeneration and finally death (Levin 1999; Lieven et al. 2006; Kisiswa et al. 2010).

1.4.4 Treatment modalities in glaucoma

The treatment of glaucoma will/ can involve several approaches including neuro-protectant (Baltmr et al. 2010; Qu et al. 2010), neuro-recovery (Casson et al. 2012a), neuro-rescue and neuro-regeneration (Levin 1999; Baltan et al. 2010) strategies.

1.5 Types of ONH photography

1.5.1 Analogue photography

Analogue photography of the ONH in 35mm slide format or other film-based media was the 'gold' standard for decades. A conventional 35mm transparency in a 3 x 2 slide mount was the most common film format (Yogesana et al. 1999; Breusegem et al. 2011). A 35mm slide can be digitised using a scanner or by re-photography (Stone et al. 2010). Recently, digital images derived from either mydriatic or non-mydriatic digital fundus cameras (Bartling et al. 2009; Bernardes et al. 2011) have superseded analogue photography for the qualitative and quantitative assessment of the ONH (Morgan et al. 2005b; Stone et al. 2010; Schuman 2012; Syed et al. 2012). The digital images facilitate stereoscopic viewing and can be easily archived in electronic patient records (Morgan et al. 2012; Syed et al. 2012) and are suitable for tele-medicine (Kassam et al. 2013).

1.5.2 Digital photography

Digital photography involves the image capture, the image processing and the image output. Image capture is produced by a charge-couple device (CCD). There are two different types of CCD imaging chips, the 'area CCD', used in

cameras, and the 'linear CCD', used in scanners (Yogesana et al. 1999; Breusegem et al. 2011). The digital images are recorded in three different colour channels red, green and blue (RGB). The specific colour range that a device can record, produce, and display images is termed the 'colour gamut'. An equal amount of RGB input, produces white whilst the absence of any input produces black colour (Bernardes et al. 2011; Balasubramanian et al. 2012). Grayscale images can also be produced (Stone et al. 2010).

Once an image is captured, it is stored as numeric data in a number of different formats for editing or output. The major digital formats are the lossless, the lossy and the no compression format. Lossless compression yields an approximately 2:1 compression ratio of the reconstructed image relative to the original and preserves the quality and conserves storage space. The most common lossless file format used is the Tagged Image File Format (.tiff) which is preferable for archiving images as it preserves all features, but at the cost of a large file size, and is a suitable format for image-editing software. Other lossless formats include Graphics Interchange Format (.gif), Portable Network Graphics (.png), and Raw Image Format where the file name extension is specific to the given camera (Tyler et al. 2003b). The lossy compression scheme is suitable for both full colour and grayscale images. The most common lossy format is the Joint Photographic Experts Group (.jpeg) which reduces the original file size to as much as 5% (Liesenfeld et al. 2000).

A common editing tool is the 'cropping tool'. It is frequently used with digitised 35mm slides to change the aspect ratio (the proportional relationship

between the width and the height of the image) to optimise the screen display or for partial display of the image (Wood et al. 2009; Bernardes et al. 2011; Gugleta et al. 2013).

The image output represents the converted numeric data into a viewable form for viewing. The image quality depends upon a number of variables related to the patient, the camera and the photographer (Greenfield 1997; Bartling et al. 2009). The image output should be consistent with the original image in terms of sharpness, illumination, contrast, exposure, colour, magnification, size and the clarity (Shuttleworth et al. 2000; Ewen et al. 2006; Gugleta et al. 2013). The sharpness is mainly dependent upon the scan focus of the camera. Focusing the fundus camera requires the adjustment of the relationship between the ONH and the camera lens such that the ONH lies within the depth of field of the camera lens and the receiving plane lies within the depth of focus of the image. The depth of focus is determined by the CCD plane which is used as a receiving plane (Bartz-Schmidt et al. 1999; Roff et al. 2001). A number of factors can influence the scan focus such as lens opacities; insufficient pupil dilation; differences in the scan focus settings between follow-up examinations, which leads to variation in the size of the pixels of the image; the patient's discomfort to bright light; the available accommodation to the photographer (Chauhan et al. 2001; Bartling et al. 2009).

The illumination of the output image should not be under- or overexposed relative to the original image (Saine 2002). The magnification between the eye

and the camera is calculated either from the axial length (Huang et al. 2012) or from the corneal curvature and the refraction (Garway-Heath et al. 1998b; Jonas et al. 2006). The magnification of the camera is proportionate to the resolution. Therefore, a camera with high magnification exhibits better definition. The resolution in digital photography dictates the number of pixels within the image. Each pixel refers to a specific area in the image. The pixel dimensions are expressed in terms of the width and the height (i.e. 3008 x 1960) (Bartling et al. 2009; Bernardes et al. 2011).

Digital images can be viewed either monoscopically or stereoscopically. Stereo-viewing of digital images is still considered to be a 'gold standard' in the assessment of the ONH (Radcliffe et al. 2010; Mansouri et al. 2011; Swamy et al. 2012). The stereo-pair may be obtained either by sequential or simultaneous imaging, with the first being the most widely used. In sequential image capture, each component of the stereo-pair is obtained separately by adjusting the angle of the camera (Correnti et al. 2003). In simultaneous image capture a single exposure is utilized to place two images side by side on a constant stereo base (Tyler et al. 2003a) and overcomes the limitation from differences in capture angle associated with sequential image capture (Rosenthal et al. 1977; Zeyen et al. 2003).

1.6 Fundamentals of perimetry

1.6.1 The normal visual field

The visual field can be defined as the portion of space in which objects are visible at the same moment during steady fixation of gaze in one direction (Imaging and Perimetry Society 2014). The monocular visual field extends to approximately 90° temporally, 60° superiorly, 60° nasally, and 75° inferiorly (Anderson and Patella 1999). The binocular overlap of the visual field extends to approximately 120° horizontally; beyond approximately 60° temporally, the field is monocular. The intersection of the vertical and the horizontal meridians represents the fixation point and corresponds to the fovea. The ONH produces a physiological blind spot, 7.5° vertically and 5.5° horizontally, which is situated approximately 15° from and, 1.5° below, fixation in the temporal field (Anderson and Patella 1999).

The normal visual field has been likened to a three-dimensional ‘island (or hill) of vision in a sea of blindness’ (Traquair 1927) whereby, under photopic conditions, the peak of the hill represents the fovea and exhibits the highest sensitivity. The contour of the island vision slopes down from the highest point to the shoreline where it meets the ‘sea of blindness’.

1.6.2 Differential light sensitivity

Perimetry, the technique used to quantify the visual field, measures the differential light threshold, $\Delta L/L$, the minimum brightness of the stimulus, Δl , necessary to evoke a response when presented against a background of a constant luminance, L . The threshold is usually expressed in terms of its

reciprocal, the sensitivity. The stimulus luminance is traditionally measured in apostilbs (asb) but is expressed in decibels referenced to the maximum stimulus luminance. In the case of the Humphrey Field Analyzer (HFA), 0dB represents 10.000asb.

The differential light sensitivity can be measured by one of two techniques. kinetic perimetry and static perimetry.

1.6.3 Kinetic perimetry

Kinetic perimetry adopts a horizontal approach to the 'hill of vision' whereby the stimulus is presented along a given meridian from the 'non-seen' to the 'seen' in a centripetal direction towards fixation. The patient is required to indicate when the stimulus is 'just seen' and this location is taken to be the threshold. The stimulus is then moved towards fixation from this location and the patient is required to report if the stimulus becomes 'not-seen'. The process is repeated for each 15° meridian. A line joining locations of equal threshold is termed an isopter. The entire process is repeated using either smaller and/ or dimmer stimuli (resulting in smaller isopters) or larger and/ or brighter stimuli (resulting in larger isopters) to achieve a topographical appreciation of the visual field.

The 'gold' standard for manual kinetic perimetry still remains the Goldmann perimeter (Goldmann 1945). The Goldmann perimeter comprises a hemispherical bowl, or cupola, with a white surface of a uniform luminance of 31.5asb (10cdm⁻²) upon which a white stimulus is presented. Six stimulus

sizes are available: each successive size stimulus has a twofold difference in the diameter and a fourfold increase in the area to that of the preceding stimulus. The smallest stimulus, Size 0, has a diameter of 0.05° and an area of $1/16 \text{ mm}^2$ and the largest stimulus, Size V, a diameter of 1.7° and can area of 64mm^2 . The Goldmann perimeter incorporates 20 discrete luminance values. The maximum luminance is 1000asb (318cdm^{-2}) and the reduction in luminance is achieved in four major steps each of 0.5 log units. Within each of these four major steps are 5 minor steps each of 0.1 log units. The recommended stimulus velocity is $4^\circ/\text{sec}$. The outcome of kinetic perimetry is expressed qualitatively in terms of the size and shape of the given isopter and the relationship to the other isopters.

The Goldmann perimeter has largely been superseded by semi-automated kinetic perimetry (SKP) available with the Octopus perimeter (Vonthein et al. 2007; Nevalainen et al. 2008). The Octopus perimeter utilises the same stimulus characteristics as the Goldmann perimeter but overcomes many of the limitations of the Goldmann perimeter, namely the correction for the reaction time of the patient, the uniformity of the stimulus velocity and the use of age-corrected prediction intervals for any given isopter.

1.6.4 Standard automated perimetry (SAP)

Standard automated perimetry (SAP) utilises a vertical approach to the 'hill of vision' whereby the luminance of a stationary whites stimulus, generally presented on a white surface of uniform white background of 31.5asb (10cdm^{-2}), is adjusted until threshold is achieved. The default stimulus for

SAP is Goldmann size III (which subtends an angle of 0.431°) which is generally presented for 200msec. The differential light sensitivity is measured in decibels (dB) where 0dB represents the maximum stimulus luminance with a resolution of 1dB (0.1 log unit). The 'gold' standard perimeter for SAP is either the HFA (Wild et al. 1999a) or the Octopus perimeter (Buerki 2007).

Threshold to a visual stimulus is classically determined in terms of the Frequency-of-Seeing (FOS) curve whereby, in the case of a luminance threshold, the frequency of a correct response is plotted against the logarithm of the corresponding luminance. Threshold is generally taken to be the luminance at which 50% of the presentations are 'seen'. A steep curve indicates low variability associated with the designated threshold and a flat curve indicates high variability. The derivation of a frequency-of-seeing curve is time consuming and the technique is not a clinically viable procedure for examining the visual field.

For perimetry, a staircase procedure is used to estimate the threshold at any given stimulus location whereby the 'true' threshold is approached in predetermined steps of equal stimulus luminance, in either increasing or a descending magnitudes, respectively. Once a change in response has been obtained from the observer, i.e. the 'true' threshold has been 'crossed', the magnitude of the luminance step is usually halved and the direction of approach towards the 'true' threshold is reversed until the 'true' threshold is crossed once again. The accuracy of the estimated threshold increases with the use of smaller steps, especially when close to the threshold; the number of

crossings of threshold and the number of repetitions (Flammer et al. 1984; Fankhauser et al. 1988; Bengtsson et al. 1998). However, this increase in accuracy is at the expense of an increased examination duration (Bebie et al. 1976).

1.6.4.1 Threshold algorithms

The first generation threshold algorithms for SAP were the Threshold algorithm of the Octopus perimeter and the Full Threshold algorithm of the HFA.

The Full Threshold algorithm of the HFA, initially estimates the threshold at each of four 'seed' locations situated at $x = +/-9^\circ$, $y = +/-9^\circ$ in each quadrant. The starting luminance at each of these four seed points is 25dB, irrespective of the age of the patient, and the threshold is estimated twice at each of these four locations using 4-2dB staircase. The start level at each of the immediate surrounding locations is determined by extrapolation from the outcome at the nearest seed location (Wild et al. 1999a) and the threshold estimate is derived using the same 4-2dB staircase. The threshold is designated as the last 'seen' stimulus luminance (Wild et al. 1999a; Wild et al. 1999b).

The second generation threshold algorithms for SAP reduced the accuracy of the threshold estimate in order to reduce the examination time and included the Dynamic and FASTPAC algorithms of the Octopus perimeter and the HFA, respectively.

The FASTPAC algorithm, introduced in 1991, also uses the four primary seed points to determine the initial stimulus luminance for the neighbouring stimulus locations. The luminance presented at the neighbouring points is 1dB brighter when the expected threshold is an even number and 2dB dimmer when the expected threshold is an odd number (Flanagan et al. 1993a; Flanagan et al. 1993b). The algorithm utilizes a 3dB step in either an ascending or a descending direction, respectively, and threshold is crossed once (Flanagan et al. 1993a). The estimated threshold is also designated as the 'last seen' stimulus luminance (Wild et al. 1999a; Wild et al. 1999b).

The third generation algorithms for the HFA were introduced in 1997 and maintained the accuracy of the threshold estimate derived by the Full Threshold algorithm whilst maintaining a similar if not slightly reduced examination duration compared to the FASTPAC algorithm. These algorithms comprised the two Swedish Interactive Threshold Algorithms (SITA), SITA Standard and SITA Fast, for SAP with the HFA (Bengtsson et al. 1997; Bengtsson and Heijl 1998). The SITA Standard algorithm uses 4-2dB staircase and is analogous to the Full Threshold algorithm. The SITA Fast algorithm uses a 4dB step, only, and is analogous to the FASTPAC algorithm (Bengtsson et al. 1997; Bengtsson et al. 1998).

Both SITA algorithms utilize two Bayesian posterior probability, or likelihood, functions (models) at each stimulus location. One function is a distribution of the probability of the likelihood of a 'seen' response at any

given value of sensitivity in the normal eye and the other function is an equivalent distribution in the glaucomatous eye (Olsson and Rootzén 1994). The shape of each function is continually adjusted following the response to each stimulus presentation. At any given moment during the examination, the height of the function represents the most probable threshold at the given location and the width describes the accuracy of the threshold estimate. The more dominant of the two functions for the given patient is used to calculate, at any given moment, the magnitude of the 'next' stimulus luminance. The thresholding procedure at any given location is terminated when a predetermined level of accuracy, as predefined by the Error Related Factor (ERF) is obtained (Bengtsson et al. 1997; Bengtsson et al. 1998). The magnitude of the ERF at each stimulus location represents a compromise between the accuracy of the threshold estimate and the examination duration. With the SITA Standard algorithm, the threshold estimate at any given location can be terminated after a single crossing of threshold (Bengtsson et al. 1997) but such a requirement is not necessary for the SITA Fast algorithm (Bengtsson et al. 1997; Bengtsson and Heijl 1998; Bengtsson et al. 1998). Both SITA algorithms determine the response time to each stimulus presentation (Bengtsson et al. 1997) and the subsequent inter-stimulus interval is based upon this individual response time characteristics. On completion of the examination, the threshold estimate is recalculated at each stimulus location based upon all the response information obtained during the examination (Bengtsson et al. 1997; McKendrick and Turpin 2005). This process is particularly useful for those locations at which the threshold estimate occurred at the beginning of the examination.

Between the two SITA algorithms, SITA Fast is approximately 60% shorter compared to SITA Standard (Budenz et al. 2002; Cedrone et al. 2008) and approximately 70% shorter compared to the Full Threshold algorithm (Bengtsson and Heijl 1998; Lalle 2001). The SITA Standard algorithm exhibits slightly higher mean sensitivity of 0.8dB (Wild et al. 1999a), 0.9dB (Artes et al. 2002), 1.0dB (Shirato et al. 1999), or even 1.9dB (Bengtsson et al. 1998) compared to the Full Threshold algorithm in normal individuals. The SITA Fast algorithm exhibits a higher mean sensitivity of 1.3dB (Wild et al. 1999a), 1.6dB (Artes et al. 2002) or even 2.2dB (Bengtsson et al. 1998) compared to Full Threshold algorithm. A similar trend has been observed between SITA algorithms and FASTPAC. The equivalent of SITA Standard has been estimated as 0.5dB lower than the SITA Fast (Wild et al. 1999a), whilst the equivalent of Full Threshold algorithm exhibits a range of 0.08dB to 0.5dB higher mean sensitivity than FASTPAC (Bengtsson et al. 1998).

In individuals with glaucoma, the SITA Standard algorithm also exhibits slightly higher mean sensitivity of 1.0dB (Shirato et al. 1999; Wild et al. 1999b) to 1.31dB (Sharma et al. 2000) compared to the Full Threshold algorithm and 0.7dB higher mean sensitivity than FASTPAC (Wild et al. 1999b). Similarly, the SITA Fast algorithm exhibits a 1.6dB higher mean sensitivity than FASTPAC; a 0.9dB higher mean sensitivity than SITA Standard and a 1.87dB higher mean sensitivity than the Full Threshold algorithm (Wild et al. 1999b). The SITA algorithms in individuals with glaucoma exhibit higher differential light sensitivity than Full Threshold and

FASTPAC algorithms, in particular, in the presence of a statistically deeper defect (Wild et al. 1999b).

1.6.4.2 Stimulus Program

The location of, and spatial distribution between, the various stimulus locations for a given visual field examination is termed the stimulus program.

The most common programs for the HFA are Programs 30-2, 24-2 and 10-2. Program 30-2 incorporates 76 stimulus locations, out an eccentricity of 27°, based upon a square grid with an inter-stimulus separation of 6° and equally centred either side of the vertical and horizontal midlines. Program 24-2 is identical to that of Program 30-2 except that it comprises 54 stimulus locations out to an eccentricity of 21° and the two extreme nasal locations situated above and below the horizontal midline. Clearly, the probability of detecting visual field loss increases with an increase in either the number of locations or in the resolution of the stimulus program, i.e., a reduction in the inter-stimulus separation, or both. Clearly, such increases are at the expense of an increase in the examination duration. The use of a 6° separation represents a compromise between the examination duration and the spatial resolution: such a grid has a 95% probability of detecting a focal defect the size of the blind spot (Fankhauser and Bebie 1979). Program 10-2 incorporates 68 stimulus locations, out an eccentricity of 9°, based upon a square grid with an inter-stimulus separation of 2° and equally centred either side of the vertical and horizontal midlines. Program 10-2 is useful for increasing the spatial

resolution of paracentral defects and for end-stage disease (Katz and Sommer 1986; Wall et al. 2009; Russell et al. 2012). It is also currently the feature of much attention in the identification of early glaucomatous field loss when the outcome from program 24-2 is normal (Asaoka 2013). Programs 30-1 and 24-1 are identical in format to Programs 30-2 and 24-2 with the exception that the stimuli are centred along the horizontal and vertical meridians (Weber and Dobek 1986). As a consequence, the outcome from these Programs can be adversely influenced by small eye movements.

1.6.4.3 Variability of the threshold estimate

The estimate of threshold varies during the given examination and between examinations of a given individual. The within-examination variability is known as the short-term fluctuation and increases with increase in eccentricity and with a decline in sensitivity to approximately 12dB after which it tends to zero. The between-examination variability is termed the long-term fluctuation and, classically, is divided into two components, the homogenous component and the heterogeneous component. The presence of the both the short- and long-term fluctuation hinders the identification of visual field loss and of progressive visual field loss (Hutchings et al. 2000).

1.7 Classification of visual field defects

The central visual field is defined as that out to an eccentricity of 30° and the peripheral field as that beyond 30°.

A generalised reduction in sensitivity across the entire field is termed either generalised or diffuse loss. An area with a reduced or absent differential light sensitivity which is surrounded by normal sensitivity is termed a scotoma, a focal defect, or a localized defect. Such an area of reduced sensitivity is termed relative and that with no light sensitivity as absolute. The blind spot is a physiological example of an absolute scotoma (Anderson and Patella 1999). If the focal loss involves fixation, the loss is termed a central scotoma and if it includes both fixation and the blind spot, it is termed a centrocecal scotoma. A focal defect adjacent to fixation is termed a paracentral defect. A scotoma involving the RNFL takes on the characteristic arcuate shape of the layer. Visual field loss involving a localized peripheral region and extending centripetally into the field is termed a contraction. When the field loss is absolute and involves the periphery, the loss is termed a contraction.

1.8 The Single Field printout of the central field

The Single Field printout for the estimated sensitivities across the central field derived by each of the two SITA algorithms contains the estimated value of sensitivity at each stimulus location; the grayscale representation of sensitivity across the field; the Total Deviation values and probability levels; the Pattern Deviation values and probability levels; the Glaucoma Hemifield Test; the Visual Field Indices; the outcome to the False-Negative and Fixation-loss catch trials; and the outcome to the False-Positive response evaluation (Heijl et al. 1986). An example of the Single Field Printout for Program 24-2 and the SITA Fast algorithm in the left eye of a patient with an age-related cataract and NTG is given in Figure 1.1.

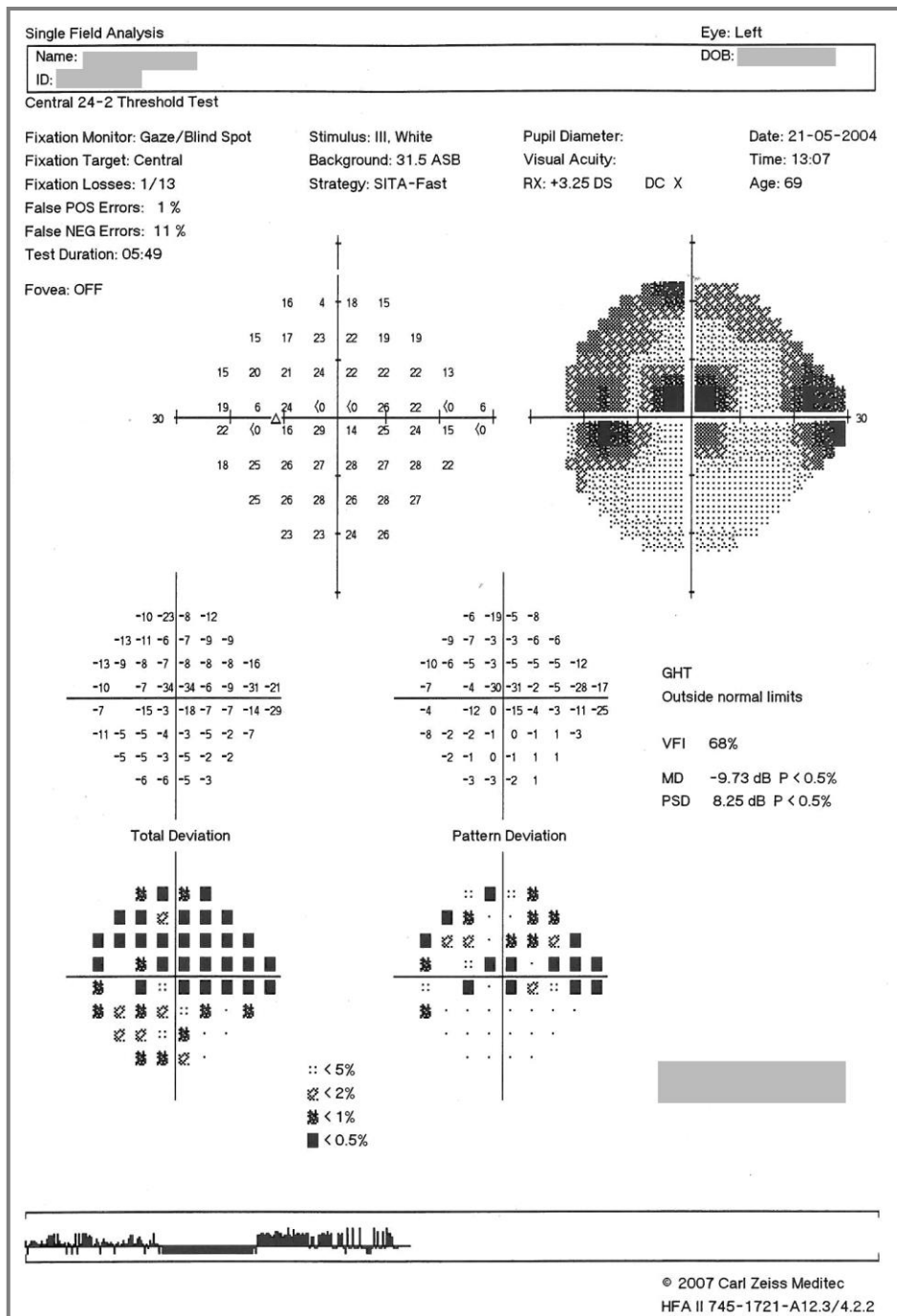


Figure 1.1. The Single Field Printout for Program 24-2 and the SITA Fast algorithm in the left eye of a patient with an age-related cataract and NTG.

1.8.1 Estimated values of sensitivity

The estimated value of sensitivity is displayed at each stimulus location as an integer value. The stimulus locations, themselves, are displayed in terms of their Cartesian coordinate position relative to fixation and this approach

enables the comparison of the estimated value of sensitivity at any given location with that obtained at one or more of its immediate neighbouring locations. The same approach is adopted for the Total and Pattern Deviation values and the associated probability levels (see below Sections 1.8.3 and 1.8.4).

1.8.2 Grayscale

The estimated values of sensitivity across the field are illustrated in terms of grayscale, with each shade of gray representing a range of 5dB. Absolute sensitivity is displayed as a black and normal sensitivity as a light gray. The grayscale interpolates between stimulus locations, is neither eccentricity nor age corrected, and masks early paracentral and arcuate loss. It is of some use in end-stage loss (Lalle 2001; Heijl and Patella 2002; Bengtsson et al. 2005).

1.8.3 Total Deviation values

The difference between the estimated value of sensitivity and the corresponding age-corrected estimate of sensitivity in the normal eye at the given location is displayed as an integer value. A negative sign indicates an estimated sensitivity worse than the estimate in the normal eye of an equivalent age.

1.8.4 Pattern Deviation values

The difference between the estimated value of sensitivity and the corresponding age-corrected estimate of sensitivity in the normal eye at the given location, having corrected for any overall increase or reduction,

respectively, in sensitivity across the field, is displayed as an integer value. A negative sign indicates an estimated sensitivity worse than the estimate in the normal eye of an equivalent age. The correction for any overall increase or reduction, respectively, in sensitivity across the field is achieved by calculation and use of the General Height (GH) Index.

The GH is defined as the 7th least negative of the 52 Total Deviation values corresponding to the Program 24-2 format, with the three locations involving the blind spot omitted, ranked from the most positive to the most negative. The 7th least negative value corresponds to the 85th percentile of the distribution of the ranked values and the rank of the value was selected, empirically, to minimise the influence of any false-positive peak (Wall 1997). The estimate of the GH is dependent upon the presence of normal values.

A positive GH index indicates that the observer has a general sensitivity which is better than that encountered in the age-corrected normal eye whilst a negative value indicates the opposite. The influence of the general sensitivity is removed by subtracting the value of the GH from the Total Deviation value at each stimulus location when the GH is positive and adding the value when the GH is negative. The GH index is not displayed on the print-out.

The calculation of the GH is dependent upon the presence of a sensitivity within the normal range at a minimum of the first seven ranked locations. The inclusion of one or more locations exhibiting an abnormal sensitivity results in an increasing overestimation of the magnitude of the diffuse component and,

therefore an under-representation of the extent of localized field loss (Asman et al. 2004). This phenomenon has subsequently being called, the ‘Pattern Deviation Reversal’ (Kothari et al. 2014) or ‘Ceiling Effect’ (Artes et al. 2011; Medeiros et al. 2012b). Any errors in the estimation of the GH may lead to errors in the calculation of indices based upon the Pattern Deviation values i.e. the VFI (Marin-Franch et al. 2014).

An alternative method has been proposed for specifying the GH the GH-rank estimator or GH-r (Marin-Franch et al. 2014). The GH-r is based upon the assumption that the mean GH for the normal population is 1.8dB. The GH-r is 1.8dB minus the 7th least negative Total Deviation value. However, this approach has yet to be implemented.

1.8.5 Total Deviation probability values

The Total Deviation probability level is displayed at each stimulus location. The probability level is that associated with the difference at each given stimulus location between the estimated value of sensitivity and the corresponding age-corrected estimate of sensitivity in the normal eye, lying within the normal range. The probability levels are $p < 0.05$, $p < 0.02$, $p < 0.01$ and $p < 0.005$, respectively.

1.8.6 Pattern Deviation probability values

The Pattern Deviation probability level is displayed at each stimulus location. The probability level is that associated with the difference at each given stimulus location between the estimated value of sensitivity and the

corresponding age-corrected estimate of sensitivity in the normal eye, having accounted for the overall elevation or reduction in sensitivity, lying within the normal range. The probability levels are as those for the Total Deviation probability values.

1.8.7 Visual field indices

The visual field indices are summary measures of various facets of the estimated sensitivity across all the stimulus locations and comprise the Mean Deviation (MD), the Pattern Standard Deviation (PSD) and the Visual Field Index (VFI).

1.8.7.1 Mean Deviation (MD)

The Mean Deviation (MD) index is the weighted mean across all stimulus locations of the difference between the estimated sensitivity and the age-corrected estimate in the normal eye. The weighting function, which is propriety to the manufacturer, Zeiss, reflects the more reliable estimate of threshold at the more paracentral locations. As the field loss worsens, the index becomes increasingly negative. Functional blindness is associated with an MD of approximately -25dB. The MD is influenced by both generalised and localized abnormality. Particularly confounding factors are the presence of cataract and refractive defocus (Ang et al. 2011; Tanna et al. 2011; Gardiner et al. 2012b; Lee et al. 2014a).

1.8.7.2 Pattern Standard Deviation (PSD)

The Pattern Standard Deviation (PSD) is the weighted standard deviation across all stimulus locations of the difference between the estimated sensitivity and the age-corrected estimate in the normal eye. The PSD reflects the magnitude of localized loss. The normal value approximates to 1dB and the PSD becomes increasingly positive as the area of the field loss increases until advanced field loss, after which the localized loss cannot be differentiated from the generalised loss and the PSD tends to 1.0dB as the field loss worsens (Heijl and Bengtsson 1998; Bengtsson et al. 2005; Gardiner et al. 2011), i.e., the PSD is limited by the lack of dynamic range of the perimeter, especially in advanced field stages (Asman et al. 2004).

1.8.7.3 Visual Field Index (VFI)

The VFI index was developed to remove the influence of generalized loss occurring in the presence of cataract (Bengtsson and Heijl 2008; Bengtsson et al. 2009). A normal visual field is defined by a 100% and a perimetrically blind field by 0%. The VFI is calculated from the sum of the outcome at each stimulus location of the Pattern Deviation probability maps when the MD is better than or equal to -20dB and from the Total Deviation probability maps when the MD is worse than -20dB. A stimulus location exhibiting a normal sensitivity is scored 100% and a location exhibiting absolute loss is scored as 0% (Bengtsson and Heijl 2008; Bengtsson et al. 2009). Locations exhibiting a sensitivity beyond the normal range at a probability level of $p < 5\%$ on the respective probability map are scored as 100% minus the modulus of the total deviation divided by the age-corrected normal value (expressed as a

percentage). The more centrally located stimuli are weighted with 3.29 and the most peripheral stimuli are weighted with 0.45 (Bengtsson and Heijl 2008; Hirasawa et al. 2013; Marvasti et al. 2013; Lee et al. 2014b). In addition, the VFI exhibits a ‘ceiling effect’ of 100% for an MD of up to approximately -4.5dB (Artes et al. 2010); however, the reduction in MD may merely reflect the influence of non-neural components.

1.8.7.4 Glaucoma Hemifield Test (GHT)

The Glaucoma Hemifield Test (GHT) compares the symmetry in the presence and the magnitude of the Pattern Deviation probability levels at each of five zones selected in the superior field to that in the inferior field. The zones are selected in relation to the distribution of the axons within the RNFL (Asman and Heijl 1992; Heijl and Patella 2002). The GHT provides a qualitative visual field classification: ‘Outside Normal Limits’, where one or more of the zones in the superior field are significantly different from the corresponding inferior zone(s); ‘Borderline’, where one or more of the zones in the superior field may be different from the corresponding inferior zone(s); ‘General Depression of Sensitivity’, where all zones are equally adversely affected; ‘Abnormally High Sensitivity’ where the threshold estimate at the stimulus locations in the zones are abnormally high; and ‘Within Normal Limits’ where the threshold estimate at the stimulus locations is within the normal range (Heijl et al. 2002; Brusini and Johnson 2007; Artes et al. 2010; Tanna et al. 2011).

1.8.8 Reliability parameters

The interpretation of the visual field examination is undertaken in the context of the reliability of the examination, itself. The reliability of the examination is expressed in terms of the proportion of incorrect responses to the False-Negative (FN) catch trials, the proportion of responses deemed to be False-Positive (FP) and the assessment of fixation stability.

1.8.8.1 False-Negative (FN) Catch Trials

A False-Negative catch trial with the Full Threshold and FASTPAC algorithms presents the stimulus at a 9dB greater luminance than the threshold estimate obtained at the given location earlier in the examination. The lower limit for an acceptable proportion of incorrect responses was originally empirically considered to be $\geq 33\%$. An incorrect response is suggestive of a loss of attention or of fatigue. However, the frequency of incorrect responses is also moderately correlated with the severity of the field loss due to the increased variability associated with the reduction in sensitivity (Bengtsson and Heijl 2000) and, therefore, the range of acceptability should be widened in such cases. The SITA algorithms use the same 9dB increment at locations of normal sensitivity, but larger increments at locations exhibiting apparent loss to compensate for the increased variability mentioned above (Bengtsson and Heijl 2000) and may be up to 20dB brighter than the previously threshold (Johnson et al. 2014). The range of acceptability for incorrect responses to the FN catch trials varies from 15-33 % (Cedrone et al. 2008; Talbot et al. 2013), to 20-25% (Asaoka et al. 2012; Park and Park 2012; Rao et al. 2013b) or even

less than 15% (Larrosa et al. 2012; Lee et al. 2012b; Sehi et al. 2012; Marvasti et al. 2013).

1.8.8.2 False-Positive (FP) Catch Trials

A False-Positive catch trial involves the non-presentation of the stimulus in a manner such that it mimics the presentation of the stimulus. The upper limit for an acceptable number of incorrect responses was originally empirically considered to be $\geq 33\%$ and a value above this figure indicates a lack of understanding of the requirements of the examination (generally referred to as ‘a trigger-happy’ patient) and is generally associated with a positive value of the GH index. The SITA algorithms designate a false-positive response as one which occurs within a ‘listen time’ window of 180msec immediately following the onset of the stimulus presentation, or as one which occurs within a further ‘listen time’ window (which commences at a fixed time after the response window and which runs into the ‘listen window’ associated with subsequent stimulus) (Olsson et al. 1997). As a consequence of the change in the method of assessment of false-positive responses, the criterion for the SITA algorithms has been revised downwards to 25%, 15% (Asaoka et al. 2011; Rao et al. 2013b ; Lee et al. 2014a), or even 10% (Wall et al. 2013).

1.8.8.3 Fixation Stability

The Fixation Stability is evaluated with the Heijl-Krakau blind spot technique and by gaze tracking. The Heijl-Krakau technique periodically presents the size III stimulus at a ‘moderately’ bright luminance into the blind spot (Heijl and Krakau 1975; Anderson and Patella 1999). A ‘seen’ response from the

observer indicates sub-optimal fixation. However, a 'seen' response can also result from an incorrect positioning of the blind spot at the start the examination and also when the individual responds to the noise associated with the presentation of the stimulus (Arnalich-Montiel et al. 2009). The upper limit for the proportion of acceptable fixation losses ranges from 30-33 or 40% (Taibbi et al. 2009; Marvasti et al. 2013), to 25-20% (Larrosa et al. 2012; Rao et al. 2013a) or even less than 15% (Cankaya and Simsek 2012; Lee et al. 2014a).

The gaze tracking technique tracks, by infrared imaging, the linear distance between the pupil centre and the 1st Perkinje image. An eye movement results in an increase in the linear distance since the pupil centre moves whilst the 1st Perkinje image remains stationary. The amplitude of the eye movement, truncated at 10°, is displayed on the print-out as an upward deflection. A downward deflection indicates a disruption to the infra-red imaging such as that caused by a blink or by a rupture of the pre-corneal tear film (Russell et al. 2012; Saunders et al. 2012).

1.8.8.4 Perimetric learning effect and fatigue effect

The outcome of the threshold can be affected by many extraneous factors including refractive defocus (Weinreb and Perlman 1986; Henson and Morris 1993), improper alignment of the trial lens (Lalle 2001), upper lid position (Cahill et al. 1987), pupil size (Flammer et al. 1984), media opacities (Heuer et al. 1988) the learning (Wood et al. 1987) and fatigue (Johnson et al. 1988) effects, exercise (Ramulu et al. 2012), accompanying music (Shue et al. 2011).

Two of the factors which exert a major influence on the outcome of the visual field are the learning and the fatigue effects.

The learning effect describes the improvement in sensitivity arising with increased familiarity of the examination in either normal individuals or individuals with glaucoma. The learning effect is evident on the first visit from the first to the second examined eye, and between the eyes, up to five visits (Wood et al. 1987). An increase in the sensitivity is more pronounced in the peripheral areas (Wood et al. 1987; Werner et al. 1989). The learning effect image is independent of age but is a function of the magnitude of the sensitivity recorded at the first examination (Heijl et al. 1989).

The fatigue effect describes the decline in sensitivity associated with the increase in the duration of the visual field examination. It can occur in normal individuals (Heijl 1977; Johnson et al. 1988), in those with ocular hypertension and in those with glaucomatous visual field loss (Wild et al. 1991; Hudson et al. 1994). The fatigue effect can be reduced by rest intervals during the examination of each eye and between eyes (Johnson et al. 1988). The fatigue effect is greater in the second eye (Searle et al. 1991).

Classically, perimetry uses a Goldmann size III stimulus. Recently, an alternative approach has been advocated: Size Threshold Perimetry (STP) or Size Modulation Perimetry whereby the stimulus size increases to either size V or size VI, dependent upon the eccentricity (Wall et al. 2013). This concept is based upon the rationale that the larger stimulus sizes exhibit less within-test

variability. A further alternative approach involves the use of multiple stimulus sizes to determine the coefficient of spatial summation (Ricco's area). Ricco's area increases with eccentricity to reflect a constant number of RGCs at the given eccentricity. However, once the stimulus size exceeds Ricco's area, oversampling of the perceptive field may occur and may mask the underlying defect (Redmond et al. 2010).

1.9 The identification of progressive visual field loss

The interval between visual field examinations for patients with glaucoma is equivocal. A lengthy interval may fail to identify progression and multiple examinations over a short interval are costly and are unlikely to identify progression in that the disease, itself, is generally slowly progressive. The recommended frequency of examinations varies from every 4 months in the first 2 years following diagnosis to every 6 months in the first 3 years (Rossetti et al. 2010). Alternatively, a 'wait and see' scheme has been proposed, involving the clustering of two or three examinations at 'baseline' and the two or three examinations over a 2year follow-up observation (Crabb and Garway-Heath 2012). Another proposal recommends a constant interval between examination, the frequency of which varies at the discretion of the ophthalmologist (Malik et al. 2013).

A further problem in the evaluation of visual field progression is the change from an established algorithm to a newly introduced algorithm which provides a better or equivalent accuracy in the estimation of threshold over a shorter

examination duration. Such an example occurred with the replacement of the Full Threshold and FASTPAC algorithms by the SITA algorithms which resulted in a more accurate estimate of threshold and narrowing of the confidence intervals for normality (Shirato et al. 1999; Sharma et al. 2000; Budenz et al. 2002).

Various approaches are used to evaluate the presence of progressive visual field loss, namely, empirical clinical judgement, defect classification systems, trend-analysis and event-based analysis.

1.9.1 Empirical Clinical Judgement

Empirical clinical judgment is largely based upon the sequential comparison, and recognition of the worsening, of the number, severity and special location of the Total and Pattern Deviation probability levels. However, the same procedure can also be applied to the visual field indices and this latter comparison can be augmented by supplementary graphical techniques such as Box and Whiskers plots.

1.9.2 Defect Classification Systems

The defect classification systems comprise predefined cross-sectional criteria for visual field abnormality within each stage of the given system. These cross-sectional systems have been used to delineate visual field progression in terms of the progression of the ensuing visual field outcome from one stage to the next (more severe) stage (Investigators 2000; Miglior et al. 2007; Musch et

al. 2008). Typical defect classification systems are those of AGIS (Gaasterland et al. 1994; Caprioli and Coleman 2008; Coleman and Miglior 2008), the CNTGS (The Collaborative Normal-Tension Glaucoma Study and Group. 1998; Leske et al. 1999) and the CIGTS (Musch et al. 1999; Lichter 2003; Vesti et al. ; Brusini and Johnson 2007), and the Bascom-Palmer (Hodapp et al. 1993) staging system (Mills et al. 2006; Park and Park 2012).

1.9.3 Trend Analysis

Trend-analysis describes the quantification of the assumed linear relationship between a given visual field outcome and the time to follow-up and provides an estimation of the rate of progression (Fitzke et al. 1995; McNaught et al. 1996; Viswanathan et al. 1998; De Moraes et al. 2011). The technique is confounded by the frequency of examinations; the levels of within- and between-examination variability; the position of the examination within the time series; the lack of agreement over the magnitude of the slope for the designation of progression; the lack of separation of the normal age-decline in sensitivity (McNaught et al. 1996; Viswanathan et al. 1998; Crabb and Garway-Heath 2012; De Moraes et al. 2012b; Russell et al. 2012). The technique will be described in more detail in Chapter 7.

1.9.4 Event Analysis

The event-based approach is that derived for, and from, the comparison of the threshold estimate at any given location at any given visual field examination to the corresponding threshold estimates at the first two examinations (Leske et al. 1999; Heijl et al. 2003). The difference is then compared to the

distribution of the test-retest variability of the threshold at the given location in individuals with stable glaucoma (Heijl et al. 2003; Heijl et al. 2008). ‘Likely’ visual field progression is designated as three or more locations exhibiting a statistically significant reduction in the estimated sensitivity compared to that derived at the two baseline examinations, which lies outside that for stable glaucoma, on three or more successive examinations (Heijl et al. 2002; Nassiri et al. 2012). The original technique was based upon the use of the Total Deviation map but is now based upon the Pattern Deviation map and therefore is essentially resistant to the effect of progressive cataract (Leske et al. 1999). The technique is currently incorporated into the Guided Progression Analysis (GPA) analysis module of the HFA.

Event analysis cannot determine the rate of change of the progression (Bengtsson et al. 2009; Artes et al. 2011; Asaoka et al. 2013; Lee et al. 2014a) and is influenced by the in between-test variability, which is high especially in extensively depressed stimulus locations (Rao et al. 2013b).

Clinical experience dictates that the various methods should be evaluated concurrently to optimise the recognition of progressive visual field loss (Chauhan et al. 2008; Iester et al. 2011).

Chapter 2

Rationale for the research

2.1 Introduction to structural and functional characteristics of the ONH

There have been numerous studies relating the magnitudes of the structural characteristics of the ONH in glaucoma to the functional outcome derived by perimetry. These studies have largely involved cross-sectional evaluation.

The structural assessment has evolved from the rudimentary, e.g. the cup-to-disc ratio, to the outcome derived by the manual analogue planimetry (Kottler et al. 1976; Jonas et al. 1988; Jonas and Montgomery 1995; Jonas et al. 1999) and onwards to the outcome derived by the current imaging techniques, such as confocal scanning laser ophthalmoscopy (CSLO) (Vizzeri et al. 2009; Kamdeu Fansi et al. 2011; Cankaya and Simsek 2012) and, concurrent with the development of this thesis, optical coherence tomography (OCT) (Huang et al. 2012; Schuman 2012; Sehi et al. 2012; Wang et al. 2012). Equally, the functional outcome has evolved from that obtained with manual kinetic perimetry (Katz and Sommer 1986; Anderson and Patella 1999; Inci Dersu 2006; Vonthein et al. 2007) to that of SAP (Wild 1988; Bengtsson et al. 1998; Bartz-Schmidt et al. 1999; Delgado et al. 2002; Heijl and Patella 2002; Turpin et al. 2007; Wesselink et al. 2009; Pan and Varma 2011) with the level of sophistication of the analysis of the latter varying from the absolute values of

sensitivity, to the visual field indices MD (Nassiri et al. 2013), PSD (Ang et al. 2011; Rao et al. 2013a) and VFI (Casas-Llera et al. 2009; Lee et al. 2014a) and to the Total and Pattern Deviation probability values (Artes et al. 2005).

However, very few studies have evaluated the progressive structural damage to the ONH with the progressive functional outcome derived by SAP over a relatively long time period (i.e. a mean of 11.8 years (Laemmer et al. 2007) and of 9.4 years (Nassiri et al. 2012). These latter studies have compared the outcome from digital planimetry with the MD index (Laemmer et al. 2007); and the outcomes from confocal CSLO with the MD index (Nassiri et al. 2012).

2.2 Previous work

The previous work within the Cardiff School of Optometry and Vision Sciences, Cardiff University, was concerned with the development of monoscopic and stereoscopic computer-assisted planimetry for the cross-sectional structural evaluation of the ONH in primary open-angle glaucoma (Sheen 2002; Sheen et al. 2004; Bourtsoukli 2005; Morgan et al. 2005a; Morgan et al. 2005b; Morgan et al. 2012). A particular feature of the custom-software for the digital viewing of the ONH is a 'floating' measurement cursor which can be moved in stereoscopic (depth) space to minimize parallax errors encountered in the measurement of the NRR undertaken at the depth of the scleral rim. A further feature of the software is the ability to zoom and pan the

digital ONH images at the observer's discretion. The work has shown that, for the identification of primary open-angle glaucoma, digital stereoscopic viewing of the ONH outweighed monoscopic viewing in terms of sensitivity and specificity and is an indicative technique for quantitative and qualitative assessments of the ONH in glaucoma (Sheen 2002; Sheen et al. 2004; Bourtsoukli 2005; Morgan et al. 2005a; Morgan et al. 2005b; Morgan et al. 2012). The use of digital stereo-planimetry was found to enhance the demarcation of subtle localized changes (focal rim notches) and to enable a more accurate quantification of the PPA (Bourtsoukli 2005); and highlighted the inappropriateness of the ISNT rule for the diagnosis of primary open-angle glaucoma (Morgan et al. 2012).

A natural extension of digital manual stereo-planimetry would be the assessment of progressive structural damage to the glaucomatous ONH and its relationship with the functional outcome.

2.3 Overall and specific aims of the work

The overall aim of the work described in this thesis was to extend the digital mono- and stereo-viewing techniques developed within the Cardiff School of Optometry and Vision Sciences to the evaluation of progressive structural damage to the glaucomatous ONH with particular emphasis on a longest possible follow-up.

The specific aims of the work described in this thesis were threefold.

Firstly, to develop and then to evaluate the efficacy of digital stereo-flicker chronoscopy for the qualitative identification of progressive glaucomatous ONH damage over a long follow-up and to determine the relationship of the latter to the progressive worsening of the visual field (Chapter 5).

Secondly, to evaluate the quantitative relationship between progressive damage to the NRR, derived by digital planimetry, and the progressive worsening of the visual field defined in terms of the traditional measures, based upon the dB notation, and in terms of a more novel approach, namely, the residual retinal ganglion cell (soma) count (Chapter 6).

Thirdly, to evaluate for the identification of early progressive glaucomatous damage over a longer follow-up than was available for the ONH imaging, the difference between the outcomes derived by the univariate linear regression of sensitivity (dB) against time to follow-up and of the residual retinal ganglion cell (soma) count against time to follow-up (Chapter 7).

2.4 Experimental Studies

The progressive structural damage of the ONH using flicker chronoscopy has only been utilized under monoscopic viewing conditions and this has been undertaken in both analogue (Heijl and Bengtsson 1989) and in digital forms (Radcliffe et al. 2010; VanderBeek et al. 2010). The study described in Chapter 5 evaluated the efficacy of digital stereo-flicker chronoscopy for the qualitative identification of progressive glaucomatous ONH damage. The cohort comprised 50 individuals with glaucoma and 11 with ocular hypertension. The median duration of follow-up was 9.9 years. The digital stereo-flicker chronoscopy in relation was evaluated not only to digital mono-flicker chronoscopy, but also to the digital stereo-viewing and digital mono-viewing of the 'side-by-side' images of the ONH.

In the subsequent study, described in Chapter 6, the correlation was determined between progressive structural damage to the NRR, quantified by digital stereo-planimetry, with the visual field outcomes expressed in dBs and, using a novel approach, the residual retinal ganglion cell (soma) count. The cohort comprised 23 individuals with glaucoma and 4 with ocular hypertension. The median duration of follow-up was 10.3 years.

The final study, described in Chapter 7, evaluated the difference between the outcomes derived by the univariate linear regression of sensitivity (dB) against time to follow-up and of the residual retinal ganglion cell (soma) count against

a long follow-up. It was hypothesized that the latter approach would result in the earlier identification of progressive early glaucomatous visual field loss. The cohort comprised 112 individuals with glaucoma. The median duration of follow-up of was 8.8 years.

2.5 Logistics

The various studies utilised retrospective longitudinal cohorts of patients attending the Glaucoma Clinics of the Cardiff Eye Unit, University Hospital of Wales (UHW). At the commencement of the research described in this thesis, the number of patients who had received concurrent ONH imaging and visual field examinations was unknown to the Cardiff Eye Unit. Equally the length of the follow-up of each patient was also unknown.

The initial part of the work presented in this thesis, therefore, comprised the acquisition of a dataset containing the ONH images obtained from the various ONH imaging devices used in the Glaucoma Clinics and the corresponding visual field outcomes.

The first stage in the acquisition of the database involved the manual search of the medical records of approximately 2800 patients who had attended the Glaucoma Clinics between 1998 and 2010. The first date enabled the earliest available images of the ONH at UHW and the later date an arbitrary cut-off

point for data collection (i.e. two years after commencement of the thesis). The search involved the identification from the medical records of the original analogue images in 35mm slide format and, subsequently, the identification of the corresponding digital images for the given patient. The analogue images in 35mm slide format were included to maximize the follow-up period for the study. These analogue images were then digitised at the Department of Media Resources at UHW using either a slide scanner or by re-photography using a macro lens. The corresponding digital images for the given patient were sourced through the electronic archival system, Imagenet, and had been acquired with two different Topcon fundus cameras.

The various different types of imaging modality necessitated the resizing and alignment of the various images to a standard reference image. For the quantitative analysis (Chapter 6), the images were referenced to the most recent fundus camera, the Topcon TRC-EX, in use at UHW. These processes were necessary to overcome the differences in the resolution and/ or the editing (i.e. cropping) of the images, which differed across the various photographic techniques.

The second stage in the acquisition of the database involved the manual search of the visual field printouts for each patient with two or more ONH images. These printouts were sourced from the five separate Humphrey Field Analyzers contained within the Department of Orthoptics at UHW.

The minimum selection criteria for entry into the database were considered to be a minimum of two ONH images and three visual field examinations. The characteristics of the individuals within the database are described in Chapter 3. From these individuals a further subset of individuals was identified who had undergone five or more visual field examinations. The latter number of visual field examinations was the minimum to undertake the GPA and also to perform univariate linear regression analysis of the given visual field outcome against time to follow-up (Wild et al. 1993; McNaught et al. 1996; Viswanathan et al. 1998; Hitchings 2008; Artes et al. 2010; Azarbod et al. 2012; De Moraes et al. 2012b; Rao et al. 2013b). Thus, the size of any given cohort for the various proposed studies was limited by the requirement for five or more visual field examinations. However, the composition of the potential cohorts was further limited by the limited number of the corresponding ONH images, particularly, those taken at the same visit as the visual field examination. A further restriction in the size of the various proposed cohorts was the absence in some patients of one or more ONH images acquired by the digital photographic technique which was to be used as the reference against which the images from the other photographic sources were to be standardised. The evolution in the size of the various cohorts used in the study is described in Chapter 3.

The third stage in the acquisition of the database was to enter the corresponding demographic and clinical history of each individual.

Concurrent with the acquisition of the database was the development of the user-friendly interface for the archiving, retrieving and viewing of the various ONH images (Chapter 4) and of the software necessary for digital stereo-flicker chronoscopy and planimetry (Chapters 5 and 6, respectively). The development of the various software utilities was undertaken in conjunction with Dr. Gavin Powell, Cardiff School of Computer Science and Informatics, Cardiff University, who wrote the coding for the various applications.

The various studies described in this thesis used a case series design. The number of individuals within each case series was determined by the number of photographic visits, the type of camera, the number of visual field examinations and the chronological association between the two diagnostic modalities. The available dataset was thus not amenable to power calculations to determine sample size.

The patients who formed the cohort for the final part of the thesis, namely, the comparison of the two univariate linear regression techniques, i.e. sensitivity in dBs and the residual retinal ganglion (soma) cell count against time to follow-up, respectively, were identified from a search of the first 1000 patients entered into 'Open Eyes', an electronic patient database, which was introduced into the Cardiff Eye Unit in 2013 (Chapter 7). The dates of the visual field examinations of those patients with a minimum of five visual field examinations over a minimum of six years were extracted from the 'Open

Eyes' database. The visual field printouts were then acquired from a manual search of the (now) three separate Humphrey Field Analyzers contained within the Department of Orthoptics at UHW.

The sensitivity values from the .pdf of the Single Field Analysis printouts of each individual were extracted using Microsoft Paint 2010 (Microsoft Corporation, Redmond, WA) and the resultant .tiff image was read into.txt format using Omnipage 18 (Nuance Communications, Inc., Burlington, MA). The dB values were converted into RGC values and output as a .csv file format via an application, produced by Dr Carlo Knupp, Senior Lecturer, Cardiff School of Optometry and Vision Sciences, Cardiff University, using Eclipse and coded in Java. The subsequent univariate linear regression analysis was undertaken by Mr. David Shaw, Senior Medical Statistician. Mr Shaw has approximately 25 years of collaboration with Professor Wild in the statistical analysis of perimetric data.

The research had ethical approval from the South East Wales Research Ethics Committee, as it came under the category of Audit. It commenced in January 2008, but was delayed by two separate Interruptions of Study which were formally agreed by Cardiff University and lasted a total of 18 months.

One further study was initiated to compare the residual RGC count in glaucoma immediately prior and subsequent to cataract extraction and

intraocular lens implantation (IOL). The rationale for this study was to demonstrate the dependency of the RGC soma calculation on the absolute values of sensitivity which are influenced by optical as well as neural factors. It was expected that the post-operative residual RGC count would be greater than the pre-operative count, thereby demonstrating the current vulnerability of the RGC calculation (Harwerth et al. 2010) in the presence of age-related cataract. A further search was undertaken for individuals with glaucoma, archived in Open Eyes, who had undergone cataract surgery with IOL at the UHW. The search period extended from 1999 to 2014. Fifty-eight individuals were identified who exhibited at least three reliable visual field examinations prior to surgery and at least three reliable visual field examinations post-operatively. The immediate pre- and the post-operative visual field examinations had to be within 1 year of the surgery. The post-operative residual RGC count was surprisingly found to be lower post-operatively. It was subsequently discovered that in all but 5 individuals, the refractive correction used for the pre-operative visual field examination has also been used for the post-operative examination, thereby causing an artificial reduction in the residual RGC count due to the induced optical defocus. Since the 'true' post-operative refractive correction was unknown, a potential correction of the sensitivities for the induced defocus could not be undertaken and, in any event, would have been both clinically and academically unsatisfactory.

Chapter 3

Characteristics of the individuals within the database compiled for the research

3.1 Acquisition of the various cohorts

As was discussed in Chapter 2, this thesis is concerned with the identification of structural (i.e. optic nerve head) and/ or functional (threshold perimetry) progressive damage in glaucoma and, where appropriate, the association between these measures.

The various experimental Chapters contained in this thesis use differing cohorts of individuals with glaucoma, depending upon the inclusion criteria for the given study. The individuals were selected from patients attending the Glaucoma Clinics of the Cardiff Eye Unit at the University Hospital of Wales.

The various cohorts were acquired from a manual search of the medical records of approximately 2800 patients who were enrolled at the Glaucoma Clinics between 1998 and 2010. The number of individuals within each cohort was limited by the availability of the requisite data and also reduced as the inclusion criteria became more stringent.

This Chapter provides a synopsis of the evolution of the numbers of individuals conforming to the various inclusion criteria and, thereby, the

numbers within the various cohorts. The evolutionary stages of the cohort acquisition are given in detail to illustrate the difficulty in obtaining a substantial number of requisite individuals.

3.2 Evaluation of structural and/or functional progressive loss

(Chapter 5 and Chapter 6)

3.2.1 Optic nerve head (ONH) images

The minimum inclusion criteria for the study of the association between structural and functional progressive loss (Chapter 5 and Chapter 6) comprised the presence of at least two optic nerve head images and of at least five visual field examinations, undertaken reliably.

The medical records of the 2800 patients were searched for the presence of analogue stereo-images, in 35mm slide format, of the ONH (i.e. the conventional form of imaging modality) to ensure the longest possible time series. The search yielded a total of 396 patients with one or more pairs of images of the ONH in 35mm slide format.

A search for the presence of digital stereo-images of the ONH for these 396 patients was then undertaken. The digital ONH images had been acquired using various Topcon fundus cameras, upgraded with a digital single-lens reflex camera, over the follow-up period and were accessed using the Topcon Imagenet software. A total of 212 individuals manifested two or more ONH stereo-images, each acquired on separate visits by either analogue or digital, or

both, imaging modalities, in one or both eyes, together with a corresponding, and complete, medical history.

The analogue 35mm slide ONH images from the 212 individuals were then digitised by the Department of Media Resources, UHW, using either a Nikon LS 2000 slide scanner, with the corresponding software for the scanning of 35mm slides, or by re-photography using a Nikon D1 digital single-lens reflex camera and a 1.05 macro lens and a copy stand placed upon a light box. The resultant images from both digitising techniques were then edited using Photoshop (Adobe, San Jose, CA) to match the colour of the original analogue image, where appropriate, and to remove dust marks and/ or the effects of abrasions on the glass cover of the slide. The size of the resulting images was 18cm x 12cm at 96 dots per inch (dpi), and was selected to ensure optimum image quality.

The resolution of the digitised analogue images varied depending upon whether the scanner or the camera was used to acquire the image and was either 2000*1312 pixels or 3008*1312 pixels. The resolution of the existing digital images depended upon the camera used to acquire the image. For the Topcon TRC-50IX camera (utilizing the Nikon D1X 20° camera) the resolution was 768*576 pixels and for the Topcon TRC-EX camera (utilizing the Sony 950P 20° camera) the resolution was 3008*1960 pixels.

The digitised ONH image series for each of the 212 individuals, together with the individual's demographic details obtained from the Cardiff Eye Unit Patient Management System (PMS), and the medical history of each individual were archived in Access, Excel and Word databases, using the standard patient identity numbering system operational at the UHW. The number of photographic visits, and the mode and resolution of photography at each visit, for the 212 individuals with two or more stereo-images by the number of photographic visits and the mode of photography is given in Table 3.1.

Mode and resolution (pixels) of photography	Number of individuals by number of photographic visits						
	≥V1	≥V2	≥V3	≥V4	≥V5	≥V6	=V7
35mm slides (2000 x 1312)	76	17	1	0	0	0	0
35mm slides (3008 x 1960)	99	43	3	0	0	0	0
Topcon TRC-IX (768 x 576)	37	127	59	21	8	2	0
Topcon TRC-EX (3008 x 1960)	0	25	18	15	2	0	1
Total	212	212	81	36	10	2	1

Table 3.1. The number of stereo-images by the number of photographic visits, and the mode and resolution of photography at each visit, for the 212 individuals with two or more stereo-images. V represents visit.

3.2.2 Visual field examination time series

The hard drives of the Humphrey Field Analyzer (HFA) 700 series perimeters, which had been, or were still, operational in the Glaucoma Clinics from 1998 onwards, were then searched for the visual field examinations of the 212 individuals with two or more stereo-images of the ONH.

3.3 The characteristics of the various cohorts with ONH stereo-images and visual field examinations

Of the 212 individuals (Table 3.2), 180 had undertaken one or more visual field examinations. The visual fields from each of the 180 individuals were then aggregated onto the hard drive of the HFA in the Glaucoma Clinic (HFA750i-12495). This perimeter contained the most contemporary analytical software version (Version 4.2) including the GPA. The visual field files were also stored on floppy discs and also printed in PDF format. Of the 180 individuals, 116 had exhibited three or more reliable visual field examinations either in both eyes (102) or in one eye, only (14). Of these 116 individuals, 74 had undertaken five or more reliable visual field examinations either in both eyes (69) or in one eye, only (5). Of the 74 individuals, 68 had undergone each pair of respective photographic and perimetric examinations within 12 months of one another, either in both eyes (64) or in one eye only (4) (Table 3.2). The reliability criteria comprised $\geq 15\%$ incorrect responses to the false-positive catch trials; $\geq 20\%$ incorrect responses to the false-negative catch trials and $\geq 20\%$ fixation losses.

Selection criterion	Number of patients
Medical notes available	~2800
Patients with ≥ 2 stereo-images of the ONH	212
Patients with ≥ 2 stereo-images of the ONH and ≥ 1 visual field examinations	180
Patients with ≥ 2 stereo-images of the ONH and ≥ 3 visual field examinations	123
Patients with ≥ 2 stereo-images of the ONH and ≥ 3 visual field examinations with reliable outcomes	116
Patients with ≥ 2 stereo-images of the ONH and ≥ 3 visual field examinations with reliable outcomes and with pairs of respective examinations each conducted within 12 months	97
Patients with ≥ 2 stereo-images of the ONH and ≥ 5 visual field examinations with reliable outcomes	74
Patients with ≥ 2 stereo-images of the ONH and ≥ 5 visual field examinations with reliable outcomes and with pairs of respective examinations each conducted within 12 months.	68

Table 3.2. The number of individuals by the frequency of the available ONH images and visual field examinations.

The number of photographic visits, and the mode and resolution of photography at each visit, for the 116 individuals with two or more stereo-images and three or more reliable visual fields are shown in Table 3.3.

The number of ONH stereo-images by the number of visual field examinations for the 116 individuals with two or more stereo-images and three or more reliable visual field examinations is presented in Table 3.4.

Mode and resolution (pixels) of photography	Number of individuals by number of photographic visits						
	≥V1	≥V2	≥V3	≥V4	≥V5	≥V6	=V7
35mm slides (2000 x 1312)	43	6	0	0	0	0	0
35mm slides (3008 x 1960)	46	15	2	0	0	0	0
Topcon TRC-IX (768 x 576)	27	77	44	19	7	2	0
Topcon TRC-EX (3008 x 1960)	0	18	15	14	2	0	1
Total	116	116	61	33	9	7	1

Table 3.3. The number of stereo-images by the number of photographic visits, and the mode and resolution of photography at each visit, for the 116 individuals with two or more stereo-images and three or more reliable visual field examinations. V represents visit.

Number of visual field examinations	Number of ONH stereo-images						
	2	3	4	5	6	7	Total
3	16	3	4	0	0	0	23
4	12	2	4	2	0	0	20
5	4	5	2	0	0	0	11
6	15	4	4	0	0	0	23
7	8	6	1	1	0	0	16
8	3	2	3	1	0	0	8
9	1	1	1	0	0	0	4
10	2	1	1	0	1	0	5
11	0	1	1	0	0	1	3
12	1	0	2	0	0	0	3
Total	62	25	23	4	1	1	116

Table 3.4. The number of ONH stereo-images by the number of visual field examinations for the 116 individuals with two or more stereo-images and three or more reliable visual field examinations.

It is clear from Table 3.4 that there was little association between the number of visual field examinations and the number of photographic visits. The majority of individuals had a greater number of visual field examinations compared to photographic visits.

The number of instances at which photography and visual field examination were conducted on the same day, is shown in Table 3.5. Only 53 of the 116 individuals (45.7%) had received both examinations on the same day, on at least one occasion.

Visits with same day photography and visual field examination	Number of Individuals (%)
1	43 (37.1)
2	8 (6.9)
3	0 (0.0)
4	1 (0.9)
5	1 (0.9)
Total	53 (45.7)

Table 3.5. The number and the corresponding percentage (%) of visits where the photography and visual field examinations were undertaken on the same day for the 116 individuals with two or more stereo-images and three or more reliable visual field examinations.

The distribution of the interval between ONH photography and the corresponding visual field examination is shown in Table 3.6.

Number of corresponding photographic and visual field examinations	Interval between a given pair of photographic visits and the corresponding visual field examinations (months)					
	Up to +/- 3	Up to +/- 6	Up to +/- 12	Up to +/- 24	Up to +/- 48	≥ 48
1	43	81	89	100	103	111
2	27	9	8	4	7	5
3	6	0	0	0	0	0
4	1	0	0	0	0	0
5	1	0	0	0	0	0
6	1	0	0	0	0	0
Cumulative number of individuals	79	90	97	104	110	116

Table 3.6. The cumulative distribution of the 116 patients (cells) with two or more stereo-images and three or more reliable visual field examinations by the number of, and interval between, the corresponding photographic and visual field examinations.

However, 97 of the 116 individuals had had at least one photographic visit and one visual field examination conducted within 12 months of each other. The number of ONH stereo-images by the number of visual field examinations for these 97 individuals is given in Table 3.7.

Number of visual field examinations	Number of ONH stereo-images						
	2	3	4	5	6	7	Total
3	7	3	4	0	0	0	14
4	8	2	4	2	0	0	16
5	3	5	2	0	0	0	10
6	14	3	4	0	0	0	21
7	6	6	1	1	0	0	14
8	2	2	3	1	0	0	8
9	1	1	1	0	0	0	3
10	2	1	1	0	1	0	5
11	0	1	1	0	0	1	3
12	1	0	2	0	0	0	3
Total	44	24	23	4	1	1	97

Table 3.7. The number of ONH stereo-images by the number of visual field examinations for the 97 individuals with two or more stereo-images and three or more reliable visual field examinations and with the pairs of respective examinations conducted within 12 months of each other.

Of the 116 individuals, 74 had had at two or more stereo-images and five or more reliable visual field examinations. The corresponding number of photographic visits, and the mode and resolution of photography at each visit, for the 74 individuals is given in Table 3.8.

Mode and resolution (pixels) of photography	Number of individuals by number of photographic visits						
	≥V1	≥V2	≥V3	≥V4	≥V5	≥V6	=V7
35mm slides (2000 x 1312)	29	4	0	0	0	0	0
35mm slides (3008 x 1960)	23	5	0	0	0	0	0
Topcon TRC-IX (768 x 576)	22	55	33	13	6	2	0
Topcon TRC-EX (3008 x 1960)	0	10	12	9	1	0	1
Total	74	74	45	22	7	2	1

Table 3.8. The number of stereo-images by the number of photographic visits, and the mode and resolution of photography at each visit, for the 74 individuals with two or more stereo-images and five or more reliable visual field examinations. V represents visit.

The frequency of ONH stereo-images by the frequency of visual field examinations in these 74 individuals is presented in Table 3.9.

Number of visual field examinations	Number of ONH stereo-images						
	2	3	4	5	6	7	Total
5	4	5	2	1	0	0	12
6	15	4	4	0	0	0	23
7	8	6	1	1	0	0	16
8	3	2	3	1	0	0	9
9	1	1	1	0	0	0	3
10	2	1	1	0	1	0	5
11	0	1	1	0	0	1	3
12	1	0	2	0	0	0	3
Total	34	20	15	3	1	1	74

Table 3.9. The number of ONH stereo-images by the number of visual field examinations for the 74 individuals with two or more stereo-images and five or more reliable visual field examinations.

The number of instances at which photography and visual field examination were conducted on the same day, is shown in Table 3.10. Forty-three of the 74 individuals (58.11%) had received both examination techniques on the same day on at least one occasion.

Visits with same day photography and visual field examination	Number of Individuals (%)
1	34 (46.0)
2	7 (9.5)
3	0 (0.0)
4	1 (1.4)
5	1 (1.4)
Total	43 (58.1)

Table 3.10. The number and the corresponding percentage (%) of visits where the photography and visual field examinations were undertaken on the same day for the 74 individuals with two or more stereo-images and five or more reliable visual field examinations and with at least one pair of respective examinations conducted within 12 months of each other.

The distribution of the interval between ONH photography and the corresponding visual field examination is shown in Table 3.11.

Number of corresponding photographic and visual field examinations	Interval between a given pair of photographic visits and the corresponding visual field examinations (months)					
	Up to +/- 3	Up to +/- 6	Up to +/- 12	Up to +/- 24	Up to +/- 48	≥ 48
1	29	58	62	71	72	74
2	23	6	6	1	1	0
3	6	0	0	0	0	0
4	1	0	0	0	0	0
5	1	0	0	0	0	0
6	1	0	0	0	0	0
Cumulative number of individuals	61	64	68	72	73	74

Table 3.11. The cumulative distribution of the 74 patients (cells) with two or more ONH stereo-images and five or more reliable visual field examinations by the number of, and interval between, the corresponding photographic and visual field examinations.

3.3.1 Resultant cohort for the qualitative assessment of progressive glaucomatous ONH damage using both mono- and stereo-flicker chronoscopy (Chapter 5)

Sixty-eight of the 74 individuals had had, at least, one photographic examination and one visual field examination conducted within 12 months of each other. The number of ONH stereo-images by the number of visual field examinations for these 68 individuals is given in Table 3.12.

Number of visual field examinations	Number of ONH stereo-images						
	2	3	4	5	6	7	Total
5	3	5	2	1	0	0	11
6	14	3	4	0	0	0	21
7	6	6	1	1	0	0	14
8	2	2	3	1	0	0	8
9	1	1	1	0	0	0	3
10	2	1	1	0	1	0	5
11	0	1	1	0	0	1	3
12	1	0	2	0	0	0	3
Total	29	19	15	3	1	1	68

Table 3.12. The number of ONH stereo-images by the number of visual field examinations for the 68 individuals with two or more stereo-images and five or more reliable visual field examinations and with at least one pair of respective examinations conducted within 12 months of each other.

Seven of the 68 individuals were excluded on the basis of inadequate image quality either of the original analogue images, of the digitised analogue images or of the existing digital images. The number of photographic visits, and the mode and resolution of photography at each visit, for the remaining 61 individuals is shown in Table 3.13.

Mode and resolution (pixels) of photography	Number of individuals by number of photographic visits						
	V1	V2	≥V3	≥V4	≥V5	≥V6	=V7
35mm slides (2000 x 1312)	21	1	0	0	0	0	0
35mm slides (3008 x 1960)	14	1	0	0	0	0	0
Topcon TRC-IX (768 x 576)	26	47	23	10	5	2	0
Topcon TRC-EX (3008 x 1960)	0	12	12	7	0	0	1
Total	61	61	35	17	5	2	1

Table 3.13. The number of stereo-images by the number of photographic visits, and the mode and resolution of photography at each visit, for the 61 individuals with two or more stereo-images and five or more reliable visual field examinations and with at least one pair of respective examinations conducted within 12 months of each other. V represents visit.

The number of ONH stereo-images by the frequency of visual field examinations in the 61 individuals is given in Table 3.14.

Number of visual field examinations	Number of ONH stereo-images						
	2	3	4	5	6	7	Total
5	1	4	2	1	0	0	8
6	14	2	4	0	0	0	20
7	6	5	1	1	0	0	13
8	2	2	3	1	0	0	8
9	1	1	1	0	0	0	3
10	2	1	1	0	1	0	5
11	0	0	1	0	0	1	2
12	0	0	2	0	0	0	2
Total	26	15	15	3	1	1	61

Table 3.14. The number of ONH stereo-images by the number of visual field examinations for the 61 individuals with two or more stereo-images and five or more reliable visual field examinations and with at least one pair of respective examinations conducted within 12 months of each other.

The demographic characteristics (median, lower and upper quartiles; range), by diagnosis, for the most severely affected eye (the age at presentation [either the first photographic visit or the first visual field examination, whichever occurred earlier]) and the length of follow-up of the reliable visual field examinations and of the photographic examinations, by diagnosis, for the 61 individuals is given in Table 3.15, followed by the clinical characteristics (median; lower and upper quartiles; range), by diagnosis, for the most severely affected eye of the 61 individuals in Table 3.16. Two cases of pigment dispersion glaucoma and one case of angle-closure glaucoma were designated as 'Others'.

Diagnosis (No of individuals)	Primary open-angle glaucoma (37)	Ocular hypertension (9)	Normal-tension glaucoma (5)	Glaucoma Suspect (7)	Others (3)
Age (yrs) at the baseline visit	69.5 (59.3, 73.3; 38.1 to 89.4)	63.0 (55.3, 64.8; 43.9 to 71.4)	69.6 (64.8, 72.4; 61.0 to 73.3)	63.8 (54.8, 66.3; 34.1 to 77.6)	45.8 (37.3, 55.3; 28.8 to 64.7)
Male : Female	16 : 21	5 : 4	4 : 1	3 : 4	2 : 1
Perimetric follow-up (yrs)	7.3 (6.2, 8.4; 3.1 to 10.0)	6.1 (5.3, 8.3; 4.0 to 10.8)	7.2 (7.0, 9.2; 5.8 to 10.3)	7.7 (6.6 , 8.8; 4.2 to 9.8)	9.5 (9.5, 9.9; 9.4 to 10.3)
Number of perimetric visits	7.0 (6.0, 8.0; 5.0 to 12.0)	6.0 (6.0, 7.0; 5.0 to 10.0)	8.0 (7.0, 11.0; 6.0 to 12.0)	6.0 (5.5, 7.5; 4.0 to 8.0)	7.0 (7.0, 7.5; 7.0 to 8.0)
Photographic follow-up (yrs)	3.9 (2.1, 5.5; 0.3 to 9.1)	3.6 (3.1, 5.8; 1.8 to 9.3)	5.3 (4.3, 6.3; 3.4 to 6.3)	4.6 (3.0, 6.0; 2.0 to 9.7)	4.4 (3.7, 5.6; 3.0 to 6.8)
Number of photographic visits	3.0 (2.0, 3.0; 2.0 to 5.0)	2.0 (2.0, 4.0; 2.0 to 6.0)	4.0 (3.0, 4.0; 2.0 to 7.0)	4.0 (2.5, 4.5; 2.0 to 5.0)	3.0 (2.5, 3.5; 2.0 to 4.0)
Maximum duration of follow-up (yrs)	8.9 (7.4, 9.8; 5.4 to 15.0)	10.6 (8.6, 11.0; 5.1 to 11.7)	9.2 (8.0, 9.3; 7.8 to 10.3)	9.7 (8.0, 10.4; 4.7 to 11.4)	10.0 (9.7, 10.1; 9.4 to 10.3)

Table 3.15. The demographic characteristics (median, lower and upper quartiles; range) of the most severely affected eye, by diagnosis, for the 61 individuals with two or more stereo-images and five or more reliable visual field examinations conducted within 12 months of each other.

Diagnosis (No of individuals)	Primary open-angle glaucoma (37)	Ocular hypertension (9)	Normal-tension glaucoma (5)	Glaucoma Suspect (7)	Others (3)
Mean Deviation (dB) at the baseline visit	-5.38 (-8.36, -2.57; -25.10 to 0.34)	-1.53 (-3.55, -0.74; -5.55 to -0.60)	-11.88 (-18.16, -7.74; -18.58 to -5.01)	-2.97 (-4.53, -2.17; -6.22 to -1.70)	-1.77 (-10.85, -1.60; -19.93 to -1.43)
Visual Field Index (%) at the baseline visit	92.0 (79.0, 97.0; 26.0 to 99.0)	98.0 (96.0, 98.0; 94.0 to 99.0)	73.0 (54.0, 74.0; 51.0 to 94.0)	94.0 (89.0, 96.5; 86.0 to 98.0)	85.0 (69.5, 90.5; 54.0 to 96.0)
Pattern Standard Deviation (dB) at the baseline visit	3.62 (2.04, 8.80; 1.54 to 14.42)	1.91 (1.56, 2.23; 1.45 to 4.58)	9.21 (8.79, 9.38; 3.36 to 13.18)	3.65 (2.70, 4.25; 1.70 to 5.26)	6.19 (4.59, 7.76; 2.98 to 9.32)
Intraocular pressure (mmHg) at the baseline visit	24.00 (20.25, 26.75; 11.00 to 39.00)	26.50 (22.06, 29.75; 19.00 to 38.00)	20.00 (17.50, 20.00; 13.00 to 22.00)	19.50 (18.00, 20.00; 12.00 to 22.00)	17.50 (16.00, 23.50; 15.00 to 29.00)
Vertical cup-to-disc ratio at the baseline visit	0.70 (0.60, 0.80; 0.30 to 0.90)	0.50 (0.40, 0.50; 0.10 to 0.70)	0.75 (0.70, 0.90; 0.65 to 0.90)	0.60 (0.60, 0.70; 0.50 to 0.75)	0.55 (0.50, 0.68; 0.20 to 0.80)

Table 3.16. The clinical characteristics (median, lower and upper quartiles; range) of the most severely affected eye, by diagnosis, for the 61 individuals with two or more stereo-images and five or more reliable visual field examinations.

3.3.2 Resultant cohort for the quantitative assessment of progressive structural and functional glaucomatous damage (Chapter 6)

The optic nerve head images of the 61 individuals had been derived from four different photographic modalities (two different digitising techniques for the analogue images and two different digital fundus cameras) (Table 3.13). The digital images from the Topcon TRC-IX camera had been cropped by the technicians immediately following image acquisition. The extent of the cropping varied both within- and between-technicians for any one patient. The images from the Topcon TRC-EX camera had not been edited. The remaining images could, therefore, only be scaled relative to the EX camera. The scaling procedure is described in Chapter 4. Of the 61 individuals, 27 manifested at least one image with the Topcon TRC-EX camera (Table 3.17) and this number represented the final cohort.

Mode and resolution (pixels) of photography	Number of individuals by number of photographic visits						
	V1	V2	V3	V4	≥V5	≥V6	=V7
35mm slides (2000 x 1312)	5	0	0	0	0	0	0
35mm slides (3008 x 1960)	7	1	0	0	0	0	0
Topcon TRC-IX (768 x 576)	15	15	5	1	1	1	0
Topcon TRC-EX (3008 x 1960)	0	11	12	7	0	0	1
Total	27	27	17	8	1	1	1

Table 3.17. The number of stereo-images by the number of photographic visits, and the mode and resolution of photography at each visit, for the 27 individuals with two or more stereo-images and five or more reliable visual field examinations with at least one pair of examinations conducted within 12 months of each other and with at least one photographic examination undertaken with the Topcon TRC-Ex camera. V represents visit.

The number of ONH stereo-images by the frequency of visual field examinations for the 27 individuals with two or more stereo-images and five or more reliable visual field examinations with at least one pair of respective photographic and visual field examinations conducted within 12 months of each other, is given in Table 3.18.

Number of visual field examinations	Number of ONH stereo-images						
	2	3	4	5	6	7	Total
5	1	1	1	0	0	0	3
6	5	1	1	0	0	0	7
7	2	2	1	0	0	0	5
8	1	1	3	0	0	0	5
9	0	1	1	0	0	0	2
10	1	0	1	0	0	0	2
11	0	0	1	0	0	1	2
12	0	0	1	0	0	0	1
Total	10	6	10	0	0	1	27

Table 3.18. The number of ONH stereo-images by the number of visual field examinations for the 27 individuals with two or more stereo-images and five or more reliable visual field examinations with at least one pair of respective examinations conducted within 12 months of each other and with at least one photographic examination undertaken with the Topcon TRC-Ex camera.

The demographic characteristics (median, upper and lower quartiles; range), by diagnosis, for the most severely affected eye (the age at presentation [either the first photographic visit or the first visual field examination, whichever occurred earlier]) and the length of follow-up of the reliable visual field examinations and of the photographic examinations, by diagnosis, of the 27 individuals is given in Table 3.19. The clinical characteristics (median; lower and upper quartiles; range), by diagnosis, for the most severely affected eye of the 27 individuals, are given in Table 3.20. One case of pigment dispersion glaucoma was designated with the ‘Others’ category.

Diagnosis (No of individuals)	Primary open-angle glaucoma (18)	Ocular hypertension (3)	Normal-tension glaucoma (4)	Glaucoma Suspect (1)	Others (1)
Age (yrs) at the baseline visit	69.3 (60.5, 71.2; 45.0 to 78.0)	63.0 (59.2, 63.7; 55.3 to 64.4)	67.2 (63.9, 70.3; 61.0 to 72.4))	68.5	45.8
Male : Female	6 : 12	2 : 1	0 : 4	0 : 1	1 : 0
Perimetric follow-up (yrs)	8.0 (7.0, 8.7; 4.7 to 9.8)	6.5 (5.9, 8.7; 5.3 to 10.8)	8.2 (7.1, 9.4; 7.0 to 10.3)	7.7	10.3
Number of perimetric visits	7.0 (6.0, 8.0; 5.0 to 11.0)	7.0 (6.5, 8.5; 6.0 to 10.0)	9.5 (7.5, 11.3; 6.0 to 12.0)	5.0	8.0
Photographic follow-up (yrs)	5.2 (3.5, 6.3; 1.8 to 9.1)	8.6 (6.1, 9.0; 3.6 to 9.3)	5.8 (4.9, 6.3; 3.4 to 6.3)	6.0	6.8
Number of photographic visits	3.0 (2.0, 3.0; 2.0 to 4.0)	4.0 (3.0, 4.0; 2.0 to 4.0)	4.0 (3.5, 4.8; 2.0 to 7.0)	4.0	4.0
Maximum duration of follow-up (yrs)	9.1 (8.2, 9.9; 5.6 to 15.0)	10.9 (8.7, 11.1; 6.4 to 11.3)	8.6 (8.0, 9.4; 7.8 to 10.3)	8.8	10.3

Table 3.19. The demographic characteristics (median, upper and lower quartiles; range), of the most severely affected eye, by diagnosis, for the 27 individuals with two or more stereo-images and at least one visit conducted through Topcon TRC-EX and five or more reliable visual field examinations conducted within 12 months of each other.

Diagnosis (No of individuals)	Primary open-angle glaucoma (18)	Ocular hypertension (3)	Normal-tension glaucoma (4)	Glaucoma Suspect (1)	Others (1)
Mean Deviation (dB) at the baseline visit	-3.59 (-8.18, -1.52; -25.10 to 0.34)	-4.62 (-5.09, -2.68; -5.55 to -0.73)	-9.81 (-13.45, -7.06; -18.16 to -5.01)	-3.75	-1.43
Visual Field Index (%) at the baseline visit	93.5 (76.8, 98.0; 26.0 to 99.0)	94.0 (94.0, 96.0; 94.0 to 98.0)	73.5 (68.3, 79.0; 54.0 to 94.0)	89.0	85.0
Pattern Standard Deviation (dB) at the baseline visit	3.39 (2.03, 9.47; 1.64 to 14.42)	2.23 (2.07, 3.41; 1.91 to 4.58)	9.00 (7.43, 9.25; 3.36 to 9.38)	4.73	6.19
Intraocular Pressure (mmHg) at the baseline visit	24.00 (21.00, 27.75; 14.00 to 36.00)	29.50 (26.75, 30.00; 21.00 to 38.00)	20.00 (17.00, 20.00; 13.00 to 22.00)	15.00	16.00
Vertical cup-to-disc ratio at the baseline visit	0.70 (0.60, 0.78; 0.30 to 0.90)	0.50 (0.50, 0.50; 0.40 to 0.50)	0.75 (0.70, 0.88; 0.65 to 0.90)	0.60	0.50

Table 3.20. The perimetric and clinical characteristics (median, upper and lower quartiles; range), at the entry visit, of the 27 individuals with two or more stereo-images and at least one visit conducted through Topcon TRC-EX and five or more reliable visual field examinations conducted within 12 months of each other.

The chronological relationship between the ONH photography and the visual field examinations was searched in the 27 individuals (Figure 3.1). The search revealed the lack of ONH photographic visits and therefore the lack of chronological concordance between the two diagnostic modalities.

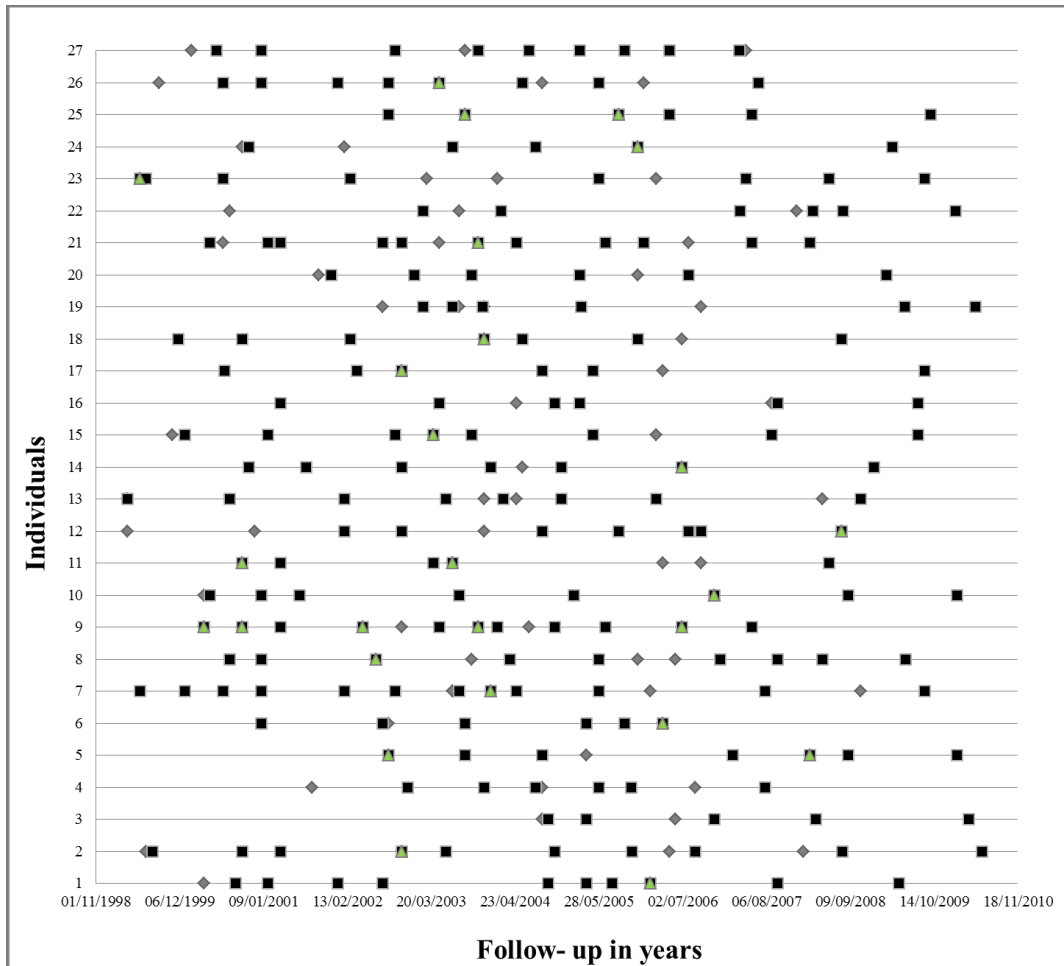


Figure 3.1. The distribution of the ONH and visual field examination in 27 patients with two or more ONH stereo-images with at least one visit conducted through Topcon TRC-EX and five or more reliable visual field examinations. ‘♦’ represents the ONH examinations, ‘■’, the visual field examination and ‘▲’ the chronological concordance of the two examinations.

3.3.3 Resultant cohort for the pointwise linear regression of residual retinal ganglion cell (RGC) count (Chapter 7)

The identification of the previous cohorts, described above, was predicated upon the identification of individuals who had had at least two photographic visits and five reliable visual field examinations, irrespective of the duration of follow-up.

It was anticipated that, in the absence of the requirement for contemporary ONH images, a more substantial cohort, based upon visual field examination alone, could be acquired for the study of functional progressive glaucomatous loss. The medical records of patients attending the Glaucoma Clinics at the Cardiff Eye Unit, UHW were therefore researched for individuals with five or more reliable visual field examinations over a longer follow-up (a minimum of 5 years).

In late 2013, an electronic patient record and archival system, 'Open Eyes', was introduced at the Cardiff Eye Unit. At the time of the search for this additional cohort (February 2014), the 'Open Eyes' archive contained the records of 1000 consecutive patients who had attended the Glaucoma Clinics between 1999 and 2014.

The search of these 1000 patients yielded 120 individuals (70 female: 50 male). Fourteen of the 120 individuals had been previously identified during the manual search for the study of structural and functional progressive

glaucomatous damage. These 14 individuals were retained within the cohort of 120 individuals since the visual field series, as would be expected, was longer than that identified by the earlier manual search.

In addition to the 120 individuals, a further 16 were included who had been utilized in the study of the association between structural and functional progressive loss and who were not listed in the 'Open Eyes' archive. Of these 136 individuals, 24 were excluded on the basis of extraction and IOL implantation during the visual field time series.

The hard drives of the HFA 700 series perimeters, which had been, or were still, operational in the Glaucoma Clinic from 1999 onwards, were then searched for the visual field examinations of the resultant 112 individuals. The visual fields from each of the 112 individuals were then aggregated onto floppy discs. The Single Field Analysis and the GPA printouts were each printed for each eye of each individual at each visual field visit. The visual field printouts were then anonymised by a numbering system and scanned and archived in .pdf format.

The demographic characteristics (median, upper and lower quartiles; range), by diagnosis, for the most severely affected eye, the age at presentation and the length of follow-up of the reliable visual field examinations, by diagnosis, for the 112 individuals is given in Table 3.21. The clinical characteristics (median, upper and lower quartiles; range), by diagnosis, for the most severely affected eye of the 112 individuals, are given in Table 3.22.

Diagnosis (No of individuals)	Primary open- angle glaucoma (70)	Ocular hypertension (11)	Normal-tension glaucoma (21)	Glaucoma Suspect (3)	Others (7)
Age (yrs) at the baseline visit	64.9 (57.7, 72.4; 32.2 to 80.1)	55.9 (52.4, 66.6; 46.3 to 72.9)	68.3 (61.8, 72.4; 41.1 to 82.9)	65.1 (60.3, 72.1; 56.0 to 82.9)	61.7 (57.1, 68.1; 45.8 to 82.1)
Male : Female	27 : 43	5 : 6	9 : 12	1 : 2	2 : 5
Perimetric follow-up (yrs)	8.5 (7.3, 9.7; 5.0 to 14.5)	9.9 (7.5 , 10.7; 5.2 to 12.4)	9.4 (8.6, 9.9; 6.3 to 10.9)	9.6 (8.6, 10.3; 7.7 to 10.9)	9.6 (8.5, 10.1; 6.4 to 10.2)
Perimetric visits	8.0 (6.3, 9.0; 5.0 to 15.0)	7.0 (6.0, 8.0; 6.0 to 10.0)	8.0 (7.0, 11.0; 5.0 to 15.0)	7.0 (6.0, 8.0; 5.0 to 9.0)	8.0 (7.5, 8.0; 5.0 to 9.0)

Table 3.21. The demographic characteristics (median, lower and upper; range) of the most severely affected eye, by diagnosis, for the 112 individuals with five or more reliable visual field examinations over a minimum follow-up of 5 years.

Diagnosis (No of individuals)	Primary open-angle glaucoma (70)	Ocular hypertension (11)	Normal-tension glaucoma (21)	Glaucoma Suspect (3)	Others (7)
Mean Deviation (dB) at the baseline visit	-4.86 (-9.42, -2.59; -25.10 to 0.34)	-1.09 (-3.54, -0.68; -13.00 to 0.15)	-3.87 (-5.01, -2.59; -19.01 to -0.01)	-2.40 (-3.08, -2.33; -2.26 to -3.75)	-5.21 (-8.30, -2.52; -10.30 to -1.45)
Visual Field Index (%) at the baseline visit	91.0 (76.3, 96.8; 26.0 to 100.0)	98.0 (95.0, 99.0; 69.0 to 100.0)	94.0 (88.0, 97.0; 43.0 to 99.0)	99.0 (94.0, 99.0; 89.0 to 99.0)	89.0 (83.5, 96.0; 78.0 to 98.0)
Pattern Standard Deviation (dB) at the baseline visit	5.51 (2.28, 10.28; 1.20 to 15.78)	1.72 (1.61, 2.52; 1.25 to 12.82)	3.36 (2.02, 6.11; 1.80 to 13.88)	1.92 (1.75, 3.33; 1.58 to 4.73)	3.03 (1.97, 4.79; 1.87 to 5.59)
Number of retinal ganglion cells derived from perimetry at the baseline visit	621,730 (491789, 762355; 90199 to 1243545)	890949 (756695, 1038451; 390239 to 1075758)	681650 (614492, 830132; 231515 to 1086445)	785756 (686.054, 809,276; 586352 to 832796)	606,858 (389,230, 901,644; 249409 to 8714052)

Table 3.22. The perimetric characteristics (median, lower and upper; range) at the entry visit, of the most severely affected eye, by diagnosis, for the 112 individuals with five or more reliable visual field examinations over a minimum follow-up of 5 years.

Chapter 4

Optic nerve head image registration, sizing and alignment, and viewing

4.1 Aim

The purpose of this Chapter is twofold: firstly to describe the hardware and the features produced by the associated custom software for viewing of the various ONH images; and secondly to describe the techniques used for scaling and aligning the ONH images from the various photographic sources.

4.2 Hardware

The ONH images were viewed with the computer-assisted stereoscopic system and customised software initially developed by Morgan and colleagues (Morgan et al. 2005a; Morgan et al. 2005b; Morgan et al. 2012) and subsequently modified for the purposes of this thesis. A personal computer was used in conjunction with a 19 inch flat screen monitor (Trinitron G420, Sony, Tokyo, Japan) featuring 16-bit colour and 1280x1024 resolution. The stereo presentation was facilitated by a Z-screen (Stereo Graphics Corporation, San Rafael, CA), placed over the screen of the monitor. The Z-screen controlled the orientation of the polarisation of the transmitted light and a set of passive polarising eyewear ensured the separation of the left and right on-screen images to the respective eyes.

4.3 Software

Custom-software firstly created a database of images for each individual and secondly generated the mono- and stereo-viewing conditions in conjunction with the Z-screen.

For any given individual, the biographical information, the designation of each ONH image for the given stereo-pair, the corresponding keratometry and refraction values, the name of the camera and the date of examination were entered into the software (Figure 4.1).

The screenshot shows a software window titled "Examination Details" with the following fields and values:

Patient Details			
First Name	Last Name	DOB	Patient ID
17	SFIGP	04/04/1939	[Redacted]

Exam Details			
Right Eye		Left Eye	
Right Image Path	[Select Image]	Right Image Path	[Select Image]
Left Image Path	[Select Image]	Left Image Path	[Select Image]

Variables			
k1	7.5	Sphere	1.0
k2	7.5	Cylinder	1.0
Camera	camera 1		
Exam Date	29/05/2014		

Buttons: OK, Cancel

Figure 4.1. A screenshot of the biographical information, the designation of each ONH image for the given stereo-pair, the keratometry values, the refraction, the name of the camera and the date of examination for a given individuals as presented from the software.

In order to generate the mono- and stereo-viewing conditions, the individual ONH images were stored in a .jpeg file format. As was discussed in Chapter 3, the images had been acquired from a variety of photographic sources, namely, 35mm slides, the Topcon TRC-IX (utilizing the Nikon D1X 20° camera) and the Topcon TRC-EX (utilizing the Sony 950P 20° camera). The multiplicity of sources and the presence, and the magnitudes, of image cropping, necessitated standardisation of the sizing and alignment of the various image outputs within any given individual.

In order to size and align the various types of image outputs, the two component images of each stereo-pair were aligned manually using the multiple align box in the software (Figure 4.2). This

alignment box enabled the images to be adjusted in size by using the zoom option and to correct any horizontal, vertical and rotational disparity between the two images. The judgement

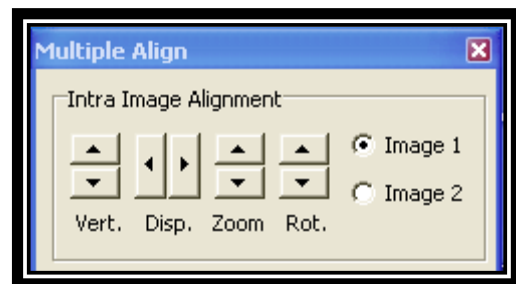


Figure 4.2. A screenshot of the multiple align box used for image alignment.

of the disparity in alignment was based upon the extent of the alignment of the ONH margin; the width and the orientation of the vessels and any anomalies or abnormalities such as PPA or ONH haemorrhage. This procedure was facilitated by the emergence of stereopsis from the two monoscopic images as the images became aligned. An identical procedure was undertaken to align the respective ONH images for the comparison of any chronological pair and this procedure could be further facilitated by flickering between the respective image pairs.

The software enabled a database which contained the ONH images of all the available stereo-pairs for each individual. The operator could choose any combination of chronological image-pairs in either stereoscopic or monoscopic viewing mode; select the frequency of the flicker (Figure 4.3); and add, delete or edit the details of the individual (Figure 4.4).

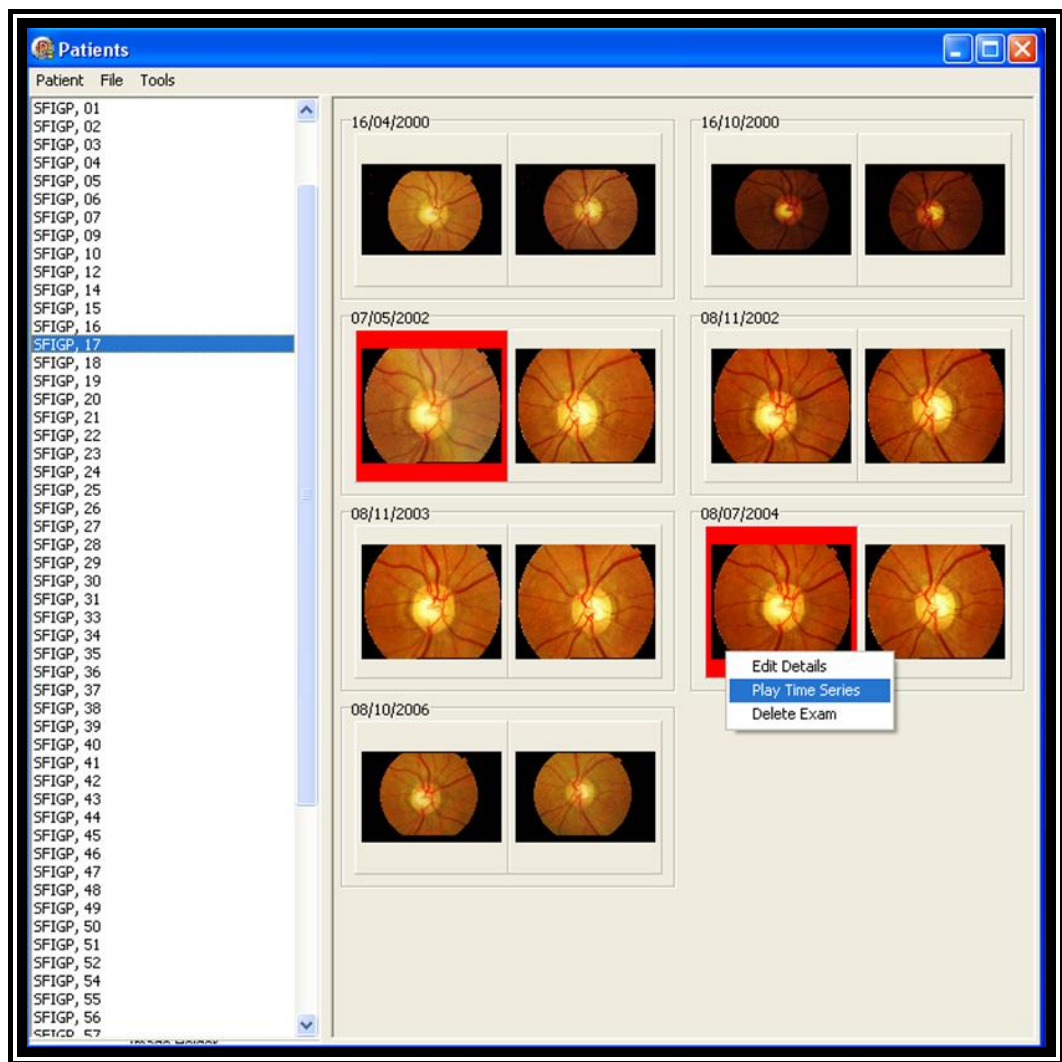


Figure 4.3. A screen capture of the database illustrating an ONH image for the right and left eyes, respectively, of a given individual at each of seven visits. The two images contained within the automatically generated red square, indicate the two time points, selected by the operator, for the given chronological comparison of the ONH characteristics.

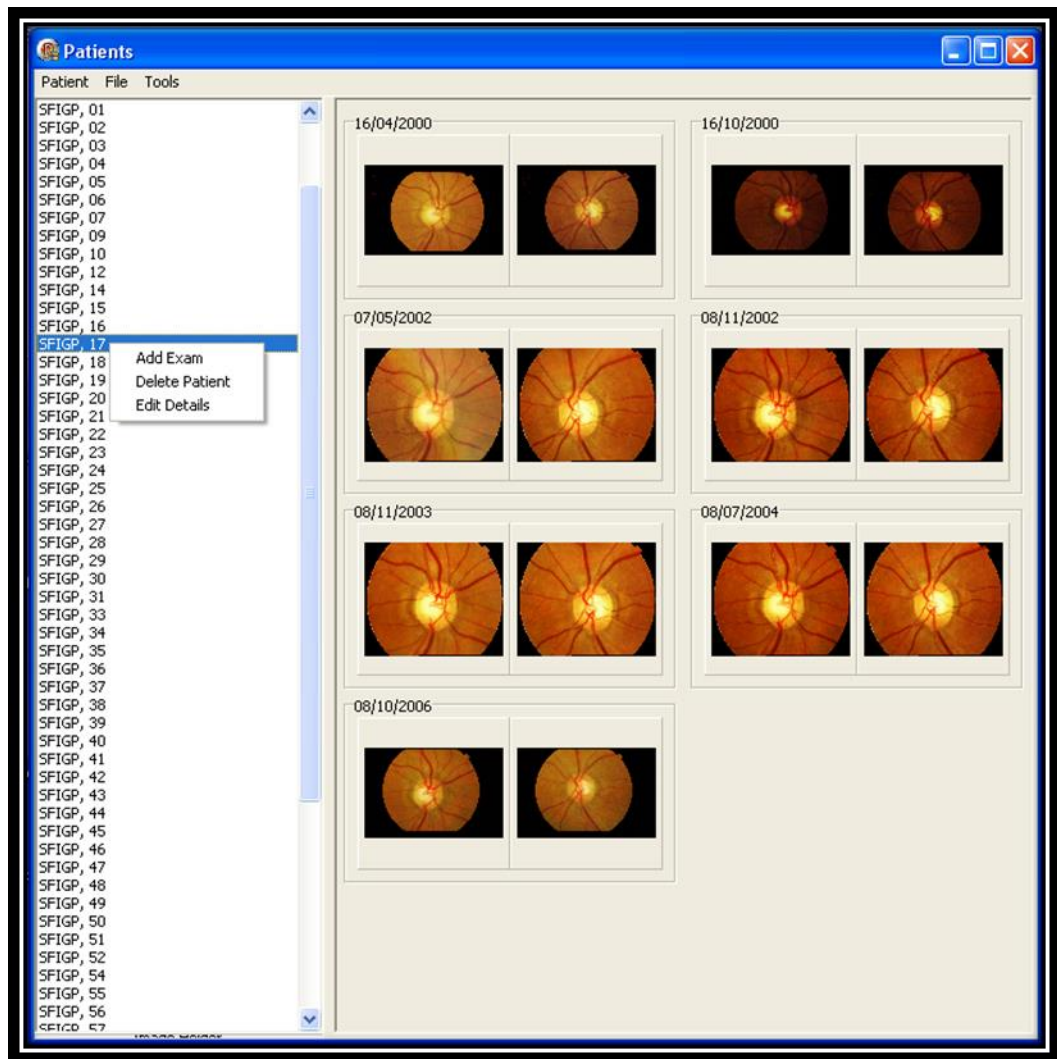


Figure 4.4. A screen capture of the database illustrating an ONH image for the right and left eyes, respectively, of a given individual at each of five visits.

The software also contained a vertical synchronisation unit which compressed each stereo-pair to half of its original height and the separate right and left images were interlaced to form a single image. The resultant interlaced image contained the same number of compressed lines from each of its component images but only half the information contained in the original images. The interlaced image was stored as a .tcf file rather than a .jpeg file in order to ensure faster loading and automated decompression of the file when viewed within the software. The .tcf file format ensured that the reading process for the given file and the sequence of the colour triplets (RGB to BGR) was achieved without loss of

information. The refresh rate of the image was set to a level that allowed the observer to perceive a single stereoscopic image.

The software enabled a range of magnification from x0.33 to x100 which was based upon the principles of sub-pixelation. For a 1:1 scale, each individual pixel of the ONH image represents one individual pixel on the screen and for a 2:1 scale, 4 pixels on the screen. When the observer operated the zoom function, any four contiguous pixels are averaged to create a sub-pixel. The sub-pixelation enhanced the resolution of the image.

The software colour-balanced, for a given individual, all the ONH images relative to the baseline image. The balancing was achieved by using the sub-pixelation technique, described above, to achieve the identical chromatic average of each image to that of the baseline by adjusting the weighted average of the red, green and blue channels. In addition, the colour-balancing was adjusted as a function of the magnification at any given stage of the zoom function.

The image for monoscopic viewing was not compressed and, obviously, did not require the polarising eyewear. By convention, the right component of each image-pair was always displayed monoscopically.

The software enabled either a static ‘side-by-side’ comparison or a flickered comparison. The frequency of the flicker (‘Flicker Rate’) was manually adjustable and ranged from 0Hz to 80Hz. The sequential comparison of the chronologically successive stereo-pairs was achieved by quad-buffer representation whereby each eye receives a separate image for each stereo-pair, the data of which is held in one of four buffers. The separate images of the left and the right views of the first stereo-pair are stored in one double buffer and the corresponding images for the comparison stereo-pair in a second double buffer. The quad-buffer method is used to obtain flicker at a frequency exceeding that of the critical fusion frequency of the eye.

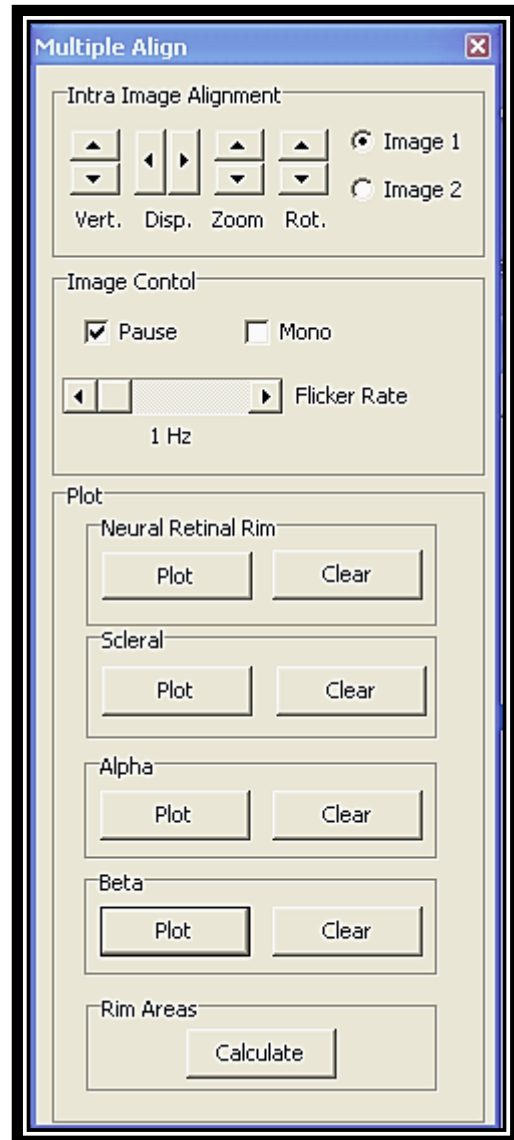


Figure 4.5. Multiple align box option

By convention, the first stereo-pair of any comparison (‘Image 1’) was always the chronological older image of the paired-comparison. The observer had the option to pause the ‘flicker’ option, immediately, and/ or to change the viewing mode from stereo- to mono-viewing, in only one screen (Figure 4.5). The software also provided the option for a greyscale viewing of the ONH images.

The software enabled planimetry of the cup, the ONH margin, and the α - and β -PPA zones, respectively, in both stereo- and mono-viewing modes. The planimetry in stereo-viewing was undertaken using a 'floating-cursor' whereby the depth of the cursor matched the depth of the given feature and hence overcame parallax errors which would have resulted had the cursor being in a fixed plane. The cup and the ONH margin and the α -zone of the PPA were each delineated in black and the β -zone of the PPA in white.

The clicking of the 'calculate' option (Figure 4.5) terminated the planimetry and saved the outcome as a .txt file in the same directory as the .tcf and the .jpeg files of the corresponding image.

The software calculated the sectorial area of each ONH parameter in digital (pixels) units for each 5° sector and also for the composite of each parameter. The centre of gravity for the cup area, as demarcated by the operator, was used as the reference point for the sectors. The sectors were labelled from the horizontal temporal meridian and followed the sequence of temporal, superior, nasal, and inferior meridians in each eye. The 5° sectorization enabled the areal calculation of any given feature in 5° multiples. The software automatically recorded the viewing mode and the outcome of planimetry in separate .txt files.

A 'Ruler' option was available which enabled a measurement of the cup depth at the given location of the cursor. A 'Rings' option was also available which enabled a series of concentric circles of fixed varying radii to act as a visual reference for either the cup or the ONH margins. A 'Reload' option reset the

images from the colour-balanced image to the original colour texture. None of these options were used in the studies described in Chapter 5 and Chapter 6.

4.4 Equalizing the ONH image size from the various photographic sources

The stereo-image pair for any given individual for the given photographic source at the given visit, was adjusted manually to a size which occupied approximately one third of the 19 inch screen of the monitor (Figure 4.6). The resultant images between Visits 1 and 2 were resized and aligned by manually increasing the size of one image and/ or reducing the size of the other, depending upon the original sizes of the respective images from the given two different photographic sources. The size for any given subsequent between-visit comparison for an individual was manually adjusted to that of the image size used for (i.e., referenced to) the comparison between Visits 1 and 2 (Figure 4.6).

In order to ensure that consistency had been achieved in the manual adjustment between the images from a given photographic source relative to those from another, scaling factors were calculated for the various combinations of photographic sources. The scaling factor was calculated for two separate comparisons. Firstly, the scaling factor was calculated between the original image size of the stereo-pair derived at any visit for an individual and the corresponding image resulting from the manual alignment of the two images at any given comparison. The latter, itself, was influenced by the sizing of the image derived from the subsequent visit. Secondly, a scaling factor was calculated between the manually aligned images for any between-visit comparison within each individual (Figure 4.6).

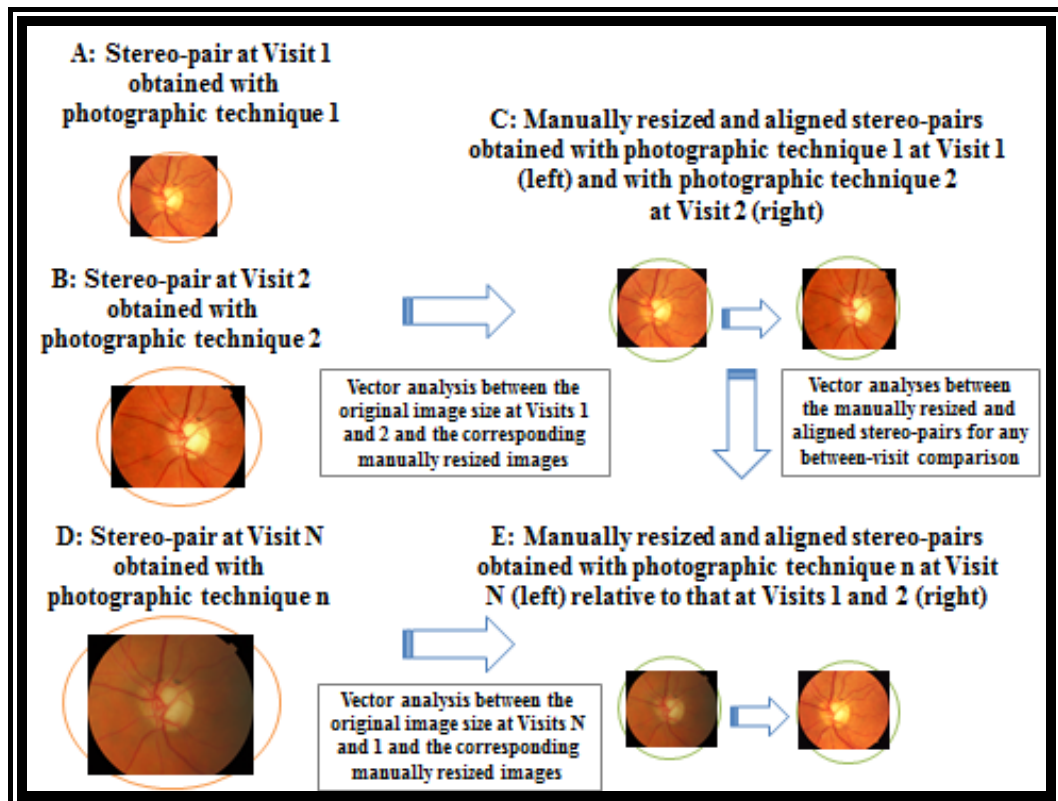


Figure 4.6. A schematic illustrating the procedure for the manual resizing of the original photographic images for any visit (A, B, D) and the manually resized and aligned stereo-pairs (E) relative to those between Visits 1 and 2 (C). The associated vector comparisons for the calculation of the scaling factor are also shown.

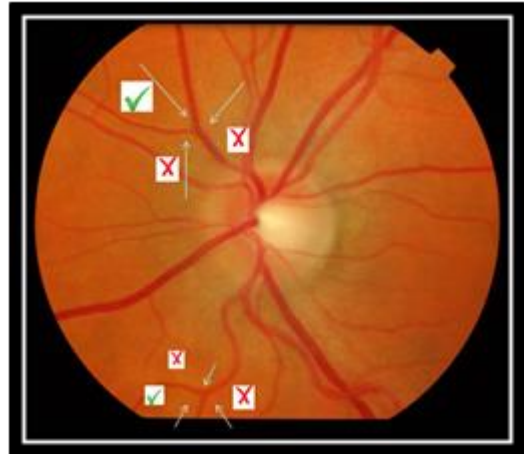
In the absence of a ‘gold standard’ method to quantify the scaling, a novel quantitative technique was adopted to provide some insight into the consistency of the scaling factor within each of the photographic sources, between individuals. Twenty-eight vectors were drawn on each of the images for the given individual, based upon 8 predetermined features inherent in the images for that individual. Each vector defined the distance and the orientation between the same two ‘key’ features within each ONH image. The difference in the lengths of the given pair of vectors between the original image from the given respective photographic source and that at any given between-visit comparison, and the difference in the lengths of the given pair of vectors between the manually resized and aligned stereo-pairs for any between-visit comparison, were

separately used to calculate the corresponding scaling factors. The former described the magnitude of the resizing of the original images whilst the latter provided the error associated with the manual resizing and alignment of the stereo-pairs between-visits. For the second approach, the technique assumed that if the manual alignment of the four images, i.e., the right and left images of each stereo-pair, was acceptable, then the error between the two visits would be minimal in terms of both the vector length and the orientation. For each analysis the scaling factor was defined as the median of the differences.

The comparison was undertaken using Image J software version J 1.47u/ Java 1.6.0_24 (32-bit) (National Institutes of Health, Bethesda, MA) which quantified the length of the given vector in pixels by taking the difference in the x and in the y coordinates, respectively, between the two edge points defining the vectors for the original and the manually-aligned images.

Eight features from the given pair of stereo ONH images (i.e. between the two given separate visits) within an individual were selected and vectors drawn between each of these 8 features using the rectangular tool of the Image J software. The total number of vectors was 28. The features had to be present across the images from all photographic sources within an individual and were generally situated one ONH diameter or more from the ONH and comprised vessel bifurcations, crossing of vessels, and prominent bends in the vessels.

The features were selected on a hierarchical basis in terms of their prominence and their likelihood of being unaffected by the glaucomatous process; were also chosen to maximise, wherever possible, the length of the vectors and to be approximately distributed across the four quadrants. A vessel bifurcation



was defined as the branching of the vessels in the direction of the periphery of the image (Figure 4.7). The centre of the Cartesian system for each individual was defined as the centre of the cup (Figure 4.8).

Figure 4.7. Two examples of the position of a vessel bifurcation, indicated by the ✓ symbol, considered suitable for the vector analysis. The ✗ symbols represent unsuitable, positions of the same bifurcations.

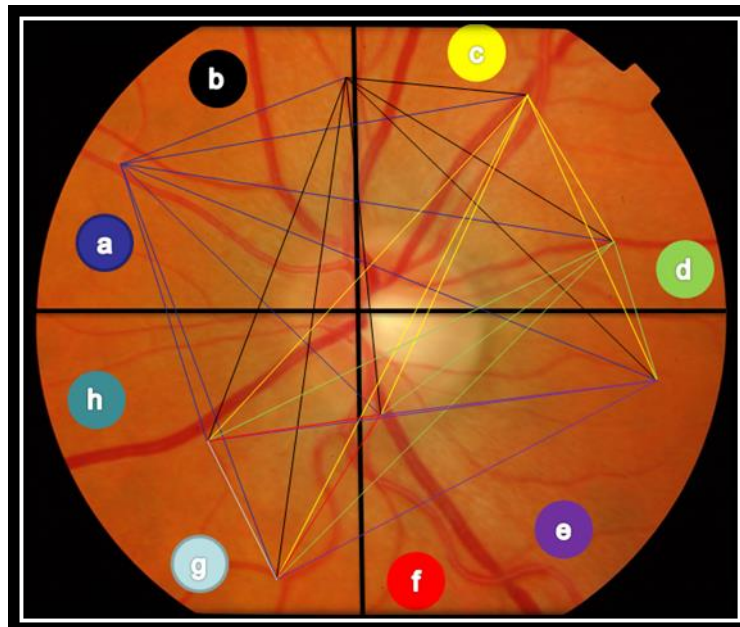


Figure 4.8. The eight features (a to h inclusive) selected for the vector analysis, and the corresponding 28 vectors, illustrated for a given stereo-pair for a given individual.

4.5 Results

The median (lower and upper quartiles; range) for the proportionate difference, in the magnitudes of the x and y coordinates of all 28 vectors considered together, between the original image and the manually resized image for each given imaging modality, at a randomly selected visit, amongst the 27 individuals are given in Table 4.1.

Imaging modality (pixels)	Number of comparisons (vectors)	Median, lower and upper quartiles; range of the proportionate difference in the magnitude of the vectors (%)	
		x coordinate	y coordinate
35mm slide (2000 x 1312)	4 (112)	-31.1 (-42.0, -20.7; -77.1 to 733.3)	-30.5 (-42.9, -26.0; -75.0 to 166.7)
35mm slide (3008 x 1960)	5 (140)	-50.0 (-59.0, -24.7; -88.5 to 100.0)	-52.1 (-58.3, -30.7; -97.7 to 966.7)
Topcon TRC- IX (768 x 576)	25 (700)	11.2 (-1.2, 26.4; -87.9 to 6520.0)	13.1 (-1.1, 25.8; -100.0 to 314.3)
Topcon TRC- EX (3008 x 1960)	27 (756)	-56.5 (-59.3, -54.1; -100.0 to 15.2)	-56.7 (-59.6, -54.2; -100.0 to 83.3)

Table 4.1. The summary statistics (median, lower and upper quartiles; range) for the proportionate difference, in the magnitudes of the x and y coordinates of all 28 vectors considered together, between the original image and the manually resized image for each given imaging modality, at a randomly selected visit, amongst the 27 individuals.

The corresponding median (lower and upper quartiles; range) for the proportionate difference, in the magnitudes of the x and y coordinates of all 28 vectors considered together, between the manually resized and aligned images, by paired photographic modalities, at a randomly selected between-visit comparison, amongst the 27 individuals are given in Table 4.2.

Imaging modality (pixels)	Number of comparisons (vectors)	Median, lower and upper quartiles; range of the proportionate difference in the magnitude of the vectors (%)	
		x coordinate	y coordinate
35mm slide (2000 x 1312)/ 35mm slide (3008 x 1960)	0	-	-
35mm slide (2000 x 1312)/ Topcon TRC- IX (768 x 576)	2 (56)	1.5 (-0.6, 3.0; -3.6 to 75.0)	-0.9 (-1.8, 0.6; -18.2 to 50.0)
35mm slide (2000 x 1312)/ Topcon TRC- EX (3008 x 1960)	4 (112)	-1.3 (-3.2, 3.1; -22.7 to 120.0)	-2.4 (-4.2, 0.0; -50.0 to 200.0)
35mm slide (3008 x 1960)/ 35mm slide (3008 x 1960)	1 (28)	-1.6 (-4.6, 0.1; -12.5 to 3.5)	-2.2 (-6.7, 1.7; -33.3 to 12.8)
35mm slide (3008 x 1960)/ Topcon TRC- IX (768 x 576)	5 (140)	-1.6 (-3.8, 0.0; -50.0 to 28.9)	-1.5 (-4.6, 0.8; -47.8 to 300.0)
35mm slide (3008 x 1960)/ Topcon TRC- EX (3008 x 1960)	5 (140)	-2.1 (-4.0, 2.2; -30.8 to 29.5)	-0.3 (-4.0, 1.4; -60.0 to 83.3)
Topcon TRC- IX (768 x 576)/ Topcon TRC- IX (768 x 576)	10 (280)	0.0 (-2.0, 1.5; -75.6 to 500.0)	0.0 (-1.7, 1.7; -30.8 to 200.0)
Topcon TRC- IX (768 x 576)/ Topcon TRC- EX (3008 x 1960)	23 (644)	0.0 (-2.0, 1.7; -100.0 to 400.0)	0.0 (-1.4, 2.1; -100.0 to 300.0)
Topcon TRC- EX (3008 x 1960)/ Topcon TRC- EX (3008 x 1960)	9 (252)	-1.2 (-2.8, 0.7; -33.3 to 300.0)	-0.4 (-2.5, 1.8; -75.0 to 400.0)

Table 4.2. The summary statistics median (lower and upper quartiles; range) for the proportionate difference, in the magnitudes of the x and y coordinates of all 28 vectors considered together, between the manually resized and aligned images, by paired photographic modalities, at a randomly selected between-visit comparison, amongst the 27 individuals.

4.6 Discussion

The median for the proportionate difference, in the magnitudes of the x and y coordinates of all 28 vectors considered together, between the manually resized and aligned images, by paired photographic modalities, at a randomly selected between-visit comparison, amongst the 27 individuals ranged from -2.4% to 1.5%. The interquartile range associated with each median reflected the narrowness of each distribution. Such values indicate the precision, overall of the manual alignment. However, the magnitudes of the range associated with each of the individual comparisons reflected the limitations of the vector analysis rather than that of the manual alignment in that such range would be clinically impossible. These values resulted from the consistency in denoting the prominent anatomical features (i.e. bifurcations) arising from variations in resolution between the photographic sources particularly when one or more images had been cropped. Clearly, such large values could not have occurred by manual visual alignment.

The outcome from stereo-imaging of the ONH is highly dependent upon the optimum alignment within a stereo-pair and between chronologically different stereo-pairs. The delineation of the ONH and NRR margins is adversely influenced by both the translation (displacement) and the rotation of one image relative to the other image within a stereo-pair or from one stereo-pair to another. Failure to correct for such effects leads to parallax errors and resultant inaccuracies in the evaluation of the NRR. Differences in disparity between image-pairs reduce the degree of stereopsis and also create discomfort in viewing for the observer. The digital alignment of the stereo-pairs is generally undertaken

manually (Heijl and Bengtsson 1989; Yogesan et al. 1999; Berger et al. 2000; Morgan et al. 2005a; Morgan et al. 2005b; Kamdeu Fansi et al. 2011; Syed et al. 2011), although some studies have attempted software controlled alignment with only limited success (Ng et al. 2015).

To the Author's knowledge, there is no commercially available software which enables a more accurate alignment than that by an experienced clinical operator. Such an operator is able to align the image-pair based upon alignment of the morphological clinical features (vessel pattern, ONH tilt etc.) and to compensate, in the same way, for rotational issues arising from photographic artefacts. The results described above indicate that the manual alignment was clinically acceptable.

Chapter 5

The qualitative assessment of progressive glaucomatous ONH damage using both mono- and stereo-flicker chronoscopy

5.1 Introduction

A novel approach to the evaluation of progressive structural damage of the ONH is flicker chronoscopy whereby two sequential monoscopic digital images of the ONH are successively viewed (i.e., flickered) with a predetermined temporal frequency (Heijl and Bengtsson 1989; Yogesan et al. 1999; Berger et al. 2000; Corona et al. 2002; Radcliffe et al. 2010; VanderBeek et al. 2010) (Chapter 4). Such a technique has only been used monoscopically. The advantage of monoscopic flicker chronoscopy over ‘side-by-side’ stereo-viewing is equivocal. Both viewing techniques exhibit comparable sensitivity in the identification of progressive ONH damage and of progressive visual loss (Radcliffe et al. 2010; VanderBeek et al. 2010) and comparable specificity when structural change is absent (Berger et al. 2000). High between-observer variability can be present with flicker chronoscopy and the outcome can also exhibit poor concordance with progressive ONH damage as designated by Heidelberg Retinal Tomography (HRT), scanning laser polarimetry (SLP), and/ or OCT and also with progressive visual field loss (Syed et al. 2011). However, mono-flicker chronoscopy exhibits better sensitivity for determining an increase in PPA (VanderBeek et al. 2010; Kamdeu Fansi et al. 2011) and in the detection of emergent disc haemorrhages

(Bengtsson and Krakau 1979; Leske et al. 2007; Bengtsson et al. 2008; Cymbor et al. 2009; VanderBeek et al. 2010; Syed et al. 2012).

A digital stereo-viewing planimetric technique has been developed by Morgan and colleagues (Morgan et al. 2005a; Morgan et al. 2005b; Morgan et al. 2012) and is discussed in Chapter 4. The accompanying software enables modification to permit mono- and stereo-flicker chronoscopy and, therefore, presents a unique opportunity to evaluate the performance of stereo-flicker chronoscopy over the traditional mono-flicker chronoscopy and also in regards to the advantages of digital imaging.

5.2 Aim

The overall aim of the study was twofold. Firstly, to compare the efficacy of digital stereo-flicker chronoscopy using the modified software of Morgan and colleagues to that from mono-flicker chronoscopy for the qualitative identification of glaucomatous ONH damage in a case series of individuals attending a glaucoma clinic with a long follow-up. Secondly, to determine the relationship between the qualitative assessment of any progressive glaucomatous ONH damage and the concomitant visual field outcome.

5.3 Methods

The cohort comprised the 61 individuals described in Section 3.3.1, Chapter 3, with two or more stereo-images and five or more reliable visual field examinations, and with each pair of respective examinations conducted within 12 months of each other. The ONH images for each individual were randomly assigned between eyes.

The summary statistics (median, lower and upper quartiles; range) of the demographics and of the clinical characteristics for the 61 individuals in the randomly assigned eye at their baseline visit are shown in Table 5.1 and Table 5.2, respectively (it should be noted that the information contained in these latter Tables is different to that contained in Tables 3.15 to 3.16 which is based upon the most severely affected eye, [Chapter 3]). The latter was used to determine the diagnosis whilst the randomly selected eye was used to encompass the full range of disease stage.

Two consultant ophthalmologists ('A' and 'B'), trained to fellowship standard in glaucoma, undertook the qualitative and the quantitative assessment of the ONH images. The ONH images were viewed with the four separate viewing techniques (mono-, mono-flicker, stereo-, and stereo-flicker) using the flat screen monitor and the embedded Z-screen together with the passive polarising filter eyewear described in Chapter 4. The 'right' image of each stereo-pair was used for each of the two mono-viewing techniques.

Diagnosis (No of individuals)	Primary open-angle glaucoma (34)	Ocular hypertension (11)	Normal-tension glaucoma (5)	Glaucoma Suspect (8)	Others (3)
Age (yrs) at the baseline visit	69.3 (59.6, 73.8; 38.9 to 89.4)	64.4 (56.3, 68.2; 43.9 to 71.4)	69.6 (64.8, 72.4; 61.0 to 73.3)	63.2 (46.7, 65.3; 34.1 to 77.6)	45.8 (37.3, 55.3; 28.8 to 64.7)
Male : Female	16 : 18	5 : 6	4 : 1	3 : 5	2 : 1
Perimetric follow-up (yrs)	7.3 (6.1, 8.4; 3.1 to 10.0)	6.3 (5.3, 8.0; 4.0 to 10.8)	9.2 (7.2, 10.3; 5.8 to 10.3)	7.8 (6.6, 8.5; 4.2 to 9.8)	9.5 (9.5, 9.9; 9.4 to 10.3)
Number of perimetric visits	7.0 (6.0, 8.0; 5.0 to 12.0)	6.0 (6.0, 8.0; 5.0 to 10.0)	8.0 (7.0, 11.0; 6.0 to 12.0)	6.5 (5.8, 7.3; 5.0 to 8.0)	7.0 (7.0, 7.5; 7.0 to 8.0)
Photographic follow-up (yrs)	3.9 (2.4, 5.8; 0.4 to 9.1)	3.4 (2.4, 4.1; 0.3 to 9.3)	5.3 (4.3, 5.3; 3.4 to 6.3)	5.0 (2.1, 5.9; 2.0 to 9.7)	4.4 (3.7, 5.6; 3.0 to 6.8)
Number of photographic visits	3.0 (2.0, 3.0; 2.0 to 5.0)	2.0 (2.0, 4.0; 2.0 to 6.0)	4.0 (3.0, 4.0; 2.0 to 7.0)	3.5 (2.0, 4.3; 2.0 to 5.0)	3.0 (2.5, 3.5; 2.0 to 4.0)
Maximum duration of follow-up (yrs)	8.9 (7.4, 9.7; 5.4 to 10.8)	10.0 (8.5, 11.0; 5.1 to 11.7)	9.2 (8.0, 9.3; 7.8 to 10.3)	9.9 (8.4, 10.9; 4.7 to 15.0)	10.0 (9.7, 10.1; 9.4 to 10.3)

Table 5.1. The demographic characteristics (median, lower and upper quartiles; range) of the randomly assigned eye of the 61 individuals at the baseline visit.

Diagnosis (No of individuals)	Primary open-angle glaucoma (34)	Ocular hypertension (11)	Normal-tension glaucoma (5)	Glaucoma Suspect (8)	Others (3)
Mean Deviation (dB) at the baseline visit	-4.07 (-6.93, -2.31; -22.09 to -0.37)	-1.09 (-2.57, -0.71; -5.55 to -0.26)	-5.74 (-7.74, -5.01; -18.16 to -1.87)	-2.64 (-4.14, -1.77; -6.22 to 0.69)	-1.60 (-8.04, -1.52; -14.48 to -1.43)
Visual Field Index (%) at the baseline visit	94.0 (84.8, 97.8; 31.0 to 99.0)	98.0 (96.5, 99.0; 94.0 to 100.0)	91.0 (74.0, 94.0; 54.0 to 98.0)	95.0 (89.0, 97.3; 86.0 to 100.0)	85.0 (69.5, 91.5; 58.0 to 98.0)
Pattern Standard Deviation (dB) at the baseline visit	2.69 (1.91, 5.15; 1.29 to 14.42)	1.73 (1.51, 1.96; 1.03 to 3.09)	4.72 (3.36, 8.79; 2.21 to 9.38)	2.70 (2.25, 3.76; 1.39 to 5.26)	2.98 (2.33, 6.15; 1.67 to 9.32)
Intraocular Pressure (mmHg) at the baseline visit	24.00 (20.80, 28.00; 11.00 to 39.00)	25.00 (22.00, 28.50; 19.00 to 38.00)	19.00 (16.80, 20.50; 13.00 to 22.00)	19.50 (17.80, 20.00; 15.00 to 20.00)	16.00 (16.00, 17.50; 16.00 to 19.00)
Vertical cup-to-disc ratio at the baseline visit	0.70 (0.61, 0.80; 0.30 to 0.90)	0.50 (0.30, 0.50; 0.10 to 0.70)	0.70 (0.69, 0.75; 0.65 to 0.90)	0.60 (0.55, 0.63; 0.50 to 0.70)	0.50 (0.35, 0.60; 0.20 to 0.70)

Table 5.2. The clinical characteristics (median, lower and upper quartile; range) of the randomly assigned eye of the 61 individuals at the baseline visit.

Each observer attended for two separate sessions of approximately 5 hours per session. Each observer evaluated all possible pairs of ONH images over the time series with each of the four viewing techniques and designated each pair of ONH images as either 'glaucoma' or 'not glaucoma'. The total viewing time across the two sessions was 4.2 hours for Observer 'A' and 5.6 hours for Observer 'B'.

The ONH images were presented in a pre-determined pseudo-random sequence which differed across individuals (Figure 5.1). The observers were masked as to the nature of the pre-determined sequence. When an observer responded 'glaucoma' to any one of the paired comparisons, the observer was further required to designate the presence or absence of glaucomatous ONH progression between the two images in the given pair. For any given pair of images, the prior image in the time series always preceded the later image such that the judgement by the observer required the identification of a 'deterioration' rather than an 'improvement'.

In the individuals with three or more available ONH images (i.e. 3 or more comparisons per viewing technique) 'Definite progression' was defined as a consistent progression in the ONH across the appropriate comparisons and was scored as '1'. 'Possible progression' was scored as '2' and was defined either as a progression between the first two or more comparisons, which was not present between the first and last images of the series, or as progression between the first and the last images, alone. 'Inconsistent progression' was scored as '3' and denoted apparent progression between a given pair of images which was not

substantiated by other comparisons. 'No-progression' was scored as '4'. An incorrect diagnosis was scored as 'x'.

A second digit defined the ranking of the four viewing techniques in identifying the earliest progression. The second digit ranged from '1 to 4' (i.e. one value for each of the four viewing techniques), with the lower value representing the earliest designation of progression.

Individuals with only two visits (i.e. one comparison per viewing technique) could only be scored as '1', '4' or 'x', due to the limitation in the number of comparisons.

The combined time for the diagnostic designation and for the identification of progression, by each observer, was recorded for each of the paired comparisons for each method.

Each observer was further instructed to evaluate the given pair of ONH images, in terms of their image quality, using a grading from 1 (poor) to 5 (excellent). The outcome of the diagnostic designation for each paired comparison for each viewing technique for each observer was evaluated relative to the hospital diagnosis at the UHW.

Individuals	1st Comparison					2nd & 3rd Comparisons					4rth, 5th & 6th Comparisons					7th to 21st Comparisons			
	2 Visits					3 Visits					4 Visits					5, 6 & 7 Visits			
SFIGP 01	M	MF	S	SF		M	MF	S	SF										
...	MF	S	SF	M															
...	S	SF	M	MF		MF	S	SF	M		M	MF	S	SF					
...	SF	M	MF	S															
...	SF	M	MF	S		S	SF	M	MF		MF	S	SF	M					
...	S	SF	M	MF		SF	M	MF	S										
...	MF	S	SF	M		SF	M	MF	S										
...	M	MF	S	SF		S	SF	M	MF		S	SF	M	MF		M	MF	S	SF
...	M	MF	S	SF		MF	S	SF	M										
...	MF	S	SF	M							SF	M	MF	S					
...	S	SF	M	MF		M	MF	S	SF		SF	M	MF	S					
...	SF	M	MF	S		M	MF	S	SF		SF	M	MF	S		MF	S	SF	M
...	SF	M	MF	S		MF	S	SF	M		S	SF	M	MF					
...	S	SF	M	MF															
...	MF	S	SF	M		M	MF	S	SF		M	MF	S	SF					
...	S	SF	M	MF		MF	S	SF	M										
...	SF	M	MF	S		S	SF	M	MF		M	MF	S	SF		S	SF	M	MF
...	SF	M	MF	S															
...	S	SF	M	MF		SF	M	MF	S										
...	MF	S	SF	M															
...	M	MF	S	SF															
...	M	MF	S	SF															
SFIGP 61	MF	S	SF	M		SF	M	MF	S		MF	S	SF	M					

Figure 5.1. A schematic illustrating, by visit, the pseudo-randomization of the four viewing techniques (mono-, mono-flicker, stereo-, stereo-flicker) across the 61 individuals.

5.4 Results

Each observer undertook 872 paired comparisons of the ONH images (218 evaluations for each of the four methods). The median (lower and upper quartiles; range) of the image quality, scored on a 0-5 scale, by observer and by viewing technique, for the 50 individuals with glaucoma (top) and for the 11 individuals with ocular hypertension (bottom), evaluated between each of the first three visits is given in Table 5.3.

The mean of the differences and the corresponding 95% limits of agreement, for the within-observer ‘test-retest’ variability in the assessment of image quality of the ONH images for the 30 individuals with glaucoma and with three or more images, for each of the viewing techniques, for each observer, within the first three visits is given in Table 5.4 (top). The between-observer variability in the assessment of image quality for the second of the two image evaluations for each of the viewing techniques within the first three visits is given in Table 5.4 (bottom). The corresponding information for the 5 individuals with ocular hypertension and with three or more ONH images is given in Table 5.5 (top and bottom). Observer ‘A’ was marginally more consistent than Observer ‘B’ for the within-observer ‘test-retest’ assessment of image quality for the images from the individuals with glaucoma or from the individuals with ocular hypertension. No particular trend was apparent by viewing technique. The agreement between observers in the assessment of image quality was good. It was slightly closer for the images from the individuals with glaucoma when assessed under stereo-viewing conditions compared to mono-viewing conditions.

Viewing method	Mono	Mono-Flicker	Stereo	Stereo-Flicker
Observer 'A'				
Image 1 Visits (1-2)	3 (3, 4; 2 to 5) 4 (3, 4; 2 to 4)	4 (3, 4; 2 to 5) 4 (3.5, 4; 4 to 3)	4 (3, 4; 2 to 5) 4 (3, 4; 3 to 4)	4 (3, 4; 2 to 5) 4 (3, 4; 2 to 4)
Image 1 Visits (1-3)	3 (3, 4; 2 to 5) 4 (4, 4; 2 to 4)	3.5 (3, 4; 2 to 5) 4 (3, 4; 2 to 4)	3.5 (3, 4; 2 to 5) 4 (3, 4; 2 to 5)	3 (3, 4; 2 to 5) 4 (3, 4; 2 to 4)
Image 2 Visits (1-2)	3.5 (3, 4; 1 to 5) 4 (3, 4; 2 to 4)	4 (3, 4; 2 to 5) 4 (3.5, 4; 4 to 2)	4 (3, 4; 2 to 5) 4 (3, 4; 3 to 4)	4 (3, 4; 2 to 5) 4 (3, 4; 2 to 4)
Image 2 Visits (2-3)	4 (3, 4; 2 to 4) 4 (3, 4; 3 to 4)	4 (3, 4; 2 to 4) 4 (4, 4; 2 to 4)	4 (3, 4; 2 to 4) 4 (3, 4; 3 to 4)	4 (3, 4; 2 to 5) 4 (3, 4; 3 to 4)
Image 3 Visits (2-3)	3 (3, 4; 2 to 5) 4 (3, 4; 2 to 4)	4 (3, 4; 2 to 4) 4 (3, 4; 2 to 4)	4 (3, 4; 2 to 5) 4 (3, 4; 2 to 4)	4 (3, 4; 2 to 4) 4 (3, 4; 2 to 4)
Image 3 Visits (1-3)	3 (3, 4; 2 to 5) 4 (3, 4; 2 to 4)	4 (3, 4; 2 to 5) 4 (3, 4; 2 to 4)	3 (3, 4; 2 to 5) 4 (3, 4; 2 to 5)	3 (3, 4; 2 to 5) 3 (3, 4; 2 to 4)
Observer 'B'				
Image 1 Visits (1-2)	3 (3, 4; 1 to 4) 3 (3, 4; 2 to 4)	3 (3, 4; 1 to 4) 3 (3, 4; 2 to 4)	3 (3, 4; 1 to 5) 3 (3, 4; 2 to 4)	3 (3, 4; 1 to 4) 4 (3, 4; 3 to 4)
Image 1 Visits (1-3)	3 (3, 3; 2 to 5) 4 (3, 4; 2 to 4)	3 (3, 4; 2 to 5) 3 (3, 4; 2 to 5)	3 (3, 4; 2 to 4) 4 (3, 4; 2 to 5)	3 (3, 4; 2 to 5) 3 (3, 4; 2 to 5)
Image 2 Visits (1-2)	3 (3, 4; 2 to 4) 4 (3, 4; 2 to 4)	3 (3, 4; 2 to 4) 4 (3, 4; 2 to 4)	4 (3, 4; 2 to 5) 4 (4, 4; 3 to 4)	4 (3, 4; 2 to 4) 4 (3, 4; 3 to 4)
Image 2 Visits (2-3)	3 (3, 4; 2 to 5) 3 (3, 4; 2 to 4)	3 (3, 4; 2 to 5) 4 (3, 4; 2 to 4)	4 (3, 4; 2 to 4) 3 (3, 4; 3 to 4)	3 (3, 4; 2 to 5) 3 (3, 3; 2 to 4)
Image 3 Visits (2-3)	3 (3, 4; 2 to 5) 3 (3, 4; 3 to 4)	3 (3, 4; 2 to 5) 3 (3, 3; 2 to 4)	4 (3, 4; 2 to 5) 3 (3, 4; 3 to 4)	3.5 (3, 4; 2 to 5) 4 (3, 4; 2 to 4)
Image 3 Visits (1-3)	3 (3, 4; 2 to 5) 3 (3, 4; 2 to 4)	3 (2, 4; 2 to 5) 3 (3, 3; 3 to 4)	4 (3, 4; 2 to 5) 4 (3, 4; 2 to 5)	3 (3, 4; 2 to 5) 3 (3, 4; 2 to 5)

Table 5.3. The median (lower and upper quartiles; range) of the image quality, scored on a 0-5 scale, by observer and by viewing technique, for the 50 individuals with glaucoma (top) and for the 11 individuals with ocular hypertension (bottom), evaluated at each of the first three visits.

Within-observer agreement for the individuals with glaucoma				
Viewing method	Mono	Mono-Flicker	Stereo	Stereo-Flicker
Observer 'A'				
Image 1 (Visits 1-2 & 1-3)	0.1 (-1.0 to 1.2)	-0.1 (-0.9 to 0.8)	0.0 (-1.3 to 1.3)	-0.3 (-1.1 to 0.6)
Image 2 (Visits 1-2 & 2-3)	0.2 (-1.1 to 1.4)	0.0 (-1.4 to 1.4)	0.0 (-1.2 to 1.4)	-0.1 (-1.7 to 1.6)
Image 3 (Visits 1-3 & 2-3)	-0.1 (-1.3 to 1.1)	0.0 (-0.9 to 1.0)	-0.1 (-1.2 to 1.1)	-0.2 (-1.2 to 0.8)
Observer 'B'				
Image 1 (Visits 1-2 & 1-3)	0.0 (-1.0 to 1.0)	-0.1 (-1.1 to 1.0)	0.1 (-1.4 to 1.5)	0.3 (-0.1 to 1.5)
Image 2 (Visits 1-2 & 2-3)	-0.2 (-1.7 to 1.2)	-0.1 (-1.4 to 1.2)	-0.4 (-1.5 to 0.7)	-0.1 (-1.4 to 1.3)
Image 3 (Visits 1-3 & 2-3)	0.1 (-1.3 to 1.5)	-0.1 (-1.7 to 1.5)	0.0 (-1.1 to 1.1)	0.0 (-1.5 to 1.5)
Between-observer difference for the individuals with glaucoma				
Image 1 (Visits 1-3)	-0.3 (-1.6 to 1.0)	-0.3 (-1.5 to 1.0)	-0.1 (-1.5 to 1.4)	0.1 (-1.3 to 1.5)
Image 2 (Visits 2-3)	0.3 (-0.7 to 1.3)	-0.2 (-1.5 to 1.0)	-0.1 (-1.3 to 1.0)	-0.1 (-1.6 to 1.3)
Image 3 (Visits 1-3)	0.0 (-1.5 to 1.5)	-0.3 (-1.7 to 1.1)	0.1 (-1.3 to 1.6)	-0.1 (-1.7 to 1.6)

Table 5.4. The mean of the differences, and the corresponding 95% limits of agreement, for the within-observer 'test-retest' variability in the assessment of image quality for each of the viewing techniques, for each observer, within the first three visits, for the individuals with glaucoma (top) and the between-observer variability in the assessment of image quality for the second of the two image evaluations for each of the viewing techniques within the first three visits (bottom).

Within-observer agreement for the individuals with ocular hypertension				
Viewing method	Mono	Mono-Flicker	Stereo	Stereo-Flicker
Observer 'A'				
Image 1 (Visits 1-2 & 1-3)	0.0 (-1.4 to 1.4)	-0.4 (-1.5 to 0.7)	-0.2 (-1.8 to 1.4)	-0.4 (-1.5 to 0.7)
Image 2 (Visits 1-2 & 2-3)	0.0 (-1.4 to 1.4)	-0.2 (-1.1 to 0.7)	0.0 (-1.4 to 1.4)	0.0 (-1.4 to 1.4)
Image 3 (Visits 1-3 & 2-3)	0.0 (0.0 to 0.0)	0.0 (0.0 to 0.0)	0.0 (-1.4 to 1.4)	-0.2 (-1.1 to 0.7)
Observer 'B'				
Image 1 (Visits 1-2 & 1-3)	0.0 (-1.4 to 1.4)	0.0 (-2.0 to 2.0)	0.4 (-0.7 to 1.5)	-0.2 (-2.3 to 1.9)
Image 2 (Visits 1-2 & 2-3)	0.0 (0.0 to 0.0)	0.0 (-1.4 to 1.4)	-0.4 (-1.5 to 0.7)	-0.4 (-1.5 to 0.7)
Image 3 (Visits 1-3 & 2-3)	-0.2 (-1.8 to 1.4)	0.2 (-0.7 to 1.1)	0.4 (-0.7 to 1.5)	0.0 (-2.0 to 2.0)
Between-observer difference for the individuals with ocular hypertension				
Image 1 (Visits 1-3)	-0.2 (-1.1 to 0.7)	0.0 (-2.0 to 2.0)	0.2 (-0.7 to 1.1)	0.0 (-1.4 to 1.4)
Image 2 (Visits 2-3)	-0.4 (-1.5 to 0.7)	-0.2 (-1.1 to 0.7)	-0.2 (-1.8 to 1.4)	-0.6 (-1.7 to 0.5)
Image 3 (Visits 1-3)	-0.2 (-1.1 to 0.7)	-0.2 (-1.8 to 1.4)	0.2 (-1.4 to 1.8)	0.2 (-1.4 to 1.8)

Table 5.5. The mean of the differences, and the corresponding 95% limits of agreement, for the within-observer 'test-retest' variability in the assessment of image quality for each of the viewing techniques, for each observer, within the first three visits, for the individuals with ocular hypertension (top) and the between-observer variability in the assessment of image quality for the second of the two image evaluations for each of the viewing techniques within the first three visits (bottom).

The median (lower and upper quartiles; range) of the time taken to reach an outcome in terms both of diagnosis and of progression for each paired comparison for each of the first three visits, by observer and by viewing technique, for the 50 individuals with glaucoma is given in Table 5.6 (top) and the mean of the differences between the two observers, and the corresponding 95% limits of agreement, in Table 5.6 (bottom). The corresponding information for the 11 individuals with ocular hypertension is given in Table 5.7 (top and bottom).

Individuals with glaucoma				
Viewing method	Mono	Mono-Flicker	Stereo	Stereo-Flicker
Observer 'A'				
Visits (1-2)	18.0 (13.3, 22.0; 8.0 to 38.0)	21.0 (15.0, 28.0; 5.0 to 60.0)	25.0 (18.0, 32.0; 7.0 to 60.0)	30.5 (23.0, 40.5; 12.0 to 63.0)
Visits (2-3)	12.5 (9.0, 15.0; 5.0 to 39.0)	15.0 (13.3, 20.0; 7.0 to 41.0)	15.0 (10.5, 23.3; 5.0 to 40.0)	24.5 (14.3, 34.0; 5.0 to 51.0)
Visits (1-3)	14.5 (12.0, 22.8; 9.0 to 36.0)	18.5 (14.0, 30.8; 5.0 to 44.0)	17.0 (12.3, 22.8; 5.0 to 50.0)	33.5 (17.0, 46.8; 10.0 to 76.0)
Observer 'B'				
Visits (1-2)	16.5 (10.3, 22.0; 3.0 to 38.0)	20.5 (14.0, 27.5; 5.0 to 55.0)	22.5 (17.0, 29.8; 7.0 to 53.0)	29.5 (21.3, 38.0; 5.0 to 72.0)
Visits (2-3)	10.0 (7.0, 14.0; 3.0 to 39.0)	15.5 (10.3, 19.8; 5.0 to 41.0)	16.0 (7.3, 23.8; 4.0 to 52.0)	26.0 (15.5, 40.0; 5.0 to 51.0)
Visits (1-3)	13.0 (9.0, 21.0; 3.0 to 39.0)	24.5 (16.0, 31.8; 3.0 to 60.0)	17.0 (11.0, 23.0; 6.0 to 50.0)	34.5 (22.5, 46.8; 9.0 to 92.0)
Between-observer difference for the individuals with glaucoma				
Visits (1-2)	1.7 (-13.9 to 17.3)	0.4 (-22.5 to 23.3)	1.9 (-18.6 to 22.5)	0.5 (-25.2 to 26.3)
Visits (2-3)	1.2 (-6.4 to 8.8)	0.6 (-11.4 to 12.5)	0.4 (-9.2 to 10.0)	-2.1 (-21.0 to 16.8)
Visits (1-3)	2.2 (-11.3 to 15.7)	-2.2 (-20.3 to 16.0)	0.3 (-8.1 to 8.7)	-2.0 (-31.7 to 27.7)

Table 5.6. Top: The median (lower and upper quartiles; range) of the time (seconds) taken to reach an outcome in terms both of diagnosis and of progression for each paired-comparison, by observer and by viewing technique, for the 50 individuals with glaucoma. Bottom: The mean of the differences between the two observers, and the corresponding 95% limits of agreement, for the time to reach an outcome in terms both of diagnosis and of progression, by viewing technique, at each of the first three visits.

In general, the median time to reach an outcome in terms both of diagnosis and of progression for each paired comparison for both observers was shortest for mono-viewing, longer but relatively similar for stereo-viewing and mono-flicker chronoscopy and longest for stereo-flicker chronoscopy. The median time to reach an outcome for stereo-flicker chronoscopy was approximately three quarters longer than that for mono-viewing. The agreement between the two

observers, in terms of the median time to outcome, exhibited no particular trend across each of the four viewing techniques.

Individuals with ocular hypertension				
Viewing method	Mono	Mono-Flicker	Stereo	Stereo-Flicker
Observer 'A'				
Visits (1-2)	16.0 (12.0, 21.0; 9.0 to 30.0)	22.0 (19.0, 26.5; 15.0 to 33.0)	21.0 (15.0, 23.5; 11.0 to 45.0)	25.0 (21.5, 33.0; 11.0 to 51.0)
Visits (2-3)	15.0 (9.0, 15.0; 9.0 to 20.0)	10.0 (9.0, 19.0; 7.0 to 30.0)	15.0 (10.0, 17.0; 4.0 to 20.0)	22.0 (21.0, 24.0; 8.0 to 38.0)
Visits (1-3)	14.0 (11.0, 15.0; 9.0 to 18.0)	17.0 (17.0, 25.0; 12.0 to 25.0)	16.0 (15.0, 17.0; 15.0 to 21.0)	34.0 (27.0, 50.0; 17.0 to 64.0)
Observer 'B'				
Visits (1-2)	15.0 (11.5, 21.5; 5.0 to 39.0)	25.0 (12.0, 27.0; 4.0 to 41.0)	17.0 (13.0, 24.0; 10.0 to 34.0)	27.0 (21.0, 33.0; 4.0 to 61.0)
Visits (2-3)	15.0 (9.0, 15.0; 9.0 to 15.0)	11.0 (10.0, 19.0; 9.0 to 40.0)	14.0 (10.0, 17.0; 7.0 to 20.0)	14.0 (9.0, 24.0; 5.0 to 38.0)
Visits (1-3)	15.0 (14.0, 20.0; 9.0 to 30.0)	17.0 (14.0, 25.0; 5.0 to 25.0)	17.0 (16.0, 21.0; 3.0 to 24.0)	36.0 (34.0, 54.0; 10.0 to 64.0)
Between-observer difference for the individuals with ocular hypertension				
Visits (1-2)	-0.3 (-18.5 to 18.0)	1.0 (-21.9 to 23.9)	2.0 (-12.0 to 16.0)	-0.2 (-10.4 to 10.0)
Visits (2-3)	1.0 (-3.4 to 5.4)	-2.8 (-11.4 to 5.8)	-0.4 (-12.9 to 12.1)	4.6 (-9.8 to 19.0)
Visits (1-3)	-4.2 (-16.5 to 8.1)	2.0 (-18.7 to 22.7)	0.6 (-13.5 to 14.7)	-1.2 (-12.7 to 10.3)

Table 5.7. Top: The median (lower and upper quartiles; range) of the time (seconds) taken to reach a diagnostic outcome for each paired comparison, by observer and by viewing technique, for the 11 individuals with ocular hypertension. Bottom: The mean of the differences between the two observers, and the corresponding 95% limits of agreement, for the time to reach a diagnostic outcome, by viewing technique, at each of the first three visits.

Observer 'A' utilized 1Hz flicker for all cases, whereas Observer 'B' utilized 1 and 2Hz flicker for mono-chronoscopy and a staircase of 1, 8, and 2 Hz flicker for the stereo-chronoscopy of each image.

5.4.1 Designation of glaucoma

The number of ‘glaucoma’ to ‘non-glaucoma’ cases, by observer and by viewing technique, for the 50 individuals with glaucoma and for the 11 individuals with ocular hypertension between Visit 1 and Visit 2 (left column) and for the 30 individuals with glaucoma and 5 individuals with ocular hypertension between Visits 1, 2 and 3 (middle columns) is presented in Table 5.8. The fourth column in Table 5.8 represents the outcomes from the 82 comparisons of the ONH images from the 17 individuals (14 with glaucoma and 3 with ocular hypertension) with four or more ONH images.

Within the limitations of the dataset, between Visits 1 and 2, Observer ‘B’ correctly identified a substantially greater number of cases of ‘glaucoma’ compared to Observer ‘A’, but identified fewer cases of ‘non-glaucoma’ (i.e. Observer ‘B’ exhibited a higher sensitivity and a lower specificity compared to Observer ‘A’).

For both observers, the mono-flicker chronoscopy, stereo-viewing and stereo-flicker chronoscopy yielded a higher number of correctly identified cases of ‘glaucoma’ compared to mono-viewing technique and a similar number of correctly identified cases of ‘non-glaucoma’. Observer ‘A’ benefited (i.e. exhibited the greater increase in correctly identified cases) from stereo-viewing more than Observer ‘B’.

Observer	Visit 1-Visit 2 50:11				Visit 2-Visit 3 30:5				Visit 1-Visit 3 30:5				Visit 1- Visit 4... Visit 1-Visit n 14:3 (64:18)			
	M	MF	S	SF	M	MF	S	SF	M	MF	S	SF	M	MF	S	SF
'A'	31:7	34:6	35:8	36:7	19:3	19:3	23:3	23:2	19:3	21:3	23:2	24:2	40:15	40:12	42:13	45:12
'B'	43:5	44:6	44:4	45:6	27:1	27:2	27:1	28:1	26:1	27:1	28:2	27:1	57:7	55:7	58:7	56:7
'A' = 'B' Correct outcome	25:4	25:4	26:3	26:4	14:2	14:1	14:1	15:1	14:1	14:1	14:2	14:1	50:0	50:0	50:0	50:0
'A' = 'B' Incorrect outcome	4:4	2:4	3:3	2:4	1:2	1:2	0:2	0:2	2:2	2:2	0:2	0:2	6:2	8:4	6:4	8:5

Table 5.8. The number of 'glaucoma' to 'non-glaucoma' cases, by observer and by viewing technique, for the 50 individuals with glaucoma and for the 11 individuals with ocular hypertension between Visit 1 and Visit 2 (left column) and for the 30 individuals with glaucoma and 5 individuals with ocular hypertension between Visits 1, 2 and 3 (middle columns). The fourth column represents the outcomes from the 82 comparisons of the ONH images from the 17 individuals (14 with glaucoma and 3 with ocular hypertension) with four or more ONH images. M represents Mono-viewing, MF Mono-flicker, S Stereo-viewing and SF Stereo-flicker.

The agreement between observers in the correct designation of glaucoma cases was poor, i.e. only 25 or 26 of the 50 cases of 'glaucoma' and 4 of the 11 cases of 'non-glaucoma'. Both observers incorrectly designated the same four individuals with no glaucoma as 'glaucoma'. Similarly, the observers both incorrectly designated up to a further four individuals with glaucoma as 'non-glaucoma'. The above trends were also largely present between Visits 2 and 3 and Visits 1 and 3 and between any subsequent visits. The non-colour balanced ONH images for each of these four individuals incorrectly designated as 'glaucoma' are illustrated in Figure 5.2. The image quality for each of the two stereo-images for these four individuals ranged between Grade 3 and Grade 4 for each observer.

The time to diagnostic outcome for the paired comparisons for all viewing techniques for Observer 'B' and for three of the four techniques for Observer 'A' for Case 1 exceeded the upper quartile of the distribution of the corresponding times for the 50 individuals with glaucoma. Indeed, for both stereo-viewing techniques, the times to diagnostic outcome for the paired comparisons for each observer were the longest of the 50 individuals. These values indicate the difficulty in making the correct clinical judgement. For Case 2, the time to diagnostic outcome for each paired comparison for Observer 'B' was beyond the upper quartile of the 50 individuals for stereo-flicker chronoscopy and less than the lower quartile for the remaining three techniques. The time to diagnostic outcome for each paired comparison for Observer 'A' was at the maximum range of the 50 individuals for the mono-viewing technique, was greater than the upper quartile for stereo-flicker chronoscopy and was at the median for the remaining two techniques. These findings suggest that both observers gave greater

importance to the most ‘sophisticated’ viewing technique, stereo-flicker chronoscopy, in the evaluation of the paired image comparisons. In the remaining two cases, Cases 3 and 4, both observers each manifested a time to diagnostic outcome for the paired comparisons which was at, or above, the upper quartile for each of the viewing techniques. These values would again suggest the difficulty associated in achieving the correct clinical outcome. Neither observer changed the frequency of flicker for any of the four cases.

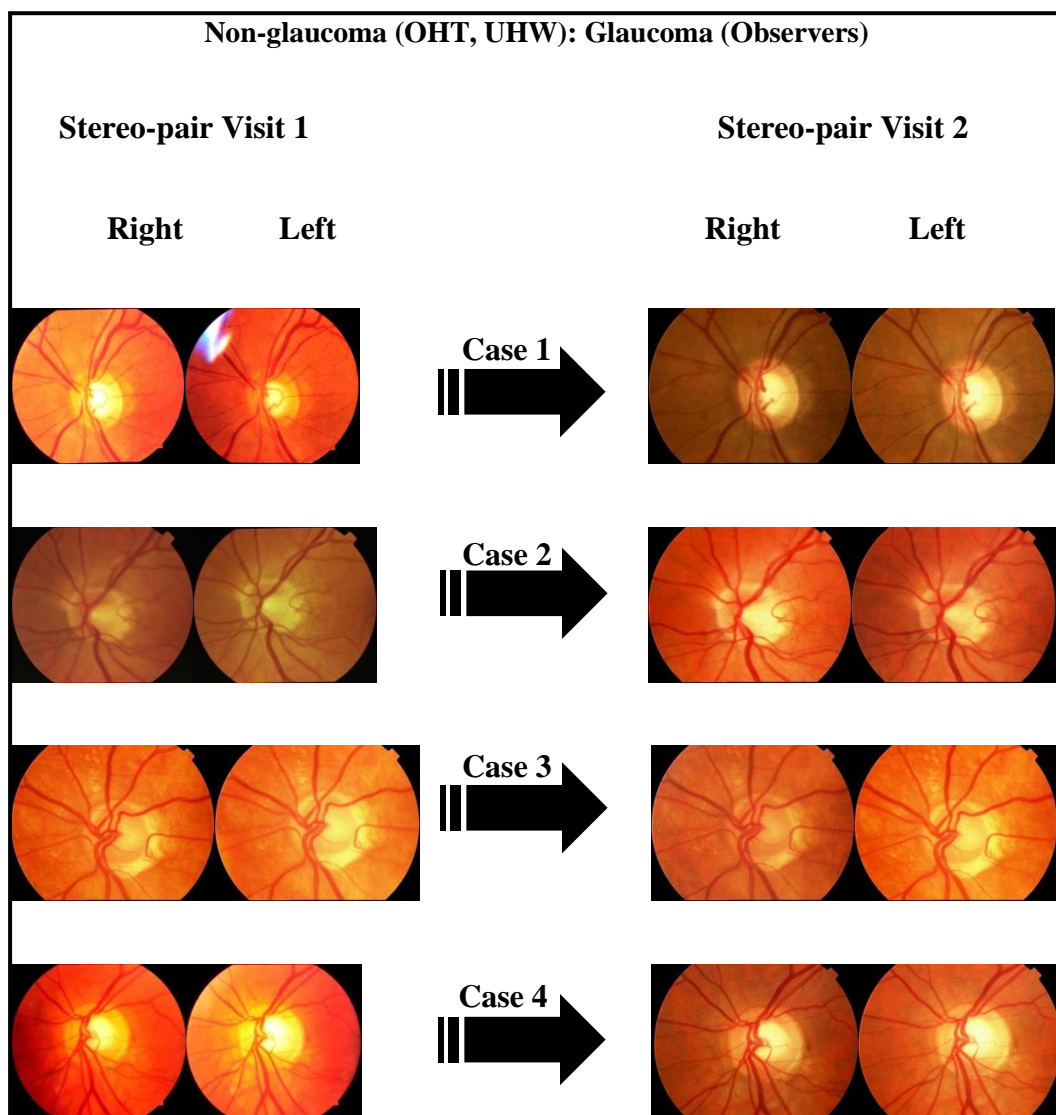


Figure 5.2. The non-colour balanced ONH images, between Visits 1 and 2, for each of the four cases of non-glaucoma incorrectly designated as ‘glaucoma’ by both observers.

The non-colour balanced ONH images for each of these four individuals incorrectly designated as 'non-glaucoma' is illustrated in Figure 5.3. The image quality for each of the two stereo-images for three of the four individuals ranged from Grade 3 to Grade 4 for each observer. For the fourth individual (Case 1), the image quality for the two stereo-pairs was graded as 2 and 3 for Observer 'A' and as Grade 1 and 2 for Observer 'B'. In addition, two individuals (Cases 1 and 3), comprised unusual manifestations of the ONH, multiple drusen and myelinated retinal nerve fibres, respectively, which clearly confounded the correct designation of 'glaucoma'.

The time to diagnostic outcome for each paired comparison for Case 1 was less than the lower quartile value for all four viewing techniques for each observer. For the mono-viewing by each observer and for the mono-flicker chronoscopy by Observer 'B' was the shortest for the 11 individuals with ocular hypertension. The times for Case 2 were at, or beyond, the upper quartile for all four viewing techniques for each observer and reflected the relative difficulty in achieving a correct diagnosis. The times achieved by both observers for Case 3 were close to the median for both mono-viewing conditions and were less than the lower quartile for the stereo-viewing techniques. These latter values reflect the relative ease in achieving the apparent correct diagnosis. The times for Case 4 were either at, or close to the median or the upper quartile, for the various viewing techniques across both observers.

Neither observer changed the frequency of the flicker for any of these four cases.

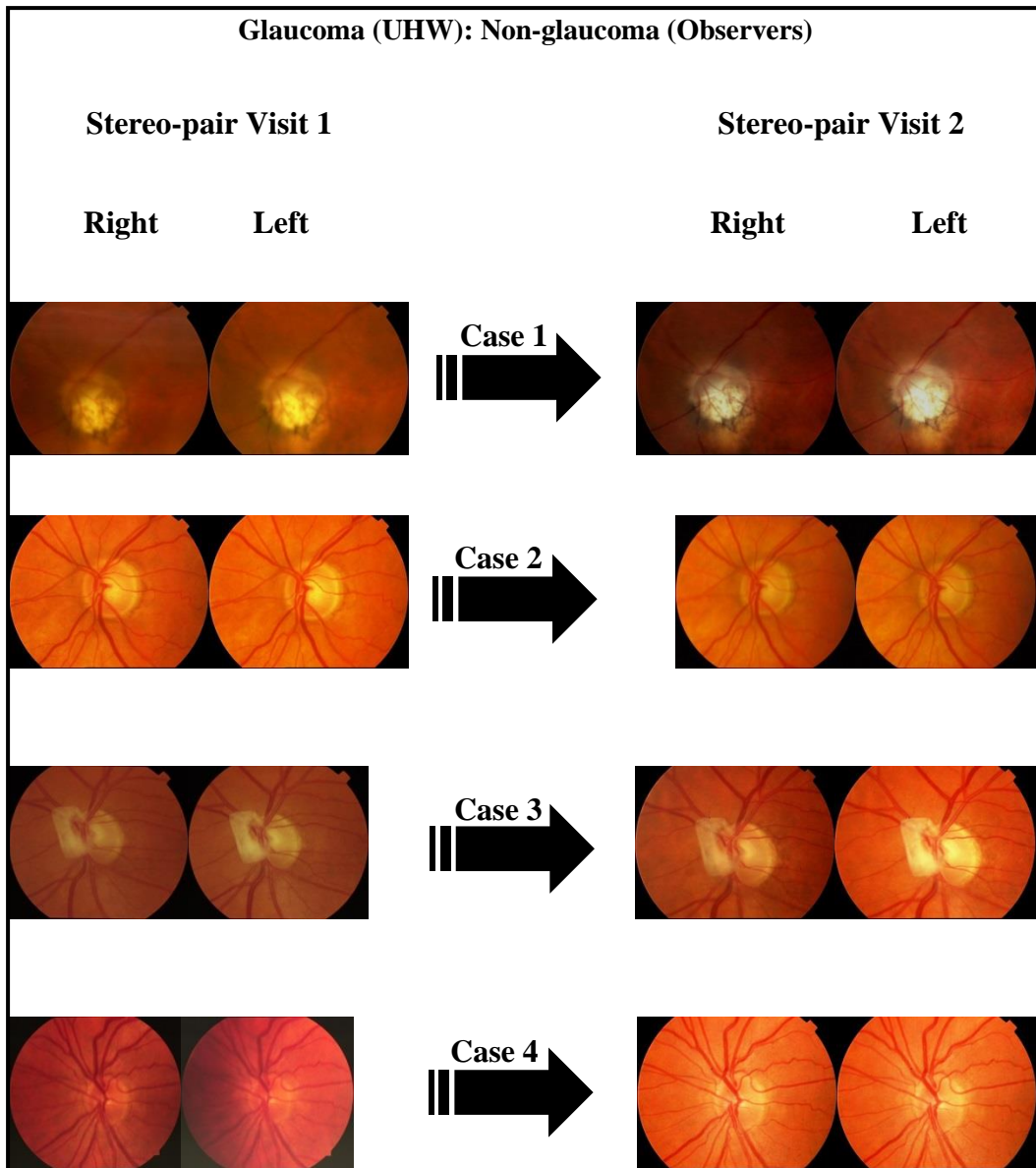


Figure 5.3. The non-colour balanced ONH images, between Visits 1 and 2, for each of the four cases of non-glaucoma incorrectly designated as ‘non-glaucoma’ by both observers.

5.4.2 Designation of progressive glaucomatous ONH damage

The number of cases of non-progression, by observer, by number of visits and by viewing technique, amongst the 50 individuals with glaucoma, is presented in Table 5.9 for the first five visits. Both non-flicker techniques yielded a higher number of non-progressive cases compared to the corresponding two flicker

techniques. Mono-viewing, alone, yielded the highest number of non-progressive cases. Similarly, the number of cases with definite progression and with possible progression, respectively, by observer, by number of visits and by viewing technique, amongst the same 50 individuals with glaucoma is presented in Table 5.10 for the first five visits. Only two individuals had attended for more than five visits (6 and 7 visits, respectively). In general, both flicker techniques yielded a higher number of cases of definite progression compared to the corresponding non-flicker techniques. No trend between techniques or between observers was apparent amongst the limited number of cases exhibiting possible progression.

The agreement between observers in the number of cases designated as definite progression was poor. With stereo-flicker chronoscopy, Observer 'A' identified 20 cases, and Observer 'B' 22 cases, of definite progression. However, agreement between the two observers was present in only 14 of these cases. No trend was present between the two observers in the recognition of definite progression across the four techniques. The agreement between observers in the number of cases designated as non-progressive was also poor. With stereo-flicker chronoscopy, agreement between observers was achieved in 7 cases. However, Observer 'A' identified 11 cases of non-progression and Observer 'B' 15 cases.

Of the four viewing techniques, stereo-flicker chronoscopy identified definite progression for each observer at an earlier stage (i.e. an earlier ONH image comparison) compared to each of the remaining three techniques (Table 5.11). Nevertheless, of the 14 cases of definite progression which were designated by

both observers, the stereo-flicker technique identified only 6 cases prior to each of the remaining three techniques. For Observer 'A' there was little difference between mono-flicker chronoscopy and stereo-flicker chronoscopy, whereas for Observer 'B' there was a noticeable difference, in that mono-flicker chronoscopy identified an earlier stage of progression definite progression in 3 cases, compared to 14 cases with stereo-flicker chronoscopy. No cases of 'progression' in the 7 cases of non-progression designated by both observers, were identified by stereo-flicker, in isolation. Of the 4 cases of ocular hypertension incorrectly designated as glaucoma by both observers, stereo-flicker chronoscopy identified definite progression, in isolation to the remaining three techniques, in two cases for Observer 'B', only (Table 5.12).

The total time for the diagnostic outcome and the evaluation of ONH progression for the 50 cases with glaucoma was shortest for mono-viewing (15 and 13.2 seconds for Observer 'A' and Observer 'B', respectively) and longest for stereo-flicker chronoscopy (29.5 and 30 seconds for Observer 'A' and Observer 'B', respectively). Mono-flicker chronoscopy and stereo-viewing were similar to one-another and approximately 5 seconds longer than mono-viewing technique (Table 5.6). The times were clinically identical for the cases designated as non-glaucomatous.

Observer	2 Visits (18 cases)				3 Visits (16 individuals)				4 Visits (8 cases)				5 Visits (5 cases)			
	M	MF	S	SF	M	MF	S	SF	M	MF	S	SF	M	MF	S	SF
'A'	11	4	11	6	6	3	4	3	3	1	4	2	3	1	3	0
'B'	12	10	10	10	9	6	7	5	7	0	5	0	2	0	1	0
Cases of agreement	10				6				5				2			
('A' = 'B')	7	4	6	6	5	1	2	1	4	0	3	0	2	0	1	0

Table 5.9. The number of cases with non-progression by observer, by number of visits and by viewing technique, for the 50 individuals with glaucoma. M represents Mono-viewing, MF Mono-flicker, S Stereo-viewing and SF Stereo-flicker.

Observer	2 Visits (18 cases)				3 Visits (16 individuals)				4 Visits (8 cases)				5 Visits (5 cases)			
	M	MF	S	SF	M	MF	S	SF	M	MF	S	SF	M	MF	S	SF
'A'	2	9	1	8	4 (1)	6 (2)	4 (4)	6 (2)	2 (1)	3 (0)	1 (0)	4 (0)	0 (0)	1 (1)	0 (0)	2 (1)
'B'	5	6	8	7	2 (4)	3 (6)	3 (4)	7 (1)	1 (0)	3 (1)	1 (1)	5 (0)	1 (0)	2 (0)	1 (0)	3 (0)
Cases of agreement (‘A’ = ‘B’)	8				6				4				2			
	1	5	1	5	1 (1)	2 (1)	0 (2)	3 (0)	1 (0)	2 (0)	1 (0)	4 (0)	0 (0)	1 (0)	0 (0)	2 (0)
Cases of incorrect outcome	0				0				2				0			
	0	0	0	0	0 (0)	0 (0)	0 (0)	0 (0)	0 (0)	1 (0)	1 (0)	1 (0)	0 (0)	0 (0)	0 (0)	0 (0)

Table 5.10. The number of cases with definite progression and with possible progression (in parenthesis) by observer, by number of visits and by viewing technique, for the 50 individuals with glaucoma. M represents Mono-viewing, MF Mono-flicker, S Stereo-viewing and SF Stereo-flicker.

Viewing technique	M	MF	S	SF	M	MF	S	SF
Visits	Observer 'A'				Observer 'B'			
3	2 (0)	5 (2)	3 (0)	5 (2)	2 (0)	3 (2)	2 (0)	6 (2)
4	0 (0)	1 (0)	0 (0)	3 (3)	0 (0)	0 (0)	0 (0)	5 (3)
5	0 (0)	1 (0)	0 (0)	1 (1)	0 (0)	0 (0)	0 (0)	3 (1)
Total	2 (0)	7 (2)	3 (0)	9 (6)	2 (0)	3 (2)	2 (0)	14 (6)

Table 5.11. The number of instances in which the given viewing technique identified definite progression at an earlier stage compared to each of the remaining three viewing techniques, by observer, by number of visits, amongst the 50 progressed individuals with glaucoma. The figure in parenthesis indicates the number of instances where agreement was present for both observers. M represents Mono-viewing, MF Mono-flicker, S Stereo-viewing and SF Stereo-flicker.

Non-glaucoma (OHT, UHW) : Glaucoma (Observers)								
Viewing technique	M	MF	S	SF	M	MF	S	SF
Cases	Observer 'A'				Observer 'B'			
Case 1 (4 visits)	1.2	1.1	1.4	1.2	2.4	1.2	1.3	1.1
Case 2 (2 visits)	4	4	4	4	4	4	4	1
Case 3 (4 visits)	4	1.1	4	3	4	3	4	1.1
Case 4 (6 visits)	3	1.2	3	1.1	3	1.2	3	1.1
Cases of progression	1	3	1	2	0	2	1	4

Table 5.12. The outcome for the 4 cases of ocular hypertension incorrectly designated as glaucoma by both observers, by viewing technique and by ranking of the earliest identification of definite progression.

5.4.3 Comparison of definite progression to that of the corresponding visual field outcome

The outcomes of the three separate visual field progression criteria, MD, VFI and EMGT GPA, in isolation and in combination, for the 61 individuals are given in Table 5.13.

Visual field progression Criteria	Diagnosis		
	Glaucoma	Non-glaucoma	Total
MD	3	-	3
VFI	4	-	4
EMGT GPA	4	2	6
MD & VFI	1	-	1
MD & EMGT GPA	-	-	0
VFI & EMGT GPA	1	-	1
MD, VFI & EMGT GPA	7	-	7
Total individuals	20	2	22

Table 5.13. The outcomes of the three separate visual field progression criteria, MD, VFI and EMGT GPA in isolation, and in combination, for the 50 individuals with glaucoma and the 11 individuals with ocular hypertension.

The outcomes of the three separate visual field progression criteria, MD, VFI and EMGT GPA in isolation, and combined, for the 14 cases of definite ONH progression designated by both observers with stereo-flicker chronoscopy are given in Table 5.14. Seven of the 14 cases of definite progression with stereo-flicker chronoscopy, also exhibited visual field progression by one or more of the progression criteria. Interestingly, of those ONHs deemed to have definite progression by each observer, alone, 35% (Observer 'A') and 45% (Observer 'B') exhibited visual field progression by one or more of the progression criteria.

Visual field progression Criteria	Cases of definite progression with stereo-flicker		
	'A' = 'B'	Observer 'A'	Observer 'B'
MD	1	1	2
VFI	2	2	2
EMGT GPA	1	1	1
MD & VFI	1	1	1
MD & EMGT GPA	-	-	2
VFI & EMGT GPA	-	-	-
MD, VFI & EMGT GPA	2	2	2
Proportion	7/14	7/20	10/22

Table 5.14. The frequency of visual field progression for each of the three separate visual field progression criteria, MD, VFI and EMGT GPA in isolation and combined, for the 14 cases of definite progression confirmed by both observers using stereo-flicker chronoscopy and for the 20 and 22 cases, respectively, of definite progression for Observer 'A' and Observer 'B', alone.

The outcomes of the three separate visual field progression criteria, MD, VFI and EMGT GPA in isolation and in combination for the 7 cases of non-progression of the ONH designated by both observers with stereo-flicker chronoscopy are given in Table 5.15. Four of the 7 cases of non-progression with stereo-flicker chronoscopy exhibited visual field progression by one or more of the progression criteria. Of the 11 ONHs deemed to exhibit non-progression by Observer 'A', 6 exhibited field progression by one or more of the progression criteria. Similarly, of the 15 ONHs deemed to exhibit non-progression by Observer 'B', 5 exhibited field progression by one or more of the progression criteria. However, there was some diversity in the type of visual field analysis exhibiting progression both within- and between-observers.

Visual field progression Criteria	Cases of non-progression with stereo-flicker		
	'A' = 'B'	Observer 'A'	Observer 'B'
MD	1	1	1
VFI	-	-	1
EMGT GPA	1	1	1
MD & VFI	-	-	-
MD & EMGT GPA	-	-	-
VFI & EMGT GPA	-	1	-
MD, VFI & EMGT GPA	2	3	2
Proportion	4/7	6/11	5/15

Table 5.15. The frequency of visual field progression for each of the three separate visual field progression criteria, MD, VFI and EMGT GPA in isolation and in combination for the 7 cases of non-progression of the ONH confirmed by both observers using stereo-flicker chronoscopy and for the 11 and 15 cases, respectively, of non-progression for Observer 'A' and Observer 'B', alone.

There was a noticeable difference, within the limited dataset, between the length of the time series of both the ONH image acquisition and the measurement of the visual field for those with or without progression of either the ONH and/ or the visual field (Table 5.16). However, the length of the time series for the visual field examinations was approximately twice that of the ONH image acquisitions.

Number of visits/ follow-up (yrs)	14 cases of definite progression with stereo- flicker chronoscopy		7 cases of non-progression with stereo-flicker chronoscopy	
	ONH & visual field progression (7/14)	Visual field non- progression (7/14)	ONH non-progression (4/7)	Visual field non-progression (3/4)
Number of perimetric visits	7.0 (6.0, 10.0; 5.0 to 12.0)	7.0 (6.0, 8.0; 4.0 to 9.0)	7.5 (6.8, 8.5; 6.0 to 10.0)	6.0 (6.0, 6.5; 6.0 to 7.0)
Number of photographic visits	3.0 (2.0,4.0; 2.0 to 4.0)	4.0 (2.5, 4.5; 2.0 to 5.0)	2.0 (2.0, 2.3; 2.0 to 3.0)	2.0 (2.0, 2.0; 2.0 to 2.0)
Perimetric follow-up (yrs)	7.7 (6.2, 8.1; 4.4 to 10.3)	7.0 (5.3, 8.6; 3.1 to 9.8)	6.5 (6.1, 7.6; 5.8 to 10.0)	6.1 (5.9 to 7.6; 5.7 to 9.2)
Photographic follow-up (yrs)	3.3 (2.4, 5.7; 1.7 to 6.1)	4.6 (3.5, 5.9; 2.1 to 6.7)	3.4 (2.3, 4.7; 2.0 to 5.9)	2.0 (1.2, 2.7; 0.4 to 2.0)

Table 5.16. The number of the perimetric and the photographic visits (median, lower and upper quartiles; range) for the 7 out of 14 cases of definite progression confirmed by both observers using stereo-flicker chronoscopy and who exhibited visual field progression (left-hand column); for the 7 out the 14 cases of definite progression confirmed by both observers using stereo-flicker chronoscopy and who did not exhibit visual field progression (middle-left column); for the 4 out of 7 cases of non-progression of the ONH confirmed by both observers using stereo-flicker chronoscopy and who exhibited visual field progression (middle-right column); and for the 3 of the 7 cases of non-progression of both the ONH and the visual field.

5.5 Discussion

The results highlight the importance of a flicker comparison, with either mono- or stereo-viewing, for the designation of glaucoma and for the identification of glaucomatous ONH progression.

Observer 'B' adopted an approach based upon high sensitivity with a resultant lower specificity. Observer 'A' adopted an approach which yielded a high specificity with a resultant lower sensitivity.

Regardless of the difference in the two approaches, the improvement of stereo-viewing over mono-viewing in the diagnostic accuracy of glaucoma was apparent. Flicker-viewing increased the diagnostic accuracy, compared to non-flicker viewing, and stereo-flicker manifested a slightly better diagnostic accuracy compared to mono-flicker viewing. That is, although the sensitivity and specificity relative to the hospital diagnosis varied between the two observers, the ranking of the four viewing techniques, in terms of diagnostic accuracy, remained the same.

The benefit-cost of the improvement in the diagnostic accuracy with increase in sophistication of the viewing technique, for Observer 'A' who exhibited a high specificity in their clinical judgement (i.e. 5 additional cases [10% of the 50 cases with glaucoma] designated from mono-viewing to stereo-flicker chronoscopy, at a cost of a doubling in viewing time for all cases) is open to debate. The corresponding benefit-cost for Observer 'B', who exhibited a high sensitivity in

their clinical judgement, was a 2 additional cases (an increase of 4% of the 50 cases with glaucoma) designated with stereo-flicker chronoscopy compared to mono-viewing. These additional two cases occurred at a cost of a doubling in viewing time for *all* cases and highlighted the time-consuming character of stereo-flicker chronoscopy. Such an outcome may not warrant the extra time involved and such an argument is also applicable to cases of non-glaucoma. However, regardless the time-consuming nature of stereo-flicker chronoscopy, it still remains a sensitive technique in the diagnosis of glaucoma.

Given the intuitive logic of the ranking of the four viewing techniques in terms of diagnostic accuracy and given that the study was not concerned with a comparison of ophthalmological competence (Breusegem et al. 2011), it seemed of little value to augment the study by recruiting one or more further ophthalmologists as observers. Such observers would merely have each generated different levels of sensitivity and specificity and it is unlikely that this would have altered the ranking of the viewing techniques in terms of diagnostic accuracy.

Given the aim of the study, the comparison of stereo-flicker chronoscopy with mono-flicker chronoscopy for the qualitative identification of progressive glaucomatous ONH damage, the outcome (i.e., the designation of ‘glaucoma’ or ‘non-glaucoma’) was based upon a comparison of a sequential image-pair, rather than upon the evaluation of a single image. The latter could also have been undertaken for the non-flicker viewing techniques, but would have resulted in an

increased length of the study, which was already extensive, and which a pilot study had indicated would not have been viable.

Little agreement was present between the various methods for the evaluation of visual field progression and little agreement between the outcome of these methods and the qualitative evaluation of ONH progression.

Four cases exhibited visual field progression in the presence of a non-progressive ONH. This lack of concordance is likely to have arisen from the longer time series of the visual field examinations compared to that of the ONH image acquisition (median visual field follow-up 6.5 years and median ONH image acquisition 3.4 years).

The 'gold' standard for the diagnosis of glaucoma was that of the UHW diagnosis. It is possible that such a standard contained cases with an inappropriate diagnosis. Indeed, two cases with a hospital diagnosis of ocular hypertension were each designated as glaucoma by both observers with all four viewing techniques over all visits. Such findings are likely to be attributable to an incorrect hospital diagnosis, particularly given that external review of the visual fields by an expert in visual field interpretation (JMW) confirmed the presence of a repeatable glaucomatous visual field defect in one case and a likely normal field in the other case. Similarly, two of the individuals with a hospital diagnosis of glaucoma were designated as non-glaucoma by each of the two observers. It

should be noted, however, that the designation of either ‘glaucoma’ or ‘non-glaucoma’ was made on the basis of the ONH appearance, alone, and in one eye only, i.e. without the knowledge of the corresponding visual field information and the comparison of the ONH symmetry between the two eyes.

As was noted previously, the designation of glaucoma was based upon a comparison of a sequential image-pair, rather than upon the evaluation of a single image. The criteria for the designation of glaucoma could, therefore, have been made on the basis either of an ONH appearance typical of glaucoma or of an ONH exhibiting progressive damage.

The hospital notes did not contain sufficient information to use, as ‘gold’ standard a UHW definition of progressive ONH damage. As a consequence the dataset was evaluated in terms of the number of cases in which both observers each designated progressive damage.

A comparison between the qualitative assessment of the ONH images and the quantitative planimetric outcome, described in the following Chapter (Chapter 6), could have been undertaken. However, given that the qualitative evaluation would have included assessment of non-quantifiable features such as the presence of disc haemorrhages and alterations of the topography of the vessels, etc, such an approach was considered unreliable and, therefore was not adopted.

Chapter 6

The quantitative assessment of progressive structural and functional glaucomatous damage

6.1 Introduction

Analogue planimetry, derived with varying degrees of sophistication in technique, and either with mono- or stereo-viewing (Chapter 4), has been used for many years to characterize the various features of the ONH (Kottler et al. 1976; Jonas et al. 1988; Jonas and Montgomery 1995; Jonas et al. 1999). More recently, digital planimetry (Chapter 1), also with varying degrees of sophistication and with either mono- or stereo-viewing, has largely replaced the manual technique (Garway-Heath et al. 1999; Yogesan et al. 1999; Barry et al. 2000; Correnti et al. 2003; Morgan et al. 2005a; Morgan et al. 2005b; Ramakrishnan et al. 2005; Hoffmann et al. 2007; Sanfilippo et al. 2009; Radcliffe et al. 2010; Morgan et al. 2012; Tsutsumi et al. 2012; Carbonaro et al. 2014).

The association between ONH structure and the functional outcome from perimetry has been the subject of a number of cross-sectional studies which have evaluated one or more ONH parameters derived either from traditional analogue planimetry (Garway-Heath et al. 1998a; Jonas et al. 1998; Junemann et al. 2000) or from digital planimetry (Garway-Heath and Hitchings 1998; Bartz-Schmidt et al. 1999; Grewal et al. 2009; Saito et al. 2010; Medeiros et al. 2012d) (Chapter 1).

Several studies have evaluated the relationship between structural progression of the ONH derived by analogue planimetry (Jonas et al. 2000; Johnson et al. 2003; Crowston et al. 2004; Jonas et al. 2004; Jonas et al. 2006; Jampel et al. 2008) or by digital planimetry (Nguyen et al. 2004; Laemmer et al. 2007) and the corresponding functional progression of the visual field. The time-frame of these various studies ranges from 0.5 to 8.7 years with analogue planimetry and from 2.8 to 11.8 years with digital planimetry.

The digital manual planimetric technique developed by Morgan and colleagues (Morgan et al. 2005a; Morgan et al. 2005b; Morgan et al. 2012) and used by (Sanfilippo et al. 2009; Carbonaro et al. 2014) incorporates a measurement cursor which can be moved in stereoscopic (depth) space to minimize parallax errors encountered in the measurement of the NRR which is made at the depth of the scleral rim. The stereoscopic images can also be zoomed and panned at the observer's discretion to clarify details of the ONH (Chapter 4).

Studies in animals and humans have established that the relationship between structural and functional outcomes is non-linear when one of the outcomes, usually a given measure of the ONH, is expressed linearly and the other outcome, usually the visual field, is expressed in log units. The various structure and function models have proposed either a linear or a logarithmic transformation for the appropriate variable to generate structural and functional outcomes on identical scales (Swanson et al. 2004; Drasdo et al. 2007; Hood et al. 2007; Drasdo et al. 2008; Gonzalez-Hernandez et al. 2009; Harwerth et al. 2010; Malik et al. 2012; Medeiros et al. 2012b).

Given the above knowledge, it would seem appropriate to develop and to evaluate the utility of digital stereo-flicker chronoscopy for the manual planimetric identification of progressive structural damage of the ONH. In addition, it would also seem appropriate to revisit the association between progressive structural damage, identified with the ‘floating cursor’ digital stereo-planimetric technique and expressed in linear units (Morgan et al. 2005a; Morgan et al. 2005b; Morgan et al. 2012) and progressive functional damage, i.e., the outcome of the visual field, expressed in linear units as the number of the residual RGC soma count.

6.2 Aim

The aim of the study, therefore, was twofold. Firstly, to quantify the NRR, as a whole and by segments and by sectors, in a case series of individuals attending a glaucoma clinic over a long follow-up, using digital manual stereo-planimetry incorporating the ‘floating cursor’ technique of Morgan and colleagues (Morgan et al. 2005a; Morgan et al. 2005b; Morgan et al. 2012) and to compare the outcomes to those derived monoscopically. Secondly, to evaluate the relationship between ONH progression (defined as a thinning of the NRR) derived with the stereo-viewing technique, and the concomitant visual field outcome, expressed, linearly, as the number of remaining RGCs.

6.3 Methods

The cohort comprised 27 of the 61 individuals described in the previous Chapter (Chapter 5) who had two or more ONH images, five or more reliable visual field examinations, and at least one photographic visit using the Topcon TRC-EX

camera. The Topcon TRC-EX camera (utilizing the Sony 950P 20° camera) was used as the reference, since the images were digital and had not undergone any form of editing (Chapter 4). The selection procedures for, and the characteristics of, these 27 individuals are described in Chapter 3. Of the 27 individuals, 23 had ‘glaucoma’ (primary open-angle glaucoma, normal-tension glaucoma, pigmentary dispersion glaucoma, or considered to be glaucoma suspect) and 4 had ocular hypertension. If an individual had more than one image from the Topcon TRC-EX camera, the more recent image was chosen as reference image.

The summary statistics (median, lower and upper quartile; range) of the demographic and the clinical characteristics (median, lower and upper quartile; range) for the 27 individuals in the randomly assigned eye at their baseline visit are shown in Table 6.1 and Table 6.2, respectively (it should be noted that the information contained in these latter Tables is different to that contained in Tables 3.19 to 3.20 which is based upon the most severely affected eye [Chapter 3]).

Diagnosis (No of individuals)	Primary open-angle glaucoma (16)	Ocular hypertension(4)	Normal-tension glaucoma (4)	Glaucoma Suspect (2)	Others (1)
Age (yrs) at the baseline visit	69.3 (60.5, 71.9; 49.7 to 78.0)	63.7 (61.1, 65.9; 55.3 to 70.2)	67.2 (63.9, 70.3; 61.0 to 72.4)	56.8 (50.9, 62.6; 45.0 to 68.5)	45.8
Male : Female	6 : 10	2 : 2	0 : 4	0 : 2	1 : 0
Perimetric follow-up (yrs)	8.1 (6.9, 8.7; 4.7 to 9.8)	6.8 (6.2, 8.1; 5.3 to 10.8)	8.2 (7.1, 9.4; 7.0 to 10.3)	7.9 (7.8, 8.0; 7.7 to 8.2)	10.3
Number of perimetric visits	7.0 (6.0, 8.3; 5.0 to 11.0)	6.5 (6.0, 7.8; 6.0 to 10.0)	9.5 (7.5, 11.3; 6.0 to 12.0)	6.0 (5.5, 6.5; 5.0 to 7.0)	8.0
Photographic follow-up (yrs)	5.5 (3.8, 6.4; 1.8 to 9.1)	6.4 (4.0, 8.8; 3.6 to 9.3)	5.8 (4.9, 6.3; 3.4 to 6.3)	4.1 (3.1, 5.0; 2.1 to 6.0)	6.8
Number of photographic visits	3.0 (2.0, 3.0; 2.0 to 4.0)	4.0 (3.5, 4.0; 2.0 to 4.0)	4.0 (3.5, 4.8; 2.0 to 7.0)	3.0 (2.5, 3.50; 2.0 to 4.0)	4.0
Maximum duration of follow-up (yrs)	8.9 (8.0, 9.7; 5.6 to 10.5)	10.5 (9.1, 11.0; 6.4 to 11.3)	8.6 (8.0, 9.4; 7.8 to 10.3)	11.9 (10.4, 13.5; 8.8 to 15.0)	10.3

Table 6.1. The demographic characteristics (median, lower and upper quartiles; range) of the randomly assigned eye of the 27 individuals at the baseline visit.

Diagnosis (No of individuals)	Primary open-angle glaucoma (16)	Ocular hypertension (4)	Normal-tension glaucoma (4)	Glaucoma Suspect (2)	Others (1)
Mean Deviation (dB) at the baseline visit	-3.82 (-9.10, -1.28; -21.88 to -0.37)	-2.67 (-3.59, -1.98; -5.55 to -0.73)	-6.38 (-10.35, -4.23; -18.16 to -1.87)	-1.53 (-2.64, 0.42; -3.75 to 0.69)	-1.43
Visual Field Index (%) at the baseline visit	95.0 (78.3, 98.3; 31.0 to 99.0)	96.5 (95.5, 97.3; 94.0 to 98.0)	84.0 (69.0, 95.0; 54.0 to 98.0)	94.5 (91.8, 97.3; 89.0 to 100.0)	98.0
Pattern Standard Deviation (dB) at the baseline visit	2.51 (1.64, 7.95; 1.41 to 14.42)	1.96 (1.84, 2.04; 1.73 to 2.04)	6.08 (3.07, 8.94; 2.21 to 9.38)	2.73 (2.06, 3.40; 1.39 to 4.07)	1.67
Intraocular Pressure (mmHg) at the baseline visit	26.00 (21.50, 29.00; 14.00 to 36.00)	26.00 (21.80, 32.00; 21.00 to 38.00)	20.00 (16.50, 21.00; 13.00 to 22.0)	17.50 (16.25, 18.75; 15.00 to 20.00)	16.00
Vertical cup-to-disc ratio at the baseline visit	0.70 (0.61, 0.80; 0.30 to 0.90)	0.50 (0.50, 0.50; 0.50 to 0.50)	0.70 (0.68, 0.80; 0.65 to 0.90)	0.55 (0.53, 0.58; 0.50 to 0.60)	0.20

Table 6.2. The clinical characteristics (median, lower and upper quartile; range) of the randomly assigned eye of the 27 individuals at the baseline visit.

The two observers (Observer A and Observer B), who had qualitatively evaluated both the diagnostic and the progressive outcomes for the 61 individuals described in Chapter 5, undertook the planimetry of the ONH images. Both observers undertook this second study of the 27 individuals on a separate occasion to that of the qualitative assessment. Each observer was instructed to designate the disc margin as the area inside of the Elschning’s scleral ring and the cup margin based upon normal clinical judgement. The order of the presentation of two viewing techniques (either mono- or stereo-viewing) was pseudo-randomized between images and between visits. The sequence of the randomization is given in Figure 6.1. The time for the planimetric outcome, by each observer, was recorded for each of the ONH images for each method.

Individual	First display of the stereo-pair							Second display of the stereo-pair							
	V1	V2	V3	V4	V5	V6	V7	Individual	V1'	V2'	V3'	V4'	V5'	V6'	V7'
#01	M	S	S					#01	S	M	M				
...	S	M						...	M	S					
...	S	M	M	M				...	M	S	S	S			
...	M	S						...	S	M					
...	M	S	M	M				...	S	M	S	S			
...	S	M	S					...	M	S	M				
...	S	M	S					...	M	S	M				
...	M	S	M	S	M			...	S	M	S	M	S		
...	M	S	M					...	S	M	S				
...	S	M						...	M	S					
...	S	M	S	S				...	M	S	M	M			
...	M	S	S	M				...	S	M	M	S			
...	M	S	M	M	M	S	S	...	S	M	S	S	S	M	M
...	S	M						...	M	S					
...	S	M						...	M	S					
...	M	S						...	S	M					
...	M	S						...	S	M					
...	S	M	M	S				...	M	S	S	M			
#27	S	M	S					...	M	S	M				

Figure 6.1. The pseudo-randomized order of presentation of the mono- and stereo-viewing techniques between images and between visits.

The planimetric results, in pixels, for any given ONH image acquired with any given camera were output in a text file (.txt) and comprised the ONH area, the

cup area, the NRR area, and the areas of the alpha and beta zones of the PPA. This output was given for each 5° segment commencing from the horizontal temporal meridian. The area in pixels of each of the 72 segments was summed to produce the ONH area for each image. All measurements were then scaled relative to that obtained with the Topcon TRC-EX camera. The scaling factor was the ratio of the ONH area of the Topcon TRC-EX image to that of the image acquired from the given other camera. The ONH area, the cup area, the NRR area, the areas of the alpha and beta zones of the PPA and the corresponding sectors were converted from pixels into mm² using the conversion factor for the TRC-EX camera, supplied by Topcon Corporation, Tokyo, Japan, of 1 pixel equals 8.36E-06 mm².

The scaled images at each visit were then further corrected for the magnification derived from the Topcon TRC-EX camera (utilizing the Sony 950P 20° camera) and that from the given eye using Littman's formula, $t = p * q * s$, where, t is the 'true diameter' of the ONH derived from the measured ONH area, on the assumption that the ONH is circular; p is the correction factor of 3.0805 for the Topcon TRC-EX camera (Morgan 26/09/2013); q is a correction factor, which is dependent on the optical dimensions of the given eye and is based upon the keratometry readings and the mean spherical refractive error (Garway-Heath et al. 1998b); and s is the diameter of the ONH acquired by the Topcon TRC-EX camera. Secondly, the true area magnification of the ONH, t^2 , was then derived from the 'true diameter', t , using the formula $t^2 = (p * q)^2 * s^2$ (Rudnicka et al. 1998).

The visual fields for the 27 individuals had all been obtained using Program 24-2 and stimulus size III with the SITA Fast algorithm of the HFA 700 series. Following, and masked to the results of, the planimetry, the fields of the 27 individuals were evaluated by a visual field expert (JMW) in terms of their reliability. Of the 27 individuals 4 were excluded on the basis of poor quality perimetry, due to one or more of the following features; a marked learning effect, $\geq 15\%$ incorrect responses to the false-positive catch trials, and poor fixation. Five of the individuals with glaucoma exhibited a progressive cataract which ultimately required extraction and IOL implantation. These 5 individuals were analysed separately from the remaining 18 individuals and the results were derived from the visual field series prior to surgery.

The number of residual retinal ganglion cells at each stimulus location within Program 24-2 for the SITA Fast algorithm were calculated for each of the 23 individuals from the equations of Harwerth and colleagues (Harwerth et al. 2010).

$$m = [0.054 * (ec * 1.32)] + 0.9 \quad (1)$$

$$b = [-1.5 * (ec * 1.32)] - 14.8 \quad (2)$$

$$rgc = \{ [(s - 1.87) - b] / m \} + 4.7 \quad (3)$$

$$SAP \text{ } rgc = \Sigma 10^{(rgc * 0.1)} \quad (4),$$

where m and b are the slope and y-intercept, respectively, for the function at a given retinal eccentricity ec ; rgc is the number of RGCs, in dBs, in the given area of the retina which corresponds to the given stimulus location which exhibits a sensitivity of s , in dBs. The constant 1.32 in equations (1) and (2) is the ratio of human to monkey axial lengths. The constant 1.87 in equation (3) is a correction for the difference between the sensitivities obtained with the Full Threshold and SITA Fast algorithms and the constant 4.7 converts RGC density (somas/mm²) to the total number of RGCs in the area of the given retina corresponding to the given 6° x 6° degree inter-stimulus separation of the Program 24-2 stimulus grid (based on a conversion factor, for the human eye, of 3.5° of visual angle per mm of retinal distance). The total number of RGCs (SAP rgc) is obtained from the anti-log of the total number of RGCs summed across the given stimulus locations.

The Single Field Analysis printouts of the HFA for each visit of each individual were scanned into .pdf format. The values of sensitivity at each given stimulus location within the given printout were extracted from the printout using Microsoft Paint 2010 (Microsoft Corporation, Redmond, WA) and saved in .tiff format.

The images in .tiff format were each converted into .txt files using OmniPage 18 (Nuance Communications, Inc., Burlington, MA). Each dB value was then converted into the corresponding RGC number via an application, produced using Eclipse which is a web-based workspace with an extensible plug-in system for

customization using the programming language Java. The output of the application was derived as a .csv (comma separated values) file.

The RGCs sub-serving the given stimulus location were mapped to the given ONH sector based upon the work of Garway-Heath and colleagues (Garway-Heath et al. 2000b) and utilizing the ONH sectors of Wirtschafter and colleagues (Wirtschafter et al. 1982) (Figure 6.2). The printout from the application contained the number of RGCs at each of the 54 locations of Program 24-2 and for each of the ONH sectors and for the superior and the inferior quadrants (Figure 6.3).

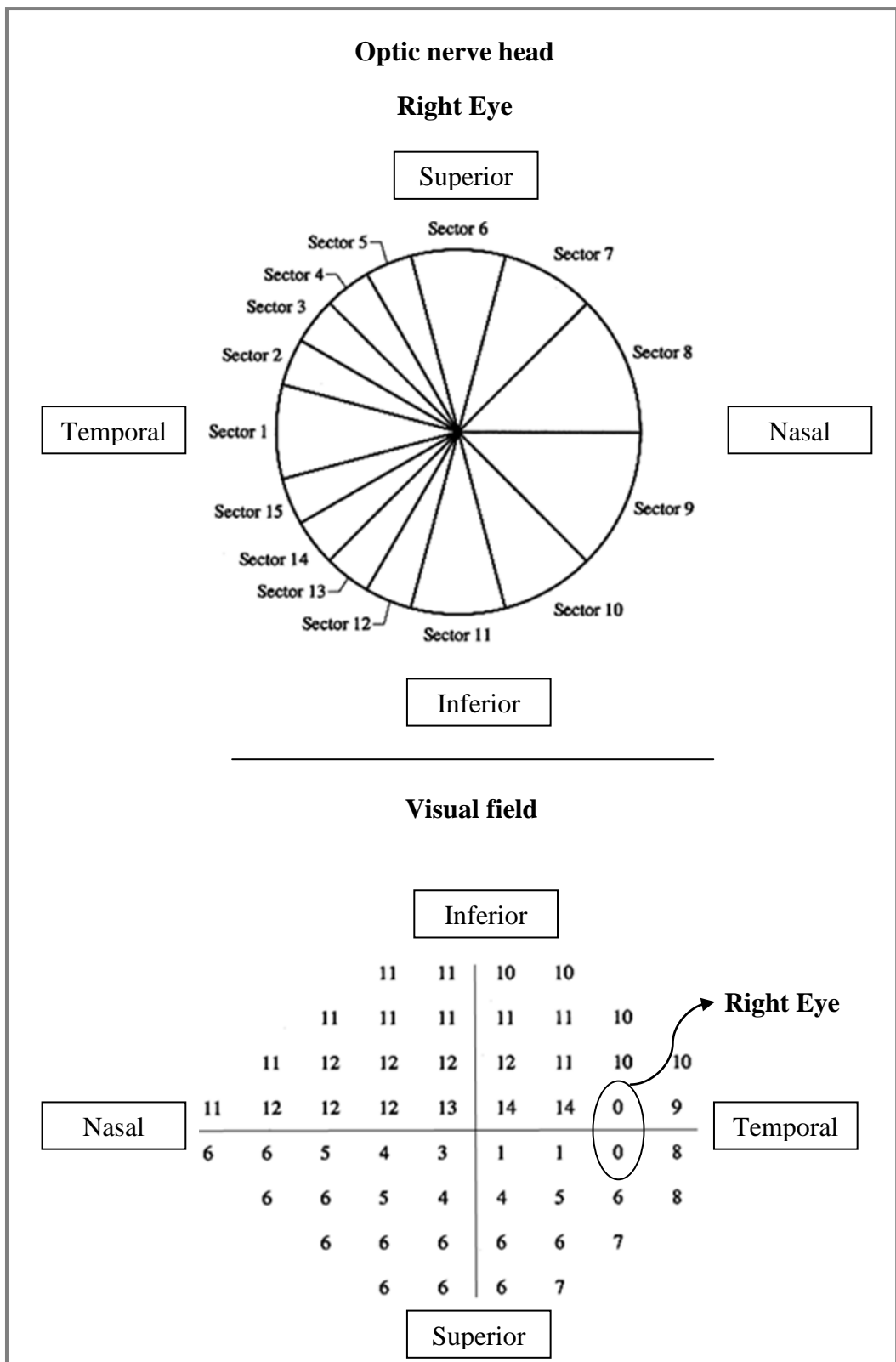


Figure 6.2. The ONH sectors from Wirtschafter and colleagues (1982) (top) and the mapping of the visual field to the ONH sectors, to estimate the RGC number of a given ONH sector subserving the given stimulus location, based upon the work of Garway-Heath and colleagues (2000) (bottom).

Overleaf: Figure 6.3. An example of the output from the application coded to calculate the RGC at each of the ONH sectors based upon the Program 24-2 stimulus grid of the HFA.

field values									
0	0	28	25	25	28	0	0	0	0
0	30	30	28	29	29	29	0	0	0
27	29	31	30	29	30	30	26	0	0
30	24	32	31	32	30	31	29	26	0
30	0	32	32	33	32	32	30	28	0
28	30	31	30	32	30	30	29	0	0
0	30	30	28	31	30	29	0	0	0
0	0	29	32	30	29	0	0	0	0
field eccentricity									
29.69848	25.80698	22.84732	21.2132	21.2132	22.84732	25.80698	29.69848	34.20526	0
25.80698	21.2132	17.49286	15.29706	15.29706	17.49286	21.2132	25.80698	30.88689	0
22.84732	17.49286	12.72792	9.486833	9.486833	12.72792	17.49286	22.84732	28.4605	0
21.2132	15.29706	9.486833	4.242641	4.242641	9.486833	15.29706	21.2132	27.16616	0
21.2132	15.29706	9.486833	4.242641	4.242641	9.486833	15.29706	21.2132	27.16616	0
22.84732	17.49286	12.72792	9.486833	9.486833	12.72792	17.49286	22.84732	28.4605	0
25.80698	21.2132	17.49286	15.29706	15.29706	17.49286	21.2132	25.80698	30.88689	0
29.69848	25.80698	22.84732	21.2132	21.2132	22.84732	25.80698	29.69848	34.20526	0
field m									
3.016908	2.739521	2.528557	2.412077	2.412077	2.528557	2.739521	3.016908	3.338151	0
2.739521	2.412077	2.146891	1.990374	1.990374	2.146891	2.412077	2.739521	3.101618	0
2.528557	2.146891	1.807246	1.576221	1.576221	1.807246	2.146891	2.528557	2.928664	0
2.412077	1.990374	1.576221	1.202415	1.202415	1.576221	1.990374	2.412077	2.836404	0
2.412077	1.990374	1.576221	1.202415	1.202415	1.576221	1.990374	2.412077	2.836404	0
2.528557	2.146891	1.807246	1.576221	1.576221	1.807246	2.146891	2.528557	2.928664	0
2.739521	2.412077	2.146891	1.990374	1.990374	2.146891	2.412077	2.739521	3.101618	0
3.016908	2.739521	2.528557	2.412077	2.412077	2.528557	2.739521	3.016908	3.338151	0
field b									
-73.603	-65.8978	-60.0377	-56.8021	-56.8021	-60.0377	-65.8978	-73.603	-82.5264	0
-65.8978	-56.8021	-49.4359	-45.0882	-45.0882	-49.4359	-56.8021	-65.8978	-75.956	0
-60.0377	-49.4359	-40.0013	-33.5839	-33.5839	-40.0013	-49.4359	-60.0377	-71.1518	0
-56.8021	-45.0882	-33.5839	-23.2004	-23.2004	-33.5839	-45.0882	-56.8021	-68.589	0
-56.8021	-45.0882	-33.5839	-23.2004	-23.2004	-33.5839	-45.0882	-56.8021	-68.589	0
-60.0377	-49.4359	-40.0013	-33.5839	-33.5839	-40.0013	-49.4359	-60.0377	-71.1518	0
-65.8978	-56.8021	-49.4359	-45.0882	-45.0882	-49.4359	-56.8021	-65.8978	-75.956	0
-73.603	-65.8978	-60.0377	-56.8021	-56.8021	-60.0377	-65.8978	-73.603	-82.5264	0
Number of Retinal Ganglion Cells									
0	0	7547	6078	6078	7547	0	0	0	0
0	9797	12104	11171	12542	10873	8905	0	0	0
6890	10873	19734	24283	20982	17373	12104	6290	0	0
9797	0	32523	66390	80403	24283	15807	8905	5481	0
9797	0	32523	80403	97373	32523	17745	9797	6447	0
7547	12104	19734	24283	32523	17373	12104	8266	0	0
0	9797	12104	11171	15807	12104	8905	0	0	0
0	0	8266	11858	9797	8266	0	0	0	0
SAP_sigma= 983402.8760966102									
RGC number in Quadrant 6 =				138736					
RGC number in Quadrant 11 =				100729					
RGC number in Quadrants (10 11 12 13) =				346060					
RGC number in Quadrants (4 5 6 7) =				300985					
RGC number in sector 10 =				41187					
RGC number in sector 12 =				123740					
RGC number in sector 13 =				80403					
RGC number in sector 4 =				89329					
RGC number in sector 5 =				54854					
RGC number in sector 7 =				18064					

Sensitivity (dB)

Stimulus eccentricity (°)

m at each stimulus eccentricity

b at each stimulus eccentricity

Number of RGCs sub-serving at each stimulus eccentricity

Number of RGCs sub-serving each sector and quadrant

6.4 Results

Observer ‘A’ took 1.2 hours to complete the planimetry of the 27 individuals and Observer ‘B’ 3.1 hours. The median (lower and upper quartiles; range) of the time taken to complete the planimetry for each of the images emanating from the second photographic visit of the time series, by diagnostic outcome, by observer and by viewing technique, for the 23 individuals with glaucoma (top) and for the 4 individuals (bottom) with ocular hypertension together with the mean of the differences between the two observers, and the corresponding 95% limits of agreement, is shown in Table 6.3.

Diagnosis	Time for mono-viewing (minutes)	Time for stereo-viewing (minutes)
Observer ‘A’		
Glaucoma	0.39 (0.30, 0.44; 0.23 to 1.10)	0.43 (0.35, 0.47; 0.20 to 1.15)
Non-glaucoma	0.45 (0.39, 0.47; 0.33 to 0.48)	0.43 (0.42, 0.44; 0.40 to 0.44)
Observer ‘B’		
Glaucoma	1.04 (0.46, 1.49; 0.26 to 4.43)	1.05 (0.49, 1.32; 0.21 to 2.38)
Non-glaucoma	0.55 (0.48, 1.31; 0.41 to 2.06)	0.52 (0.50, 1.41; 0.48 to 2.30)
Between-observer difference (‘B’-‘A’) to complete planimetry		
Glaucoma	-0.80 (-0.94 to 2.53)	0.57 (-0.66 to 1.80)
Non-glaucoma	0.59 (-1.10 to 2.27)	0.68 (-1.35 to 2.70)

Table 6.3. The median (lower and upper quartiles; range) of the times (minutes) to complete planimetry of the 23 images acquired at the second photographic visit, by diagnosis, by observer and by viewing technique, together with the mean of the differences between the two observers, and the corresponding 95% limits of agreement.

The time to complete the planimetry for the individuals with glaucoma was similar for the two viewing techniques; however, it was notably longer for each technique for Observer ‘B’ compared to Observer ‘A’.

The descriptive statistics (median, upper and lower quartiles; range) for the true values of the ONH area, NRR area, cup area, ONH diameter, and CDR for the 23 of the 27 individuals who had undertaken perimetry reliably, by diagnosis, by observer and by viewing technique, are given in Tables 6.4.

Individuals with glaucoma (20)				
Feature	Observer A		Observer B	
	Mono	Stereo	Mono	Stereo
ONH area (mm²)	2.37 (2.09, 2.66; 1.27 to 3.34)	2.38 (2.11, 2.67; 1.35 to 3.39)	2.10 (1.73, 2.39; 1.12 to 2.87)	2.09 (1.71, 2.40; 1.14 to 3.15)
NRR area (mm²)	1.40 (1.07, 1.56; 0.28 to 2.19)	1.30 (0.95, 1.49; 0.28 to 2.35)	1.03 (0.77, 1.28; 0.43 to 1.92)	1.00 (0.78, 1.29; 0.50 to 1.84)
Cup area (mm²)	1.01 (0.78, 1.33; 0.20 to 1.63)	1.09 (0.74, 1.47; 0.20 to 1.89)	0.98 (0.71, 1.21; 0.15 to 1.94)	0.98 (0.72, 1.23; 0.13 to 1.89)
ONH diameter (mm)	1.54 (1.44, 1.63; 1.13 to 1.83)	1.54 (1.45, 1.63; 1.16 to 1.84)	1.45 (1.31, 1.55; 1.06 to 1.69)	1.45 (1.31, 1.55; 1.07 to 1.77)
CDR	0.67 (0.58, 0.72; 0.33 to 0.90)	0.67 (0.62, 0.76; 0.34 to 0.92)	0.70 (0.64, 0.74; 0.31 to 0.89)	0.70 (0.63, 0.76; 0.28 to 0.87)
Individuals with ocular hypertension (3)				
Feature	Observer A		Observer B	
	Mono	Stereo	Mono	Stereo
ONH area (mm²)	2.63 (2.59, 2.71; 2.51 to 3.34)	2.69 (2.61, 2.78; 2.54 to 3.80)	2.33 (2.29, 2.50; 2.27 to 2.87)	2.35 (2.28, 2.42; 2.25 to 2.70)
NRR area (mm²)	1.46 (1.43, 1.47; 1.25 to 2.22)	1.41 (1.33, 1.53; 1.10 to 2.10)	1.14 (1.10, 1.22; 0.99 to 1.51)	1.15 (1.05, 1.30; 0.93 to 1.37)
Cup area (mm²)	1.15 (1.13, 1.29; 0.83 to 1.70)	1.41 (1.20, 1.55; 1.70 to 0.95)	1.21 (1.16, 1.28; 0.95 to 1.70)	1.20 (1.10, 1.27; 1.65 to 1.01)
ONH diameter (mm)	1.62 (1.61, 1.64; 1.58 to 1.83)	1.64 (1.62, 1.67; 1.59 to 1.95)	1.53 (1.51, 1.58; 1.51 to 1.69)	1.53 (1.51, 1.55; 1.50 to 1.64)
CDR	0.67 (0.66, 0.69; 0.52 to 0.73)	0.68 (0.67, 0.73; 0.61 to 0.77)	0.72 (0.69, 0.74; 0.64 to 0.77)	0.72 (0.68, 0.73; 0.66 to 0.78)

Table 6.4. The descriptive statistics (median, upper and lower quartiles; range) for the true values of the ONH area, NRR area, cup area, ONH diameter, and CDR for the 20 individuals with glaucoma (top) and for the 3 individuals with ocular hypertension (bottom), by observer and by viewing technique.

The between-observer difference in the NRR area (mm^2) at baseline between Observer B and A against the mean of the NRR area (mm^2) derived by the two observers is given in Figure 6.4.

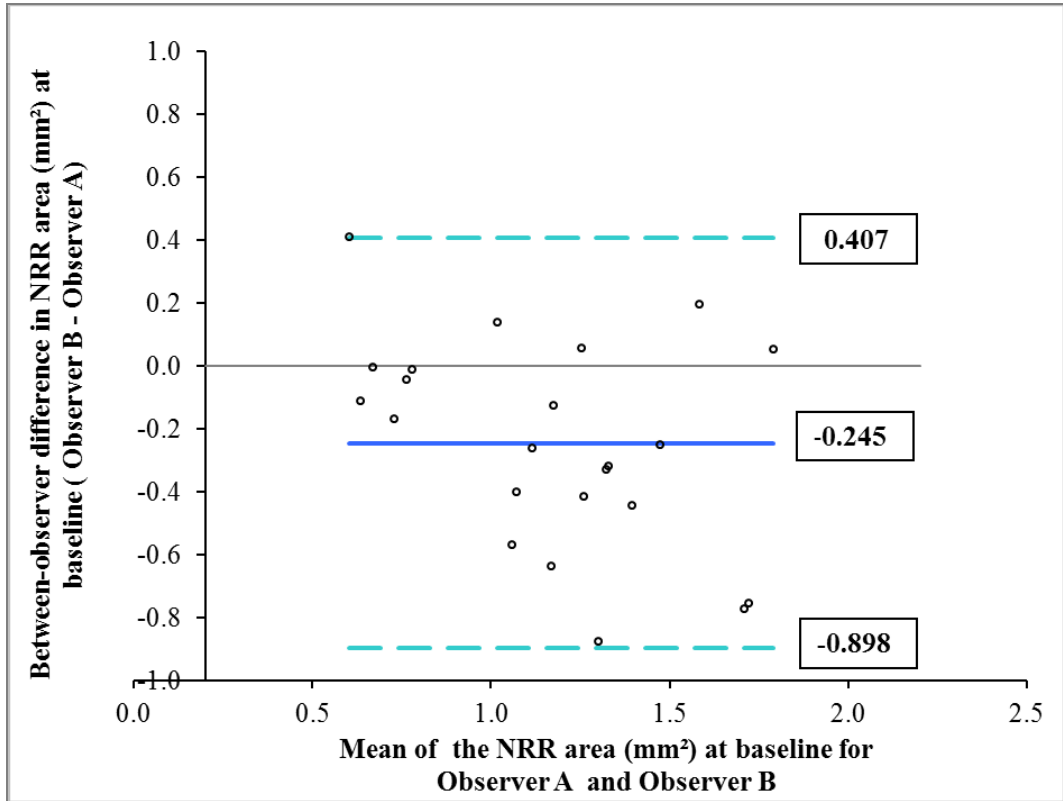


Figure 6.4. The between-observer difference in the NRR area (mm^2) at baseline between Observer B and A against the mean of the NRR area (mm^2) derived by the two observers. The solid line indicates the mean of the differences and the dotted line the 95% limits of agreement.

Observer A tended to overestimate the extent of the NRR area compared to Observer B (mean and median of the differences -0.245 mm^2 and -0.251 mm^2 , respectively). This between-observer difference was approximately 21% of the median NRR area averaged between the two observers.

The true NRR area (mm^2) against the true ONH area (mm^2) at the baseline photographic visit by observer for the 20 individuals with glaucoma, and for the 3 individuals with ocular hypertension, is given in Figure 6.5 (top) for 'Observer A' and in Figure 6.5 (bottom) for 'Observer B'.

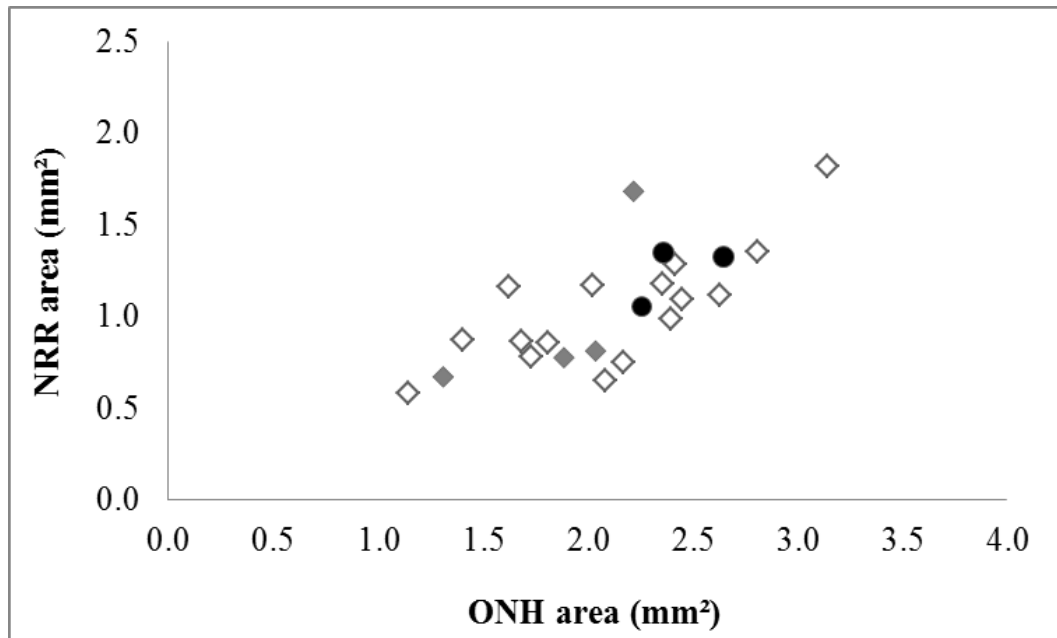
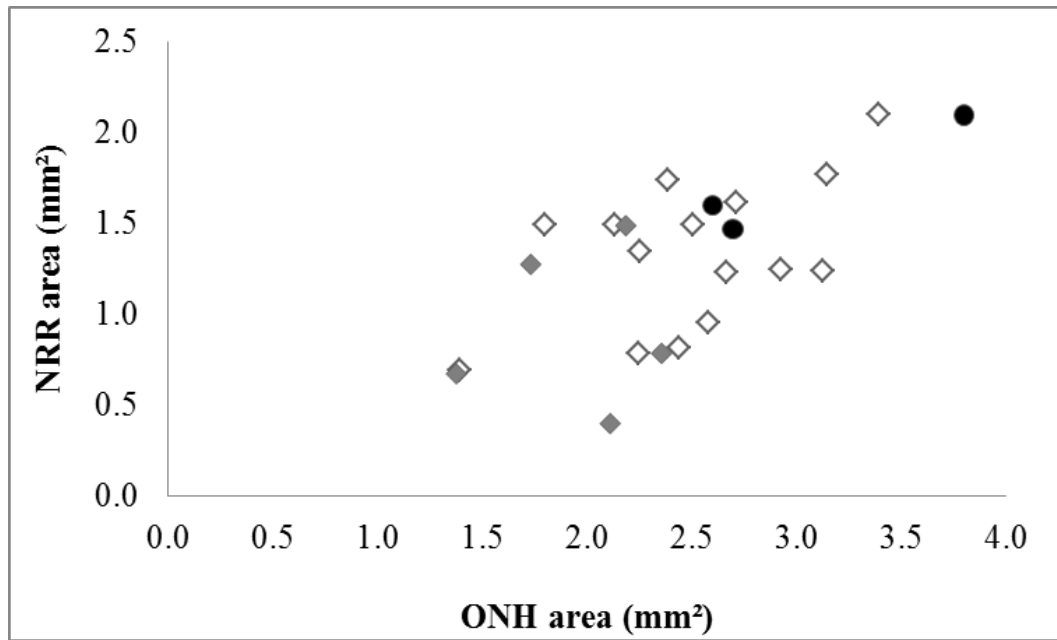


Figure 6.5. The true NRR area (mm²) against the true ONH area (mm²) at the baseline photographic visit by observer for the 23 individuals who had undertaken perimetry reliably (top) Observer A; (bottom) Observer B. The diamonds represent the 20 individuals with glaucoma (the filled diamonds indicate those with progressive cataract) and the filled circles the 3 individuals with ocular hypertension.

The VFI (%) at the baseline visual field examination against the true NRR area (mm²) at the baseline photographic visit for the 20 individuals with glaucoma, and for the 3 individuals with ocular hypertension, is given in Figure 6.6 (top) for ‘Observer A’ and in Figure 6.6 (bottom) for ‘Observer B’. The VFI declined

(worsened) in a curvilinear manner with reduction in the NRR area derived by each observer.

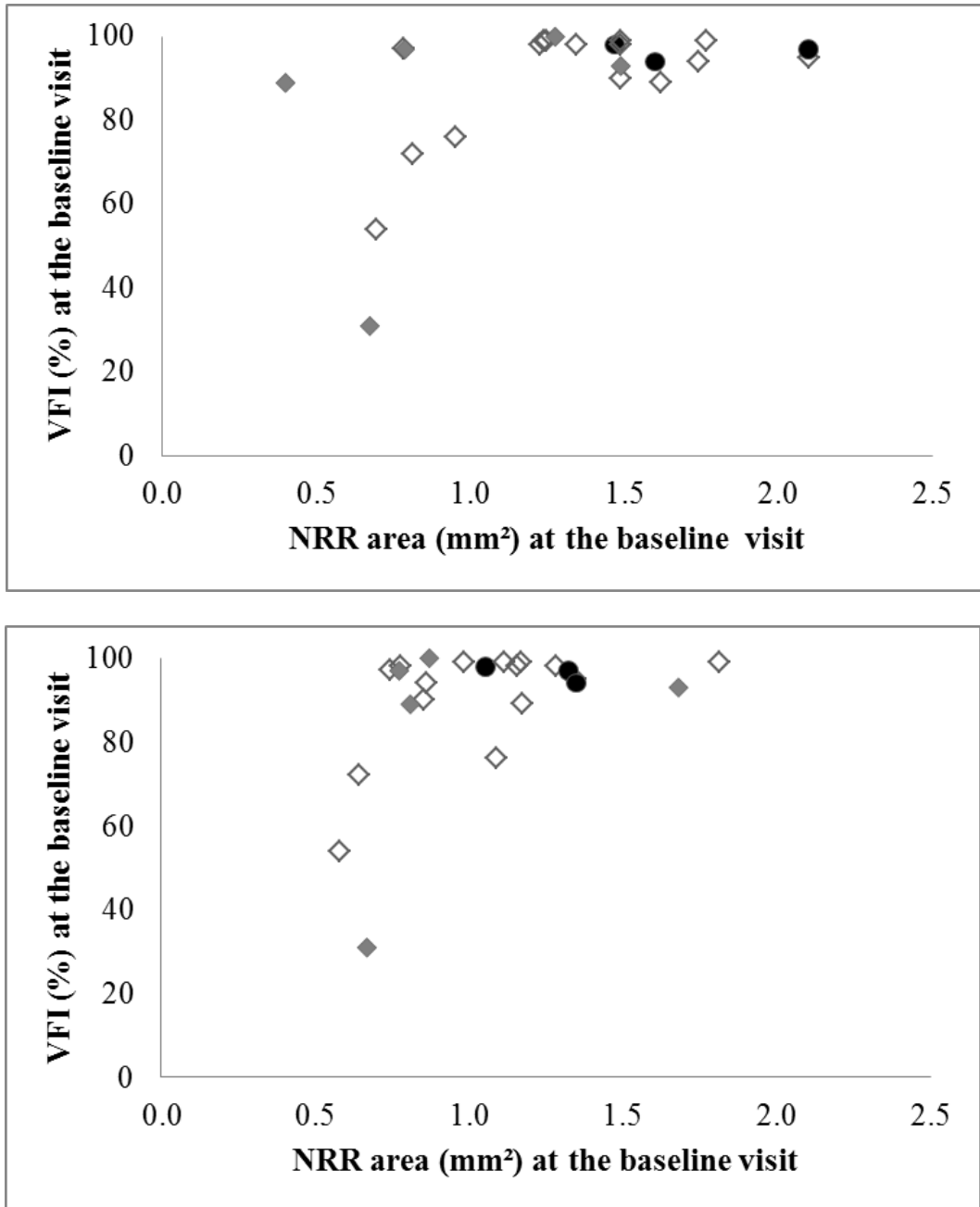


Figure 6.6. The VFI (%) at the baseline visual field examination against the true NRR area (mm²) at the baseline photographic visit for the 23 individuals for ‘Observer A’ (top) and ‘Observer B’ (bottom). The diamonds represent the 20 individuals with glaucoma (the filled diamonds indicate those with progressive cataract) and the filled circles the 3 individuals with ocular hypertension.

The MD (dB) at the baseline visual field examination against the true NRR area (mm²) at the baseline photographic visit for the 20 individuals with glaucoma,

and for the 3 individuals with ocular hypertension, is given in Figure 6.7 (top) for ‘Observer A’ and Figure 6.7 (bottom) for ‘Observer B’. The MD decreased (worsened) in a curvilinear manner with reduction in the NRR area derived by each observer.

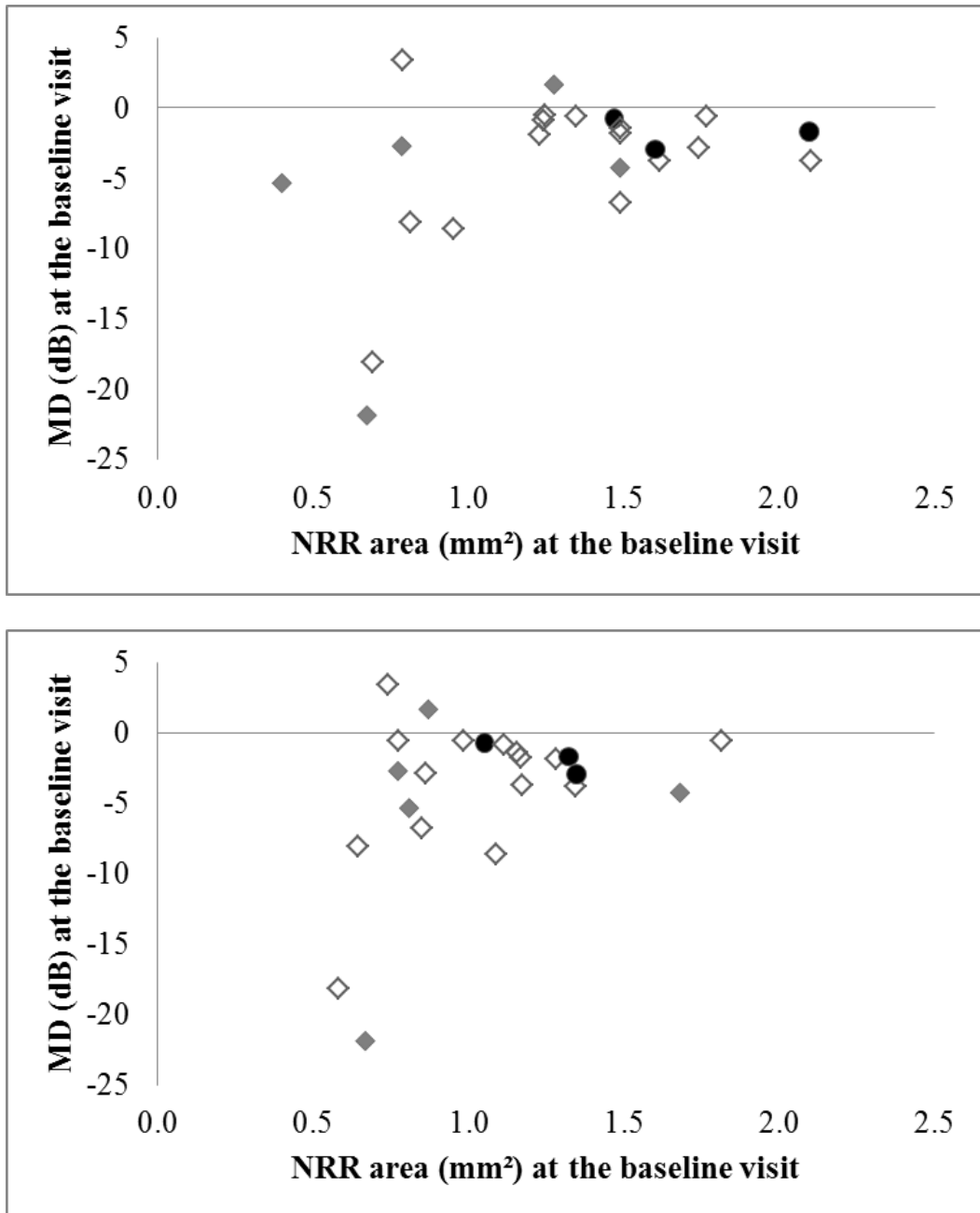


Figure 6.7. The MD (dB) at the baseline visual field examination against the true NRR area (mm²) at the baseline photographic visit for the 23 individuals for ‘Observer A’ (top) and ‘Observer B’ (bottom). The diamonds represent the 20 individuals with glaucoma (the filled diamonds indicate those with progressive cataract) and the filled circles the 3 individuals with ocular hypertension.

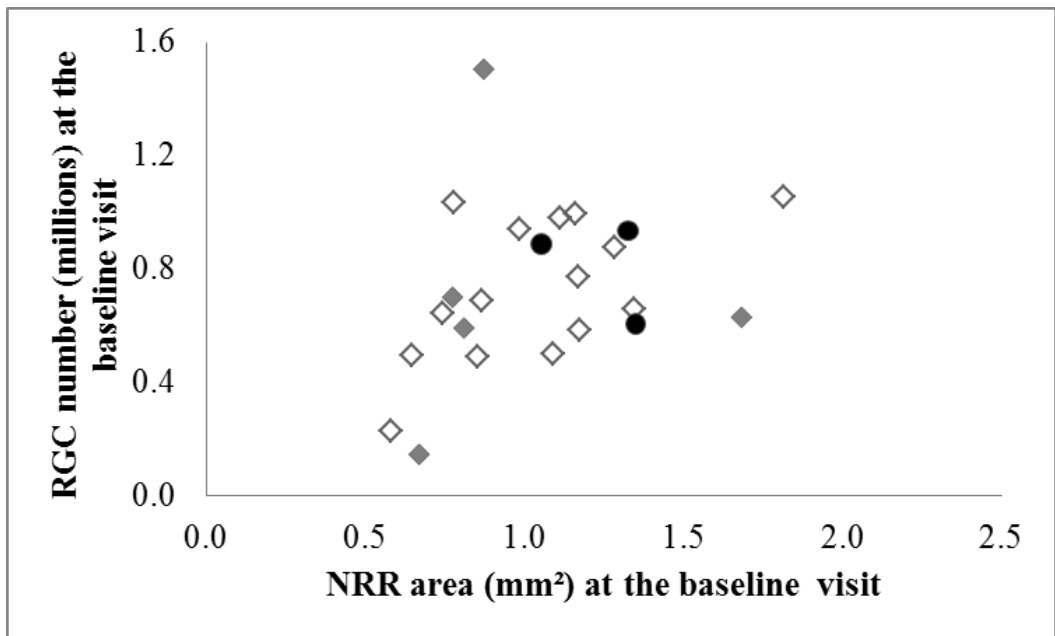
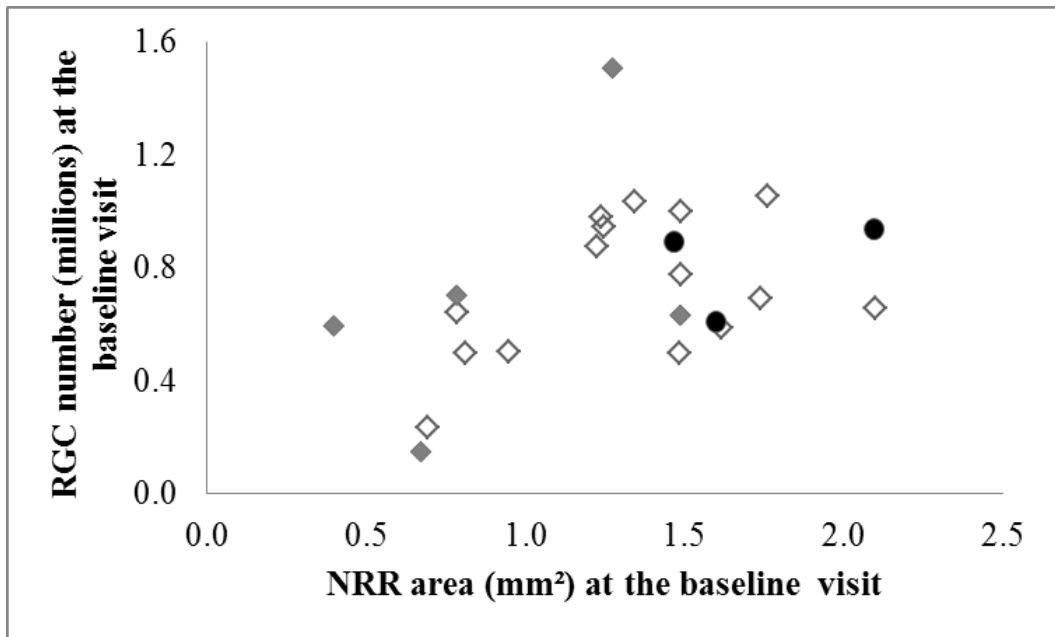


Figure 6.8. The number of RGCs (millions) at the baseline visual field examination against the true NRR area (mm²) at the baseline photographic visit for the 23 individuals for ‘Observer A’ (top) and ‘Observer B’ (bottom). The diamonds represent the 20 individuals with glaucoma (the filled diamonds indicate those with progressive cataract) and the filled circles the 3 individuals with ocular hypertension.

The number of RGCs (millions) at the baseline visual field examination against the true NRR area (mm²) at the baseline photographic visit for the 20 individuals with glaucoma, and for the 3 individuals with ocular hypertension, is given in Figure 6.8 (top) for ‘Observer A’ and Figure 6.8 (bottom) for ‘Observer B’. The

number of RGCs decreased in a more linear manner with reduction in the NRR area derived by each observer.

The between-observer difference in the proportionate change in the NRR area (%) at baseline between Observer B and A against the mean of the proportionate change in the NRR area (%) derived by the two observers is given in Figure 6.9. The mean of the differences in the proportionate changes between the two observers was -7.9% suggesting that Observer A identified less change in the NRR. However, this latter assumption was influenced by two notable outliers in the distribution of differences and the median of the differences was -1.8% indicating a much closer between-observer agreement than the mean in the identification of progressive change in the NRR.

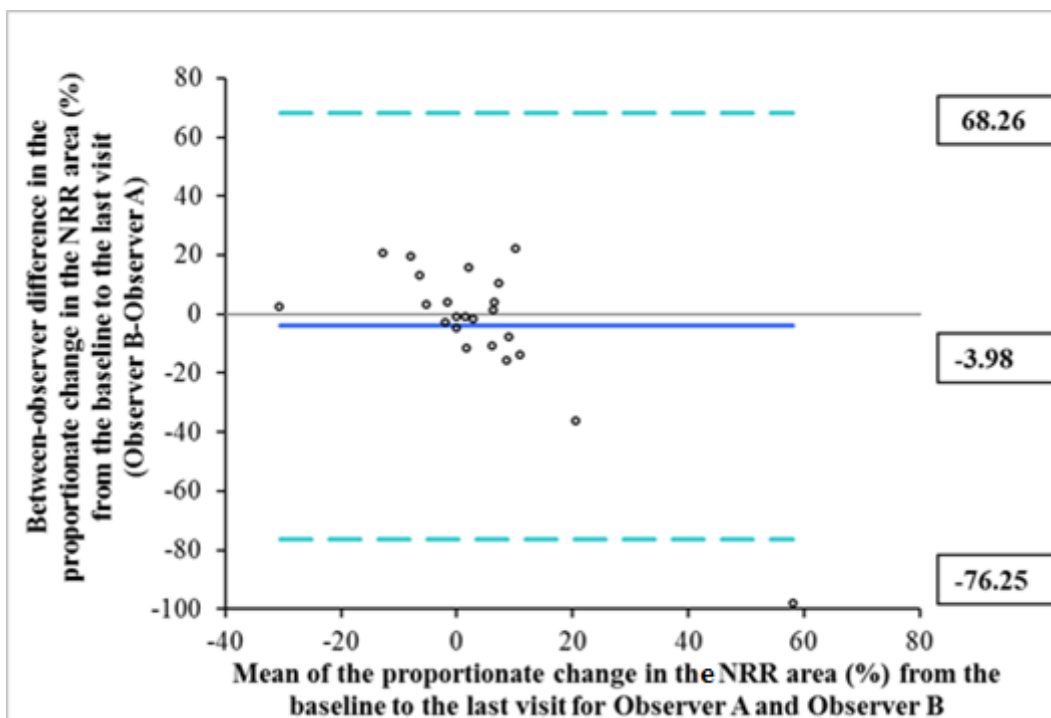


Figure 6.9. The between-observer difference in the proportionate change in the NRR area (%) at baseline between Observer B and A against the mean of the proportionate change in the NRR area (%) derived by the two observers. The solid line indicates the mean of the differences and the dotted line the 95% limits of agreement.

The frequency of visual field progression by trend-analysis (the statistical significance of the slopes of the VFI and MD against time to follow-up) and by event-analysis (EMGT GPA progression criteria) amongst the 23 individuals is shown in Table 6.5. Four individuals exhibited visual field progression by two or more of the three criteria and four by one criterion, alone.

Criteria	Visual field progression
MD	1
VFI	1
EMGT GPA	2
MD and VFI	2
MD and EMGT GPA	-
VFI and EMGT GPA	-
MD, VFI and EMGT GPA	2

Table 6.5. The frequency of visual field progression by trend-analysis (the statistical significance of the slopes of the VFI and MD against time to follow-up) and by event-analysis (EMGT GPA progression criteria) amongst the 23 individuals.

The proportionate change in VFI (%) from the baseline to the last visit against the corresponding proportionate change in the NRR (%), for each observer, is presented in Figure 6.10. There was no relationship between the proportionate change in the VFI, derived by either observer, and the proportionate change in the NRR area.

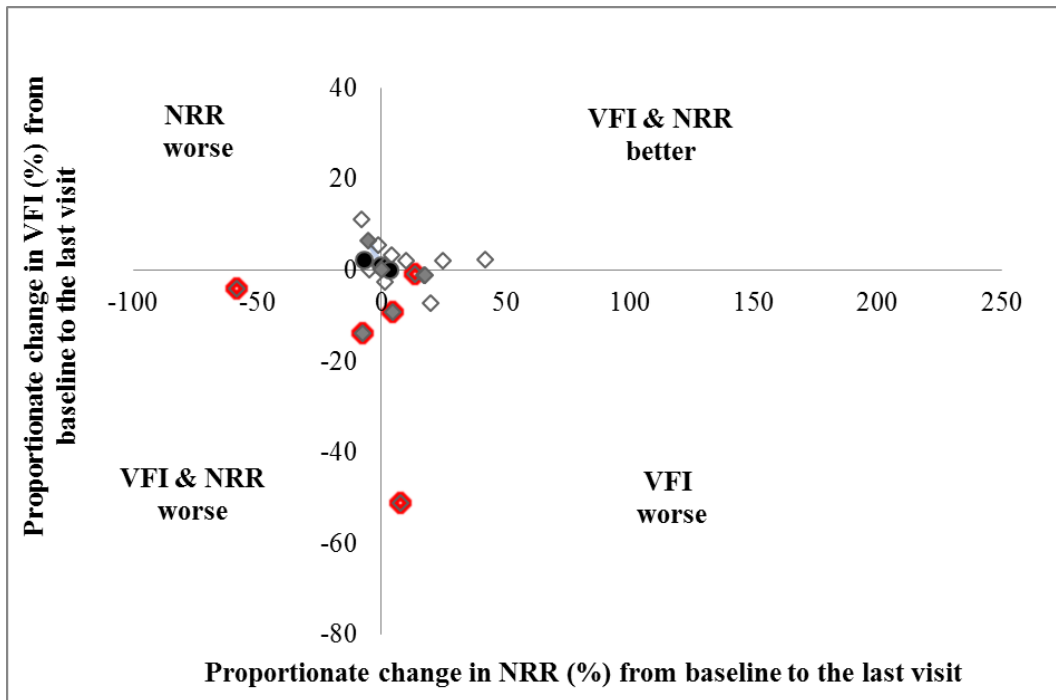
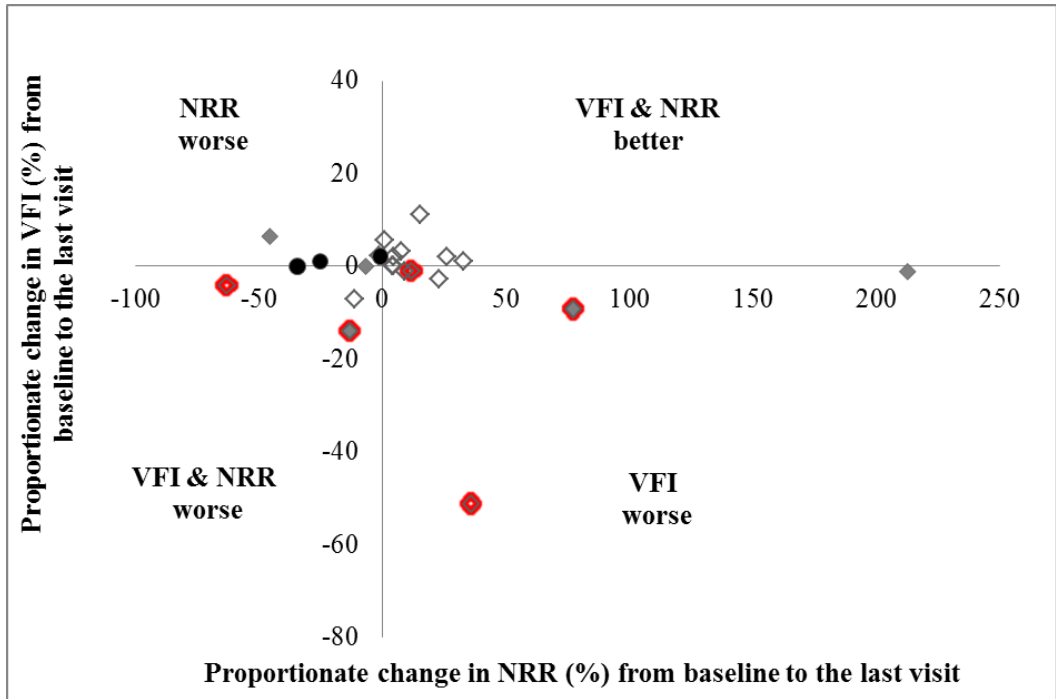


Figure 6.10. The proportionate change (%) in VFI from the baseline to the last visit against the corresponding proportionate change in the NRR (%), for Observer A (top) and Observer B (bottom). The diamonds represent the 20 individuals with glaucoma (the filled diamonds indicate those with progressive cataract) and the circles the 3 individuals with ocular hypertension. The red circles represent those exhibiting a statistically significant negative slope ($p < 0.5\%$) of the VFI against time to follow-up.

The proportionate change in MD (%) from the baseline to the last visit against the corresponding proportionate change in the NRR (%), by observer, is presented in Figure 6.11. There was no relationship between the proportionate change in the MD, derived by either observer, and the proportionate change in the NRR area.

The proportionate change in the number of RGCs (%) from the baseline to the last visit against the corresponding proportionate change in the NRR (%), by observer, is presented in Figure 6.12. There was also no relationship between the proportionate change in the number of RGCs, derived by either observer, and the proportionate change in the NRR area.

The proportionate change from the baseline to the last visit in the number of RGCs for the superior and inferior sectors, respectively, against the corresponding proportionate change in the NRR (%), is given in Figures 6.13 and 6.14. There was no relationship, for either sector, between the proportionate changes in the NRR, derived by either observer, and the proportionate changes in the number of RGCs. The proportionate change in VFI and the MD could not be calculated for the four sectors owing to the proprietary nature of the age-corrected normal values.

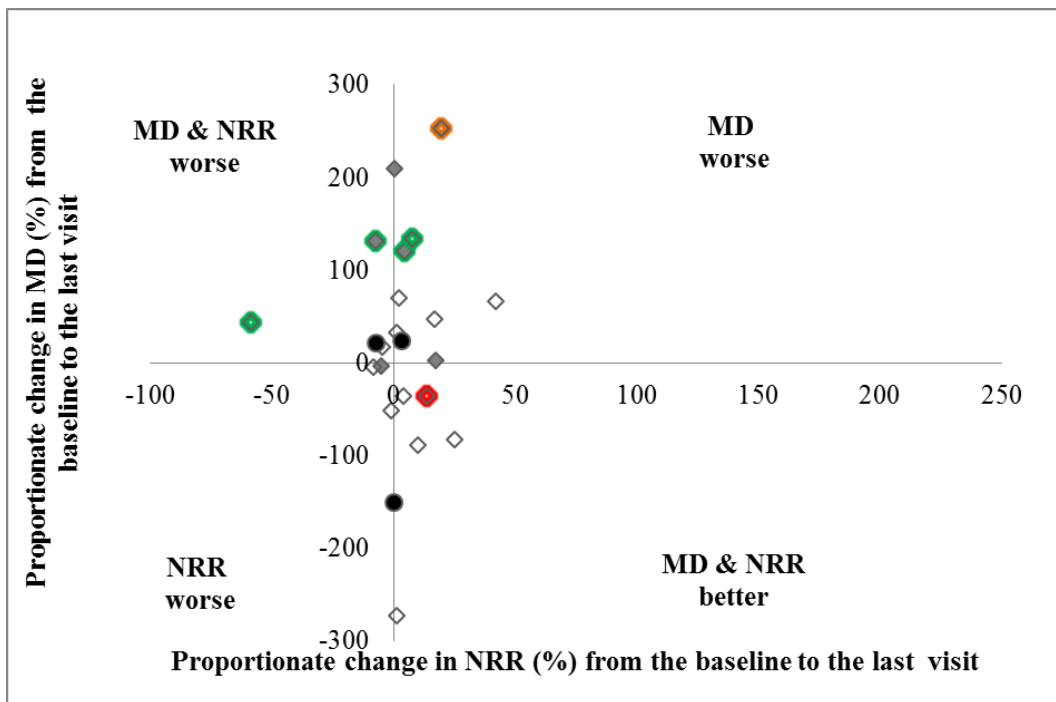
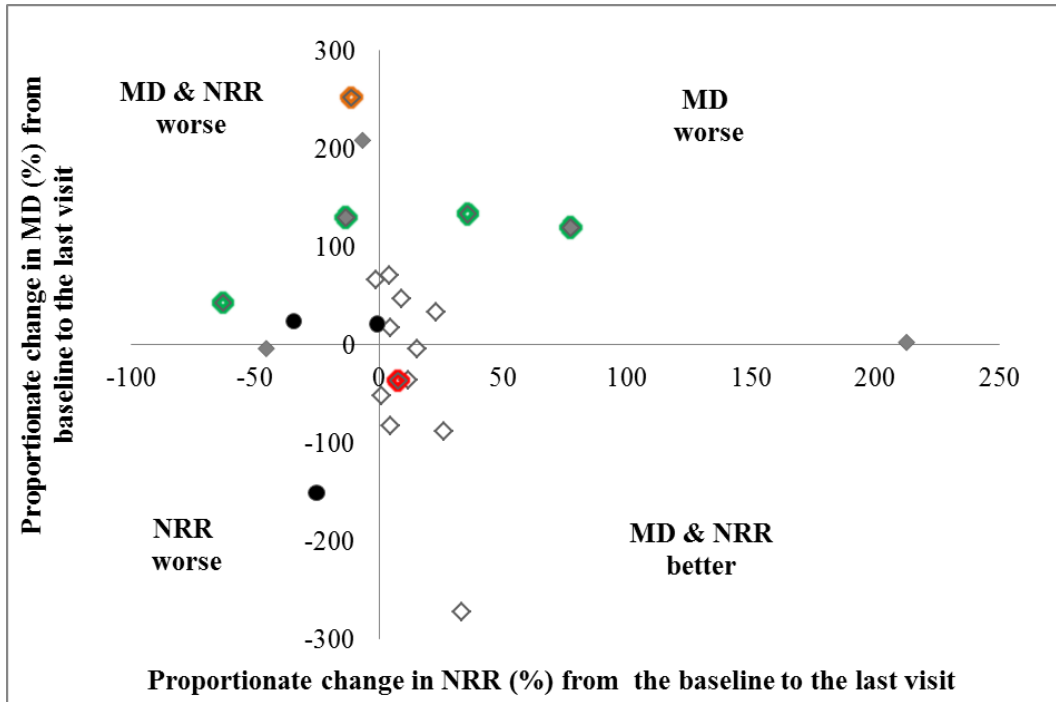


Figure 6.11. The proportionate change in MD (%) from the baseline to the last visit against the corresponding proportionate change in the NRR (%), for Observer A (top) and Observer B (bottom). The diamonds represent the 20 individuals with glaucoma (the filled diamonds indicate those with progressive cataract) and the circles the 3 individuals with ocular hypertension. The red circles represent those exhibiting a statistically significant negative slope ($p < 0.5\%$) of the VFI against time to follow-up; the orange circles those individuals with a statistically significant negative slope ($p < 0.5\%$) for the MD against time to follow-up; and the green circles those individuals with a statistically significant negative slope ($p < 0.5\%$) of both the VFI and the MD against time to follow-up.

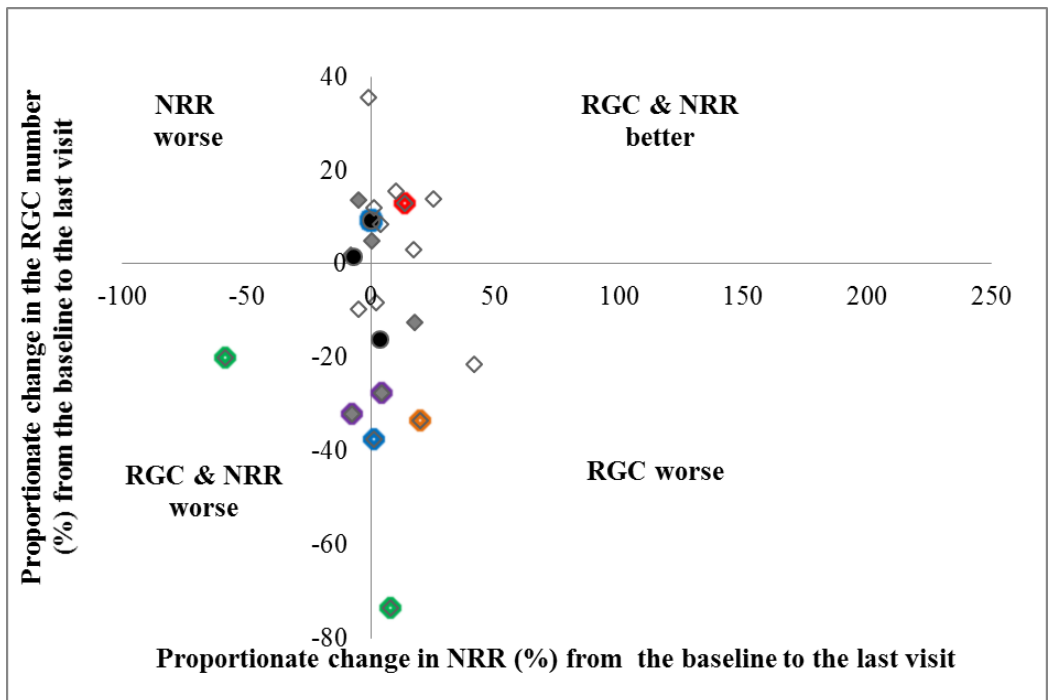
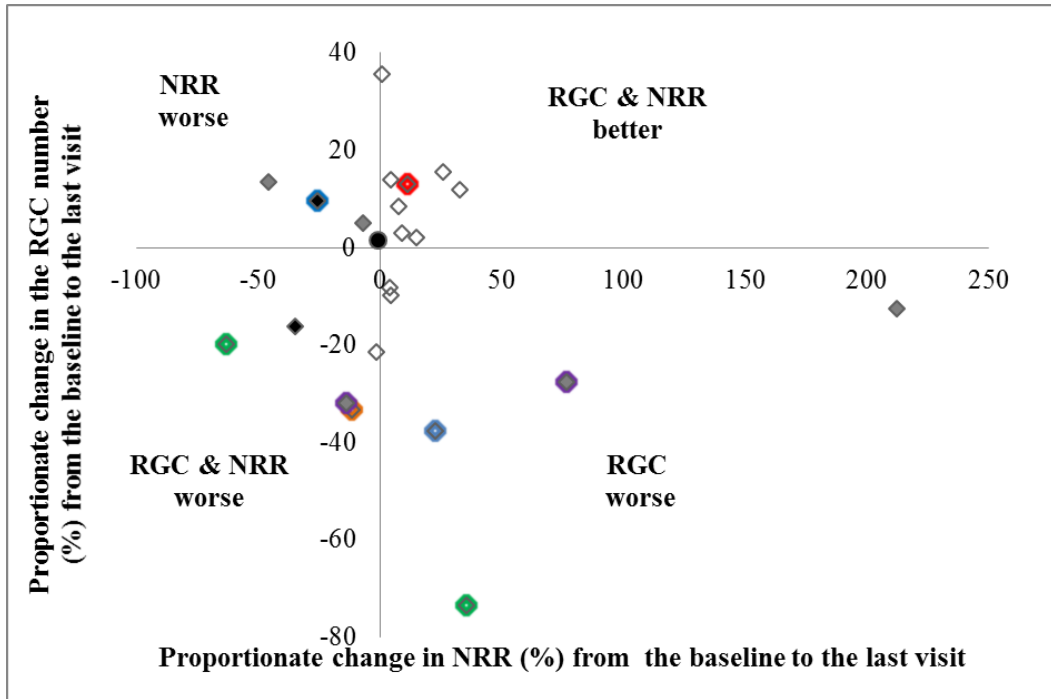


Figure 6.12. The proportionate change in the number of RGCs (%) from the baseline to the last visit against the corresponding proportionate change in the NRR (%), for Observer A (top) and Observer B (bottom). The diamonds represent the 20 individuals with glaucoma (the filled diamonds indicate those with progressive cataract) and the circles the 3 individuals with ocular hypertension. The red circles represent those exhibiting a statistically significant negative slope ($p < 0.5\%$) of the VFI against time to follow-up; the orange circles those individuals with a statistically significant negative slope ($p < 0.5\%$) for the MD against time to follow-up; the green circles those individuals with a statistically significant negative slope ($p < 0.5\%$) of both the VFI and the MD against time to follow-up; the purple circles those individuals with a statistically significant negative slope ($p < 0.5\%$) of both the VFI and the MD against time to follow-up and ‘likely progression’ with the EMGT GPA criteria and the blue circles those individuals exhibiting ‘likely progression’ with the EMGT GPA criteria.

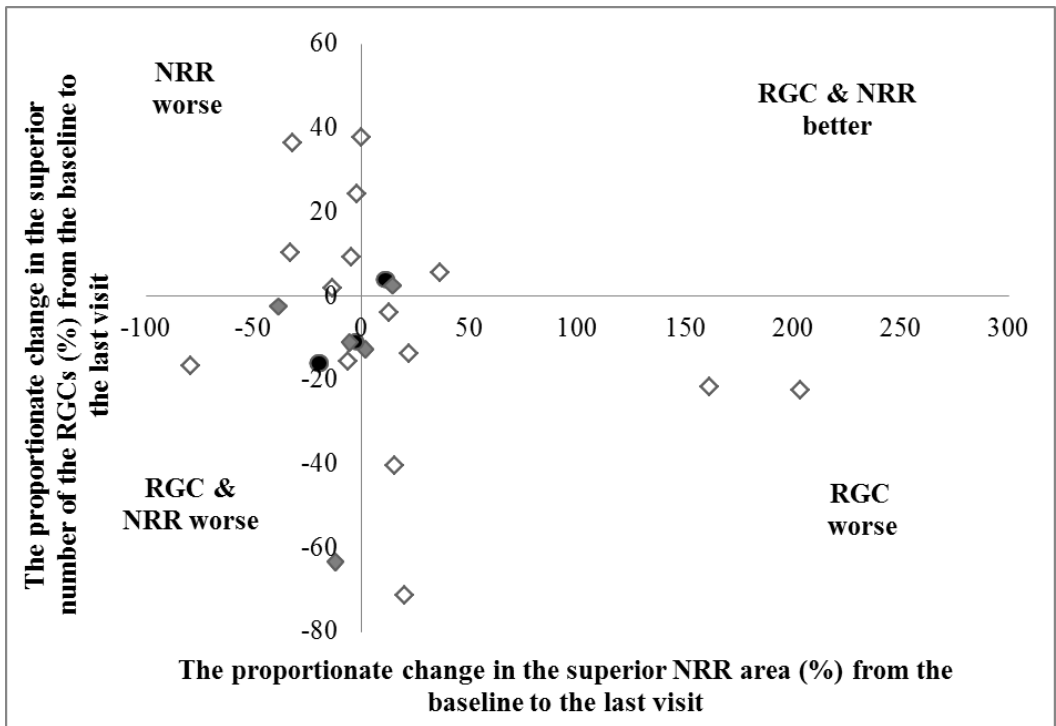
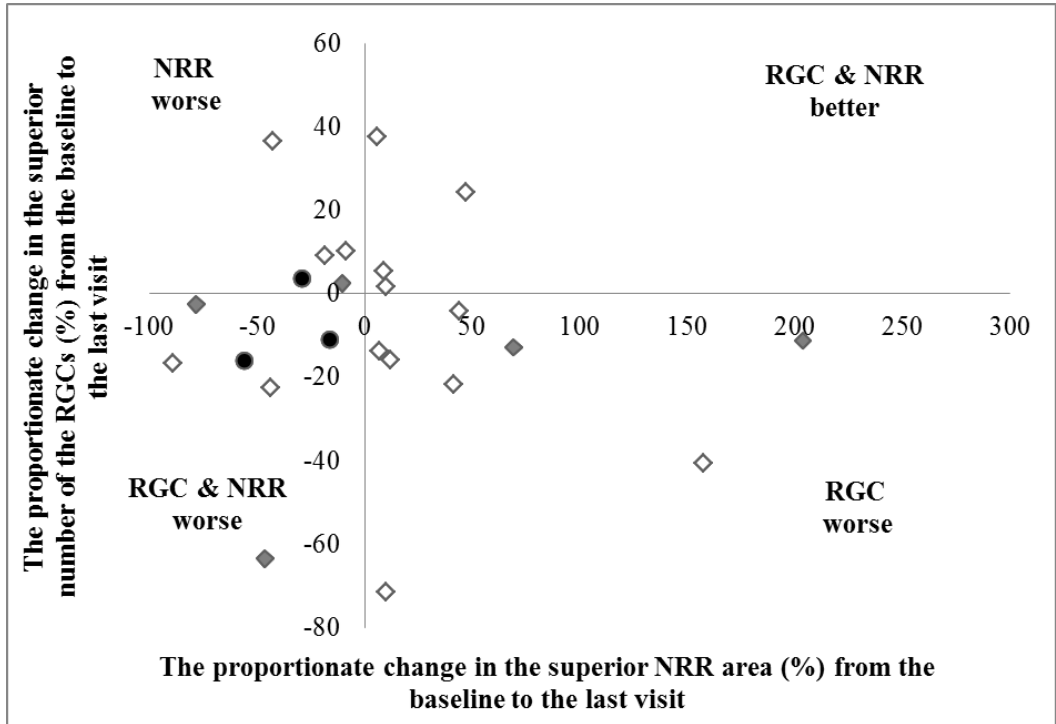


Figure 6.13. The proportionate change in the superior number of RGCs (%) from the baseline to the last visit against the corresponding proportionate change in the superior NRR area (%), for Observer A (top) and Observer B (bottom). The diamonds represent the 20 individuals with glaucoma (the filled diamonds indicate those with progressive cataract) and the circles the 3 individuals with ocular hypertension.

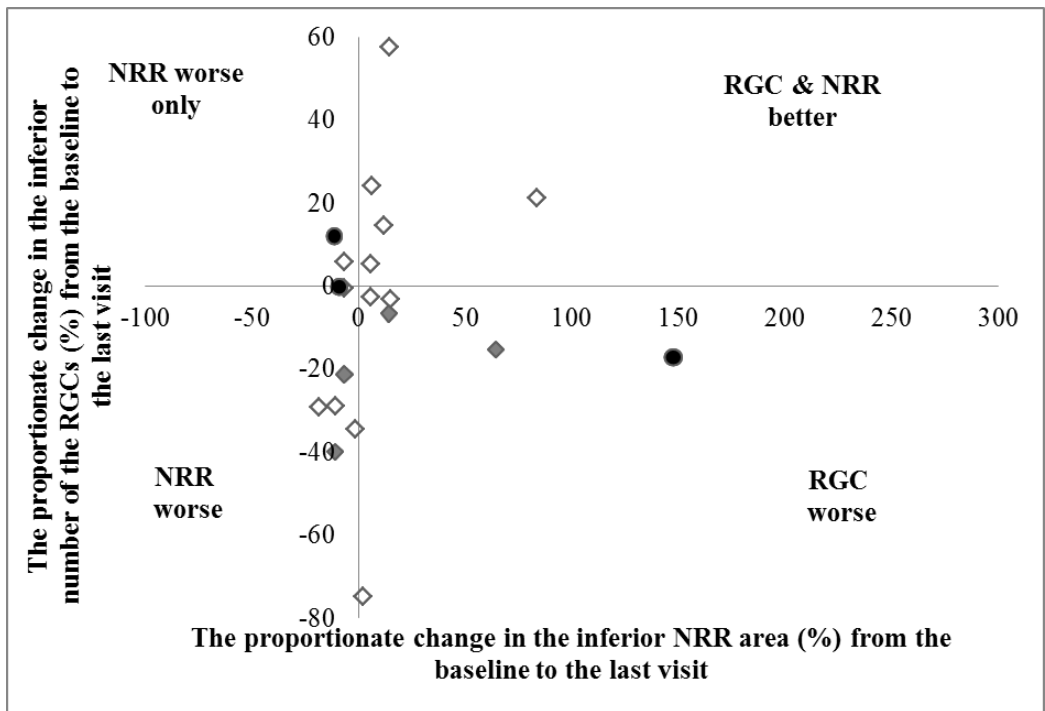
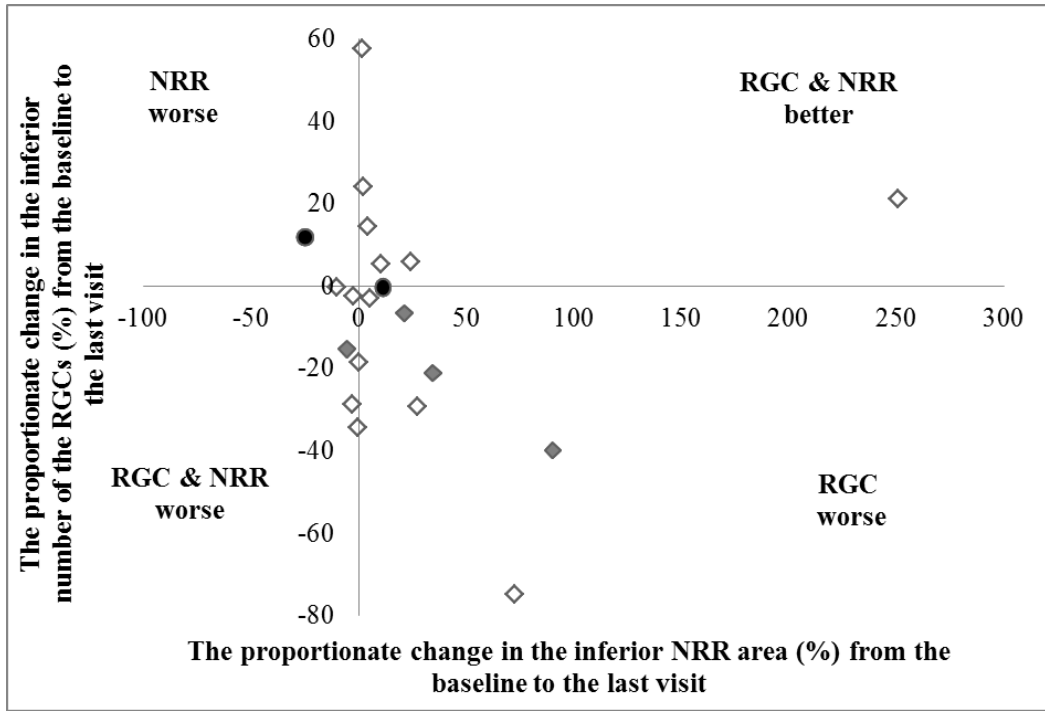


Figure 6.14. The proportionate change in the inferior number of RGCs (%) from the baseline to the last visit against the corresponding proportionate change in the inferior NRR area (%), for Observer A (top) and Observer B (bottom). The diamonds represent the 20 individuals with glaucoma (the filled diamonds indicate those with progressive cataract) and the circles the 3 individuals with ocular hypertension.

The between-observer difference in the proportionate change of the NRR area (%) against the time interval (years) is given in Figure 6.15.

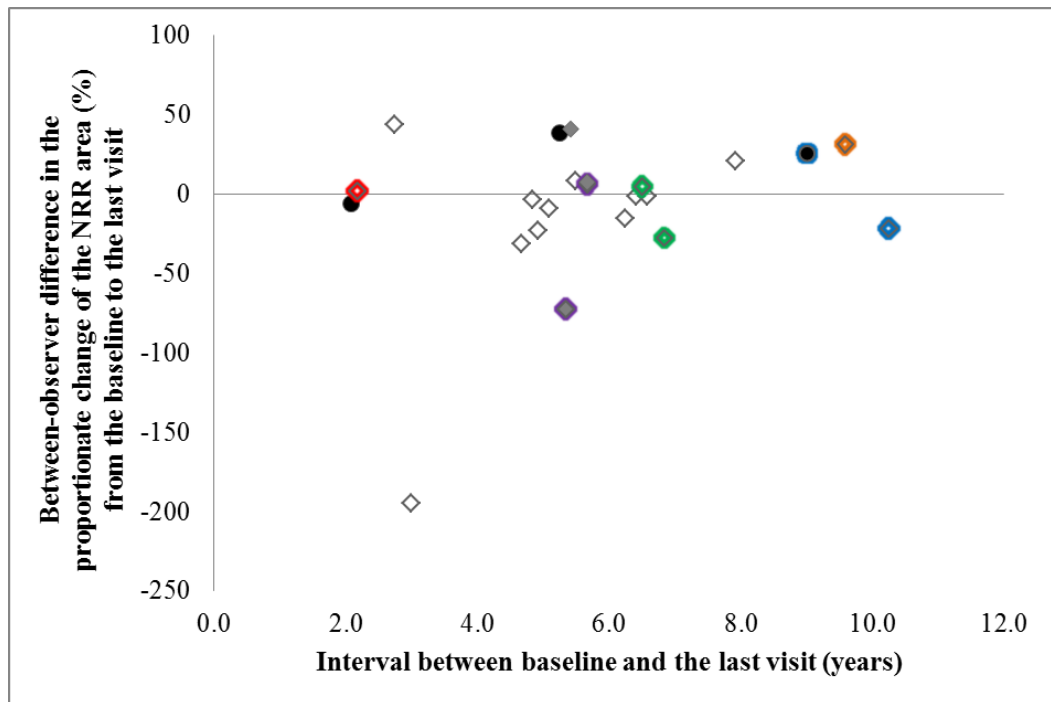


Figure 6.15. The between-observer difference in the proportionate change of the NRR area (%) against the time interval (years). The diamonds represent the 20 individuals with glaucoma (the filled diamonds indicate those with progressive cataract) and the circles the 3 individuals with ocular hypertension. The red circles represent those exhibiting a statistically significant negative slope ($p < 0.5\%$) of the VFI against time to follow-up; the orange circles those individuals with a statistically significant negative slope ($p < 0.5\%$) for the MD against time to follow-up; the green circles those individuals with a statistically significant negative slope ($p < 0.5\%$) of both the VFI and the MD against time to follow-up; the purple circles those individuals with a statistically significant negative slope ($p < 0.5\%$) of both the VFI and the MD against time to follow-up and 'likely progression' with the EMGT GPA criteria and the blue circles those individuals exhibiting 'likely progression' with the EMGT GPA criteria.

6.5 Discussion

The results indicate a weak curvilinear association between structure (defined as the extent of the NRR area and delineated by manual stereo-digital planimetry using a floating cursor) and function (defined separately in terms of the visual field indices, MD and VFI). A slightly stronger, but linear, association was present between NRR and residual RGC count. The outcomes of the planimetry, and hence the strengths of these various associations, varied between the two ophthalmologists.

The results also indicate that there was no association between structural progression (defined in terms of a proportionate reduction in the NRR area and delineated by digital manual stereo-planimetry using a floating cursor) and functional progression (defined in terms of the proportionate change in the MD, the VFI and the residual RGCs count, respectively). The outcomes of the planimetry again varied between the two ophthalmologists. The association was not improved by the separate consideration of the superior and inferior sectors of the ONH.

Considerable care had been taken to ensure that the images from the various photographic sources had been standardised between camera variations in image size (Chapter 4). All measurements from the various cameras were corrected for the magnification of the given camera, then standardised relative to the reference camera, and finally scaled to correct for refractive error based on an algorithm incorporating keratometry readings and mean spherical error. The images were then colour balanced relative to baseline image of the time series.

The dimensions of the optic disc ONH area (Table 6.4) and the relationship between the neuroretinal rim area and the cup area (Figure 6.5) are compatible with those generally accepted in the literature (Varma 1993; Garway-Heath and Hitchings 1998; Jonas et al. 1999; Hoffmann et al. 2007; Sanfilippo et al. 2009; Andersson et al. 2011; Cankaya and Simsek 2012).

The weak curvilinear association between the visual field indices MD and VFI at baseline and the corresponding NRR area was expected given the derivation of these two indices from the logarithmic dB scale of perimetry. Nevertheless, it is contrary to the linear association with MD of $r=0.57$ (Saito et al. 2010). As would be expected, the association between visual field outcome expressed linearly in terms of residual RGCs count exhibited a linear function with NRR area.

The extent of the disparity between the two consultant ophthalmologists, both of whom were trained to fellowship standard in glaucoma and whose sub-specialty was glaucoma, in terms of not only the qualitative analysis, but also the planimetry, was unexpected. The mean and median of the differences between ophthalmologists in the identification of the NRR area at baseline was approximately 21% of the median NRR area averaged across the two ophthalmologists. Clearly, appreciation of the subtle features of the glaucomatous ONH varies between ophthalmologists. The corresponding difference for the identification of progressive change in the NRR was approximately 4%. However, both ophthalmologists performed planimetry which resulted in an apparent improvement in the NRR in the same 11 cases. The improvement identified by Observer A was greater than 20% in 6 of these 11 cases and up to

10% in the remaining 5 cases. The corresponding improvement for Observer B was less than 10% in 6 cases and greater than or equal to 10% in the remaining five cases. These figures highlight the subjective nature of planimetry. It is not possible, of course, to separate a measured reduction in the NRR from a ‘true’ reduction and the corresponding between-observer evaluation cannot be undertaken.

Any number of additional ophthalmologists could have been recruited to participate in the study. However, the study was not intended to determine differences between ophthalmologists in the qualitative and quantitative identification of glaucoma and progressive glaucoma.

Digital stereo-planimetry was used as the ‘gold standard’ rather than mono-planimetry, since the advantage of stereo-planimetry in the diagnosis of glaucoma has been well documented and was noted in the results described in Chapter 5. The use of a ‘floating cursor’ enhanced the visualization of the ONH features; however, the association between progressive functional and progressive structural damage was not seemingly improved by such a technique.

The structural-functional associations were based upon the topographical mapping proposed by Garway-Heath which in turn is based upon the ONH segmentation of Wirtschafter and colleagues (Wirtschafter et al. 1982). Alternative models of ONH segmentation could have been used such as those of (Abramoff et al. 2007; Lee et al. 2010; Muramatsu et al. 2011; Fraz et al. 2012; Jiang et al. 2012a) however, the approach by Garway-Heath has become the ‘gold

standard'. Nevertheless, such segmentation has been defined by empirical observation and may, in itself, be a limiting factor to the structure and function relationship.

The structural and functional progression was evaluated between the baseline and the most recent point in the time series to maximise the potential for deterioration in one or both outcomes.

The lack of an association between progressive functional and progressive structural damage is dependent upon a number of factors including the quality of visual field examination and the number of individuals exhibiting progression of either modality within the cohort and the extent of any progression. The latter is influenced by the length of the time series in the given study and by the quality of the ophthalmological patient care. The length of the time series varied between the individuals in the cohort. However, there was no relationship between the apparent progression of either, or both, structural and functional outcomes and the length of the time series. The individuals in the cohort all attended a university teaching hospital under the care of a consultant ophthalmologist with an international reputation in glaucoma.

Clearly, a weakness of the study was the sparsity of ONH images for any given individual relative to the number of visual field examinations. In addition, the ONH photography and visual field examination was not necessarily conducted on the same day. In order to obtain a realistic cohort for the study, it was necessary to include individuals with a maximum interval between the two techniques of up

to 12 months. The lack of a sufficient number of ONH images for any given individual prevented the calculation of the rate of NRR change with time.

The ONH area and NRR area was calculated based on the assumption that each of these variables is a circle. The latter approach is consistent with other studies (Barkana 2007; Laemmer et al. 2007). However, the areas were each calculated from a composite of the individual seventy-two 5° sectors (Saito et al. 2010; Morgan et al. 2012). This technique is more sensitive to localized departures from the assumed circular nature of both the ONH and the NRR. Nevertheless this approach does not account for any theoretical between-individual ‘rotation’ of the ONH relative to the orientation at which the measurements are referenced to. However, cases of clinically detectable tilted discs were excluded from the cohort.

Overall, the results from this chapter and those from Chapter 5 suggests that the subjective evaluation of the ONH in isolation, and expressed either qualitatively or quantitatively is insufficient for the optimum diagnostic sensitivity and specificity and for the evaluation of progressive loss.

Chapter 7

Pointwise linear regression of residual retinal ganglion cell count

7.1 Introduction

The nature of the progressive structural and functional relationship in glaucoma remains inconclusive and the outcomes described in Chapter 6 failed to clarify the matter even when the functional outcome was considered in terms of the proportional reduction in the residual RGC based upon the visual field as a whole.

Currently, there is no consensus on the optimum method to identify progressive visual field loss and, therefore, there is no accepted standard against which comparisons can be made. It was stated in Chapter 1 that progressive visual field loss can be evaluated using empirical clinical judgement, defect classification systems, trend-analysis (e.g., pointwise linear regression analysis [PLR]) and event-analysis (e.g., Guided Progression Analysis [GPA] based upon glaucoma change probability maps) (Ang et al. 2011; Rao et al. 2013b; Talbot et al. 2013).

It was also stated in Chapter 1 that univariate linear regression analysis of the visual field outcome against time to follow-up can be based upon either a global summary measure of the visual field such as the visual field indices MD (Gardiner et al. 2012b; Polaczek-Krupa and Grabska-Liberek 2012), PSD (Ang et al. 2011; Rao et al. 2013a), VFI (Medeiros et al. 2012c; Hirasawa et al. 2013; Gros-Otero et al. 2014; Lee et al. 2014b) Diffuse Defect (DD) (Monhart et al.

2006) and Local Defect (LD) (Buerki 2007) or upon the outcome at each individual stimulus location such as the absolute value of sensitivity (Bengtsson et al. ; Iester et al. 2011) or of the Pattern Deviation value (Gardiner et al. 2011; Marin-Franch et al. 2014). A minimum of five reliable visual field examinations is required (McNaught et al. 1996; Artes et al. 2010; Teng et al. 2010; Azarbod et al. 2012). The technique is a 'within-individual' analysis which does not depend upon the comparison with an established database of 'stable' patients. Progression is defined in terms of the statistical significance, and magnitude, of the slope of the function (Wild et al. 1993; McNaught et al. 1996; Viswanathan et al. 1998; Azarbod et al. 2012).

As was discussed previously, the outcome of the visual field examination, the differential light sensitivity, is expressed in logarithmic units (dB) which is referenced to the maximum luminance of the stimulus. By definition, the dB scale is an exponential measure: a change of 3dB represents either a doubling or a halving of the stimulus luminance. Therefore, when the (functional) outcome from the visual field expressed in dB is plotted against the (structural) outcome from the ONH or RNFL expressed as a linear measure, the function is curvilinear (Malik et al. 2012; Medeiros et al. 2012a). For example, when the differential light sensitivity is plotted on a linear scale, identical increments or decrements in dB at differing levels of sensitivity exhibit differing increments or decrements. When the functional and structural outcomes are both plotted on either logarithmic or linear scales, the relationship is essentially linear at any given eccentricity.

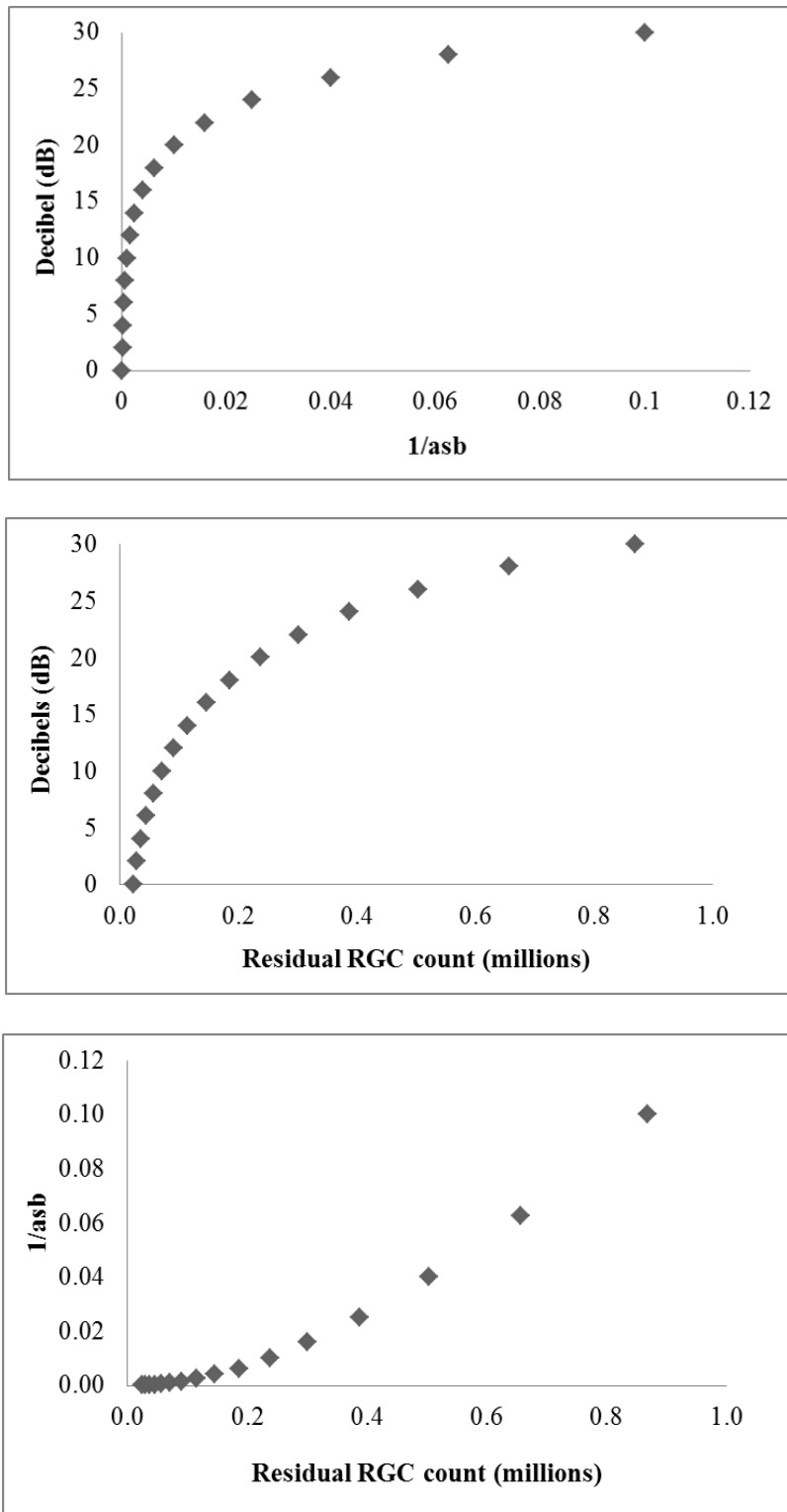


Figure 7.1. The relationship between the various transformations of the mean differential light sensitivity recorded with stimulus size III using Program 24-2 and specified in dB. Note the differences in the scaling of the various axis.

A more appropriate expression of the visual field outcome maybe that of residual RGC count which is a linear entity. Such an expression should overcome the

limitation of the logarithmic dB scale in expressing the linear magnitude of the functional loss corresponding to a small dB reduction at high levels of differential light sensitivity and the overestimation of the linear magnitude, when expressed in dB, at the low levels of differential light sensitivity (Garway-Heath et al. 2000a; Medeiros et al. 2013) (Figure 7.1). The use of a linear entity based upon the number of the residual RGCs for the evaluation of progressive visual field loss should, therefore, identify progressive loss in previously normal or near normal areas of the visual field ‘earlier’ than that based upon the corresponding outcome defined in terms of the logarithmic dB scale and lessen the magnitude of the apparent progression in moderate to severe glaucoma. Such an approach would provide a more equivalent relationship with the progressive structural outcome.

7.2 Aim

The aim of the study was to compare, at each stimulus location, the outcome of univariate linear regression of differential light sensitivity (expressed in dBs) against time to follow-up with that of the corresponding residual ganglion cell count against time to follow-up in the (early) identification of progressive visual field loss for a long-time series.

7.3 Methods

The medical records of 1000 consecutive patients who had attended the Glaucoma Clinics at the Cardiff Eye Unit, UHW, between 1999 and 2014, were searched using the electronic database ‘Open Eyes’. The minimum criteria for inclusion were a diagnosis of primary open-angle glaucoma, in the absence of

any concomitant ocular disease other than age-related cataract, and 5 visual field examinations, undertaken reliably, over a minimum follow-up of 5 years.

Perimetry had been undertaken with the Humphrey Field Analyzer Mark II, using either the SITA Fast or the SITA Standard strategy and Program 24-2. The reliability criteria were $\geq 15\%$ incorrect responses to the false-positive catch trials, $\geq 20\%$ incorrect responses to the false-negative catch trials and $\geq 20\%$ fixation losses.

The search yielded a total of 112 patients. The results of the visual field examinations for these patients were then retrieved from the hard drives of the HFA 700 series perimeters, which had been, or were still, operational in the Department of Orthoptics from 1999 onwards. The Single Field Analysis printouts for each patient were then scanned and archived in .pdf format.

The corresponding global indices (MD, PSD and VFI) were recorded and archived from each visual field examination for each individual. An ordinary least squares univariate linear regression analysis was separately undertaken for each of the three visual field indices, MD, PSD and VFI, and for the global residual RGC count using the Statistical Analysis System 9.4 (SAS, Cary NC). The output contained the estimate of the slope, the lower and upper 95% confidence limits of the estimate and the statistical significance of the slope (Figure 7.2).

06:08 Friday, November 14, 2014

sub	Dependent	Parameter	Estimate	pm	Probt	LowerCL	UpperCL	expest
9	md	Intercept	10.93	.	0.0091	3.87	17.99	.
		age	-0.22	0.13	0.0059	-0.35	-0.09	.
	psd	Intercept	-0.20	.	0.9132	-4.52	4.12	.
		age	0.04	0.08	0.2708	-0.04	0.12	.
	lpsd	Intercept	-0.45	.	0.6478	-2.73	1.83	.
		age	0.02	0.04	0.2819	-0.02	0.06	1.02015
	vfi	Intercept	117.72	.	<.0001	104.98	130.45	.
		age	-0.36	0.23	0.0085	-0.59	-0.13	.
	lvfi	Intercept	4.79	.	<.0001	4.66	4.92	.
		age	-0.00	0.00	0.0084	-0.01	-0.00	0.99628
	rgc	Intercept	2974555.59	.	0.0006	1852214.84	4096896.33	.
		age	-38640.02	20305.56	0.0035	-58945.59	-18334.46	.
	lrgc	Intercept	16.19	.	<.0001	15.04	17.34	.
		age	-0.05	0.02	0.0016	-0.07	-0.03	0.95474
	10	md	Intercept	-2.40	.	0.8242	-30.45	25.66
age			-0.07	0.42	0.6657	-0.49	0.35	.
psd		Intercept	11.61	.	0.5172	-33.82	57.04	.
		age	-0.03	0.69	0.9157	-0.71	0.66	.
lpsd		Intercept	2.56	.	0.2011	-2.09	7.21	.
		age	-0.00	0.07	0.8705	-0.07	0.07	0.99562
vfi		Intercept	44.62	.	0.5589	-149.95	239.19	.
		age	0.52	2.93	0.6476	-2.41	3.46	.
lvfi		Intercept	3.96	.	0.0112	1.50	6.43	.
		age	0.01	0.04	0.6719	-0.03	0.04	1.00613
rgc		Intercept	70460.05	.	0.8654	-1012296.38	1153216.48	.
		age	7475.57	16332.71	0.2727	-8857.14	23808.28	.
lrgc		Intercept	12.38	.	<.0001	10.44	14.32	.
		age	0.01	0.03	0.2836	-0.02	0.04	1.01311
11		md	Intercept	-0.75	.	0.8949	-17.41	15.91
	age		-0.02	0.22	0.7869	-0.24	0.20	.
	psd	Intercept	4.24	.	0.5976	-18.70	27.18	.
		age	-0.03	0.30	0.7658	-0.33	0.27	.
	lpsd	Intercept	1.82	.	0.6374	-9.28	12.93	.
		age	-0.02	0.14	0.7517	-0.16	0.13	0.98439
	vfi	Intercept	96.52	.	0.0048	55.88	137.17	.
		age	0.01	0.53	0.9611	-0.52	0.54	.
	lvfi	Intercept	4.57	.	<.0001	4.15	4.99	.
		age	0.00	0.01	0.9577	-0.01	0.01	1.00010
	rgc	Intercept	1363099.87	.	0.1906	-1211209.18	3937408.93	.
		age	-8447.22	33471.60	0.4806	-41918.82	25024.39	.
	lrgc	Intercept	14.41	.	0.0009	10.93	17.89	.
		age	-0.01	0.05	0.4555	-0.06	0.03	0.98793

Figure 7.2. The output of the univariate linear regression analysis illustrating the slope of each of the three visual field indices, MD, PSD and VFI, and of the global residual RGC count against time to follow-up; the lower and upper 95% confidence limits of the estimate and the statistical significance of the estimate, at each stimulus location arranged in Program 24-2 format. Outcomes exhibiting a statistical significant estimate of the slope are highlighted in yellow.

The dB values of sensitivity at each given stimulus location for each given Single Field Analysis printout were then extracted and converted into the corresponding RGC value using the identical methods to those described in Chapter 6 (page 145 to page 149). The values of sensitivity at each given stimulus location within the given printout were firstly extracted from the printout using Microsoft Paint 2010 (Microsoft Corporation, Redmond, WA) and saved in .tiff format. The images in .tiff format were then converted into .txt files using OmniPage 18 (Nuance Communications, Inc., Burlington, MA). Each dB value was then converted into

the corresponding RGC number using the formulae of Harwerth et al, (Harwerth et al. 2005; Harwerth et al. 2010) which is given in full in Chapter 6, via an application programmed in Java and outputted as a .csv file.

The dB and residual RGC count at each stimulus location in each eye were then separately regressed against time to follow-up using ordinary least squares univariate linear regression analysis. The calculation was undertaken using the same Statistical Analysis System 9.4.

The output contained the estimate of the slope, the lower and upper 95% confidence limits of the estimate and the statistical significance of the estimate at each stimulus location arranged in a Program 24-2 format for the dB values and the residual RGC count, respectively (Figures 7.3a and b).

The SAS System											09:14 Monday, December 15, 2014 197			
ID-EYE-PARAM	row	Regress	Statistic	c1	c2	c3	c4	c5	c6	c7	c8	c9		
S046-L-FieldValues	1	age	Estimate	.	.	-0.3620	-0.7298	-0.3685	-0.6430	.	.	.		
			LowerCL	.	.	-0.9635	-1.0932	-1.0915	-1.6047	.	.	.		
			Probt	.	.	0.1825	0.0036	0.2471	0.1463	.	.	.		
			UpperCL	.	.	0.2395	-0.3664	0.3545	0.3188	.	.	.		
S046-L-FieldValues	2	age	Estimate	.	-0.7957	-0.3871	-0.5332	-0.5651	-0.5764	-0.6631	.	.		
			LowerCL	.	-1.4015	-0.7992	-1.0589	-0.8371	-1.0001	-1.0563	.	.		
			Probt	.	0.0198	0.0605	0.0478	0.0031	0.0173	0.0075	.	.		
			UpperCL	.	-0.1899	0.0250	-0.0074	-0.2932	-0.1527	-0.2699	.	.		
S046-L-FieldValues	3	age	Estimate	-0.5059	-0.8004	-0.6944	-0.5012	-0.6736	-0.6258	-0.5976	-0.6603	.		
			LowerCL	-0.9101	-1.2904	-1.2710	-0.8129	-1.0985	-1.1901	-1.0220	-1.2220	.		
			Probt	0.0235	0.0085	0.0270	0.0091	0.0096	0.0358	0.0152	0.0294	.		
			UpperCL	-0.1016	-0.3105	-0.1179	-0.1894	-0.2487	-0.0614	-0.1731	-0.0986	.		
S046-L-FieldValues	4	age	Estimate	-0.6195	.	-0.4134	-0.3659	-0.2448	-0.4046	-0.7192	-0.6755	-0.6205		
			LowerCL	-1.4200	.	-0.9056	-0.6759	-0.6788	-0.9789	-1.1096	-1.1970	-1.3156		
			Probt	0.1033	.	0.0833	0.0289	0.2067	0.1299	0.0052	0.0208	0.0703		
			UpperCL	0.1810	.	0.0788	-0.0559	0.1891	0.1697	-0.3288	-0.1540	0.0747		
S046-L-FieldValues	5	age	Estimate	-1.0405	.	-0.4826	-0.3348	-0.3354	-0.7514	-0.6424	-0.8168	-0.9690		
			LowerCL	-1.6437	.	-0.9474	-0.7853	-0.7256	-1.3630	-1.3932	-1.3435	-1.3058		
			Probt	0.0068	.	0.0444	0.1143	0.0781	0.0251	0.0792	0.0105	0.0007		
			UpperCL	-0.4373	.	-0.0178	0.1157	0.0548	-0.1399	0.1084	-0.2901	-0.6322		
S046-L-FieldValues	6	age	Estimate	-1.0248	-1.1137	-0.8164	-0.7993	-0.9871	-0.9303	-0.7774	-0.8586	.		
			LowerCL	-1.3323	-1.6667	-1.6340	-1.3604	-1.3119	-1.2537	-1.3685	-1.5908	.		
			Probt	0.0004	0.0035	0.0502	0.0146	0.0006	0.0007	0.0196	0.0296	.		
			UpperCL	-0.7173	-0.5608	0.0012	-0.2381	-0.6623	-0.6069	-0.1864	-0.1264	.		
S046-L-FieldValues	7	age	Estimate	.	-0.9500	-0.8701	-1.0261	-0.7830	-0.7320	-0.8923	.	.		
			LowerCL	.	-1.6955	-1.3680	-1.4234	-1.2927	-1.1048	-1.4667	.	.		
			Probt	.	0.0222	0.0064	0.0012	0.0109	0.0039	0.0104	.	.		
			UpperCL	.	-0.2035	-0.3721	-0.6289	-0.2732	-0.3591	-0.3178	.	.		
S046-L-FieldValues	8	age	Estimate	.	.	-0.8533	-1.1298	-1.0023	-1.2193	.	.	.		
			LowerCL	.	.	-1.8015	-2.0721	-1.6169	-1.8278	.	.	.		
			Probt	.	.	0.0686	0.0274	0.0086	0.0036	.	.	.		
			UpperCL	.	.	0.0950	-0.1876	-0.3076	-0.6108	.	.	.		

Figure 7.3a. The slope of the univariate linear regression of differential light sensitivity (dB) against time to follow-up, the lower and upper 95% confidence limits of the estimate and the statistical significance of the estimate, at each stimulus location arranged in Program 24-2 format.

The SAS System											09:14 Monday, December 15, 2014 198			
ID-EYE-PARAM	row	Regress	Statistic	c1	c2	c3	c4	c5	c6	c7	c8	c9		
S046-L-GanglionCell	9	age	Estimate	.	.	-136.5182	-371.0315	-193.0546	-268.9772	.	.	.		
			LowerCL	.	.	-363.3603	-533.1193	-531.7586	-610.6078	.	.	.		
			Probt	.	.	0.1825	0.0020	0.2028	0.0989	.	.	.		
			UpperCL	.	.	90.3238	-200.9436	145.6495	72.6534	.	.	.		
S046-L-GanglionCell	10	age	Estimate	.	-366.1570	-233.8544	-496.4353	-541.9394	-456.1409	-383.9574	.	.		
			LowerCL	.	-631.4422	-477.5287	-982.6777	-753.3983	-801.3538	-579.3766	.	.		
			Probt	.	0.0164	0.0567	0.0468	0.0012	0.0193	0.0039	.	.		
			UpperCL	.	-100.8718	9.8199	-10.1929	-330.4805	-110.9200	-188.5382	.	.		
S046-L-GanglionCell	11	age	Estimate	-230.7737	-582.6143	-744.9637	-1124.798	-1594.0815	-1007.353	-550.6926	-349.5584	.		
			LowerCL	-409.5278	-935.4921	-1380.546	-1775.592	-2431.6756	-1784.294	-940.5790	-631.5368	.		
			Probt	0.0210	0.0081	0.0297	0.0067	0.0045	0.0207	0.0150	0.0244	.		
			UpperCL	-52.0196	-229.7364	-109.3815	-474.0054	-756.4873	-230.4127	-160.8063	-67.5800	.		
S046-L-GanglionCell	12	age	Estimate	-360.7635	.	-866.4748	-3044.585	-2369.1994	-1133.554	-855.3883	-367.5738	-182.2263		
			LowerCL	-786.7983	.	-1816.991	-5827.330	-7188.8637	-2680.126	-1338.971	-629.4943	-371.4271		
			Probt	0.0814	.	0.0661	0.0374	0.2621	0.1183	0.0061	0.0154	0.0561		
			UpperCL	65.2713	.	84.0412	-261.8405	2450.4649	413.0180	-371.0054	-105.6533	6.9744		
S046-L-GanglionCell	13	age	Estimate	-680.4723	.	-862.5881	-2462.491	-2457.5508	-1896.978	-654.0932	-423.4361	-313.5679		
			LowerCL	-1021.159	.	-1647.694	-5776.368	-5994.8238	-3723.692	-1583.049	-700.1197	-407.8220		
			Probt	0.0037	.	0.0369	0.1144	0.1342	0.0444	0.1301	0.0110	0.0004		
			UpperCL	-339.7853	.	-77.4826	851.3863	1079.7222	-70.2647	274.8629	-146.7524	-219.3137		
S046-L-GanglionCell	14	age	Estimate	-482.3895	-751.1594	-864.8174	-1655.007	-2007.1188	-1315.485	-613.0545	-320.4513	.		
			LowerCL	-614.2432	-1076.773	-1830.118	-2677.448	-2338.8425	-1736.099	-1146.765	-614.9811	.		
			Probt	0.0002	0.0019	0.0695	0.0088	0.0000	0.0005	0.0318	0.0381	.		
			UpperCL	-350.5358	-425.5453	100.4830	-632.5661	-1675.3950	-894.8706	-79.3445	-25.9215	.		
S046-L-GanglionCell	15	age	Estimate	.	-461.2404	-707.7097	-951.4064	-751.1233	-542.2409	-471.4525	.	.		
			LowerCL	.	-836.3209	-1054.431	-1262.220	-1215.0116	-820.2934	-789.6235	.	.		
			Probt	.	0.0251	0.0033	0.0005	0.0088	0.0041	0.0125	.	.		
			UpperCL	.	-86.1599	-360.9880	-640.5933	-287.2351	-264.2044	-153.2814	.	.		
S046-L-GanglionCell	16	age	Estimate	.	.	-434.9542	-579.4773	-494.3991	-451.1549	.	.	.		
			LowerCL	.	.	-1015.894	-1104.592	-763.8686	-628.2932	.	.	.		
			Probt	.	.	0.1123	0.0364	0.0053	0.0012	.	.	.		
			UpperCL	.	.	145.9858	-54.3624	-224.9296	-274.0166	.	.	.		

Figure 7.3b. The slope of the univariate linear regression of residual RGC count against time to follow-up, the lower and upper 95% confidence limits of the estimate and the statistical significance of the estimate, at each stimulus location arranged in Program 24-2 format.

A further output contained the magnitude of the statistical significance associated with the estimate of the slope at each location arranged in Program 24-2 format and denoted in terms an asterisk where ‘*’ indicated $p < 0.05$; ‘**’ $p < 0.01$; ‘***’ ; $p < 0.001$; and ‘****’ $p < 0.0001$ (Figure 7.4).

```

The SAS System                                09:14 Monday, December 15, 2014 46
sub      eye      table      row      _1      _2      _3      _4      _5      _6      _7      _8      _9
S046     L        GS         9         .         .         .         .         .         .         .         .         .
10        .         .         .         .         .         .         .         .         .         .         .         .
11        *         *         .         .         .         .         .         .         .         .         .         .
12        .         .         .         .         .         .         .         .         .         .         .         .         .
13        .         .         .         .         .         .         .         .         .         .         .         .         .
14        .         .         .         .         .         .         .         .         .         .         .         .         .
15        .         .         .         .         .         .         .         .         .         .         .         .         .
16        .         .         .         .         .         .         .         .         .         .         .         .         .

S046     L        MS         1         .         .         .         .         .         .         .         .         .
2         .         .         .         .         .         .         .         .         .         .         .         .
3         .         .         .         .         .         .         .         .         .         .         .         .         .
4         .         .         .         .         .         .         .         .         .         .         .         .         .
5         .         .         .         .         .         .         .         .         .         .         .         .         .
6         .         .         .         .         .         .         .         .         .         .         .         .         .
7         .         .         .         .         .         .         .         .         .         .         .         .         .
8         .         .         .         .         .         .         .         .         .         .         .         .         .

S046     R        GS         9         .         .         .         .         .         .         .         .         .
10        .         .         .         .         .         .         .         .         .         .         .         .         .
11        .         .         .         .         .         .         .         .         .         .         .         .         .
12        .         .         .         .         .         .         .         .         .         .         .         .         .
13        .         .         .         .         .         .         .         .         .         .         .         .         .
14        .         .         .         .         .         .         .         .         .         .         .         .         .
15        .         .         .         .         .         .         .         .         .         .         .         .         .
16        .         .         .         .         .         .         .         .         .         .         .         .         .

S046     R        MS         1         .         .         .         .         .         .         .         .         .
2         .         .         .         .         .         .         .         .         .         .         .         .         .
3         .         .         .         .         .         .         .         .         .         .         .         .         .
4         .         .         .         .         .         .         .         .         .         .         .         .         .
5         .         .         .         .         .         .         .         .         .         .         .         .         .
6         .         .         .         .         .         .         .         .         .         .         .         .         .
7         .         .         .         .         .         .         .         .         .         .         .         .         .
8         .         .         .         .         .         .         .         .         .         .         .         .         .

```

Figure 7.4. An illustration of the significance printout, is given in Figures 7.3. The statistical significance of the estimate of the slope of the univariate linear regression of differential light sensitivity (dB) (top) and residual RGC count (bottom) against time to follow-up arranged in Program 24-2 format for the individual presented in Figures 7.3 a and b. ‘*’ indicates $p < 0.05$; ‘**’ $p < 0.01$; ‘***’ ; $p < 0.001$; and ‘****’ $p < 0.0001$.

7.4 Results

The visual fields from one eye of each individual were pseudo-randomly selected for the analysis to ensure an equal distribution between right and left eyes. The summary statistics (median, lower and upper quartiles; range) for the age and gender characteristics of the 112 individuals; together with the number of visual field examinations; the duration of visual field follow-up; the visual field indices and the residual RGC count of the baseline visual field in the randomly selected eye, are given in Table 7.1.

Age (years)	64.9 (57.5, 71.8; 32.2 to 82.9)
Gender (male : female)	44 : 68
Number of visual field examinations	8.0 (6.0, 9.0; 5.0 to 15.0)
Duration of visual field follow-up (years)	9.0 (7.3, 9.9; 5.0 to 14.5)
Mean Deviation (dB) at the baseline visit	-2.79 (-6.17, -1.08; -25.10 to 1.46)
Pattern Standard Deviation (dB) at the baseline visit	2.42 (1.77, 5.66; 1.03 to 13.73)
Visual Field Index (%) at the baseline visit	96 (87.8, 98.0; 26.0 to 100.0)
Number of residual RGCs at the baseline visit	752796 (579123, 953804; 90199 to 8714052)

Table 7.1. The summary statistics (median, lower and upper quartiles; range) for the age and gender characteristics of the 112 individuals together with the number of visual field examinations; the duration of visual field follow-up; the visual field indices and the residual RGC count of the baseline visual field in the randomly selected eye.

7.4.1 Global approach

Of the 112 individuals, 70 exhibited a statistically significant progressive slope, in the designated eye, for one or more of the visual field indices including the global residual RGC count. The outcomes are shown in Tables 7.2 and 7.3.

Thirty-two individuals exhibited a statistically improving slope in the designated eye for one or more of the visual field indices including the global residual RGC count; however, only seven of these slopes were statistically significant. The outcomes are shown in Tables 7.3 and 7.4.

Eye (number of individuals)	Mean Deviation	Pattern Standard Deviation	Visual Field Index	Residual RGC count
Right eyes (27)	20/27	19/27	16/27	16/27
Left eyes (43)	31/43	20/43	30/43	35/43

Table 7.2. The number of statistically significant progressive slopes by each of the various visual field indices and by the global residual RGC count for each eye.

Index (unit/ year)	Progressive slope	Statistically significant progressive slope	Improving slope	Statistically significant 'improved' slopes
Mean Deviation (dB/ year)	-0.39 (-0.64, -0.17; -2.58 to -0.01)	-0.56 (-0.85, -0.34; -2.32 to -0.15)	0.12 (0.06,0.20; 0.02 to 1.20)	0.28 (0.24, 0.74; 0.20 to 1.20)
Pattern Standard Deviation (dB/ year)	0.16 (0.07,0.38; 0.0 to 1.47)	0.26 (0.16,0.66; 0.04 to 1.47)	-0.10 (-0.22, -0.04; -1.21 to -0.01)	-1.07 (-1.14, -0.62; -1.21 to -0.16)
Visual Field Index (%/year)	-0.81 (-1.92, -0.19; -7.11 to -0.01)	-1.65 (-2.50,-0.66; -6.78 to -0.07)	0.15 (0.04, 0.34; 0.01 to 3.01)	0.61 (0.42, 1.25; 0.03 to 3.01)
Residual RGC count (count/ year)	-24951 (-36600, -10685; -255007 to -519)	-33859 (-42693,-26598; -98539 to -8595)	12563 (7675,17602; 92 to 127890)	11660

Table 7.3. The summary statistics (median, lower and upper quartiles; range) of the slope of the given visual field index against time to follow-up for the total number of progressive slopes, of statistically significant progressive slopes, of improving slopes, and of statistically significant improving slopes.

Eye (number of individuals)	Mean Deviation	Pattern Standard Deviation	Visual Field Index	Residual RGC count
Right eyes (5)	2/5	2/5	2/5	1/5
Left eyes (2)	1/2	1/2	2/2	0/2

Table 7.4. The number of statistically significant improving slopes by each of the various visual field indices and by the global residual RGC count for each eye.

The relationship of the number of the statistically significant progressive slopes between the various indices, are shown in Figure 7.5 and in tabular format in Table 7.5.

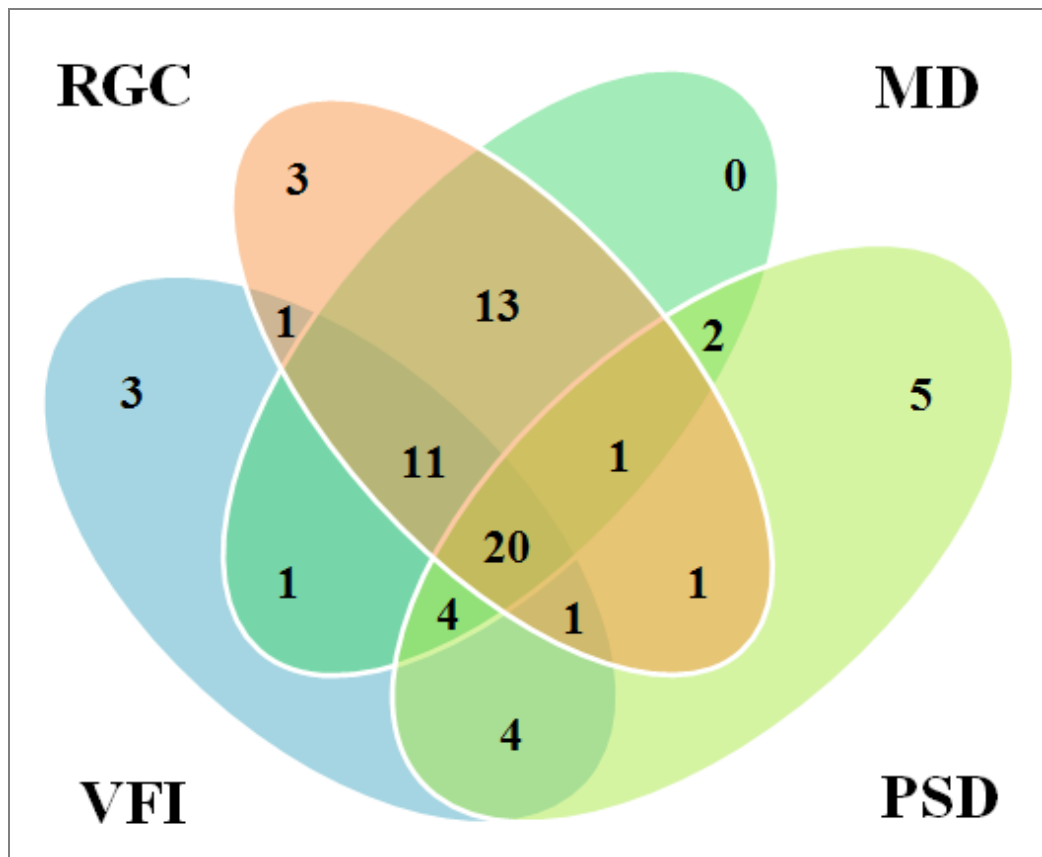


Figure 7.5. The relationship of the number of statistically significant progressive slopes between the various indices. Turquoise represents the statistically significant progressive slopes with the MD index; green, the statistically significant progressive slopes with the PSD index; orange, the statistically significant progressive slopes with the global residual RGC count; and blue, the statistically significant progressive slopes with the VFI index.

Twenty individuals exhibited a statistically significant progressive slope with all four measures; 11 individuals with the residual RGC count, MD and VFI; and 13 significant slopes with residual RGC count and MD.

Technique of progression	Frequency (70/112)
PSD	5
VFI	3
RGC	3
MD, PSD	2
MD, VFI	1
MD, RGC	13
PSD, VFI	4
PSD, RGC	1
VFI, RGC	1
MD, PSD, VFI	4
MD, PSD, RGC	1
MD, VFI, RGC	11
PSD, VFI, RGC	1
MD, PSD, VFI, RGC	20
Total	70

Table 7.5. The outcomes illustrated in Figure 7.5, expressed in tabulated format.

A statistically significant decline in the residual RGC count together with a statistically significant decline in either or both the PSD and the VFI indices could be construed as progression of a localized visual field defect. However, the data in Table 7.5 do not seem to support this notion.

7.4.2 Pointwise approach

Of the 112 individuals, 102 exhibited a total of 1312 statistically significant negative (progressive) slopes with either, or both, the univariate linear pointwise regressions of the absolute value of sensitivity (dB) and the residual RGC count against time to follow-up. The summary statistics (median, lower and upper

quartiles; range) of these 1312 locations is given in Table 7.6. Of the 1100 locations exhibiting a statistically significant negative slope common to both regression outcomes, 166 exhibited a greater statistical significance for the residual RGC count and 108 for the absolute value of sensitivity. One hundred and seven locations exhibited a statistically negative significant slope for the residual RGC count, only, and 111 for the absolute value of sensitivity, only.

Total number of locations associated with a statistically significant negative slope	Number of locations	Median (lower and upper quartiles; range)
Total	1312	10.0 (3.0,20.8; 0.0 to 47.0)
Absolute value of sensitivity (dB)	1206	8.5 (3.0, 18.8; 0.0 to 46.0)
Residual RGC count	1202	8.0 (2.3, 17.8; 0.0 to 47.0)
Common to both outcomes	1100	7.0 (2.0, 16.0; 0.0 to 46.0)
Common locations with equal statistical significance	821	6.0 (2.0, 11.0; 0.0 to 34.0)
Greater statistical significance: Absolute value of sensitivity (dB)	108	0.0 (0.0, 1.0; 0.0 to 9.0)
Greater statistical significance: Residual RGC count	166	0.5 (0.0, 2.0; 0.0 to 16.0)
Additional locations: Absolute value of sensitivity (dB)	111	0.0 (0.0, 1.0; 0.0 to 10.0)
Additional locations: Residual RGC count	107	0.5 (0.0, 1.0; 0.0 to 8.0)

Table 7.6.The summary statistics (median, lower and upper quartiles; range) of the number of locations for the 102 individuals associated with a statistically significant negative slope for the absolute values of sensitivity (dB) and for the residual RGC count, against time to follow-up.

The number of individuals against the number of statistically significant negative slopes for each regression outcome is given in Figure 7.6. Both techniques exhibited comparable results.

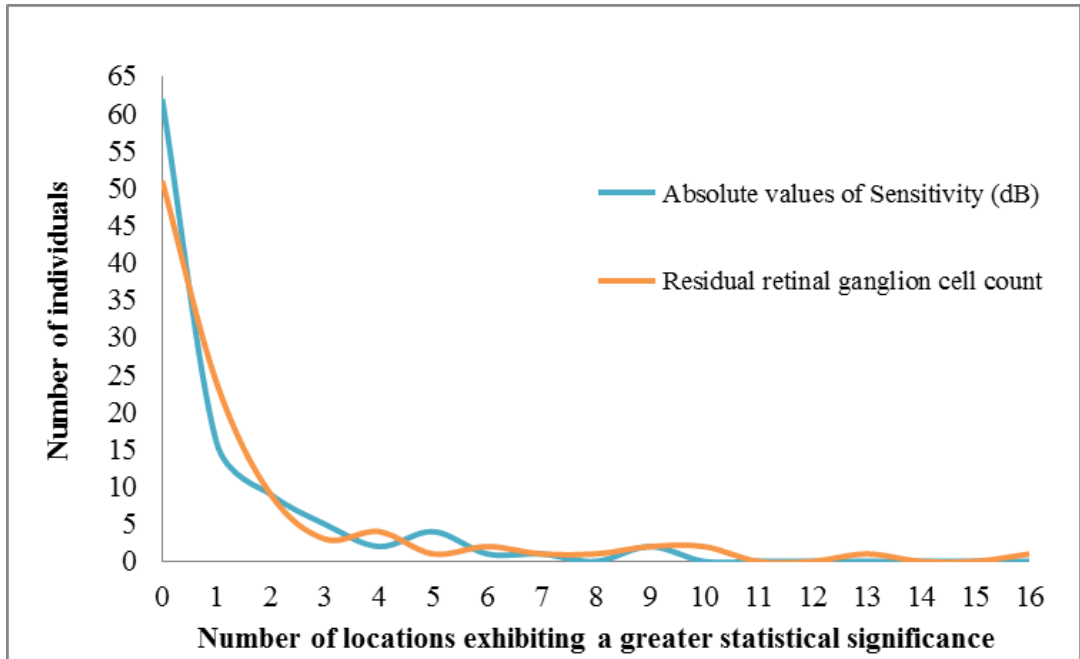


Figure 7.6. The number of individuals against the number of statistically significant negative slopes for each regression outcome.

The number of individuals by the number of additional statistically significant negative slopes for each regression outcome is given in Figure 7.7. Similarly, the two techniques exhibited comparable results. Approximately 80% of the additional locations with statistically significant negative slopes were contiguous with other locations exhibiting statistically significant negative slopes.

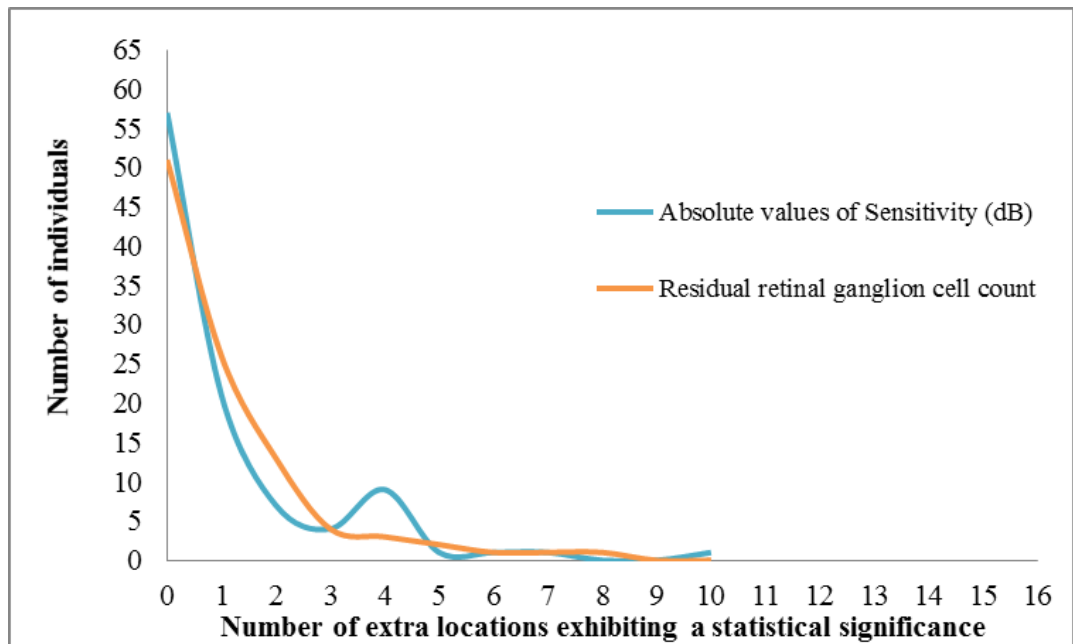


Figure 7.7. The number of individuals against the number of additional statistically significant negative slopes for each regression outcome.

Of the 102 individuals with statistically significant negative slopes, 22 also exhibited one or more statistically significant positive slopes (median 2.0; lower and upper quartiles 1.0, 2.8; range 1.0 to 4.0). The median number of locations exhibiting negative slopes for these 22 individuals was 2.0 (lower and upper quartiles 1.0, 11.8; range 1.0 to 24.0 (Table 7.7). The relationship between these two outcomes amongst the 22 individuals is illustrated in Figures 7.8 and 7.9.

Significant locations	Residual RGC count (negative slope)	Residual RGC count (positive slope)	Negative slope dB	Positive slope dB
Total locations	120	38	127	36
Median (lower, upper quartiles; range)	2.0 (1.0, 9.5; 0.0 to 24.0)	2.0 (1.0, 2.0; 0.0 to 3.0)	2.0 (1.0, 10.0; 0.0 to 25.0)	1.0 (1.0, 2.0; 1.0 to 3.0)

Table 7.7. The summary statistics (median, lower and upper quartiles; range) of the distributions of the statistically significant negative and positive slopes for residual RGC count, and for the absolute values of sensitivity (dB), against time to follow-up, respectively, amongst the 22 individuals.

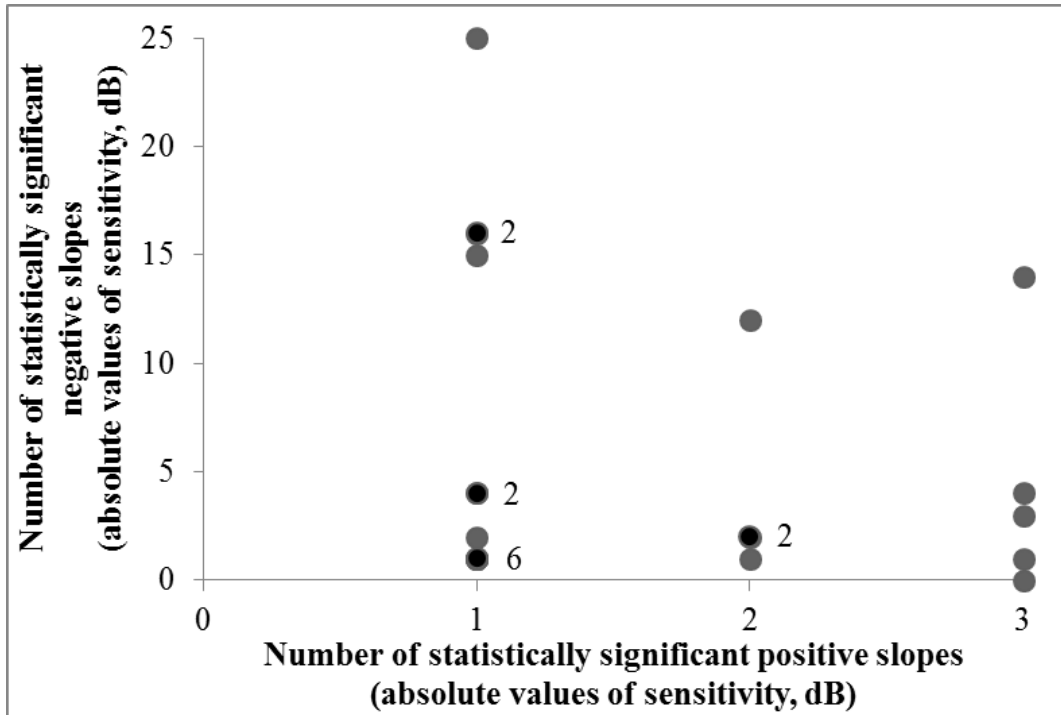


Figure 7.8. The relationship between the number of statistically significant negative slopes and the corresponding number of positive slopes for the absolute values of sensitivity (dB). The figure adjacent to a symbol indicates the number of overlapping data points.

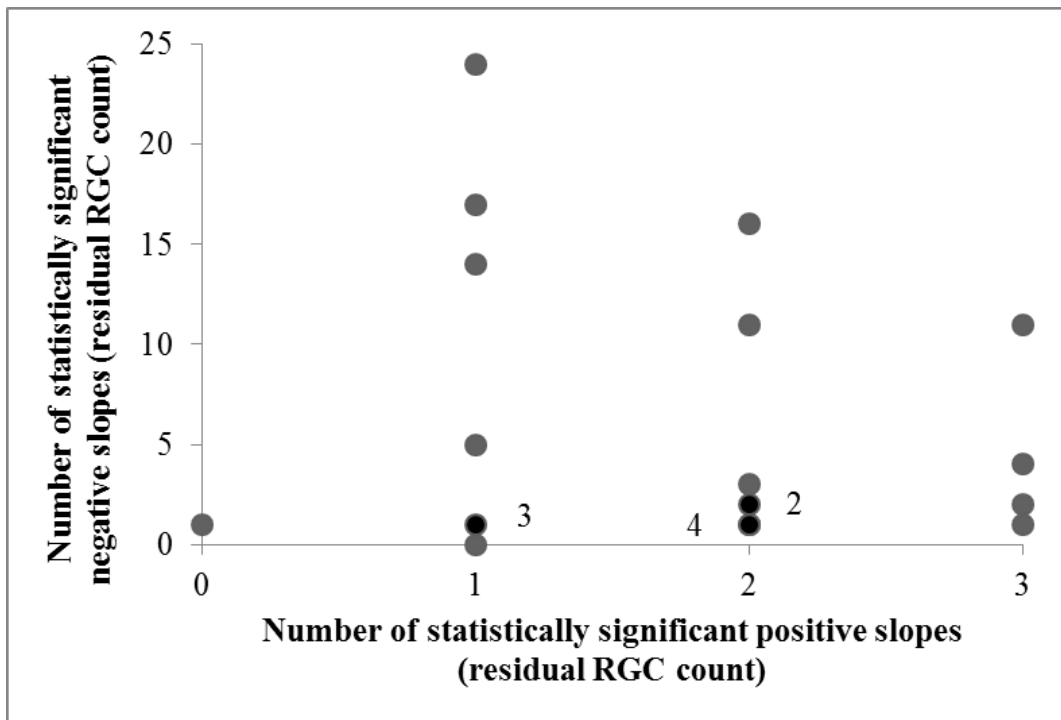


Figure 7.9. The relationship between the number of statistically significant negative slopes and the corresponding number of positive slopes for the residual RGC count. The figure adjacent to a symbol indicates the number of overlapping data points.

The number of locations exhibiting a statistically significant negative slope for each regression outcome, but with one outcome manifesting a more statistically significant slope compared to the other, by the mean of the absolute sensitivity at the two baseline more examinations is given in Figure 7.10. Within the limitations of the dataset, between a baseline mean of approximately 31dB to 26dB inclusive, more statistically significant slopes were present for residual RGC count compared to that for absolute sensitivity. For baseline means between 25.5dB to approximately 23dB, the proportions of more statistically significant slopes were similar between the two outcomes. Below a baseline mean of approximately 23dB, a difference in the magnitude of the statistical significance of the slopes between the two regression outcomes could not be discerned.

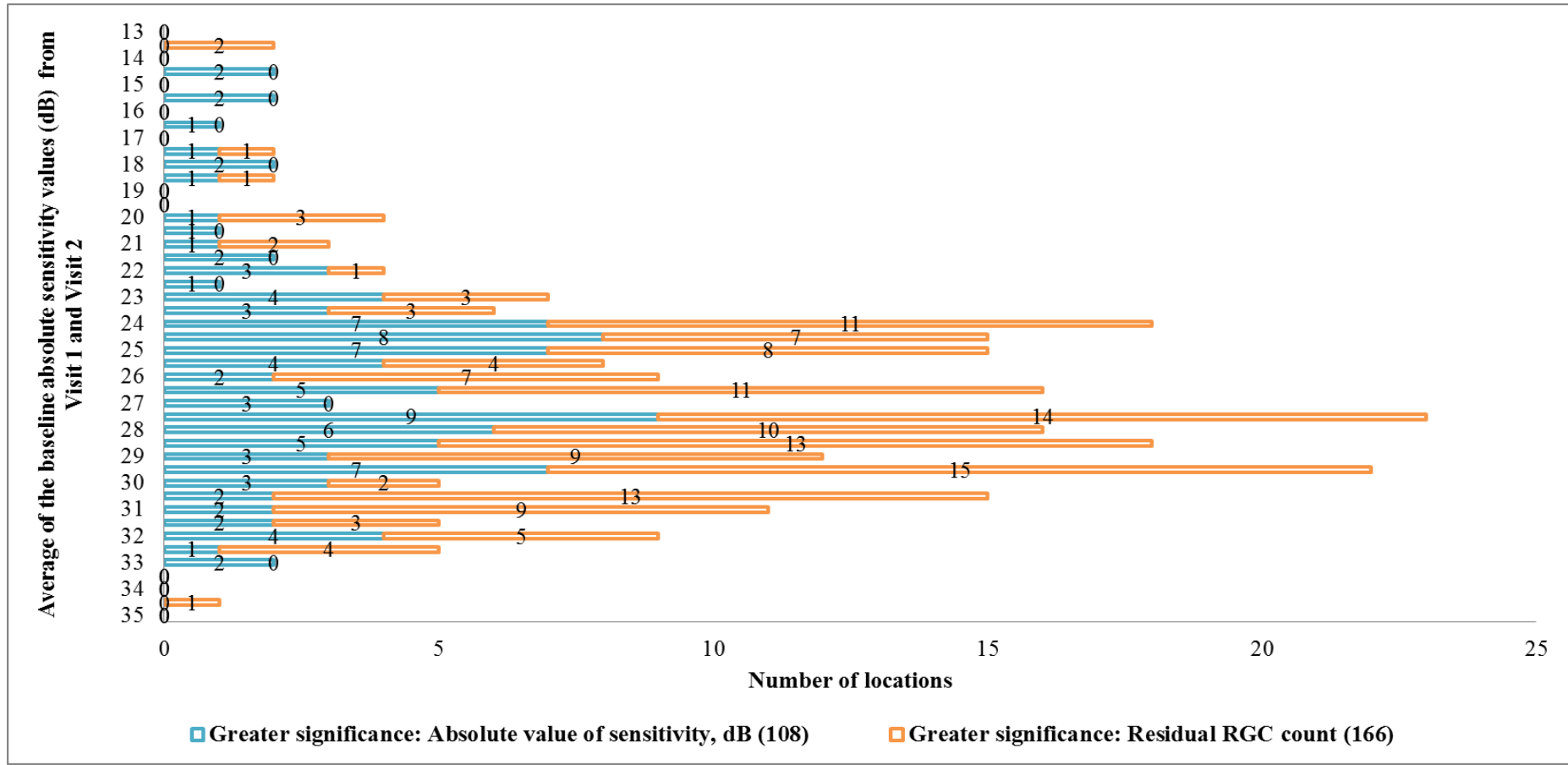


Figure 7.10. The number of locations exhibiting a statistically significant negative slope for each regression outcome, but with one outcome manifesting a more statistically significant slope compared to the other, by the mean of the absolute sensitivity at the two baseline examinations.

The number of additional locations exhibiting a statistically significant negative slope for one outcome compared to the absence of progression with the other outcome, by the mean of the absolute sensitivity at the two baseline examinations is given in Figure 7.11. Within the limitations of the dataset, between a baseline mean of approximately 31dB to 25.5dB inclusive, more additional locations with statistically significant slopes were present for residual RGC count compared to that for absolute sensitivity. For baseline means between 25dB to approximately 22dB, a difference between the two outcomes could not be discerned. Below a baseline mean of approximately 22dB, more statistically significant slopes were present, overall, for the absolute value sensitivity.

The summary statistics (median, lower and upper quartiles; range) of the absolute values of sensitivity (dB) averaged across Visits 1 and 2 is given in Table 7.8.

	Greater statistical significance		Additional locations	
	Absolute value of sensitivity (dB)	Residual RGC count	Absolute value of sensitivity (dB)	Residual RGC count
Number of locations	108	166	107	111
Baseline average Visits 1 and 2	26.3 (24.0, 28.5; 14.5 to 33.0)	28.0 (25.2,29.5; 13.5 to 34.5)	26.0 (19.3,30.0; 0.0 to 33.5)	27.5 (25.0,29.5; 8.5 to 33.5)

Table 7.8. The summary statistics (median, lower and upper quartiles; range) of the absolute values of sensitivity (dB) averaged across Visits 1 and 2.

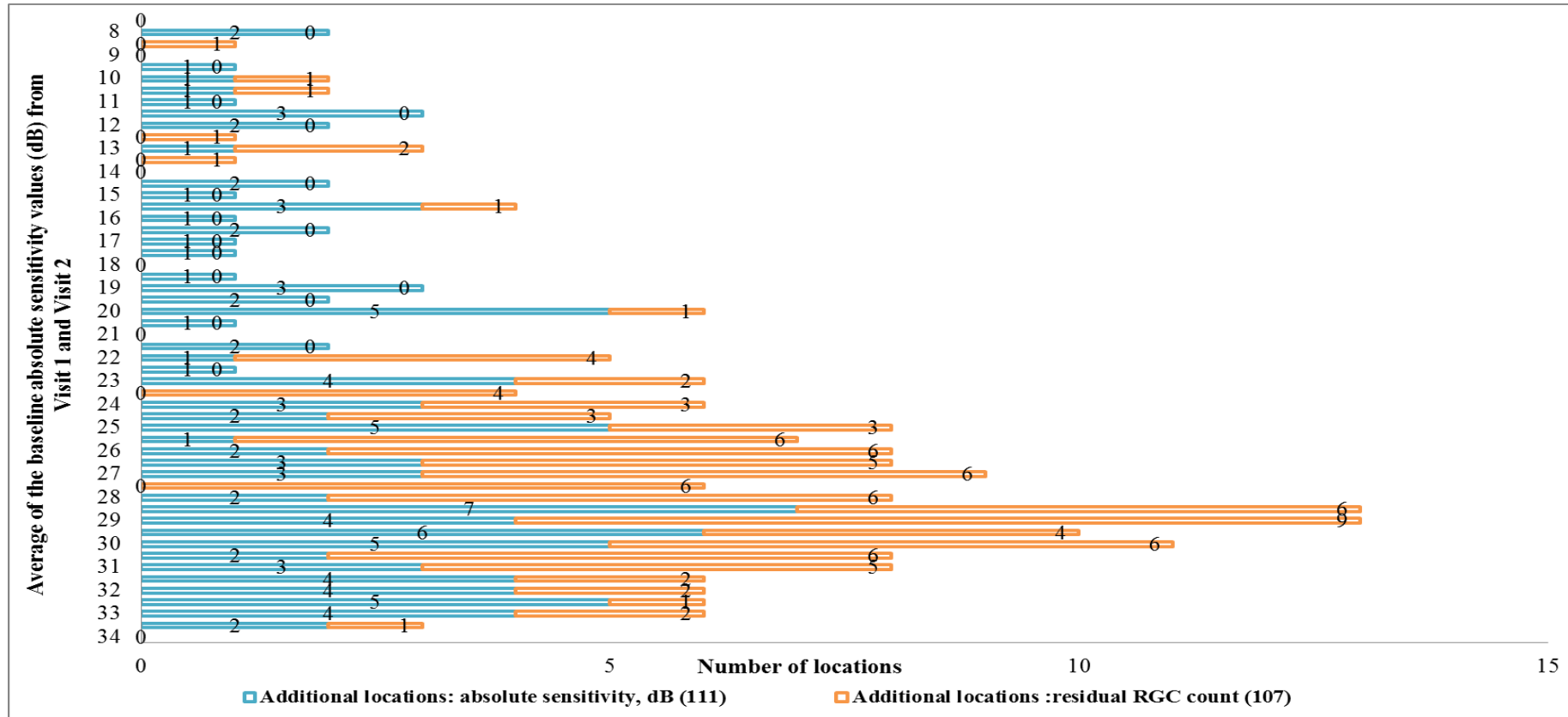


Figure 7.11. The number of additional locations exhibiting a statistically significant negative slope for one outcome compared to the absence of progression with the other outcome, by the mean of the absolute sensitivity at the two baseline examinations. Note the scaling of both the ordinate and the abscissa is different to that of Figure 7.10.

Of the 112 individuals, 10 individuals exhibited a total of 51 statistically significant positive slopes with either, or both, the univariate linear pointwise regressions of the absolute value of sensitivity (dB) and the residual RGC count against time to follow-up. The summary statistics (median, lower and upper quartiles; range) of these 51 locations is given in Table 7.9.

Total number of locations associated with a statistically significant negative slope	Number of locations	Median (lower and upper quartiles; range)
Total	51	3.5 (2.3, 4.0; 1.0 to 18.0)
Absolute value of sensitivity (dB)	40	2.0 (2.0, 3.5; 1.0 to 13.0)
Residual RGC count	48	3.0 (2.0, 3.5; 1.0 to 18.0)
Common to both outcomes	37	2.0 (2.0, 2.5; 1.0 to 13.0)
Common locations with equal statistical significance	32	2.0 (2.0, 2.5; 1.0 to 9.0)
Greater statistical significance: Absolute value of sensitivity (dB)	0	0.0 (0.0, 0.0; 0.0 to 0.0)
Greater statistical significance: Residual RGC count	5	0.0 (0.0, 0.0; 0.0 to 5.0)
Additional locations: Absolute value of sensitivity (dB)	3	0.0 (0.0, 0.5; 0.0 to 1.0)
Additional locations: Residual RGC count	11	1.0 (0.0, 1.0; 0.0 to 5.0)

Table 7.9. The summary statistics (median, lower and upper quartiles; range) of the number of locations for the 10 individuals associated with a statistically significant positive slope for the absolute values of sensitivity (dB) and for the residual RGC count, against time to follow-up.

7.5 Discussion

The results (Figures 7.10 and 7.11) generally indicate that the outcome of the univariate linear regression, at each stimulus location, of the residual ganglion cell count against time to follow-up identifies progression at higher levels of baseline sensitivity compared to the corresponding outcome of the differential light sensitivity (expressed in dB) against time to follow-up. This outcome was manifested by a greater statistical significance of the slope and/ or number of stimulus locations exhibiting progressive loss in the absence of progressive loss based upon the absolute values of sensitivity (dB). These results are in agreement with the hypothesis of Garway-Heath and colleagues (Garway-Heath et al. 2000a).

The outcomes of the univariate linear regression analyses at each stimulus location were evaluated in terms of the statistical significance of the slope rather than the magnitude of the slope, itself. The age-related decline in absolute sensitivity at each location in the normal eye is unknown. As a consequence, various empirical values have been proposed for the definition of progressive loss. A reduction in sensitivity of 1 dB/ year (approximately ten times the normal age-related decline compiled from cross-sectional data) with a statistical significance at $p < 0.01$ at two or more locations corresponding to the RNFL distribution is considered to be 'exclusive progression' (Viswanathan et al. 1998; Manassakorn et al. 2006; Strouthidis et al. 2007; Heijl et al. 2009; Heijl et al. 2013b; Nassiri et al. 2013; Anderson 2015). Alternatively, for stimulus locations beyond 15° eccentricity, a more conservative criterion of 2dB/ year at $p < 0.01$ or $p < 0.05$ has been proposed to account for the increased within- and between-

examination variability compared to the more central locations (Spry and Johnson 2002; Artes et al. 2005; De Moraes et al. 2012b; Anderson 2015). The use of a less stringent significance level of $p < 0.05$ and a reduction 0.5dB/ year increases the sensitivity to detect progressive loss at the expense of a reduction in specificity (Wilkins et al. 2005; De Moraes et al. 2012b). The Guidelines of the European Glaucoma Society (EGS 2008) consider a clinically significant rate of progression to be 2-4 dB/ year (Rossetti et al. 2010). The age-related decline, in the normal eye, of the residual RGC count at each location is also unknown. However, a decline of 7877 ganglion cells/ year (Medeiros et al. 2012b) across the central field, as a whole, has been proposed from a knowledge of the number of residual ganglion cell soma and the RNFL thickness. The magnitudes at each stimulus location of the statistically significant slopes for both regression outcomes, although available (Figures 7.3a and 7.3b) were not analysed given that they were not directly comparable and that the respective normal age-related decline is unknown for the residual RGC count. A knowledge of the age-related decline for each modality could be used to standardize each modality in terms of the ratio of the measured slope to the age-corrected slope. Such standardization would then permit a comparison of the rate of change compared to that of the normal for absolute sensitivity and for residual RGC count at each stimulus location for each individual. The next stage of the work will involve the derivation of the respective normal age-related declines, at each stimulus location obtained from cross-sectional data.

The slope of the univariate linear regression analysis for each of the visual field indices MD, PSD and VFI against to follow-up would be expected to approximate to zero in the normal eye in that each of these measures are age corrected. Progressive loss is identified by the presence of a statistically significant progressive slope and the magnitude of the slope varies across studies depending upon the characteristics of the cohort and the nature of the study. The median rate of statistically significant progression for the MD in the current study was -0.56dB/ year. This value lies within the range for the mean of -0.29dB/ year (Cho et al. 2012), to mean of -1.26dB/ year (Smith et al. 1996). The median rate of statistically significant progression for the VFI of -1.65%/ year in the current study was compatible with that for the mean of -1.30%/ year (Casas-Llera et al. 2009). The median rate of statistically significant progression for PSD in the current study was 0.26dB/ year which is slightly less than that of 0.71dB/ year (Smith et al. 1996). The decline in residual RGC count of -33859 (lower quartile -42693, upper quartile -26598)/ year is almost identical to that of -33369 cells/ year derived from SAP and OCT of the RNFL thickness, combined (Medeiros et al. 2012b).

It can be conjectured that the relative lack of agreement between the global indices reinforces the need to considered progressive visual field loss in terms of each individual stimulus locations.

A strength of the study was the relatively long time series of the visual field examinations (9.0 years; IQR 7.3, 9.9; range 5.0 to 14.5) and the corresponding large number of reliable visual field examinations within the time series (8.0

examinations; 6.0, 9.0; 5.0 to 15.0). A weakness of the study was the lack of a structural comparison (i.e., the optic nerve head and/ or RNFL thickness) over the same time series with which to validate the apparent visual field progression defined with either regression outcome.

The outcome of the analysis derives from univariate regression analysis (i.e. trend analysis). The outcome could be compared to that derived from the GPA analysis that follows the EMGT progressive criteria (i.e. event analysis). However, the current version of the GPA software (Version 4.2) does not permit the integration of the outcomes from the SITA Standard and SITA Fast algorithms.

Retinal ganglion cell soma and axon estimations were derived from the model of Harwerth (Harwerth et al. 2005; Harwerth et al. 2010) since the model has been used relatively extensively in the context of glaucoma (Medeiros et al. 2012a; Medeiros et al. 2012b; Medeiros et al. 2012c; Medeiros et al. 2012d; Medeiros et al. 2013). However, various other models of the cross-sectional structure and function relationship, based upon either RGC axonal thickness or density, could have been used including the linear models of Hood and Kardon (Hood et al. 2007; Raza et al. 2011; Raza and Hood 2015), Harwerth (Garway-Heath et al. 2000a; Harwerth et al. 2010; Asaoka et al. 2012; Medeiros et al. 2012b; Porciatti and Ventura 2012) and Drasdo (Drasdo et al. 2007; Drasdo et al. 2008) and the logarithmic ‘Hockey-Stick’ model of Swanson (Swanson et al. 2004).

A Mean Sensitivity of 0dB corresponded to a residual RGC count of 23906. Thus, the linear relationship between the RGC count and the absolute values of sensitivity is limited by the dynamic range of SAP in that residual RGCs may exist in the presence of perimetric blindness. The limitation of the dynamic range might be overcome by the use of Goldmann stimulus size V. Alternatively; the apparent count may reflect the non-neuronal component which is evident by OCT of the RNFL.

Recently, the linearity of visual field progression, expressed in terms of the MD (Pathak et al. 2013), and in terms of pointwise linear regression analysis (Pathak et al. 2015) has been challenged in that an exponential model would appear to be more appropriate. However, a linear approach has also been advocated (Bryan et al. 2013). In the current study, all 46 individuals who exhibited a statistically significant progression of the VFI by linear regression analysis manifested progression with exponential regression analysis at the same probability level. One individual exhibited progression by exponential regression only. Similarly, of the 51 individuals who exhibited statistically significantly progressive slopes for the global residual RGC count 47 exhibited an identical outcome by exponential regression. Clearly, the pointwise dataset is such that the efficacy of alternative regression models such as linear and exponential can be evaluated in the future.

Chapter 8

Overall Discussion, conclusion and future work

The study which has relied upon the analysis of retrospective data, has highlighted the importance of the acquisition of good quality data, collected at regular intervals and integrated with other diagnostic techniques, not only for the benefit of the patient, but also for the benefit of research.

8.1 Optic nerve head image registration, sizing and alignment, and viewing

A novel quantitative approach was utilized to ensure the consistency in scaling and aligning of the ONH images from the various photographic sources. Twenty-eight vectors were drawn on each of the images for the given individual, based upon 8 predetermined features inherent in the images for the given individual. Each vector defined the distance and the orientation between the same two 'key' features within each ONH image.

The magnitude of the resizing, and the error associated with the manual resizing and alignment of the stereo-pairs, was described by the difference in the lengths of the given pair of vectors: for each analysis, the scaling factor was defined as the median of the differences. The median of the proportionate difference in the magnitudes of the x and y coordinates of all 28 vectors, considered together, between the manually resized and aligned images ranged from -2.4% to 1.5%. Such values indicate a satisfactory overall precision in the manual alignment.

Automated registrations of ONH images acquired with digital photography and by SLP (Ng et al. 2015) and between monoscopic ONH images (Radcliffe et al. 2010; Syed et al. 2012) have been described and a similar approach should be adopted for stereo-images acquired across the complete spectrum of analogue and differing digital modalities. In particular, it will be essential to develop a reliable automated digital alignment technique between each stereo image-pair which is based upon the recognition of individual morphological clinical features (vessel pattern, ONH tilt etc.) and which simultaneously, compensates for rotational issues arising from photographic artefacts. Such a technique will offer a simple and reliable tool for routine clinical practice to assist in the identification of glaucoma and/ or the presence of glaucomatous progression.

8.2 The qualitative assessment of progressive glaucomatous ONH damage using both mono- and stereo-flicker chronoscopy

The study evaluated the efficacy of digital stereo-flicker chronoscopy compared to that of mono-flicker chronoscopy for the qualitative identification of glaucomatous ONH damage in a case series of 61 individuals attending a glaucoma clinic over a long follow-up. Although both ophthalmologists who evaluated the ONH images exhibited little agreement with each other, the flicker comparison, with either mono- or stereo-viewing, increased the diagnostic accuracy for glaucoma and for the identification of glaucomatous progression. In particular, stereo-flicker manifested a slightly better diagnostic accuracy compared to mono-flicker viewing.

The relationship was determined between the qualitative assessment of progressive glaucomatous ONH damage and the corresponding visual field outcome. The relationship was confounded by the diversity in the length of the time series of both the ONH images and of the visual field examinations. However, there was little agreement between the various methods for the evaluation of visual field progression and little relationship between visual field progression and ONH progression.

8.3 The quantitative assessment of progressive structural and functional glaucomatous damage

The NRR was quantified, as a whole, by segments and by sectors, in a case series of 23 individuals attending a glaucoma clinic over a long follow-up, using digital manual stereo- and monoscopic planimetry incorporating the ‘floating cursor’ technique of Morgan and colleagues (Morgan et al. 2005a; Morgan et al. 2005b; Morgan et al. 2012). The use of a ‘floating cursor’ enhanced the visualization of the ONH features. The relationship was then investigated between ONH progression (defined as a thinning of the NRR) and the concomitant visual field progression (defined in terms of the MD, VFI and residual RGC count).

Digital manual stereo-planimetry was used as the ‘gold standard’ rather than mono-planimetry. A weak curvilinear association was present, at baseline, between the extent of the NRR area and the magnitudes of the MD and VFI and a slightly stronger, linear, association between NRR and residual RGC count.

No association was present between structural and functional progression for either the NRR as a whole or for the superior and the inferior sectors. The structural and functional progression was evaluated between the baseline and the most recent point in the time series in order to maximise the potential for deterioration in one or both outcomes. The quantification of the ONH through planimetry, and hence the strengths of the various associations, varied between the two ophthalmologists.

The lack of an association between progressive functional and progressive structural damage was limited by variations in: the quality of the visual field examinations; the number of individuals exhibiting progression with either modality; the extent of progression which inevitably is influenced by the length of the time series; and the quality of the ophthalmological care between individuals. No relationship was present between the apparent progression of either, or both, structural and functional outcomes and the length of the time series.

During the study, the introduction and clinical acceptance of spectral domain OCT for use in glaucoma has radically altered the image resolution and the objective quantification of the ONH and of the RNFL, in particular. Optical coherence tomography of the ONH parameters has already superseded digital manual planimetry (Ramakrishnan et al. 2005; Sung et al. 2009; Lee et al. 2010; Liu et al. 2011; Chauhan et al. 2012; Huang et al. 2012; Naghizadeh et al. 2012; Tatham et al. 2013; Bussel et al. 2014; Leung 2014; Rao et al. 2015).

Current research involves the construction of the automated depth segmentation of the ONH in three dimensional space from OCT ONH images (Abramoff et al. 2009; Sharma et al. 2011; Moghimi et al. 2012; Lee et al. 2013). However, the extent to which the outcome of clinical practice is dependent upon observation of a high resolution digital stereo-image, complete with ‘floating’ cursor is unknown. Such automated depth segmentation will inevitably replace the traditional stereo-viewing, but it would be useful to determine the utility of such a technique in the context of current automated depth segmentation. In addition, the utility of automated depth segmentation of the ONH should be applied to the evaluation of progressive structural damage by alignment of the serial images.

8.4 Pointwise linear regression of residual RGC count

The outcome of the univariate linear regression of differential light sensitivity (expressed in dB) against time to follow-up with that of the corresponding residual ganglion cell count against time to follow-up in the (early) identification of progressive visual field loss for a long-time series was compared at each stimulus location. The study involved 112 individuals, with five or more reliable visual field examinations, over a minimum follow-up of 5 years.

The results indicated that the residual RGC count identified progression at higher levels of sensitivity at baseline compared to that for the differential light sensitivity. This outcome was manifested by a greater statistical significance of the slope and/ or a greater number of stimulus locations exhibiting statistically significant progressive loss. The outcomes were evaluated in terms of the statistical significance of the slope rather than the magnitude of the slope.

A univariate regression analysis was also undertaken for each of the visual field indices (MD, VFI, and PSD) and the corresponding residual RGC count against time to follow-up. The results indicated agreement between the MD, VFI and PSD and residual RGC count in 20 of the 70 individuals who exhibited statistically significant progression by one or more index. In a further 28 individuals, a statistically significantly progressive residual RGC count was associated with at least one other index exhibiting statistically significant progression. It may well be that an index based upon residual RGC count will be a more sensitive measure for identifying visual field progression; however, the sensitivity and specificity of the residual RGC count for identifying progressive loss is unknown.

The magnitudes at each stimulus location of the statistically significant slopes for both regression outcomes are available and could be further analysed. Given a knowledge of the (cross-sectional) age-related decline for each modality the slopes for each modality could be standardised in terms of the ratio of the measured slope to the age-corrected slope. The next stage of the work will involve the derivation of the respective normal age-related declines, at each stimulus location.

A subsequent stage of the work will involve the comparison of the outcomes derived from the two regressions with that derived from the Event-based analysis of Heijl and Bengtsson (Leske et al. 1999; Heijl et al. 2003; Heijl et al. 2008).

The calculation of the residual RGC count is based upon the absolute value of sensitivity and does not exclude the influence of ‘optical’ (i.e. non-neural factors). A next stage of the work will be to correct the calculation of residual RGC count for these optical factors by, for example, adjusting for the current General Height index or other types of separation (Marin-Franch et al. 2014). An important part of this work will be to evaluate the residual RGC counts pre- and post-operatively in patients undergoing cataract extraction and IOL implantation, as proposed in the aborted study outlined in Chapter 2.

A further aspect will be the automated registration of the spatial distribution of residual RGC soma derived by perimetry with that of RGC axonal thickness derived by OCT.

The outcomes of the current study should be placed in the context of the continuing advance in available computing power enabling greater and greater capability for the storage, processing, display and electronic transfer of ONH images provides a concurrently greater opportunity for improve the health care via the development of electronic based health care monitoring and management. The extensive use of the internet and the evolution in mobile technology, worldwide, can be utilized to provide ‘immediate’ outcomes for patients with glaucoma, e.g., applications, or text alerts, to improve compliance in taking medication and online visual field testing, etc., whilst retaining patient confidentiality. In the context of the current study, stereo-ONH images obtained remotely could be compressed, sent via email, uploaded in a predefined internet

space and viewed by the receiving clinician for almost real-time evaluation. The application of such technology not only has obvious benefits for developing countries, but also can reduce the cost of health care provision, whilst improving quality of care. In countries such as the United States, Canada and Australia, public healthcare programs are willing to reimburse for tele-glaucoma and tele-retinal screening programs, which are considered cost-effective, although the legislation for their activation may vary by state/provincial governments (Kassam et al. 2013).

The use of meta-data, for example those of the epidemiological characteristics of glaucoma; the relationship between the rate of structural and functional progression in relation to age of detection of the disease; the type of, and compliance with, therapy; the development of more statistically appropriate values for normality of current or future diagnostic devices with the ensuing advantage of improved/ optimal specificity and sensitivity etc.; provide the potential for the ongoing optimisation of glaucoma care and delivery, for e-learning; for e-research including the development and use of future pharmacological therapies, and other advantages not yet known. Similar concepts have also been discussed elsewhere (Strouthidis et al. 2014; Wright and Diamond 2015).

The deconstruction of the structure and function relationship via the analysis of meta-data should also lead to the development of optimized pharmaceutical or surgical strategies for the treatment of the various different types, and stages, of glaucoma and the eradication of the disease.

References

- Abramoff, M. D., Alward, W. L., Greenlee, E. C., Shuba, L., Kim, C. Y., Fingert, J. H. and Kwon, Y. H. (2007). Automated segmentation of the optic disc from stereo color photographs using physiologically plausible features. *Invest Ophthalmol Vis Sci* **48**:1665-1673.
- Abramoff, M. D., Lee, K., Niemeijer, M., Alward, W. L., Greenlee, E. C., Garvin, M. K., Sonka, M. *et al.* (2009). Automated segmentation of the cup and rim from spectral domain OCT of the optic nerve head. *Invest Ophthalmol Vis Sci* **50**:5778-5784.
- Ahn, J. K. and Park, K. H. (2002). Morphometric change analysis of the optic nerve head in unilateral disk hemorrhage cases. *Am J Ophthalmol* **134**:920-922.
- Altangerel, U., Bayer, A., Henderer, J. D., Katz, L. J., Steinmann, W. C. and Spaeth, G. L. (2005). Knowledge of chronology of optic disc stereophotographs influences the determination of glaucomatous change. *Ophthalmology* **112**:40-43.
- American Academy of Ophthalmology. (2010). Primary angle-closure glaucoma PPP-2010 [Online]. Available at :<http://www.aaopt.org/preferred-practice-pattern/primary-angle-closure-ppp--october-2010> [Accessed: 20/01/2015].
- Anastasopoulos, E., Founti, P. and Topouzis, F. (2015). Update on pseudoexfoliation syndrome pathogenesis and associations with intraocular pressure, glaucoma and systemic diseases. *Curr Opin Ophthalmol* **26**:82-89.
- Anderson, A. J. (2015). Estimating the true distribution of visual field progression rates in glaucoma. *Invest Ophthalmol Vis Sci* **56**:1603-1608.
- Anderson, D. R. and Patella, V. M. (eds). (1999). Automated Static Perimetry Second ed. St. Louis: Mosby Inc.
- Andersson, S., Heijl, A. and Bengtsson, B. (2011). Optic disc classification by the Heidelberg Retina Tomograph and by physicians with varying experience of glaucoma. *Eye* **25**:1401-1407.

Ang, G. S., Mustafa, M. S., Scott, N., Diaz-Aleman, V. T. and Azuara-Blanco, A. (2011). Perimetric progression in open-angle glaucoma and the Visual Field Index (VFI). *J Glaucoma* **20**:223-227.

Arnalich-Montiel, F., Casas-Llera, P., Munoz-Negrete, F. J. and Rebolleda, G. (2009). Performance of glaucoma progression analysis software in a glaucoma population. *Graefes Arch Clin Exp Ophthalmol* **247**:391-397.

Artes, P. H., Iwase, A., Ohno, Y., Kitazawa, Y. and Chauhan, B. C. (2002). Properties of perimetric threshold estimates from Full Threshold, SITA Standard, and SITA Fast strategies. *Invest Ophthalmol Vis Sci* **43**:2654-2659.

Artes, P. H., Nicolela, M. T., LeBlanc, R. P. and Chauhan, B. C. (2005). Visual field progression in glaucoma: Total versus Pattern Deviation analyses. *Invest Ophthalmol Vis Sci*. **12**:4600-4606.

Artes, P. H., Chauhan, B. C., Keltner, J. L., Cello, K. E., Johnson, C. A., Anderson, D. R., Gordon, M. O. *et al.* (2010). Longitudinal and cross-sectional analyses of visual field progression in participants of the Ocular Hypertension Treatment Study. *Arch Ophthalmol* **128**:1528-1532.

Artes, P. H., O'Leary, N., Hutchison, D. M., Heckler, L., Sharpe, G. P., Nicolela, M. T. and Chauhan, B. C. (2011). Properties of the Statpac Visual Field Index. *Invest Ophthalmol Vis Sci* **52**:4030-4038.

Asaoka, R., Crabb, D. P., Yamashita, T., Russell, R. A., Wang, Y. X. and Garway-Heath, D. F. (2011). Patients have two eyes! Binocular versus better eye visual field indices. *Invest Ophthalmol Vis Sci* **52**:7007-7011.

Asaoka, R., Russell, R. A., Malik, R., Crabb, D. P. and Garway-Heath, D. F. (2012). A novel distribution of visual field test points to improve the correlation between structure-function measurements. *Invest Ophthalmol Vis Sci* **53**:8396-8404.

Asaoka, R. (2013). Measuring visual field progression in the central 10° using additional information from central 24° visual fields and 'lasso regression'. *PLoS One* **8**:1-7.

Asaoka, R., Russell, R. A., Malik, R., Garway-Heath, D. F. and Crabb, D. P. (2013). Five-year forecasts of the Visual Field Index (VFI) with binocular and monocular visual fields. *Graefes Arch Clin Exp Ophthalmol* **251**:1335-1341.

Asman, P. and Heijl, A. (1992). Glaucoma Hemifield Test. Automated visual field evaluation. *Arch Ophthalmol* **110**:812-819.

Asman, P., Wild, J. M. and Heijl, A. (2004). Appearance of the Pattern Deviation map as a function of change in area of localized field loss. *Invest Ophthalmol Vis Sci* **45**:3099-3106.

Azarbod, P., Mock, D., Bitrian, E., Afifi, A. A., Yu, F., Nouri-Mahdavi, K., Coleman, A. L. *et al.* (2012). Validation of point-wise exponential regression to measure the decay rates of glaucomatous visual fields. *Invest Ophthalmol Vis Sci* **53**:5403-5409.

Azuara-Blanco, A., Costa, P. V. and Wilson, P. R. (2002a). Optic nerve and retinal nerve fiber layer. In: Dunitz, M.L. (ed.) *Handbook of Glaucoma*. First ed. Kent: Taylor and Francis, pp. 49-66.

Azuara-Blanco, A., Costa, P. V. and Wilson, P. R. (2002b). Secondary Glaucomas. In: Dunitz, M.L. (ed.) *Handbook of Glaucoma*. First ed. Kent: Taylor and Francis, pp. 119-146.

Balasubramanian, M., Bowd, C., Weinreb, R. N., Vizzeri, G., Alencar, L. M., Sample, P. A., O'Leary, N. *et al.* (2010). Clinical evaluation of the proper orthogonal decomposition framework for detecting glaucomatous changes in human subjects. *Invest Ophthalmol Vis Sci* **51**:264-271.

Balasubramanian, M., Kriegman, D. J., Bowd, C., Holst, M., Weinreb, R. N., Sample, P. A. and Zangwill, L. M. (2012). Localized glaucomatous change detection within the proper orthogonal decomposition framework. *Invest Ophthalmol Vis Sci* **53**:3615-3628.

Baltan, S., Inman, D. M., Danilov, C. A., Morrison, R. S., Calkins, D. J. and Horner, P. J. (2010). Metabolic vulnerability disposes retinal ganglion cell axons to dysfunction in a model of glaucomatous degeneration. *J Neurosci* **30**:5644-5652.

Baltmr, A., Duggan, J., Nizari, S., Salt, T. E. and Cordeiro, M. F. (2010). Neuroprotection in glaucoma - Is there a future role? *Exp Eye Res* **91**:554-566.

Barkana, Y., Ritch, R. (2007). Size Matters: Why optic disk size should be measured when assessed for glaucoma? *Journal of Current Glaucoma Practice* **1**:17-20.

Barry, C. J., Eikelboom, R., Kanagasingham, Y., Jitskaia, L., Morgan, W., House, P. and Cuypers, M. (2000). Comparison of optic disc image assessment methods when examining serial photographs for glaucomatous progression. *Br J Ophthalmol* **84**:28-30.

Bartling, H., Wanger, P. and Martin, L. (2009). Automated quality evaluation of digital fundus photographs. *Acta Ophthalmol* **87**:643-647.

Bartz-Schmidt, K. U., Thumann, G., Jonescu-Cuypers, C. P. and Krieglstein, G. K. (1999). Quantitative morphologic and functional evaluation of the optic nerve head in chronic open-angle glaucoma. *Surv Ophthalmol* **44 Suppl 1**:41-53.

Bebie, H., Fankhauser, F. and Spahr, J. (1976). Static perimetry: strategies. *Acta Ophthalmol (Copenh)* **54**:325-338.

Bengtsson, B. and Krakau, C. E. (1979). Flicker comparison of fundus photographs. A technical note. *Acta Ophthalmol (Copenh)* **57**:503-506.

Bengtsson, B., Olsson, J., Heijl, A. and Rootzen, H. (1997). A new generation of algorithms for computerized threshold perimetry, SITA. *Acta Ophthalmol Scand* **75**:368-375.

Bengtsson, B., Heijl, A. and Olsson, J. (1998). Evaluation of a new threshold visual field strategy, SITA, in normal subjects. Swedish Interactive Thresholding Algorithm. *Acta Ophthalmol Scand* **76**:165-169.

Bengtsson, B. and Heijl, A. (1998). SITA Fast, a new rapid perimetric threshold test. Description of methods and evaluation in patients with manifest and suspect glaucoma. *Acta Ophthalmol Scand* **76**:431-437.

Bengtsson, B. and Heijl, A. (2000). False-negative responses in glaucoma perimetry: indicators of patient performance or test reliability? *Am J Ophthalmol* **130**:689.

Bengtsson, B., Bizios, D. and Heijl, A. (2005). Effects of input data on the performance of a neural network in distinguishing normal and glaucomatous visual fields. *Invest Ophthalmol Vis Sci* **46**:3730-3736.

Bengtsson, B. and Heijl, A. (2008). A Visual Field Index for calculation of glaucoma rate of progression. *Am J Ophthalmol* **145**:343-353.

Bengtsson, B., Leske, M. C., Yang, Z. and Heijl, A. (2008). Disc hemorrhages and treatment in the Early Manifest Glaucoma Trial. *Ophthalmology* **115**:2044-2048.

Bengtsson, B., Patella, V. M. and Heijl, A. (2009). Prediction of glaucomatous visual field loss by extrapolation of linear trends. *Arch Ophthalmol* **127**:1610-1615.

Berger, J. W., Patel, T. R., Shin, D. S., Piltz, J. R. and Stone, R. A. (2000). Computerized stereochronoscopy and alternation flicker to detect optic nerve head contour change. *Ophthalmology* **107**:1316-1320.

Bernardes, R., Serranho, P. and Lobo, C. (2011). Digital ocular fundus imaging: a Review. *Ophthalmologica* **226**:161-181.

Bock, R., Meier, J., Nyul, L. G., Hornegger, J. and Michelson, G. (2010). Glaucoma risk index: automated glaucoma detection from color fundus images. *Med Image Anal* **14**:471-481.

Boland, M. V. and Quigley, H. A. (2007). Risk factors and open-angle glaucoma: classification and application. *J Glaucoma* **16**:406-418.

Boland, M. V. and Quigley, H. A. (2011). Evaluation of a combined index of optic nerve structure and function for glaucoma diagnosis. *BMC Ophthalmol* **11**:6.

Bourne, R. R. A. (2012). The optic nerve head in glaucoma. *Community Eye Health* **25**:55-57.

Bourtsoukli, I. (2005). Aspects of structural and functional assessment in open-angle glaucoma. PhD Thesis, Cardiff University

Breusegem, C., Fieuws, S., Stalmans, I. and Zeyen, T. (2011). Agreement and accuracy of non-expert ophthalmologists in assessing glaucomatous changes in serial stereo optic disc photographs. *Ophthalmology* **118**:742-746.

Broadway, D. C. and Drance, S. M. (1998). Glaucoma and Vasospasm. *Br J Ophthalmol* **82**:862-870.

Broadway, D. C., Nicolela, M. T. and Drance, S. M. (1999). Optic disk appearances in primary open-angle glaucoma. *Surv Ophthalmol* **43**:223-243.

Broman, A. T., Quigley, H. A., West, S. K., Katz, J., Munoz, B., Bandeen-Roche, K., Tielsch, J. M. *et al.* (2008). Estimating the rate of progressive visual field damage in those with open-angle glaucoma, from cross-sectional data. *Invest Ophthalmol Vis Sci* **49**:66-76.

Brusini, P. and Johnson, C. A. (2007). Staging functional damage in glaucoma: review of different classification methods. *Surv Ophthalmol* **52**:156-179.

Brusini, P., Zeppieri, M., Tosoni, C., Parisi, L. and Salvetat, M. L. (2010). Optic disc damage staging system. *J Glaucoma* **19**:442-449.

Bryan, S. R., Vermeer, K. A., Eilers, P. H., Lemij, H. G. and Lesaffre, E. M. (2013). Robust and censored modeling and prediction of progression in glaucomatous visual fields. *Invest Ophthalmol Vis Sci* **54**:6694-6700.

Buckingham, B. P., Inman, D. M., Lambert, W., Oglesby, E., Calkins, D. J., Steele, M. R., Vetter, M. L. *et al.* (2008). Progressive ganglion cell degeneration precedes neuronal loss in a mouse model of glaucoma. *J Neurosci* **28**:2735-2744.

Budenz, D. L., Rhee, P., Feuer, W. J., McSoley, J., Johnson, C. A. and Anderson, D. R. (2002). Sensitivity and specificity of the Swedish interactive threshold algorithm for glaucomatous visual field defects. *Ophthalmology* **109**:1052-1058.

Buerki, E. a. M., M. . (2007). An update to Octopus perimetry. *European Ophthalmic Review*. pp. 20-22.

Bussel, II, Wollstein, G. and Schuman, J. S. (2014). OCT for glaucoma diagnosis, screening and detection of glaucoma progression. *Br J Ophthalmol* **98**:15-19.

Cahill, K. V., Burns, J. A. and Weber, P. A. (1987). The effect of blepharoptosis on the field of vision. *Ophthal Plast Reconstr Surg* **3**:121-125.

Cankaya, A. B. and Simsek, T. (2012). Topographic differences between large and normal optic discs: a confocal scanning laser ophthalmoscopy study. *Eur J Ophthalmol* **22**:63-69.

Caprioli, J. and Coleman, A. L. (2008). Intraocular pressure fluctuation a risk factor for visual field progression at low intraocular pressures in the advanced glaucoma intervention study. *Ophthalmology* **115**:1123-1129

Caprioli, J. and Coleman, A. L. (2010). Blood pressure, perfusion pressure, and glaucoma. *Am J Ophthalmol* **149**:704-712.

Carbonaro, F., Hysi, P. G., Fahy, S. J., Nag, A. and Hammond, C. J. (2014). Optic disc planimetry, corneal hysteresis, central corneal thickness, and intraocular pressure as risk factors for glaucoma. *Am J Ophthalmol* **157**:441-446.

Casas-Llera, P., Rebolleda, G., Munoz-Negrete, F. J., Arnalich-Montiel, F., Perez-Lopez, M. and Fernandez-Buenaga, R. (2009). Visual field index rate and event-based glaucoma progression analysis: comparison in a glaucoma population. *Br J Ophthalmol* **93**:1576-1579.

Casson, R. J., Chidlow, G., Ebnetter, A., Wood, J. P., Crowston, J. and Goldberg, I. (2012a). Translational neuroprotection research in glaucoma: a review of definitions and principles. *Clin Experiment Ophthalmol* **40**:350-357.

Casson, R. J., Chidlow, G., Wood, J. P., Crowston, J. G. and Goldberg, I. (2012b). Definition of glaucoma: clinical and experimental concepts. *Clin Experiment Ophthalmol* **40**:341-349.

Cavallerano, A. (2001). Secondary Open-Angle Glaucoma. In: Litwak, A. (ed.) *Glaucoma Handbook*. Boston, Oxford, Auckland, Johannesburg, Melbourne, New Delhi: Butterworth-Heinemann, pp. 275-287.

Cedrone, C., Mancino, R., Cerulli, A., Cesareo, M. and Nucci, C. (2008). Epidemiology of primary glaucoma: prevalence, incidence, and blinding effects. *Prog Brain Res* **173**:3-14.

Chandra, A., Bandyopadhyay, A. K. and Bhaduri, G. (2013). A comparative study of two methods of optic disc evaluation in patients of glaucoma. *Oman J Ophthalmol* **6**:103-107.

Chauhan, B. C., McCormick, T. A., Nicolela, M. T. and LeBlanc, R. P. (2001). Optic disc and visual field changes in a prospective longitudinal study of patients with glaucoma: comparison of scanning laser tomography with conventional perimetry and optic disc photography. *Arch Ophthalmol* **119**:1492-1499.

Chauhan, B. C., Garway-Heath, D. F., Goni, F. J., Rossetti, L., Bengtsson, B., Viswanathan, A. C. and Heijl, A. (2008). Practical recommendations for measuring rates of visual field change in glaucoma. *Br J Ophthalmol* **92**:569-573.

Chauhan, B. C., Nicolela, M. T. and Artes, P. H. (2009). Incidence and rates of visual field progression after longitudinally measured optic disc change in glaucoma. *Ophthalmology* **116**:2110-2118.

Chauhan, B. C., O'Leary, N., Almobarak, F. A., Reis, A. S., Yang, H., Sharpe, G. P., Hutchison, D. M. *et al.* (2012). Enhanced detection of open-angle glaucoma with an anatomically accurate Optical Coherence Tomography-derived neuroretinal rim parameter. *Ophthalmology* **120**:335-343.

Cho, J. W., Sung, K. R., Yun, S. C., Na, J. H., Lee, Y. and Kook, M. S. (2012). Progression detection in different stages of glaucoma: mean deviation versus visual field index. *Jpn J Ophthalmol* **56**:128-133.

Coleman, A. L. and Miglior, S. (2008). Risk factors for glaucoma onset and progression. *Surv Ophthalmol Suppl* **153**:3-10.

Corona, E., Mitra, S., Wilson, M., Krile, T., Kwon, Y. H. and Soliz, P. (2002). Digital stereo image analyzer for generating automated 3-D measures of optic disc deformation in glaucoma. *IEEE Trans Med Imaging* **21**:1244-1253.

Correnti, A. J., Wollstein, G., Price, L. L. and Schuman, J. S. (2003). Comparison of optic nerve head assessment with a digital stereoscopic camera (discam), scanning laser ophthalmoscopy, and stereophotography. *Ophthalmology* **110**:1499-1505.

Coudrillier, B., Tian, J., Alexander, S., Myers, K. M., Quigley, H. A. and Nguyen, T. D. (2012). Biomechanics of the human posterior sclera: age- and glaucoma-related changes measured using inflation testing. *Invest Ophthalmol Vis Sci* **53**:1714-1728.

Crabb, D. P. and Garway-Heath, D. F. (2012). Intervals between visual field tests when monitoring the glaucomatous patient: wait-and-see approach. *Invest Ophthalmol Vis Sci* **53**:2770-2776.

Crowston, J. G., Hopley, C. R., Healey, P. R., Lee, A. and Mitchell, P. (2004). The effect of optic disc diameter on vertical cup-to-disc ratio percentiles in a population based cohort: the Blue Mountains Eye Study. *Br J Ophthalmol* **88**:766-770.

Cymbor, M., Lear, L. and Mastrine, M. (2009). Concordance of flicker comparison versus side-by-side comparison in glaucoma. *Optometry* **80**:437-441.

Dacey, D. M. and Brace, S. (1992). A coupled network for parasol but not midget ganglion cells in the primate retina. *Vis Neurosci* **9**:279-290.

Dacey, D. M. (1993). Morphology of a small-field bistratified ganglion cell type in the macaque and human retina. *Vis Neurosci* **10**:1081-1098.

Dacey, D. M. and Lee, B. B. (1994). The 'blue-on' opponent pathway in primate retina originates from a distinct bistratified ganglion cell type. *Nature* **367**:731-735.

De Moraes, C. G., Liebmann, J. M., Liebmann, C. A., Susanna, R., Jr., Tello, C. and Ritch, R. (2011). Visual field progression outcomes in glaucoma subtypes. *Acta Ophthalmol* **91**:288-293.

De Moraes, C. G., Demirel, S., Gardiner, S. K., Liebmann, J. M., Cioffi, G. A., Ritch, R., Gordon, M. O. *et al.* (2012a). Rate of visual field progression in eyes with optic disc hemorrhages in the Ocular Hypertension Treatment Study. *Arch Ophthalmol* **130**:1541-1546.

De Moraes, C. G., Liebmann, C. A., Susanna, R., Jr., Ritch, R. and Liebmann, J. M. (2012b). Examination of the performance of different pointwise linear regression progression criteria to detect glaucomatous visual field change. *Clin Experiment Ophthalmol* **40**:190-196.

Delgado, M. F., Nguyen, N. T., Cox, T. A., Singh, K., Lee, D. A., Dueker, D. K., Fechtner, R. D. *et al.* (2002). Automated perimetry: a report by the American Academy of Ophthalmology. *Ophthalmology* **109**:2362-2374.

Dignam, K. and Stutman, R. (2001). Epidemiology and risk factors for glaucoma. In: Litwak, A. (ed.) *Glaucoma Handbook*. Boston, Oxford, Auckland, Johannesburg, Melbourne, New Delhi: Butterworth-Heinemann pp. 9-20.

Drance, S. M. (2008). What can we learn from the disc appearance about the risk factors in glaucoma? *Can J Ophthalmol* **43**:322-327.

Drasdo, N., Millican, C. L., Katholi, C. R. and Curcio, C. A. (2007). The length of Henle fibers in the human retina and a model of ganglion receptive field density in the visual field. *Vision Res* **47**:2901-2911.

Drasdo, N., Mortlock, K. E. and North, R. V. (2008). Ganglion cell loss and dysfunction: relationship to perimetric sensitivity. *Optom Vis Sci* **85**:1036-1042.

Eilaghi, A., Flanagan, J. G., Simmons, C. A. and Ethier, C. R. (2010). Effects of scleral stiffness properties on optic nerve head biomechanics. *Ann Biomed Eng* **38**:1586-1592.

Ewen, A., Lee, K. E., Klein, B. E. and Klein, R. (2006). Comparability of cup and disk diameters measured from non-stereoscopic digital and stereoscopic film images. *Am J Ophthalmol* **141**:1126-1128.

Fankhauser, F. and Bebie, H. (1979). Threshold fluctuations, interpolations and spatial resolution in perimetry. In: Greve, E.L. (ed.) *Documenta Ophthalmologica Proceedings Series. 19. Third International Visual Field Symposium*. The Hague: Junk Publishers, pp. 295-309.

Fankhauser, F., Bebie, H. and Flammer, J. (1988). Threshold fluctuations in the Humphrey Field Analyzer and in the Octopus automated perimeter. *Invest Ophthalmol Vis Sci* **29**:1466.

Fansi, A. A., Papamatheakis, D. G. and Harasymowycz, P. J. (2009). Racial variability of glaucoma risk factors between African Caribbeans and Caucasians in a Canadian urban screening population. *Can J Ophthalmol* **44**:576-581.

Fingeret, M., Medeiros, F. A., Susanna, J. R. and Weinreb, R. N. (2005). Five rules to evaluate the optic disc and retinal nerve fiber layer for glaucoma. *Optometry* **76**:661-668.

Fitzke, F. W., Crabb, D. P., McNaught, A. I., Edgar, D. F. and Hitchings, R. A. (1995). Image processing of computerised visual field data. *Br J Ophthalmol* **79**:207-212.

Flammer, J., Drance, S. M., Fankhauser, F. and Augustiny, L. (1984). Differential light threshold in automated static perimetry. Factors influencing short-term fluctuation. *Arch Ophthalmol* **102**:876-879.

Flanagan, J. G., Moss, I. D., Wild, J. M., Hudson, C., Prokopich, L., Whitaker, D. and O'Neill, E. C. (1993a). Evaluation of FASTPAC: a new strategy for threshold estimation with the Humphrey Field Analyzer. *Graefes Arch Clin Exp Ophthalmol* **231**:465-469.

Flanagan, J. G., Wild, J. M. and Trope, G. E. (1993b). Evaluation of FASTPAC, a new strategy for threshold estimation with the Humphrey Field Analyzer, in a glaucomatous population. *Ophthalmology* **100**:949-954.

Foster, P. J., Buhrmann, R., Quigley, H. A. and Johnson, G. J. (2002). The definition and classification of glaucoma in prevalence surveys. *Br J Ophthalmol* **86**:238-242.

Fraz, M. M., Remagnino, P., Hoppe, A., Uyyanonvara, B., Rudnicka, A. R., Owen, C. G. and Barman, S. A. (2012). Blood vessel segmentation methodologies in retinal images – A survey. *Comput Methods Programs Biomed* **108**:407-433.

Friedman, D. S., Jampel, H. D., Munoz, B. and West, S. K. (2006). The prevalence of open-angle glaucoma among blacks and whites 73 years and older: the Salisbury Eye Evaluation Glaucoma Study. *Arch Ophthalmol* **124**:1625-1630.

Fukuchi, T., Yoshino, T., Sawada, H., Seki, M., Togano, T., Tanaka, T., Ueda, J. *et al.* (2010). Progression rate of total, and upper and lower visual field defects in open-angle glaucoma patients. *Clin Ophthalmol* **18**:1315-1323.

Gaasterland, D. E., Ederer, F., Sullivan, E. K., Caprioli, J. and Cyrlin, M. N. (1994). Advanced Glaucoma Intervention Study: 2. visual field test scoring and reliability. *Ophthalmology* **101**:1445-1455.

Gardiner, S. K., Johnson, C. A. and Demirel, S. (2011). Cup size predicts subsequent functional change in early glaucoma. *Optom Vis Sci* **88**:1470-1476.

Gardiner, S. K., Fortune, B., Wang, L., Downs, J. C. and Burgoyne, C. F. (2012a). Intraocular pressure magnitude and variability as predictors of rates of structural change in non-human primate experimental glaucoma. *Exp Eye Res* **103**:1-8.

Gardiner, S. K., Johnson, C. A. and Demirel, S. (2012b). Factors predicting the rate of functional progression in early and suspected glaucoma. *Invest Ophthalmol Vis Sci* **53**:3598-3604.

Garway-Heath, D. F., Wollstein, G. and Hitchings, R. A. (1997). Aging changes of the optic nerve head in relation to open-angle glaucoma. *Br J Ophthalmol* **81**:840-845.

Garway-Heath, D. F. and Hitchings, R. A. (1998). Quantitative evaluation of the optic nerve head in early glaucoma. *Br J Ophthalmol* **82**:352-361.

Garway-Heath, D. F., Ruben, S. T., Viswanathan, A. and Hitchings, R. A. (1998a). Vertical cup/disc ratio in relation to optic disc size: its value in the assessment of the glaucoma suspect. *Br J Ophthalmol* **82**:1118-1124.

Garway-Heath, D. F., Rudnicka, A. R., Lowe, T., Foster, P. J., Fitzke, F. W. and Hitchings, R. A. (1998b). Measurement of optic disc size: equivalence of methods to correct for ocular magnification. *Br J Ophthalmol* **82**:643-649.

Garway-Heath, D. F., Poinosawmy, D., Wollstein, G., Viswanathan, A., Kamal, D., Fontana, L. and Hitchings, R. A. (1999). Inter- and intra-observer variation in the analysis of optic disc images: comparison of the Heidelberg Retina Tomograph and computer-assisted planimetry. *Br J Ophthalmol* **83**:664-669.

Garway-Heath, D. F., Caprioli, J., Fitzke, F. W. and Hitchings, R. A. (2000a). Scaling the hill of vision: the physiological relationship between light sensitivity and ganglion cell numbers. *Invest Ophthalmol Vis Sci* **41**:1774-1782.

Garway-Heath, D. F., Poinosawmy, D., Fitzke, F. W. and Hitchings, R. A. (2000b). Mapping the visual field to the optic disc in normal tension glaucoma eyes. *Ophthalmology* **107**:1809-1815.

Garway-Heath, D. F., Lascaratos, G., Bunce, C., Crabb, D. P., Russell, R. A. and Shah, A. (2013). The United Kingdom Glaucoma Treatment Study: a multicenter, randomized, placebo-controlled clinical trial: design and methodology. *Ophthalmology* **120**:68-76.

Goldmann, H. (1945). Ein selbstregistrierendes projektionskugelperimeter. *Ophthalmologica* **109**:71-79.

Gonzalez-Hernandez, M., Pablo, L. E., Armas-Dominguez, K., de la Vega, R. R., Ferreras, A. and de la Rosa, M. G. (2009). Structure-function relationship depends on glaucoma severity. *Br J Ophthalmol* **93**:1195-1199.

Gordon, M. O., Beiser, J. A., Brandt, J. D., Heuer, D. K., Higginbotham, E. J., Johnson, C. A., Keltner, J. L. *et al.* (2002). The Ocular Hypertension Treatment Study: baseline factors that predict the onset of primary open-angle glaucoma. *Arch Ophthalmol* **120**:714-720.

Greenfield, D. S. (1997). Stereoscopic optic disc photography In: Schuman, S.J. (ed.) *Imaging in Glaucoma*. second ed. Thorofare New Jersey: Slack Incorporated, pp. 3-15.

Grewal, D. S., Sehi, M. and Greenfield, D. S. (2009). Diffuse glaucomatous structural and functional damage in the hemifield without significant pattern loss. *Arch Ophthalmol* **127**:1442-1448.

Gros-Otero, J., Castejon, M., Paz-Moreno, J., Mikropoulos, D. and Teus, M. (2014). Perimetric progression using the Visual Field Index and the Advanced Glaucoma Intervention Study score and its clinical correlations. *J Optom* **122**:1-7.

Guerri, N., Polo, V., Larrosa, J. M., Ferreras, A., Fuertes, I. and Pablo, L. E. (2012). Performance of imaging devices versus optic disc and nerve fiber layer photography in a clinical practice guideline for glaucoma diagnosis. *Eur J Ophthalmol* **22**:554-562.

Gugleta, K., Waldmann, N., Polunina, A., Kochkorov, A., Katamay, R., Flammer, J. and Orgul, S. (2013). Retinal neurovascular coupling in patients with glaucoma and ocular hypertension and its association with the level of glaucomatous damage. *Graefes Arch Clin Exp Ophthalmol* **251**:1577-1585.

Hafez, A. S., Bizzarro, R. L. G. and Lesk, M. R. (2003). Evaluation of optic nerve head and peripapillary retinal blood flow in glaucoma patients, ocular hypertensives, and normal subjects. *Am J Ophthalmol* **136**:1022-1031.

Hancox O.D, M. D. (1999). Optic disc size, an important consideration in the glaucoma evaluation. *Clinical Eye and Vision Care* **11**:59-62.

Hankins, M. W., Peirson, S. N. and Foster, R. G. (2008). Melanopsin: an exciting photopigment. *Trends Neurosci* **31**:27-36.

Harwerth, R. S., Carter-Dawson, L., Smith, E. L., 3rd and Crawford, M. L. (2005). Scaling the structure-function relationship for clinical perimetry. *Acta Ophthalmol Scand* **83**:448-455.

Harwerth, R. S., Wheat, J. L., Fredette, M. J. and Anderson, D. R. (2010). Linking structure and function in glaucoma. *Prog Retin Eye Res* **29**:249-271.

Hasnain, S. S. (2006). Scleral edge, not optic disc or retina, is the primary site of injury in chronic glaucoma. *Med Hypotheses* **67**:1320-1325.

He, Z., Vingrys, A. J., Armitage, J. A. and Bui, B. V. (2011). The role of blood pressure in glaucoma. *Clin Exp Optom* **94**:133-149.

Healey, P. R. and Mitchell, P. (1999). Optic disk size in open-angle glaucoma: the Blue Mountains Eye Study. *Am J Ophthalmol* **128**:515-517.

Healey, P. R. and Mitchell, P. (2004). Visibility of lamina cribrosa pores and open-angle glaucoma. *Am J Ophthalmol* **138**:871-872.

Healey, P. R., Mitchell, P., Gilbert, C. E., Lee, A. J., Ge, D., Snieder, H., Spector, T. D. *et al.* (2007). The inheritance of peripapillary atrophy. *Invest Ophthalmol Vis Sci* **48**:2529-2534.

Heijl, A. and Krakau, C. E. (1975). An automatic static perimeter, design and pilot study. *Acta Ophthalmol (Copenh)* **53**:293-310.

Heijl, A. (1977). Time changes of contrast thresholds during automatic perimetry. *Acta Ophthalmol (Copenh)* **55**:696-708.

Heijl, A., Lindgren, G. and Olsson, J. (1986). A package for the statistical analysis of visual fields. In: Greve, E.L. and Heijl, A. (eds.) *Documenta Ophthalmologica Proceedings Series 49. Seventh International Visual Field Symposium*. The Netherlands: Junk Publishers, pp. 153-168.

Heijl, A., Lindgren, G. and Olsson, J. (1989). The effect of perimetric experience in normal subjects. *Arch Ophthalmol* **107**:81-86.

Heijl, A. and Bengtsson, B. (1989). Diagnosis of early glaucoma with flicker comparisons of serial disc photographs. *Invest Ophthalmol Vis Sci* **30**:2376-2384.

Heijl, A. and Bengtsson, B. (1998). Linear regression analysis in glaucoma visual field follow-up. In: Wall, M. and Wild, J.M. (eds.) *Perimetry Update 1998/1999*. New York, The Hague: Kugler Publications, pp. 125-130.

Heijl, A., Leske, M. C., Bengtsson, B., Hyman, L., Bengtsson, B. and Hussein, M. (2002). Reduction of intraocular pressure and glaucoma progression: results from the Early Manifest Glaucoma Trial. *Arch Ophthalmol* **120**:1268-1279.

Heijl, A. and Patella, V. M. (eds). (2002). *Essential Perimetry* Third ed. Dublin, California: Carl Zeiss Meditec.

Heijl, A., Leske, M. C., Bengtsson, B., Bengtsson, B. and Hussein, M. (2003). Measuring visual field progression in the Early Manifest Glaucoma Trial. *Acta Ophthalmol Scand* **81**:286-293.

Heijl, A., Bengtsson, B., Chauhan, B. C., Lieberman, M. F., Cunliffe, I., Hyman, L. and Leske, M. C. (2008). A comparison of visual field progression criteria of 3 major glaucoma trials in Early Manifest Glaucoma Trial patients. *Ophthalmology* **29**:29.

Heijl, A., Bengtsson, B., Hyman, L. and Leske, M. C. (2009). Natural history of open-angle glaucoma. *Ophthalmology* **116**:2271-2276.

Heijl, A., Leske, M. C., Hyman, L., Yang, Z. and Bengtsson, B. (2011). Intraocular pressure reduction with a fixed treatment protocol in the Early Manifest Glaucoma Trial. *Acta Ophthalmol* **89**:749-754.

Heijl, A., Bengtsson, B. and Oskarsdottir, S. E. (2013a). Prevalence and severity of undetected manifest glaucoma: results from the Early Manifest Glaucoma Trial Screening. *Ophthalmology* **120**:1541-1545.

Heijl, A., Buchholz, P., Norrgren, G. and Bengtsson, B. (2013b). Rates of visual field progression in clinical glaucoma care. *Acta Ophthalmol* **91**:406-412.

Henson, D. B. and Morris, E. J. (1993). Effect of uncorrected refractive errors upon central visual field testing. *Ophthalmic Physiol Opt* **13**:339-343.

Heuer, D. K., Anderson, D. R., Knighton, R. W., Feuer, W. J. and Gressel, M. G. (1988). The influence of simulated light scattering on automated perimetric threshold measurements. *Arch Ophthalmol* **106**:1247-1251.

Hirasawa, K., Shoji, N., Morita, T. and Shimizu, K. (2013). A modified glaucoma staging system based on Visual Field Index. *Graefes Arch Clin Exp Ophthalmol* **251**:2747-2752.

Hitchings, R. A. (2008). Glaucoma: an area of darkness. *Eye* **23**:1764-1774.

Hodapp, E., Parrish, I. I. R. K. and Anderson, D. R. (1993). Clinical decisions in glaucoma. St Louis: The CV Mosby Co, pp. 52-61.

Hoffmann, E. M., Zangwill, L. M., Crowston, J. G. and Weinreb, R. N. (2007). Optic disk size and glaucoma. *Surv Ophthalmol* **52**:32-49.

Hood, D. C., Anderson, S. C., Wall, M. and Kardon, R. H. (2007). Structure versus function in glaucoma: an application of a linear model. *Invest Ophthalmol Vis Sci* **48**:3662-3668.

Hoyng, P. (2005). Disc Haemorrhages. In: Iester, M., Garway-Heath, D. and Lemij, H.G. (eds.) *Optic Nerve Head and Retinal Nerve Fibre Analysis*. Savona, Italy: European Glaucoma Society, pp. 25-27.

Huang, D., Chopra, V., Lu, A. T., Tan, O., Francis, B. and Varma, R. (2012). Does optic nerve head size variation affect circumpapillary retinal nerve fiber layer thickness measurement by optical coherence tomography? *Invest Ophthalmol Vis Sci* **53**:4990-4997.

Hudson, C., Wild, J. M. and O'Neill, E. C. (1994). Fatigue effects during a single session of automated static threshold perimetry. *Invest Ophthalmol Vis Sci* **35**:268-280.

Hutchings, N., Wild, J. M., Hussey, M. K., Flanagan, J. G. and Trope, G. E. (2000). The long-term fluctuation of the visual field in stable glaucoma. *Invest Ophthalmol Vis Sci* **41**:3429-3436.

Iester, M., Capris, E., De Feo, F., Polvicino, M., Brusini, P., Capris, P., Corallo, G. *et al.* (2011). Agreement to detect glaucomatous visual field progression by using three different methods: a multicentre study. *Br J Ophthalmol* **95**:1276-1283.

Imaging and Perimetry Society (2014). What is Perimetry? [Online]. Available at: <http://www.perimetry.org/Perimetr.htm> [Accessed: 15-04-2015].

Inci Dersu, M. N. W. (2006). Understanding Visual Fields Part 2: Humphrey Visual Fields. *Journal of Ophthalmic Medical Technology* **2**:1-7.

Jackson, J. (2001). Primary angle-closure glaucoma. In: Litwak, A. (ed.) *Glaucoma Handbook*. Boston, Oxford, Auckland, Johannesburg, Melbourne, New Delhi: Butterworth-Heinemann pp. 291-307.

Jakobs, T. C., Libby, R. T., Ben, Y., John, S. W. and Masland, R. H. (2005). Retinal ganglion cell degeneration is topological but not cell type specific in DBA/2J mice. *J Cell Biol* **171**:313-325.

Jampel, H. D., Friedman, D., Quigley, H., Vitale, S., Miller, R., Knezevich, F. and Ding, Y. (2008). Agreement among glaucoma specialists in assessing progressive disc changes from photographs in open-angle glaucoma patients. *Am J Ophthalmol* **12**:12.

Jiang, X., Lambers, M. and Bunke, H. (2012a). Structural performance evaluation of curvilinear structure detection algorithms with application to retinal vessel segmentation. *Pattern Recognit Lett.* **33**:2048-2056.

Jiang, X., Varma, R., Wu, S., Torres, M., Azen, S. P., Francis, B. A., Chopra, V. *et al.* (2012b). Baseline risk factors that predict the development of open-angle glaucoma in a population: the Los Angeles Latino Eye Study. *Ophthalmology* **119**:2245-2253.

Johnson, C. A., Adams, C. W. and Lewis, R. A. (1988). Fatigue effects in automated perimetry. *Appl Opt* **27**:1030-1037.

Johnson, C. A., Sample, P. A., Zangwill, L. M., Vasile, C. G., Cioffi, G. A., Liebmann, J. R. and Weinreb, R. N. (2003). Structure and function evaluation (SAFE): II. Comparison of optic disk and visual field characteristics. *Am J Ophthalmol* **135**:148-154.

Johnson, C. A., Sherman, K., Doyle, C. and Wall, M. (2014). A comparison of false-negative responses for Full Threshold and SITA standard perimetry in glaucoma patients and normal observers. *J Glaucoma* **23**:288-292.

Johnson, E. C. and Morrison, J. C. (2009). Friend or foe? Resolving the impact of glial responses in glaucoma. *J Glaucoma* **18**:341-353.

Jonas, J. B., Gusek, G. C. and Naumann, G. O. (1988). Optic disc, cup and neuroretinal rim size, configuration and correlations in normal eyes. *Invest Ophthalmol Vis Sci* **29**:1151-1158.

Jonas, J. B. and Montgomery, D. M. (1995). Determination of the neuroretinal rim area using the horizontal and vertical disc and cup diameters. *Graefes Arch Clin Exp Ophthalmol* **233**:690-693.

Jonas, J. B., Sturmer, J., Papastathopoulos, K. I., Meier-Gibbons, F. and Dichtl, A. (1995). Optic disc size and optic nerve damage in normal pressure glaucoma. *Br J Ophthalmol* **79**:1102-1105.

Jonas, J. B., Budde, W. M. and Lang, P. (1998). Neuroretinal rim width ratios in morphological glaucoma diagnosis. *Br J Ophthalmol* **82**:1366-1371.

Jonas, J. B., Budde, W. M. and Panda-Jonas, S. (1999). Ophthalmoscopic evaluation of the optic nerve head. *Surv Ophthalmol* **43**:293-320.

Jonas, J. B., Bergua, A., Schmitz-Valckenberg, P., Papastathopoulos, K. I. and Budde, W. M. (2000). Ranking of optic disc variables for detection of glaucomatous optic nerve damage. *Invest Ophthalmol Vis Sci* **41**:1764-1773.

Jonas, J. B., Budde, W. M., Nemeth, J., Grundler, A. E., Mistlberger, A. and Hayler, J. K. (2001). Central retinal vessel trunk exit and location of glaucomatous parapapillary atrophy in glaucoma. *Ophthalmology* **108**:1059-1064.

Jonas, J. B., Martus, P., Horn, F. K., Junemann, A., Korth, M. and Budde, W. M. (2004). Predictive factors of the optic nerve head for development or progression of glaucomatous visual field loss. *Invest Ophthalmol Vis Sci* **45**:2613-2618.

Jonas, J. B. (2005). Clinical implications of peripapillary atrophy in glaucoma. *Curr Opin Ophthalmol* **16**:84-88.

Jonas, J. B., Stroux, A., Martus, P. and Budde, W. (2006). Keratometry, optic disc dimensions, and degree and progression of glaucomatous optic nerve damage. *J Glaucoma* **15**:206-212.

Jonas, J. B., Jonas, S. B., Jonas, R. A., Holbach, L., Dai, Y., Sun, X. and Panda-Jonas, S. (2012). Parapapillary atrophy: histological gamma zone and delta zone. *PLoS One* **7**:1-7.

Junemann, A. G., Martus, P., Wisse, M. and Jonas, J. (2000). Quantitative analysis of visual field and optic disk in glaucoma: retinal nerve fiber bundle-associated analysis. *Graefes Arch Clin Exp Ophthalmol* **238**:306-314.

Kaas, J. H., Huerta, M. F., Weber, J. T. and Harting, J. K. (1978). Patterns of retinal terminations and laminar organization of the lateral geniculate nucleus of primates. *J Comp Neurol* **182**:517-553.

Kamdeu Fansi, A. A., Boisjoly, H., Chagnon, M. and Harasymowycz, P. J. (2011). Combining rim area to disc area asymmetry ratio and Moorfields regression analysis of confocal scanning laser ophthalmoscopy for glaucoma screening. *Can J Ophthalmol* **46**:261-266.

Kass, M. A., Heuer, D. K., Higginbotham, E. J., Johnson, C. A., Keltner, J. L., Miller, J. P., Parrish, R. K., 2nd *et al.* (2002). The Ocular Hypertension Treatment Study: a randomized trial determines that topical ocular hypotensive medication delays or prevents the onset of primary open-angle glaucoma. *Arch Ophthalmol* **120**:701-713; discussion 829-730.

Kassam, F., Yogesan, K., Sogbesan, E., Pasquale, L. R. and Damji, K. F. (2013). Teleglaucoma: improving access and efficiency for glaucoma care. *Middle East Afr J Ophthalmol* **20**:142-149.

Katz, J. and Sommer, A. (1986). Asymmetry and variation in the normal hill of vision. *Arch Ophthalmol* **104**:65-68.

Kim, E. and Varma, R. (2010). Glaucoma in Latinos/Hispanics. *Curr Opin Ophthalmol* **21**:100-105.

Kisiswa, L., Dervan, A. G., Albon, J., Morgan, J. E. and Wride, M. A. (2010). Retinal ganglion cell death postponed: giving apoptosis a break? *Ophthalmic Res* **43**:61-78.

Konstas, A. G., Mikropoulos, D. G. and Irkec, M. (2010). Open-angle glaucoma and ocular perfusion. *Br J Ophthalmol* **94**:1273-1274.

Kothari, R., Bokariya, P., Singh, R., Singh, S. and Narang, P. (2014). Correlation of pattern reversal visual evoked potential parameters with the Pattern Standard Deviation in primary open-angle glaucoma. *Int J Ophthalmol* **7**:326-329.

Kottler, M. S., Rosenthal, A. R. and Falconer, D. G. (1976). Analog vs. digital photogrammetry for optic cup analysis. *Invest Ophthalmol* **15**:651-654.

Krupin, T., Liebmann, J. M., Greenfield, D. S., Rosenberg, L. F., Ritch, R. and Yang, J. W. (2005). The Low-pressure Glaucoma Treatment Study (LoGTS) study design and baseline characteristics of enrolled patients. *Ophthalmology* **112**:376-385.

Laemmer, R., Schroeder, S., Martus, P., Viestenz, A. and Mardin, C. Y. (2007). Quantification of neuroretinal rim loss using digital planimetry in long-term follow-up of normals and patients with ocular hypertension. *J Glaucoma* **16**:430-436.

Lalle, P. A. (2001). Evaluation of Automated Perimetry. In: Litwak, A. (ed.) *Glaucoma Handbook*. Boston, Oxford, Auckland, Johannesburg, Melbourne, New Delhi: Butterworth-Heinemann, pp. 97-167.

Larrosa, J. M., Polo, V., Ferreras, A., Gil, L., Fuertes, I. and Pablo, L. E. (2012). Predictive value of confocal scanning laser for the onset of visual field loss in glaucoma suspects. *Ophthalmology* **119**:1558-1562.

Lawrenson, G. J. (2007). Histopathology and Pathogenesis of Glaucomatous Optic Neuropathy. In: Edgar, D. and Rudnicka, A.R. (eds.) *Glaucoma Identification and Co-management*. Philadelphia: Elsevier Limited, pp. 27-35.

Lee, E. J., Kim, T. W., Weinreb, R. N. and Kim, H. (2012a). Reversal of lamina cribrosa displacement after intraocular pressure reduction in open-angle glaucoma. *Ophthalmology* **120**:553-559.

Lee, J., Kim, J. and Kee, C. (2012b). Characteristics of patients with a localized retinal nerve fiber layer defect and normal optic disc appearance. *Eye* **26**:1473-1478.

Lee, J. M., Cirineo, N., Ramanathan, M., Nouri-Mahdavi, K., Morales, E., Coleman, A. L. and Caprioli, J. (2014a). Performance of the Visual Field Index in glaucoma patients with moderately advanced visual field loss. *Am J Ophthalmol* **157**:39-43.

Lee, J. W., Morales, E., Yu, F., Afifi, A. A., Kim, E. A., Abdollahi, N., Nouri-Mahdavi, K. *et al.* (2014b). Effect of cataract extraction on the visual field decay rate in patients with glaucoma. *JAMA Ophthalmol* **132**:1296-1302.

Lee, K., Niemeijer, M., Garvin, M. K., Kwon, Y. H., Sonka, M. and Abramoff, M. D. (2010). Segmentation of the optic disc in 3-D OCT scans of the optic nerve head. *IEEE Trans Med Imaging* **29**:159-168.

Lee, M., Yoo, H. and Ahn, J. (2013). Comparison of disc analysis algorithms provided by cirrus OCT and stereo optic-disc photography in normal and open angle glaucoma patients. *Curr Eye Res* **38**:605-613.

Leske, M. C. (1983). The epidemiology of open-angle glaucoma: a Review. *Am J Epidemiol* **118**:166-191.

Leske, M. C., Connell, A. M., Schachat, A. P. and Hyman, L. (1994). The Barbados Eye Study. Prevalence of open-angle glaucoma. *Arch Ophthalmol* **112**:821-829.

Leske, M. C., Heijl, A., Hyman, L. and Bengtsson, B. (1999). Early Manifest Glaucoma Trial: design and baseline data. *Ophthalmology* **106**:2144-2153.

Leske, M. C., Heijl, A., Hyman, L., Bengtsson, B. and Komaroff, E. (2004). Factors for progression and glaucoma treatment: the Early Manifest Glaucoma Trial. *Curr Opin Ophthalmol* **15**:102-106.

Leske, M. C., Heijl, A., Hyman, L., Bengtsson, B., Dong, L. and Yang, Z. (2007). Predictors of long-term progression in the Early Manifest Glaucoma Trial. *Ophthalmology* **114**:1965-1972.

Leung, C. K. (2014). Diagnosing glaucoma progression with optical coherence tomography. *Curr Opin Ophthalmol* **25**:104-111.

Levin, L. A. (1999). Direct and indirect approaches to neuroprotective therapy of glaucomatous optic neuropathy. *Surv Ophthalmol* **43** 98-101.

Li, H., Healey, P. R., Tariq, Y. M., Teber, E. and Mitchell, P. (2013). Symmetry of optic nerve head parameters measured by the Heidelberg Retina Tomograph 3 in healthy eyes: the Blue Mountains Eye Study. *Am J Ophthalmol* **155**:518-523.

Li, Y., Li, C., Chen, Z., He, J., Tao, Z. and Yin, Z. Q. (2012). A microRNA, mir133b, suppresses melanopsin expression mediated by failure dopaminergic amacrine cells in RCS rats. *Cell Signal* **24**:685-698.

Lichter, P. R. (2003). Glaucoma clinical trials and what they mean for our patients. *Am J Ophthalmol* **136**:136-145.

Lichter, P. R., Musch, D. C., Gillespie, B. W., Guire, K. E., Janz, N. K., Wren, P. A. and Mills, R. P. (2001). Interim clinical outcomes in the Collaborative Initial Glaucoma Treatment Study comparing initial treatment randomized to medications or surgery. *Ophthalmology* **108**:1943-1953.

Liesenfeld, B., Kohner, E., Piehlmeier, W., Kluthe, S., Aldington, S., Porta, M., Bek, T. *et al.* (2000). A telemedical approach to the screening of diabetic retinopathy: digital fundus photography. *Diabetes Care* **23**:345-348.

Lieven, C. J., Hoegger, M. J., Schlieve, C. R. and Levin, L. A. (2006). Retinal ganglion cell axotomy induces an increase in intracellular superoxide anion. *Invest Ophthalmol Vis Sci* **47**:1477-1485.

Lindberg, J. G. (1989). Clinical investigations on depigmentation of the pupillary border and translucency of the iris in cases of senile cataract and in normal eyes in elderly persons. *Acta Ophthalmol Suppl* **190**:1-96.

Litwak, B. A. (2001). *Glaucoma Handbook*. Boston, Oxford, Auckland, Johannesburg, Melbourne, New Delhi: Butterworth-Heinemann, p. 364.

Liu, M., Guo, L., Salt, T. E. and Cordeiro, M. F. (2014). Dendritic changes in rat visual pathway associated with experimental ocular hypertension. *Curr Eye Res* **39**:953-963.

Liu, Y.-Y., Chen, M., Ishikawa, H., Wollstein, G., Schuman, J. S. and Rehg, J. M. (2011). Automated macular pathology diagnosis in retinal OCT images using multi-scale spatial pyramid and local binary patterns in texture and shape encoding. *Med Image Anal* **15**:748-759.

Malik, R., Swanson, W. H. and Garway-Heath, D. F. (2012). Structure-function relationship in glaucoma: past thinking and current concepts. *Clin Experiment Ophthalmol* **40**:369-380.

Malik, R., Baker, H., Russell, R. A. and Crabb, D. P. (2013). A survey of attitudes of glaucoma subspecialists in England and Wales to visual field test intervals in relation to NICE guidelines. *BMJ Open* **3**:5.

Manassakorn, A., Nouri-Mahdavi, K., Koucheiki, B., Law, S. K. and Caprioli, J. (2006). Pointwise linear regression analysis for detection of visual field progression with absolute versus corrected threshold sensitivities. *Invest Ophthalmol Vis Sci* **47**:2896-2903.

Mansouri, K., Leite, M. T., Medeiros, F. A., Leung, C. K. and Weinreb, R. N. (2011). Assessment of rates of structural change in glaucoma using imaging technologies. *Eye* **25**:269-277.

Maresco, G. J. a. G., S. (2002). Anatomy, physiology and pathophysiology In: Azuara-Blanco, A. and Costa, P.V. and Wilson, P.R. (eds.) *Hanbook of Glaucoma*. London: Dunitz, M. Ltd, pp. 3-16.

Marin-Franch, I., Swanson, W. H. and Malinovsky, V. E. (2014). A novel strategy for the estimation of the general height of the visual field in patients with glaucoma. *Graefes Arch Clin Exp Ophthalmol* **252**:801-809.

Martus, P., Stroux, A., Budde, W. M., Mardin, C. Y., Korth, M. and Jonas, J. B. (2005). Predictive factors for progressive optic nerve damage in various types of chronic open-angle glaucoma. *Am J Ophthalmol* **139**:999-1009.

Marvasti, A. H., Tatham, A. J., Zangwill, L. M., Girkin, C. A., Liebmann, J. M., Weinreb, R. N. and Medeiros, F. A. (2013). The relationship between Visual Field Index and estimated number of retinal ganglion cells in glaucoma. *PLoS One* **8**:1-7.

McKendrick, A. M. and Turpin, A. (2005). Advantages of terminating Zippy Estimation by Sequential Testing (ZEST) with dynamic criteria for white-on-white perimetry. *Optom Vis Sci* **82**:981-987.

McNaught, A. I., Crabb, D. P., Fitzke, F. W. and Hitchings, R. A. (1996). Visual field progression: comparison of Humphrey Statpac2 and pointwise linear regression analysis. *Graefes Arch Clin Exp Ophthalmol* **234**:411-418.

Medeiros, F. A., Lisboa, R., Weinreb, R. N., Girkin, C. A., Liebmann, J. M. and Zangwill, L. M. (2012a). A combined index of structure and function for staging glaucomatous damage. *Arch Ophthalmol* **130**:1107-1116.

Medeiros, F. A., Zangwill, L. M., Anderson, D. R., Liebmann, J. M., Girkin, C. A., Harwerth, R. S., Fredette, M. J. *et al.* (2012b). Estimating the rate of retinal ganglion cell loss in glaucoma. *Am J Ophthalmol* **154**:814-824.

Medeiros, F. A., Zangwill, L. M., Girkin, C. A., Liebmann, J. M. and Weinreb, R. N. (2012c). Combining structural and functional measurements to improve estimates of rates of glaucomatous progression. *Am J Ophthalmol* **153**:1197-1205.

Medeiros, F. A., Zangwill, L. M., Mansouri, K., Lisboa, R., Tafreshi, A. and Weinreb, R. N. (2012d). Incorporating risk factors to improve the assessment of rates of glaucomatous progression. *Invest Ophthalmol Vis Sci* **53**:2199-2207.

Medeiros, F. A., Lisboa, R., Weinreb, R. N., Liebmann, J. M., Girkin, C. and Zangwill, L. M. (2013). Retinal ganglion cell count estimates associated with early development of visual field defects in glaucoma. *Ophthalmology* **120**:736-744.

Miglior, S., Torri, V., Zeyen, T., Pfeiffer, N., Vaz, J. C. and Adamsons, I. (2007). Intercurrent factors associated with the development of open-angle glaucoma in the European Glaucoma Prevention Study. *Am J Ophthalmol* **144**:266-275.

Miglior, S. and Bertuzzi, F. (2013). Relationship between intraocular pressure and glaucoma onset and progression. *Curr Opin Pharmacol* **13**:32-35.

Mills, R. P., Budenz, D. L., Lee, P. P., Noecker, R. J., Walt, J. G., Siegartel, L. R., Evans, S. J. *et al.* (2006). Categorizing the stage of glaucoma from pre-diagnosis to end-stage disease. *Am J Ophthalmol* **141**:24-30.

Mitchell, P., Smith, W., Attebo, K. and Healey, P. R. (1996). Prevalence of open-angle glaucoma in Australia. The Blue Mountains Eye Study. *Ophthalmology* **103**:1661-1669.

Moghim, S., Hosseini, H., Riddle, J., Lee, G. Y., Bitrian, E., Giacconi, J., Caprioli, J. *et al.* (2012). Measurement of optic disc size and rim area with spectral-domain OCT and scanning laser ophthalmoscopy. *Invest Ophthalmol Vis Sci* **53**:4519-4530.

Monhart, M., Bebie, H., Buerki, E. and Palmowski-Wolfe, A. (2006). Calculation of the abnormal response area as an indicator of visual field changes. *Invest Ophthalmol Vis Sci* **47**:150-156.

Moore, D., Harris, A., Wudunn, D., Kheradiya, N. and Siesky, B. (2008). Dysfunctional regulation of ocular blood flow: A risk factor for glaucoma? *Clin Ophthalmol* **2**:849-861.

Morgan, J. E. (2002). Retinal ganglion cell shrinkage in glaucoma. *J Glaucoma* **11**:365-370.

Morgan, J. E., Sheen, N. J., North, R. V., Choong, Y. and Ansari, E. (2005a). Digital imaging of the optic nerve head: monoscopic and stereoscopic analysis. *Br J Ophthalmol* **89**:879-884.

Morgan, J. E., Sheen, N. J., North, R. V., Goyal, R., Morgan, S., Ansari, E. and Wild, J. M. (2005b). Discrimination of glaucomatous optic neuropathy by digital stereoscopic analysis. *Ophthalmology* **112**:855-862.

Morgan, J. E., Datta, A. V., Erichsen, J. T., Albon, J. and Boulton, M. E. (2006). Retinal ganglion cell remodelling in experimental glaucoma. *Adv Exp Med Biol* **572**:397-402.

Morgan, J. E. (2012). Retina ganglion cell degeneration in glaucoma: an opportunity missed? A Review. *Clin Experiment Ophthalmol* **40**:364-368.

Morgan, J. E., Bourtsoukli, I., Rajkumar, K. N., Ansari, E., Cunliffe, I. A., North, R. V. and Wild, J. M. (2012). The accuracy of the inferior>superior>nasal>temporal neuroretinal rim area rule for diagnosing glaucomatous optic disc damage. *Ophthalmology* **119**:723-730.

Morrison, C., J. (2007). Anatomy and physiology of the optic nerve. In: Lanning, B.K. and Foroozan, R. (eds.) *Optic Nerve Disorders*. Second ed. San Francisco, California: The American Academy of Ophthalmology, pp. 2-19.

Muir, K. W., Jin, J. and Freedman, S. F. (2004). Central corneal thickness and its relationship to intraocular pressure in children. *Ophthalmology* **111**:2220-2223.

Muramatsu, C., Nakagawa, T., Sawada, A., Hatanaka, Y., Hara, T., Yamamoto, T. and Fujita, H. (2011). Automated segmentation of optic disc region on retinal fundus photographs: Comparison of contour modeling and pixel classification methods. *Comput Methods Programs Biomed* **101**:23-32.

Musch, D. C., Lichter, P. R., Guire, K. E. and Standardi, C. L. (1999). The Collaborative Initial Glaucoma Treatment Study: study design, methods, and baseline characteristics of enrolled patients. *Ophthalmology* **106**:653-662.

Musch, D. C., Gillespie, B. W., Niziol, L. M., Cashwell, L. F. and Lichter, P. R. (2008). Factors associated with intraocular pressure before and during 9 Years of treatment in the Collaborative Initial Glaucoma Treatment Study. *Ophthalmology* **115**:927-933.

Musch, D. C., Shimizu, T., Niziol, L. M., Gillespie, B. W., Cashwell, L. F. and Lichter, P. R. (2012). Clinical characteristics of newly diagnosed primary, pigmentary and pseudoexfoliative open-angle glaucoma in the Collaborative Initial Glaucoma Treatment Study. *Br J Ophthalmol* **96**:1180-1184.

Naghizadeh, F., Garas, A., Vargha, P. and Hollo, G. (2012). Structure-function relationship between the Octopus perimeter cluster mean sensitivity and sector retinal nerve fiber layer thickness measured with the RTVue Optical Coherence Tomography and Scanning Laser Polarimetry. *J Glaucoma* **23**:11-18.

Nassiri, N., Nilforushan, N., Coleman, A. L., Law, S. K., Caprioli, J. and Nouri-Mahdavi, K. (2012). Longitudinal structure-function relationships with scanning laser ophthalmoscopy and standard achromatic perimetry. *Arch Ophthalmol* **130**:826-832.

Nassiri, N., Moghimi, S., Coleman, A. L., Law, S. K., Caprioli, J. and Nouri-Mahdavi, K. (2013). Global and pointwise rates of decay in glaucoma eyes deteriorating according to pointwise event analysis. *Invest Ophthalmol Vis Sci* **54**:1208-1213.

Nevalainen, J., Paetzold, J., Krapp, E., Vonthein, R., Johnson, C. A. and Schiefer, U. (2008). The use of semi-automated kinetic perimetry (SKP) to monitor advanced glaucomatous visual field loss. *Graefes Arch Clin Exp Ophthalmol* **246**:1331-1339.

Ng, W. S., Legg, P., Avadhanam, V., Aye, K., Evans, S. H., North, R. V., Marshall, A. D. *et al.* (2015). Automated registration of multimodal optic disc images: clinical assessment of alignment accuracy. *J Glaucoma* **25**:1-6.

Nguyen, N. X., Meindl, C., Horn, F. K., Dzialach, M., Langenbacher, A., Junemann, A. and Mardin, C. Y. (2004). Digital planimetry for long-term follow-up of glaucomatous optic disk injuries in patients with normal-pressure glaucoma. *Ophthalmologie* **101**:589-594.

Nickells, R. W. (2007). From ocular hypertension to ganglion cell death: a theoretical sequence of events leading to glaucoma. *Can J Ophthalmol* **42**:278-287.

Nicolela, M. T. and Drance, S. M. (1996). Various glaucomatous optic nerve appearances: clinical correlations. *Ophthalmology* **103**:640-649.

O'Neill, E. C., Danesh-Meyer, H. V., Kong, G. X., Hewitt, A. W., Coote, M. A., Mackey, D. A. and Crowston, J. G. (2010). Optic disc evaluation in optic neuropathies: the optic disc assessment project. *Ophthalmology* **118**:964-970.

Oddone, F. and Centofanti, M. (2005). Normal anatomy of the optic nerve head and retinal nerve fibre layer In: Iester, M., Garway-Heath, D.F. and Lemij, H. (eds.) *Optic Nerve Head and Retinal Nerve Fibre Analysis* Savona, Italy: European Glaucoma Society, pp. 15-17.

Olsson, J. and Rootzén, H. (1994). An image model for quantal response analysis in perimetry. *Scandinavian Journal of Statistics* **21**:375-387.

Olsson, J., Bengtsson, B., Heijl, A. and Rootzen, H. (1997). An improved method to estimate frequency of false-positive answers in computerized perimetry. *Acta Ophthalmol Scand* **75**:181-183.

Owen, V. M., Crabb, D. P., White, E. T., Viswanathan, A. C., Garway-Heath, D. F. and Hitchings, R. A. (2008). Glaucoma and fitness to drive: using binocular visual fields to predict a milestone to blindness. *Invest Ophthalmol Vis Sci* **49**:2449-2455.

Pablo, L. E., Ferreras, A., Fogagnolo, P., Figus, M. and Pajarin, A. B. (2009). Optic nerve head changes in early glaucoma: a comparison between stereophotography and Heidelberg retina tomography. *Eye* **24**:123-130.

Pan, Y. and Varma, R. (2011). Natural history of glaucoma. *Indian J Ophthalmol* **59**:19-23.

Panarelli, J. F., Banitt, M. R., Sidoti, P. A., Budenz, D. L. and Singh, K. (2015). Clinical impact of 8 prospective, randomized, multicenter glaucoma trials. *J Glaucoma* **24**:64-68.

Park, H. Y. and Park, C. K. (2012). Diagnostic capability of lamina cribrosa thickness by enhanced depth imaging and factors affecting thickness in patients with glaucoma. *Ophthalmology* **120**:745-752.

Park, S. C., Hsu, A. T., Su, D., Simonson, J. L., Al-Jumayli, M., Liu, Y., Liebmann, J. M. *et al.* (2013). Factors associated with focal lamina cribrosa defects in glaucoma. *Invest Ophthalmol Vis Sci* **54**:8401-8407.

Pathak, M., Demirel, S. and Gardiner, S. K. (2013). Non-linear, multilevel mixed-effects approach for modeling longitudinal standard automated perimetry data in glaucoma. *Invest Ophthalmol Vis Sci* **54**:5505-5513.

Pathak, M., Demirel, S. and Gardiner, S. K. (2015). Non-linear trend analysis of longitudinal pointwise visual field sensitivity in suspected and early glaucoma. *Transl Vis Sci Technol* **4**:1-8.

Peeters, A., Webers, C. A., Prins, M. H., Zeegers, M. P., Hendrikse, F. and Schouten, J. S. (2010). Quantifying the effect of intraocular pressure reduction on the occurrence of glaucoma. *Acta Ophthalmol* **88**:5-11.

Polaczek-Krupa, B. and Grabska-Liberek, I. (2012). Evaluation of the significance of some diagnostic parameters in making an early diagnosis of primary open-angle glaucoma. *Med Sci Monit* **18**:456-460.

Porciatti, V. and Ventura, L. M. (2012). Retinal ganglion cell functional plasticity and optic neuropathy: a comprehensive model. *J Neuroophthalmol* **32**:354-358.

Qu, J., Wang, D. and Grosskreutz, C. L. (2010). Mechanisms of retinal ganglion cell injury and defense in glaucoma. *Exp Eye Res* **91**:48-53.

Quaranta, L., Katsanos, A., Russo, A. and Riva, I. (2013). 24-hour intraocular pressure and ocular perfusion pressure in glaucoma. *Surv Ophthalmol* **58**:26-41.

Quigley, H. A. (1996). Number of people with glaucoma worldwide. *Br J Ophthalmol* **80**:389-393.

Quigley, H. A. and Broman, A. T. (2006). The number of people with glaucoma worldwide in 2010 and 2020. *Br J Ophthalmol* **90**:262-267.

Quigley, M. G., Patel, V., Dube, P., Wittich, W. and Harasymowycz, P. (2008). Comparing optic nerve head size measurements by the Heidelberg Retina Tomograph with fundus photography performed with a novel focusing technique. *J Glaucoma* **17**:480-483.

Radcliffe, N. M., Liebmann, J. M., Rozenbaum, I., Sbeity, Z., Sandler, S. F., Tello, C. and Ritch, R. (2008). Anatomic relationships between disc hemorrhage and parapapillary atrophy. *Am J Ophthalmol* **146**:735-740.

Radcliffe, N. M., Sehi, M., Wallace, I. B., Greenfield, D. S., Krupin, T. and Ritch, R. (2010). Comparison of stereo disc photographs and alternation flicker using a novel matching technology for detecting glaucoma progression. *Ophthalmic Surg Lasers Imaging* **41**:629-634.

Radius, R. L. and Gonzales, M. (1981). Anatomy of the lamina cribrosa in human eyes. *Arch Ophthalmol* **99**:2159-2162.

Radius, R. L. (1987). Anatomy of the optic nerve head and glaucomatous optic neuropathy. *Surv Ophthalmol* **32**:35-44.

Ramakrishnan, R., Kader, M. A. and Budde, W. M. (2005). Optic disc morphometry with optical coherence tomography: comparison with planimetry of fundus photographs and influence of parapapillary atrophy and pigmentary conus. *Indian J Ophthalmol* **53**:187-191.

Ramulu, P. Y., Maul, E., Hochberg, C., Chan, E. S., Ferrucci, L. and Friedman, D. S. (2012). Real-world assessment of physical activity in glaucoma using an accelerometer. *Ophthalmology* **119**:1159-1166.

Rao, H. L., Jonnadula, G. B., Addepalli, U. K., Senthil, S. and Garudadri, C. S. (2013a). Effect of cataract extraction on Visual Field Index in glaucoma. *J Glaucoma* **22**:164-168.

Rao, H. L., Kumbar, T., Kumar, A. U., Babu, J. G., Senthil, S. and Garudadri, C. S. (2013b). Agreement between event-based and trend-based glaucoma progression analyses. *Eye* **27**:803-808.

Rao, H. L., Yadav, R. K., Addepalli, U. K., Begum, V. U., Senthil, S., Choudhari, N. S. and Garudadri, C. S. (2015). The ISNT rule in glaucoma: revisiting with spectral domain optical coherence tomography. *Acta Ophthalmol* **93**:208-213.

Raza, A. S., Cho, J., de Moraes, C. G., Wang, M., Zhang, X., Kardon, R. H., Liebmann, J. M. *et al.* (2011). Retinal ganglion cell layer thickness and local visual field sensitivity in glaucoma. *Arch Ophthalmol* **129**:1529-1536.

Raza, A. S. and Hood, D. C. (2015). Evaluation of a method for estimating retinal ganglion cell counts using visual fields and optical coherence tomography. *Invest Ophthalmol Vis Sci* **56**:2254-2268.

Redmond, T., Garway-Heath, D. F., Zlatkova, M. B. and Anderson, R. S. (2010). Sensitivity loss in early glaucoma can be mapped to an enlargement of the area of complete spatial summation. *Invest Ophthalmol Vis Sci* **51**:6540-6548.

Ritch, R. (2001). Perspective on exfoliation syndrome. *J Glaucoma* **10**:S33-35.

Roff, E. J., Hosking, S. L. and Barnes, D. A. (2001). The influence of contour line size and location on the reproducibility of topographic measurement with the Heidelberg Retina Tomograph. *Ophthalmic Physiol Opt* **21**:173-181.

Rolando, M. (2005). Features of the glaucomatous optic nerve head. In: Iester, M., Garway-Heath, D.F. and Lemij, H. (eds.) *Optic Nerve Head and Retinal Nerve Fibre Analysis*. Savona, Italy: European Glaucoma Society, pp. 19-20.

Rosenthal, A. R., Kottler, M. S., Donaldson, D. D. and Falconer, D. G. (1977). Comparative reproducibility of the digital photogrammetric procedure utilizing three methods of stereophotography. *Invest Ophthalmol Vis Sci* **16**:54-60.

Rossetti, L., Goni, F., Denis, P., Bengtsson, B., Martinez, A. and Heijl, A. (2010). Focusing on glaucoma progression and the clinical importance of progression rate measurement: a Review. *Eye* **24** 1-7.

Rudnicka, A. R., Burk, R. O., Edgar, D. F. and Fitzke, F. W. (1998). Magnification characteristics of fundus imaging systems. *Ophthalmology* **105**:2186-2192.

Rudnicka, A. R., Mt-Isa, S., Owen, C. G., Cook, D. G. and Ashby, D. (2006). Variations in primary open-angle glaucoma prevalence by age, gender, and race: a Bayesian meta-analysis. *Invest Ophthalmol Vis Sci* **47**:4254-4261.

Russell, R. A., Crabb, D. P., Malik, R. and Garway-Heath, D. F. (2012). The relationship between variability and sensitivity in large-scale longitudinal visual field data. *Invest Ophthalmol Vis Sci* **53**:5985-5990.

Saine, P. J. (2002). Fundus photography : instrumentation and technique. In: Saine, P.J. and Tyler, M.E. (eds.) *Ophthalmic Photography: Retinal Photography, Angiography, and Electronic Imaging*. Second ed. Boston, Oxford, Auckland, Johannesburg, Melbourne, New Delhi: Butterworth-Heinemann pp. 13-96.

Saito, H., Tsutsumi, T., Iwase, A., Tomidokoro, A. and Araie, M. (2010). Correlation of disc morphology quantified on stereophotographs to results by Heidelberg Retina Tomograph II, GDx variable corneal compensation, and visual field tests. *Ophthalmology* **117**:282-289.

Samarawickrama, C., Wang, J. J., Huynh, S. C., Pai, A., Burlutsky, G., Rose, K. A. and Mitchell, P. (2010). Ethnic differences in optic nerve head and retinal nerve fibre layer thickness parameters in children. *Br J Ophthalmol* **94**:871-876.

Sanfilippo, P. G., Cardini, A., Hewitt, A. W., Crowston, J. G. and Mackey, D. A. (2009). Optic disc morphology-rethinking shape. *Prog Retin Eye Res* **28**:227-248.

Saunders, L. J., Russell, R. A. and Crabb, D. P. (2012). Practical landmarks for visual field disability in glaucoma. *Br J Ophthalmol* **96**:1185-1189.

Schuman, J. S. (2012). Detection and diagnosis of glaucoma: ocular imaging. *Invest Ophthalmol Vis Sci* **53**:2488-2490.

Searle, A. E., Wild, J. M., Shaw, D. E. and O'Neill, E. C. (1991). Time-related variation in normal automated static perimetry. *Ophthalmology* **98**:701-707.

See, J. L., Nicolela, M. T. and Chauhan, B. C. (2009). Rates of neuroretinal rim and peripapillary atrophy area change: a comparative study of glaucoma patients and normal controls. *Ophthalmology* **116**:840-847.

Sehi, M., Bhardwaj, N., Chung, Y. S. and Greenfield, D. S. (2012). Evaluation of baseline structural factors for predicting glaucomatous visual-field progression using optical coherence tomography, scanning laser polarimetry and confocal scanning laser ophthalmoscopy. *Eye* **26**:1527-1535.

Sharma, A., Oakley, J. D., Schiffman, J. C., Budenz, D. L. and Anderson, D. R. (2011). Comparison of automated analysis of Cirrus HD OCT spectral-domain optical coherence tomography with stereo photographs of the optic disc. *Ophthalmology* **118**:1348-1357.

Sharma, A. K., Goldberg, I., Graham, S. L. and Mohsin, M. (2000). Comparison of the Humphrey Swedish Interactive Thresholding Algorithm (SITA) and Full Threshold strategies. *J Glaucoma* **9**:20-27.

Sharpe, R. A., Nelson, L. A., Stewart, J. A. and Stewart, W. C. (2013). Intraocular pressure efficacy of glaucoma medications versus placebo in Phase II compared to later phase trials. *Br J Ophthalmol* **97**:121-125.

Sheen, N. J. (2002). Evaluation of stereoscopic imaging techniques in the detection of glaucoma. PhD Thesis, Cardiff University.

Sheen, N. J., Morgan, J. E., Poulsen, J. L. and North, R. V. (2004). Digital stereoscopic analysis of the optic disc: evaluation of a teaching program. *Ophthalmology* **111**:1873-1879.

Shirato, S., Inoue, R., Fukushima, K. and Suzuki, Y. (1999). Clinical evaluation of SITA: a new family of perimetric testing strategies. *Graefes Arch Clin Exp Ophthalmol* **237**:29-34.

Shue, B., Chatterjee, A., Fudemberg, S., Katz, L. J., Moster, M. R., Navarro, M. J., Pro, M. *et al.* (2011). The effects of Mozart's music on the performance of glaucoma patients on automated perimetry. *Invest Ophthalmol Vis Sci* **52**:7347-7349.

Shuttleworth, G. N., Khong, C. H. and Diamond, J. P. (2000). A new digital optic disc stereo camera: intraobserver and interobserver repeatability of optic disc measurements. *Br J Ophthalmol* **84**:403-407.

Smith, S. D., Katz, J. and Quigley, H. A. (1996). Analysis of progressive change in automated visual fields in glaucoma. *Invest Ophthalmol Vis Sci* **37**:1419-1428.

Soares, A. S., Artes, P. H., Andreou, P., Leblanc, R. P., Chauhan, B. C. and Nicolela, M. T. (2004). Factors associated with optic disc hemorrhages in glaucoma. *Ophthalmology* **111**:1653-1657.

Spaeth, G. L. (1994). A new classification of glaucoma including focal glaucoma. *Surv Ophthalmol* **38**:9-17.

Spaeth, G. L., Lopes, J. F., Junk, A. K., Grigorian, A. P. and Henderer, J. (2006). Systems for staging the amount of optic nerve damage in glaucoma: a critical review and new material. *Surv Ophthalmol* **51**:293-315.

Spry, P. G. D. and Johnson, C. A. (2002). Identification of progressive glaucomatous visual field loss. *Surv Ophthalmol* **47**:158-173.

Sramek, J. S. (2002). Ophthalmic photography: maximizing diagnostic information. In: Saine, P.J. and Tyler, M.E. (eds.) *Ophthalmic Photography: Retinal Photography, Angiography, and Electronic Imaging*. Second ed. Boston, Oxford, Auckland, Johannesburg, Melbourne, New Delhi: Butterworth-Heinemann pp. 323-368.

Stein, J. D., Kim, D. S., Niziol, L. M., Talwar, N., Nan, B., Musch, D. C. and Richards, J. E. (2011). Differences in rates of glaucoma among Asian Americans and other racial groups, and among various Asian ethnic groups. *Ophthalmology* **118**:1031-1037.

Stone, R. A., Ying, G. S., Pearson, D. J., Bansal, M., Puri, M., Miller, E., Alexander, J. *et al.* (2010). Utility of digital stereo images for optic disc evaluation. *Invest Ophthalmol Vis Sci* **51**:5667-5674.

Strouthidis, N. G., Scott, A., Viswanathan, A. C., Crabb, D. P. and Garway-Heath, D. F. (2007). Monitoring glaucomatous visual field progression: the effect of a novel spatial filter. *Invest Ophthalmol Vis Sci* **48**:251-257.

Strouthidis, N. G., Chandrasekharan, G., Diamond, J. P. and Murdoch, I. E. (2014). Teleglaucoma: ready to go? *Br J Ophthalmol* **98**:1605-1611.

Sung, K. R., Wollstein, G., Bilonick, R. A., Townsend, K. A., Ishikawa, H., Kagemann, L., Noecker, R. J. *et al.* (2009). Effects of age on optical coherence tomography measurements of healthy retinal nerve fiber layer, macula, and optic nerve head. *Ophthalmology* **116**:1119-1124.

Swamy, L., Smith, S. and Radcliffe, N. M. (2012). Optic nerve complex imaging in glaucoma Medicare Beneficiaries. *Ophthalmic Epidemiol* **19**:249-255.

Swanson, W. H., Felius, J. and Pan, F. (2004). Perimetric defects and ganglion cell damage: interpreting linear relations using a two-stage neural model. *Invest Ophthalmol Vis Sci* **45**:466-472.

Syed, Z. A., Radcliffe, N. M., De Moraes, C. G., Liebmann, J. M. and Ritch, R. (2011). Detection of progressive glaucomatous optic neuropathy using automated alternation flicker with stereophotography. *Arch Ophthalmol* **129**:521-522.

Syed, Z. A., Radcliffe, N. M., De Moraes, C. G., Smith, S. D., Liebmann, J. M. and Ritch, R. (2012). Automated alternation flicker for the detection of optic disc haemorrhages. *Acta Ophthalmol* **90**:645-650.

Taibbi, G., Fogagnolo, P., Orzalesi, N. and Rossetti, L. (2009). Reproducibility of the Heidelberg Retina Tomograph III Glaucoma Probability Score. *J Glaucoma* **18**:247-252.

Talbot, R., Goldberg, I. and Kelly, P. (2013). Evaluating the accuracy of the Visual Field Index for the Humphrey Visual Field Analyzer in patients with mild to moderate glaucoma. *Am J Ophthalmol* **156**:1272-1276.

Tanna, A. P., Bandi, J. R., Budenz, D. L., Feuer, W. J., Feldman, R. M., Herndon, L. W., Rhee, D. J. *et al.* (2011). Interobserver agreement and intraobserver reproducibility of the subjective determination of glaucomatous visual field progression. *Ophthalmology* **118**:60-65.

Tatham, A. J., Weinreb, R. N., Zangwill, L. M., Liebmann, J. M., Girkin, C. A. and Medeiros, F. A. (2013). The relationship between cup-to-disc ratio and estimated number of retinal ganglion cells. *Invest Ophthalmol Vis Sci* **54**:3205-3214.

Taylor, H. R. (2009). Glaucoma: where to now? *Ophthalmology* **116**:821-822.

Teng, C. C., De Moraes, C. G., Prata, T. S., Tello, C., Ritch, R. and Liebmann, J. M. (2010). Beta-Zone parapapillary atrophy and the velocity of glaucoma progression. *Ophthalmology* **117**:909-915.

The AGIS, I. (2000). The Advanced Glaucoma Intervention Study (AGIS): 7. The relationship between control of intraocular pressure and visual field deterioration. *Am J Ophthalmol* **130**:429-440.

The Collaborative Normal-Tension Glaucoma Study Group. (1998). Comparison of glaucomatous progression between untreated patients with normal-tension glaucoma and patients with therapeutically reduced intraocular pressures. *Am J Ophthalmol* **126**:487-497.

Tielsch, J. M., Katz, J., Singh, K., Quigley, H. A., Gottsch, J. D., Javitt, J. and Sommer, A. (1991). A population-based evaluation of glaucoma screening: the Baltimore Eye Survey. *Am J Epidemiol* **134**:1102-1110.

Traquair, H. M. (ed.) (1927). An introduction to clinical perimetry. first ed. St. Louis: C. V. Mosby Company.

Tsutsumi, T., Tomidokoro, A., Araie, M., Iwase, A., Sakai, H. and Sawaguchi, S. (2012). Planimetrically determined vertical cup/disc and rim width/disc diameter ratios and related factors. *Invest Ophthalmol Vis Sci* **53**:1332-1340.

Turpin, A., Jankovic, D. and McKendrick, A. M. (2007). Retesting visual fields: utilizing prior information to decrease test-retest variability in glaucoma. *Invest Ophthalmol Vis Sci* **48**:1627-1634.

Tyler, M. E., Saine, P. J. and Bennett, T. M. (2003a). The basics: History, basic eye anatomy, and the fundus camera. In: Andjelkovic, N. (ed.) *Practical Retinal Photography and Digital Imaging Techniques*. Boston, Oxford, Auckland, Johannesburg, Melbourne, New Delhi: Butterworth-Heinemann, pp. 1-22.

Tyler, M. E., Saine, P. J. and Bennett, T. M. (2003b). Digital imaging basics. In: Andjelkovic, N. (ed.) *Practical Retinal Photography and Digital Imaging Techniques*. Boston, Oxford, Auckland, Johannesburg, Melbourne, New Delhi: Butterworth-Heinemann, pp. 127-150.

Uhler, T. A. and Piltz-Seymour, J. (2008). Optic disc hemorrhages in glaucoma and ocular hypertension: implications and recommendations. *Curr Opin Ophthalmol* **19**:89-94.

VanderBeek, B. L., Smith, S. D. and Radcliffe, N. M. (2010). Comparing the detection and agreement of parapapillary atrophy progression using digital optic disk photographs and alternation flicker. *Graefes Arch Clin Exp Ophthalmol* **248**:1313-1317.

Varma, R., Spaeth, G. and Parker, K. (1993). The optic nerve in glaucoma. Philadelphia: J. B. Lippincott Company, p. 354.

Varma, R., Ying-Lai, M., Francis, B. A., Nguyen, B. B., Deneen, J., Wilson, M. R. and Azen, S. P. (2004). Prevalence of open-angle glaucoma and ocular hypertension in Latinos: the Los Angeles Latino Eye Study. *Ophthalmology* **111**:1439-1448.

Varma, R., Lee, P. P., Goldberg, I. and Kotak, S. (2011). An assessment of the health and economic burdens of glaucoma. *Am J Ophthalmol* **152**:515-522.

Vesti, E., Johnson, C. A. and Chauhan, B. C. (2003). Comparison of different methods for detecting glaucomatous visual field progression. *Invest Ophthalmol Vis Sci* **44**:3873-3879.

Viswanathan, A., Fitzke, F. W. and Hitchings, R. A. (1998). Pointwise linear regression of glaucomatous visual fields. In: Wall, M. and Wild, J.M. (eds.) *Perimetry Update 1998/1999*. New York, The Hague: Kugler Publications, pp. 139-145.

Vizzeri, G., Weinreb, R. N., Martinez de la Casa, J. M., Alencar, L. M., Bowd, C., Balasubramanian, M., Medeiros, F. A. *et al.* (2009). Clinicians agreement in establishing glaucomatous progression using the Heidelberg Retina Tomograph. *Ophthalmology* **116**:14-24.

Vonthein, R., Rauscher, S., Paetzold, J., Nowomiejska, K., Krapp, E., Hermann, A., Sadowski, B. *et al.* (2007). The normal age-corrected and reaction time-corrected isopter derived by semi-automated kinetic perimetry. *Ophthalmology* **114**:1065-1072.

Wall, M. (1997). *Perimetry Update 1996/1997*. New York, The Hague, The Netherlands: Kugler Publications, pp. 185-190.

Wall, M., Johnson, C. A., Kardon, R. H. and Crabb, D. P. (2009). Use of a continuous probability scale to display visual field damage. *Arch Ophthalmol* **127**:749-756.

Wall, M., Doyle, C. K., Eden, T., Zamba, K. D. and Johnson, C. A. (2013). Size Threshold Perimetry performs as well as conventional automated perimetry with stimulus sizes III, V, and VI for glaucomatous loss. *Invest Ophthalmol Vis Sci* **54**:3975-3983.

Wang, M., Lu, A. T., Varma, R., Schuman, J. S., Greenfield, D. S. and Huang, D. (2012). Combining information from 3 anatomic regions in the diagnosis of glaucoma with time-domain optical coherence tomography. *J Glaucoma* **23**:129-135.

Wax, M. B. (2011). The case for autoimmunity in glaucoma. *Exp Eye Res* **93**:187-190.

Weber, J. and Dobek, K. (1986). What is the most suitable grid for computer perimetry in glaucoma patients? *Ophthalmologica* **192**:88-96.

Weinreb, R. N. and Perlman, J. P. (1986). The effect of refractive correction on automated perimetric thresholds. *Am J Ophthalmol* **101**:706-709.

Werner, E. B., Petrig, B., Krupin, T. and Bishop, K. I. (1989). Variability of automated visual fields in clinically stable glaucoma patients. *Invest Ophthalmol Vis Sci* **30**:1083-1089.

Weinreb, R. N., Aung, T. and Medeiros, F. A. (2014). The pathophysiology and treatment of glaucoma: a Review. *JAMA* **311**:1901-1911.

Wesselink, C., Heeg, G. P. and Jansonius, N. M. (2009). Glaucoma monitoring in a clinical setting: glaucoma progression analysis versus nonparametric progression analysis in the Groningen Longitudinal Glaucoma Study. *Arch Ophthalmol* **127**:270-274.

Wild, J. M. (1988). Techniques and developments in automated perimetry: a review. *Ophthalmic Physiol Opt* **8**:295-308.

Wild, J. M., Searle, A. E., Dengler-Harles, M. and O'Neill, E. C. (1991). Long-term follow-up of baseline learning and fatigue effects in the automated perimetry of glaucoma and ocular hypertensive patients. *Acta Ophthalmol (Copenh)* **69**:210-216.

Wild, J. M., Hussey, M. K., Flanagan, J. G. and Trope, G. E. (1993). Pointwise topographical and longitudinal modeling of the visual field in glaucoma. *Invest Ophthalmol Vis Sci* **34**:1907-1916.

Wild, J. M., Pacey, I. E., Hancock, S. A. and Cunliffe, I. A. (1999a). Between-algorithm, between-individual differences in normal perimetric sensitivity: Full Threshold, FASTPAC, and SITA. Swedish Interactive Threshold algorithm. *Invest Ophthalmol Vis Sci* **40**:1152-1161.

Wild, J. M., Pacey, I. E., O'Neill, E. C. and Cunliffe, I. A. (1999b). The SITA perimetric threshold algorithms in glaucoma. *Invest Ophthalmol Vis Sci* **40**:1998-2009.

Wilkins, M. R., Fitzke, F. W. and Khaw, P. T. (2005). Pointwise linear progression criteria and the detection of visual field change in a glaucoma trial. *Eye* **20**:98-106.

Williams, P. A., Howell, G. R., Barbay, J. M., Braine, C. E., Sousa, G. L., John, S. W. and Morgan, J. E. (2013). Retinal ganglion cell dendritic atrophy in DBA/2J glaucoma. *PLoS One* **8**:1-10.

Wirtschafter, J. D., Becker, W. L., Howe, J. B. and Younge, B. R. (1982). Glaucoma visual field analysis by computed profile of nerve fiber function in optic disc sectors. *Ophthalmology* **89**:255-267.

Wood, J. M., Wild, J. M., Hussey, M. K. and Crews, S. J. (1987). Serial examination of the normal visual field using Octopus automated projection perimetry. Evidence for a learning effect. *Acta Ophthalmol (Copenh)* **65**:326-333.

Wood, N. E. H., Guo, L. and Cordeiro, F. (2009). Imaging individual ganglion cells in the human retina. In: Grehn, F. and Stamper, R. (eds.) *Essentials in Ophthalmology*. Heidelberg, Germany: Springer, pp. 1-12.

Wright, H. R. and Diamond, J. P. (2015). Service innovation in glaucoma management: using a Web-based electronic patient record to facilitate virtual specialist supervision of a shared care glaucoma programme. *Br J Ophthalmol* **99**:313-317.

Wynsberghe, V. D., Noback, R. C. and Carola, R. (1995). *Human Anatomy & Physiology*. third ed. New York: McGraw-Hill.

Xu, J., Ishikawa, H., Wollstein, G., Bilonick, R. A., Sung, K. R., Kagemann, L., Townsend, K. A. *et al.* (2008). Automated assessment of the optic nerve head on stereo disc photographs. *Invest Ophthalmol Vis Sci* **49**:2512-2517.

Yogesan, K., Barry, C. J., Jitskaia, L., Eikelboom, R. H., Morgan, W. H., House, P. H. and van Saarloos, P. P. (1999). Software for 3-D visualization/analysis of optic disc images. *IEEE Eng Med Biol Mag* **18**:43-49.

Zeyen, T., Miglior, S., Pfeiffer, N., Cunha-Vaz, J. and Adamsons, I. (2003). Reproducibility of evaluation of optic disc change for glaucoma with stereo optic disc photographs. *Ophthalmology* **110**:340-344.